PRECISION/PERSONALIZED PEDIATRIC ONCOLOGY AND IMMUNE THERAPIES: RATHER CUSTOMIZE THAN RANDOMIZE

EDITED BY: Irene Slavc, Giannoula Lakka Klement, Jaroslav Sterba, Ondrej Slaby and Dalibor Valik

PUBLISHED IN: Frontiers in Oncology

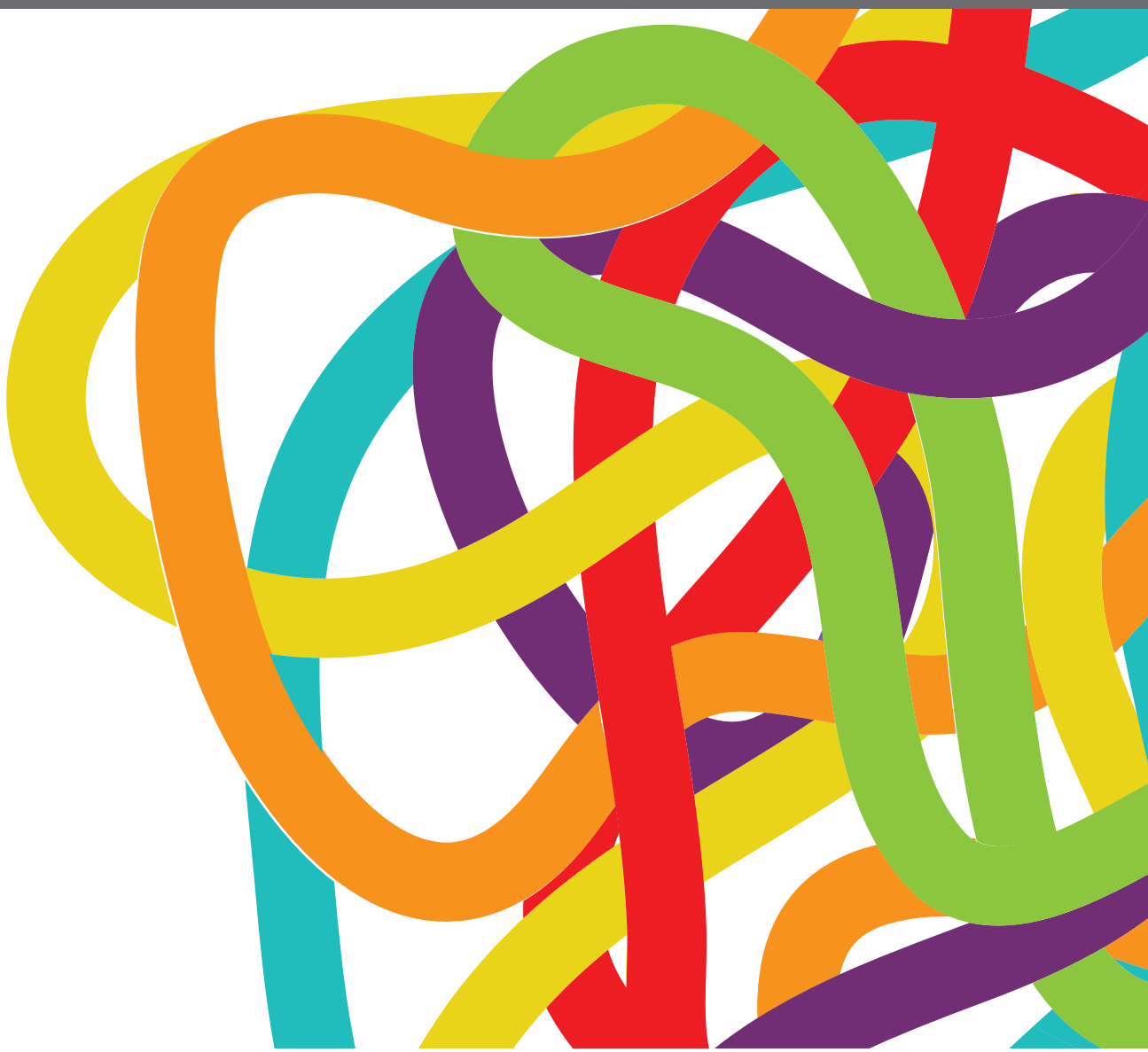

frontiers Research Topics

ISSN 1664-8714
ISBN 978-2-88963-718-8
DOI 10.3389/978-2-88963-718-8

About Frontiers

Frontiers is more than just an open-access publisher of scholarly articles: it is a pioneering approach to the world of academia, radically improving the way scholarly research is managed. The grand vision of Frontiers is a world where all people have an equal opportunity to seek, share and generate knowledge. Frontiers provides immediate and permanent online open access to all its publications, but this alone is not enough to realize our grand goals.

Frontiers Journal Series

The Frontiers Journal Series is a multi-tier and interdisciplinary set of open-access, online journals, promising a paradigm shift from the current review, selection and dissemination processes in academic publishing. All Frontiers journals are driven by researchers for researchers; therefore, they constitute a service to the scholarly community. At the same time, the Frontiers Journal Series operates on a revolutionary invention, the tiered publishing system, initially addressing specific communities of scholars, and gradually climbing up to broader public understanding, thus serving the interests of the lay society, too.

Dedication to Quality

Each Frontiers article is a landmark of the highest quality, thanks to genuinely collaborative interactions between authors and review editors, who include some of the world's best academicians. Research must be certified by peers before entering a stream of knowledge that may eventually reach the public - and shape society; therefore, Frontiers only applies the most rigorous and unbiased reviews.
Frontiers revolutionizes research publishing by freely delivering the most outstanding research, evaluated with no bias from both the academic and social point of view. By applying the most advanced information technologies, Frontiers is catapulting scholarly publishing into a new generation.

What are Frontiers Research Topics?

Frontiers Research Topics are very popular trademarks of the Frontiers Journals Series: they are collections of at least ten articles, all centered on a particular subject. With their unique mix of varied contributions from Original Research to Review Articles, Frontiers Research Topics unify the most influential researchers, the latest key findings and historical advances in a hot research area! Find out more on how to host your own Frontiers Research Topic or contribute to one as an author by contacting the Frontiers Editorial Office: researchtopics@frontiersin.org

PRECISION/PERSONALIZED PEDIATRIC ONCOLOGY AND IMMUNE THERAPIES: RATHER CUSTOMIZE THAN RANDOMIZE

Topic Editors:
Irene Slavc, Medical University of Vienna, Austria
Giannoula Lakka Klement, Floating Hospital for Children, United States
Jaroslav Sterba, Masaryk University, Czechia
Ondrej Slaby, Central European Institute of Technology (CEITEC), Czechia
Dalibor Valik, Masaryk Memorial Cancer Institute, Czechia

Citation: Slavc, I., Klement, G. L., Sterba, J., Slaby, O., Valik, D., eds. (2020). Precision/Personalized Pediatric Oncology and Immune Therapies: Rather Customize Than Randomize. Lausanne: Frontiers Media SA. doi: 10.3389/978-2-88963-718-8

Table of Contents

frontiers in Oncology

EDITORIAL
published: 24 March 2020
doi: 10.3389/fonc.2020.00377

Editorial: Precision/Personalized Pediatric Oncology and Immune Therapies: Rather Customize Than Randomize

*Michal Kýr[1,2], Giannoula Lakka Klement[1,3,4], Lenka Zdrazilova-Dubska[5,6], Regina Demlova[6,7], Dalibor Valik[1,5,6], Ondrej Slaby[8,9], Irene Slavc[10] and Jaroslav Sterba[1,2]**

[1] Department of Pediatric Oncology, University Hospital Brno, Brno, Czechia, [2] Faculty of Medicine, Masaryk University, Brno, Czechia, [3] CSTS Health Care, Toronto, ON, Canada, [4] Floating Hospital for Children at Tufts Medical Center, Boston, MA, United States, [5] Department of Laboratory Medicine, Masaryk Memorial Cancer Institute, Brno, Czechia, [6] Department of Pharmacology, Faculty of Medicine, Masaryk University, Brno, Czechia, [7] Department of Clinical Trials, Masaryk Memorial Cancer Institute, Brno, Czechia, [8] Department of Pathology, University Hospital Brno, Brno, Czechia, [9] Central European Institute of Technology (CEITEC), Masaryk University, Brno, Czechia, [10] Department of Pediatrics and Adolescent Medicine, Medical University of Vienna, Vienna, Austria

Keywords: personalized medicine, precision oncology, pediatric oncology, trial models, drug models, personalized precision pediatric oncology, clinical trial designs

Editorial on the Research Topic

Precision/Personalized Pediatric Oncology and Immune Therapies: Rather Customize Than Randomize

OPEN ACCESS

Edited and reviewed by:
Giuseppe Giaccone,
Cornell University, United States

***Correspondence:**
Jaroslav Sterba
sterba.jaroslav@fnbrno.cz

Specialty section:
This article was submitted to Cancer Molecular Targets and Therapeutics, a section of the journal Frontiers in Oncology

Received: *20 January 2020*
Accepted: *04 March 2020*
Published: *24 March 2020*

Citation:
Kýr M, Klement GL, Zdrazilova-Dubska L, Demlova R, Valik D, Slaby O, Slavc I and Sterba J (2020) Editorial: Precision/Personalized Pediatric Oncology and Immune Therapies: Rather Customize Than Randomize. Front. Oncol. 10:377. doi: 10.3389/fonc.2020.00377

Personalization of treatment based on biological markers is being utilized in clinical medicine with increasing frequency. This trend, despite an effort to identify possible common patterns, reflects the reality that no two patients are alike, and no single clinical course is identical; not even within a group of seemingly similar patients (1). There are numerous clinical variations related to host or environment-dependent factors. Numerous examples of these interpersonal differences have been recognized with drugs such as pain-control medications, heart medications, or antimicrobials. The differences have been attributed to increased pharmacometabolic capacity, to different individual microbiomes and to genetic differences between individuals (2). The latter has led to development of an entirely new specialty—pharmacogenomics. While this clinical heterogeneity is well-appreciated in most major medical specialties, clinical oncology seems to represent, surprisingly enough, one of the exceptions (3, 4).

Individualized treatments aim to optimize patient outcomes based on specific knowledge about diseases and their biological heterogeneity (5). This individualization of therapy is being adopted even in adult oncology where, at least traditionally, new therapeutic directions depended on success in large randomized clinical trials. Even in cancers where the numbers of adult patients are sufficient for large randomized double-blind clinical trials, the recent trends are to select the most suitable, genetically homogeneous, target population. This trend has been more inherent to pediatrics, where malignancies are implicitly considered rare diseases. However, the smaller populations and a personalized approach, has led to a very small number of drugs being approved for pediatric indications. The small number of patients and more personalized combinations of drugs tended to complicate statistical analysis and created problems for providing evidence of treatment efficacy in children with rare malignancies (Kyr et al.).

When a large homogeneous population can be used—a randomized, double blind, placebo controlled trial should remain the gold standard. However, this is rarely possible considering cancer heterogeneity and interpersonal differences in drug response. In pediatrics, the numbers of patients are relatively small and the diseases heterogeneous. The process of randomization and

blinding were originally developed to protect the subjects and the investigators from pre-existing subjective preferences for a procedure or a compound under evaluation (6, 7). Randomization was intended to minimalize the effect of confounders, to achieve comparable groups and to permit calculation of an unbiased estimate of the treatment effect. While the use of "blinding" in order to eliminate bias is obvious, there is another important tool that makes randomized trials powerful with regard to rendering reliable and unbiased results. It is the balancing effect between investigated groups, especially with respect unknown covariates that cannot be easily eliminated through model adjustments nor stratification. As stressed above, randomization requires sufficient number of patients and adequate sample size to work. A test sample >200 is said to be less likely to be imbalanced for an important covariate (8). But in rare diseases, where the sample sizes are small (rarely more than a hundred), the usefulness of randomization for balancing of the groups is lost. Similarly, randomized, double blind, placebo-controlled trials may not be suitable for populations that are selected on a common, but infrequent genetic alteration(s). Those groups are also quite small. While the gold standard of clinical trials, a randomized, double blind, placebo controlled trial, may have made logical sense in the era before genomics, it may need to be modified for the era informed by testing for individualized traits and smaller groups.

The concept of time-dependent variations is equally important (9). As documented in numerous recent publications, variations within an individual and implicitly, within the individual's *macroscopic tumor*, occur at velocity rates that cannot be measured by any contemporary techniques (10). It is this variability that constitutes a fundamental concern with the use of treatment group randomization. For a set of individuals being randomized using current rules, a critical prior assumption is made that *all randomized individuals are, and will remain, biologically homogenous*, and any further events can only be related to the time point of randomization. A further assumption is then made that *no change within the set of investigated subjects occurs during the study period* except the changes due to treatment. This is not true for cancers, which are known to evolve through continuously accumulating additional genomic alterations through mutations. Consequently, even if randomization was performed at baseline, the randomization effect is lost in any repeated evaluation during subsequent phases of such trials (11).

Single patient trial designs or "$N = 1$" trials (12) are an alternative to population-based clinical trials, but a broad clinical application of this approach is hindered by the absence of a standardized work-up. Current practices are based on physician-specific or institution-enabled assessments of the biological characteristics of the patient and of the cancer tissue. This usually occurs in the form of a multidisciplinary institutional expert consensus referred to as "tumor boards" (13). This personalized treatment approach allows for consideration of disease heterogeneity as well as of time-dependent variations. This *clinical plasticity*, allows for treatment to be modified at various phases of the patient's journey based on disease course or on the patient's pharmacometabolic capacity to tolerate the selected treatment. The much-needed standardization of the pre-treatment workup of a patient selected to undergo personalized therapy would enable collection of outcomes from these "$N = 1$" trials in pediatric cancer across many institutions, enable statistical analysis, and provide evidence for changing therapeutic paradigms.

Another issue arising in rare diseases, and therefore personalized pediatric oncology, is the identification of *future target population likely to benefit from a trial result*—the so called "patient horizon" (14). Patient horizon is either the number of patients in the trial, or the number who have the condition under treatment. This well-known concept is rarely utilized. To improve understanding of this concept let us take an extreme situation where all patients from the target population were randomized in 1:1 ratio for effective and ineffective treatment. In this case half of the patients are forced to receive an ineffective treatment as a price for knowing the absolute truth about the relative treatment efficacy between the two treatments. Yet, the same result could be obtained by giving either of the treatment randomly without any knowledge.

An optimal size of a trial balances both extremes and maximizes the number of patients who benefit. The exact number of patients may not be known, but the order of magnitude of the optimal number can be calculated using *the square root of the patient horizon size* for a simple trial design. For example, for a finite population of 1,000 subjects, the optimal size of a trial is a few tenths. Considering disease rarity, especially in the era of molecular medicine, the issue of the target population size (the patient horizon) becomes relevant not in pediatric oncology, but in medicine in general (14).

ISSUES TO BE ADDRESSED

There are two principal issues to be addressed in current cancer medicine pertaining to:

(i) Regulatory mechanisms of drug approval and market authorization.
(ii) Evaluation of real-life clinical efficacy.

Regulatory Considerations

A newly proposed drug approval marketing authorization pathway shall require an initial "Candidate Medicinal Product Safety Evaluation" (CMPSE, currently Phase I) and subsequent "Dose Defining Study" (DDS, currently Phase II). As we explained above a current medicinal product approval pathway is mechanistically "drug-centric" as the present practice relies on the ability of a Phase III clinical trial to provide evidence that the addition of a single compound to a standard treatment regimen is of clinical benefit *leading to marketing authorization*. This approach has become so biased that most resulting Phase III registration trial data do not provide clinically meaningful benefit (3); *on top of that, testing for "me-too" drugs toward endpoints as "substantial equivalence or non-inferiority" is vastly contributing*. Furthermore, it disregards the clinical need for different pathways for approval of

medicines intended for use (A) in the entire world population (e.g., vaccines, antipyretics, pain killers, etc.) and for those intended for (B) specific subpopulations (e.g., LDL-C marker based treatments). In the latter setting, clinical laboratory diagnostics (CDx) are used as a guide or companion to a medicinal product to determine its applicability to a subject. A regulatory approval of medications targeting (C) somatic mutations, and/or (D) diseases that follow Mendelian inheritance or germline mutation (e.g., tyrosinemia type I. and the drug nitisinone) requires a special approval pathway and expedited translation to clinical practice. Summing up from a regulatory point of view, the testing phases CMPSE Phase I + DDS Phase II would allow for *conditional medicinal product (pre)approval*.

Real-life clinical practice-based evaluation should then focus on designing "patient-centric" treatment strategies. Considering there are about 300 active drugs in oncology, and the number of 2 drugs combinations is about 45,000, or 4.4 million combinations for 3 drug combinations, Phase I testing for all these drug combinations is neither feasible nor realistic. New models such as: (i) identification of smaller pediatric cancer patient cohorts likely to benefit from a specific treatment because they have the relevant gene alteration(s), or (ii) the increasing use of multilayer profiling (markers) to diagnose, classify and monitor response in pediatric cancers (Fedorova et al.; Polaskova et al.) are therefore gaining in popularity. There is a need to validate combination treatment strategies, not just individual drugs or individual biomarkers. Attention should be directed at studying drug dosing in respective preclinical models and at identifying optimal biological dose rather than persist with the present maximum-tolerated dose. With most targeted agents, a target occupancy dose, i.e., dose required to stop/minimize pathway phosphorylation and RP2D /dose used in clinical setting (15) is the more appropriate identifier of a clinically relevant dose. As noted in many pre-clinical studies, combinations of targeted agents are often synergistic, and potentiate the effects of chemotherapy. A very good example of how combination therapy dosing can negatively influence the overall success of an innovative drug is the Mylotarg (gemtuzumab ozogamicin, alias GO) story. *Gemtuzumab ozogamicin is a recombinant humanized IgG4 kappa antibody that is used to treat CD33 positive AML. It is conjugated with calicheamicin derivative, a cytotoxic antitumor antibiotic. The drug was initially tested in a randomized controlled trial leading to FDA approval via accelerated review in May 2000. However, the drug had intolerable toxicity and mortality at the 9 mg/m^2 dose, and was voluntarily withdrawn from the market on 15th October 2010. It was subsequently tested at a much lower drug dose (3 mg/m^2 instead of 9 mg/m^2) and was shown to be just as effective with greatly improved safety profile. GO was therefore re-approved by the FDA on 1st September 2017 at lower dose* (16). Taken together, if a new compound allowed to enter the real-life clinical practice-based evaluation (i.e., CMPSE + DDS passed) brings clinically meaningful benefit, this will lead to the full marketing authorization and consequently, reimbursement of such a novel compound.

The use of chemotherapy in combination with a targeted biological agent is a commonly employed approach for enhancing the ability of chemotherapy to fight cancer. Commonly, the assumption that the inhibitory effect of the biological agent would be additive to the effect achieved by traditional chemotherapy or radiation is made. However, because of the synergistic action, the addition of a targeted biologic agent to a maximum tolerated dose (MTD) of chemotherapy, may make an already maximally toxic regimen almost lethal. In most cases, any benefit of tumor response ends up being concealed by unacceptable toxicities, and no overall survival benefit is seen. Yet, because the present design of clinical trials permits modification of only one variable between the two study arms, the dose of chemotherapy in the experimental treatment arm is rarely modified. The use of metronomic chemotherapy, with its goal of long-term "tumor control," lower toxicity, and prevention of tumor progression (rather than immediate reduction in tumor size), may represent a more realistic strategy for testing targeted and immune therapies as add on to chemotherapy (13). However, because this low toxicity regimen can have a delayed onset of radiologically visible effect, it is often abandoned too early for a patient to benefit. An example of how biomarker assessment can help document the effects of targeted therapy earlier than it could be documented radiologically is provided in this issue (Polaskova et al.) discussing three patients with multiply relapsed Burkitt lymphoma treated with personalized therapy and their response being monitored using target phosphorylation.

In summary, data for real-life evidence-based medicine addressing patient-focused clinical efficacy can be derived from time-dependent single-case designs. The new comprehensive efficacy evaluation model we present here, should be focused on treatment strategies using drug combinations rather than testing a single-compound within a randomized setting. We should modify the Phase III wherever feasible. The drug approval pathway should consist of "Candidate Medicinal Product Safety Evaluation" (previously Phase I) and "Dose Defining Study" (previously Phase II). This will bypass the often futile end-of-life enrollments in single drug clinical trials and bring about substantial cost reductions in development and implementation of new medicinal anticancer compounds to the market.

AUTHOR CONTRIBUTIONS

All authors listed have made a substantial, direct and intellectual contribution to the work, and approved it for publication.

ACKNOWLEDGMENTS

LM2018125, AZV MZCR 16-33209A, 16-34083A, LQ1605, LO1604, LO1413, and LQ1601 projects from the National Program of Sustainability II (MEYS).

REFERENCES

1. Liu K, Meng XL. There is individualized treatment. Why not individualized inference? *Annu Rev Stat Its Appl.* (2016) 3:79–111. doi: 10.1146/annurev-statistics-010814-020310
2. Roden DM, McLeod HL, Relling MV, Williams MS, Mensah GA, Peterson JF, et al. Pharmacogenomics. *Lancet.* (2019) 394:521–32. doi: 10.1016/S0140-6736(19)31276-0
3. Davis C, Naci H, Gurpinar E, Poplavska E, Pinto A, Aggarwal A. Availability of evidence of benefits on overall survival and quality of life of cancer drugs approved by European Medicines Agency: retrospective cohort study of drug approvals 2009-13. *BMJ.* (2017) 359:j4530. doi: 10.1136/bmj.j4530
4. *New Studies Question Whether Novel Anti-Cancer Drugs Are Worth Their Extra Cost [ESMO 2019 Press Release]*. (2019). Available online at: https://www.esmo.org/Press-Office/Press-Releases/ESMO-Congress-anticancer-drugs-cost-Marino-Vokinger (accessed January 9, 2020).
5. Allison KH, Sledge GW. Heterogeneity and cancer. *Oncology.* (2014) 28:2–3.
6. Yoshioka A. Use of randomisation in the Medical Research Council's clinical trial of streptomycin in pulmonary tuberculosis in the 1940s. *BMJ.* (1998) 317:1220–3. doi: 10.1136/bmj.317.7167.1220
7. Bartholomew M. James Lind's treatise of the scurvy (1753). *Postgrad Med J.* (2002) 78:695–96. doi: 10.1136/pmj.78.925.695
8. Lachin JM. Properties of simple randomization in clinical trials. *Control Clin Trials.* (1988) 9:312–26. doi: 10.1016/0197-2456(88)90046-3
9. Demlova R, Zdrazilova-Dubska L, Sterba J, Stanta G, Valik D. Host-dependent variables: The missing link to personalized medicine. *Eur J Surg Oncol.* (2018) 44:1289–94. doi: 10.1016/j.ejso.2018.04.014
10. Chen R, Mias GI, Li-Pook-Than J, Jiang L, Lam HYK, Chen R, et al. Personal omics profiling reveals dynamic molecular and medical phenotypes. *Cell.* (2012) 148:1293–307. doi: 10.1016/j.cell.2012.02.009
11. Lindsey JK, Lambert P. On the appropriateness of marginal models for repeated measurements in clinical trials. *Stat Med.* (1998) 17:447–69. doi: 10.1002/(SICI)1097-0258(19980228)17:4<447::AID-SIM752>3.0.CO;2-G
12. Nikles J, Mitchell G. N-of-1 trials in medical contexts. In: Nikles J, Mitchell G, editors. *The Essential Guide to N-of-1 Trials in Health*. Dordrecht: Springer Netherlands (2015). p. 43–55. doi: 10.1007/978-94-017-7200-6
13. Klement GL, Arkun K, Valik D, Roffidal T, Hashemi A, Klement C, et al. Future paradigms for precision oncology. *Oncotarget.* (2016) 7:46813–31. doi: 10.18632/oncotarget.9488
14. Stallard N, Miller F, Day S, Hee SW, Madan J, Zohar S, et al. Determination of the optimal sample size for a clinical trial accounting for the population size. *Biometrical J.* (2017) 59:609–25. doi: 10.1002/bimj.201500228
15. Le Tourneau C, Gan HK, Razak ARA, Paoletti X. Efficiency of new dose escalation designs in dose-finding phase I trials of molecularly targeted agents. *PLoS ONE.* (2012) 7:e51039. doi: 10.1371/journal.pone.0051039
16. Umukoro C. *A Start, Stop, GO Story in AML – Gemtuzumab Ozogamicin (Mylotarg®)*. (2017) Available online at: https://amlglobalportal.com/medical-information/a-start-stop-go-story-in-aml-gemtuzumab-ozogamicin-mylotarg (accessed January 9, 2020).

Conflict of Interest: The authors declare that the research was conducted in the absence of any commercial or financial relationships that could be construed as a potential conflict of interest.

frontiers in Oncology

ORIGINAL RESEARCH
published: 17 July 2019
doi: 10.3389/fonc.2019.00644

Individualization of Treatment Improves the Survival of Children With High-Risk Solid Tumors: Comparative Patient Series Analysis in a Real-Life Scenario

Michal Kyr[1,2], Kristyna Polaskova[1,2], Zuzana Kuttnerova[1,2], Tomas Merta[1,2], Jakub Neradil[1,2,3], Jitka Berkovcova[4], Ondrej Horky[4], Marta Jezova[5], Renata Veselska[1,2,3], Giannoula Lakka Klement[1,6], Dalibor Valik[7] and Jaroslav Sterba[1,2]*

[1] Department of Pediatric Oncology, University Hospital Brno and School of Medicine, Masaryk University, Brno, Czechia, [2] International Clinical Research Centre, St. Anne's University Hospital Brno, Brno, Czechia, [3] Laboratory of Tumor Biology, Department of Experimental Biology, School of Science, Masaryk University, Brno, Czechia, [4] Laboratory of Molecular Pathology, Department of Oncological Pathology, Masaryk Memorial Cancer Institute, Brno, Czechia, [5] Department of Pathology, University Hospital Brno and School of Medicine, Masaryk University, Brno, Czechia, [6] CSTS Health Care Inc., Toronto, ON, Canada, [7] Department of Laboratory Medicine, Masaryk Memorial Cancer Institute, Brno, Czechia

Introduction: The individualization of treatment is attractive, especially in children with high-risk cancer. In such a rare and very heterogeneous group of diseases, large population-based clinical randomized trials are not feasible without international collaboration. We therefore propose comparative patient series analysis in a real-life scenario.

Methods: Open cohort observational study, comparative analysis. Seventy patients with high-risk solid tumors diagnosed between 2003 and 2015 and in whom the treatment was individualized either empirically or based on biomarkers were analyzed. The heterogeneity of the cohort and repeated measurements were advantageously utilized to increase effective sample size using appropriate statistical tools.

Results: We demonstrated a beneficial effect of empirically given low-dose metronomic chemotherapy (HR 0.46 for relapses, $p = 0.017$) as well as various repurposed or targeted agents (HR 0.15 for deaths, $p = 0.004$) in a real-life scenario. However, targeted agents given on the basis of limited biological information were not beneficial.

Conclusions: Comparative patient series analysis provides institutional-level evidence for treatment individualization in high-risk pediatric malignancies. Our findings emphasize the need for a comprehensive, multi omics assessment of the tumor and the host as well whenever molecularly driven targeted therapies are being considered.

OPEN ACCESS

Edited by:
Wafik S. El-Deiry, Alpert Medical School, Brown University, United States

Reviewed by:
Ken Lieuw, Walter Reed National Military Medical Center, United States
AeRang Kim, Children's National Health System, United States

***Correspondence:**
Michal Kyr
kyr.michal2@fnbrno.cz

Specialty section:
This article was submitted to Cancer Molecular Targets and Therapeutics, a section of the journal Frontiers in Oncology

Received: *14 March 2019*
Accepted: *01 July 2019*
Published: *17 July 2019*

Citation:
Kyr M, Polaskova K, Kuttnerova Z, Merta T, Neradil J, Berkovcova J, Horky O, Jezova M, Veselska R, Klement GL, Valik D and Sterba J (2019) Individualization of Treatment Improves the Survival of Children With High-Risk Solid Tumors: Comparative Patient Series Analysis in a Real-Life Scenario. Front. Oncol. 9:644. doi: 10.3389/fonc.2019.00644

Low-dose metronomic chemotherapy or local control of the disease may be a more rational option in situations where targeted treatment cannot be justified by robust evidence and comprehensive biological information. "Targeted drugs" may be given empirically with a realistic benefit expectation when based on robust rationale.

Keywords: cancer, children, personalized medicine, targeted therapy, comparative effectiveness research, clinical trials, metronomic

INTRODUCTION

The success rate of cancer treatment in children has increased substantially in the past three decades (1). Despite progress, there are high-risk groups of children with cancer who do not respond to standard (maximum tolerated dose-based, MTD) treatments and continue to have poor outcomes. For this subset of patients with poor outcomes, the individualization of treatment is an emerging strategy. Such individualization may be understood as using not only targeted agents but also metronomic chemotherapies given beyond standard treatment options, if any, due to the specifically poor prognosis. This meaning of individualization i.e., customization of treatment beyond standard treatment using metronomic chemotherapy, repurposed, or targeted agents, is used throughout this paper. These approaches are well-described and employed in clinical practice (2–4).

Personalized treatment is a well-established concept aimed at optimizing patient therapy on the basis of the tumor and patient-specific biological profile. Pediatric malignancies are rare diseases in which specific alterations make personalization of therapy amenable. Classical population-based randomized clinical trials (RCT), considered a gold standard for evidence-based medicine, are incompatible with personalization of treatment for children with cancer. There is a need for the modernization of clinical trial methodologies, particularly the speed of the clinical trial process, and innovative designs (5, 6).

The aim of this study was to evaluate the efficacy of various individualized treatment approaches given either empirically or guided by biological information and to present an application of complex analytical solutions. High-risk malignancies in children form rare entities, which creates challenges in the evaluation of such small samples (7). Individualized alternatives to population-based clinical trials are the n-of-1 trials. Unfortunately, the use of the classical n-of-1 approach is not suitable in most pediatric patients with high-risk malignancies. We therefore suggest combining classical population-based and n-of-1 trials to form a series of n-of-1 trials. Existing statistical methodology enables handling specific statistical issues arising in such design. We present an application of such analytical tools, specifically extended Cox, frailty, and joint models, on a cohort of patients on individualized treatment. These tools are able to address repeated events, time varying covariates, known and unknown heterogeneity, and informative censoring problems, all of which are inherent to the individualized treatment settings. The key idea of increasing effective statistical power lies in combining rare entities to gather a larger heterogeneous sample, utilizing repeated measurements and appropriately addressing these factors in statistical analysis. This analysis was performed in a pragmatic real-life scenario that addresses more relevant clinical questions (6, 8). Comparative effectiveness research (9, 10) is an established concept and pragmatic observational studies render patient-centered real-life results that cannot be obtained through classical RCTs.

METHODS

Sample Population

Children with relapsed and/or high-risk solid tumors for whom specific individualized treatment was recommended and who signed (or whose legal guardians signed) an informed consent were retrospectively or in a prospective manner enrolled in the data registry. Disease was defined as high-risk if the expected 5-years survival rate on standard therapies was <25%. Institutional review board approval for the study was obtained. Patients from the Pediatric Oncology Department, University Hospital Brno diagnosed between 2003 and 2015, and treated using individualized treatment strategy were analyzed. The retrospective cohort enrolled 11 patients treated until 2012 and 59 patients treated in 2013 and beyond constituted the prospective cohort.

Treatment Assignment

Patients included in this cohort received standard first and/or subsequent lines of treatment regimens, if available, and individualized treatment. Altogether, the standard treatment regimens used MTD-based chemotherapy, surgery and/or radiation and originated from international pediatric oncology collaborative study groups. When standard treatment options were depleted or due to the high-risk nature of the disease, patients received individually assembled treatment consisting of metronomic chemotherapy, repurposed drugs and/or targeted agents such as antibodies or signal pathway inhibitors. At various time points of the treatment, a patient may have received molecular board consultation utilizing clinical and tumor biological data based on which a customized recommendation for specific targeted treatment was adopted. Thus, one can recognize the empirical period in which the treatments were given without knowledge based on biological studies, and the personalized (or targeted) period in which the tumor tissue studies opened the possibility to use a specific drug. Not all the drugs given in the targeted period needed to be given based on biological guidance (e.g., concomitant metronomic chemotherapy). Similarly, the selected targeted drugs did not need to be given during the whole targeted period, and even agents usually used as targeted could be given empirically (e.g.,

based on published data) in either of the periods. Thus, any of the drugs could be used in either of the period also as comedication, continuing medication from one period to the other, etc. It is necessary to understand that there were no protocol guidelines that would manage the choice of the treatment, time of its commencement or duration. Decision-making took place on daily clinical practice. Such a practice-based approach with intertwining treatments makes the perception of the design difficult compared to, e.g., simple two-arm-single-agent trial design. The simplification of our concept can be imagined as the patient timeline during which treatments were given to the patient based on best clinical judgement and, from a certain point, i.e., the tumor board consultation, the judgement could have been influenced by new biological information. Since that time, the targeted period has been considered.

In the absence of guidelines or protocols for individualized treatment strategies, the recommendations were based on best clinical practice arising from experienced clinical judgment, in-house protocols, published knowledge from either preclinical and/or clinical studies and biological studies comprising immunohistochemistry, TruSight Tumor 26 panel (Illumina Inc., San Diego, California, USA) for DNA level gene alterations and/or the phosphorylation profile of selected kinases and other signaling molecules (Human Phospho-RTK Array kit and Human Phospho-MAPK Array kit; R&D Systems, Minneapolis, MN, USA), if available. Modifications or new recommendations may have been made repeatedly for the same patient when toxicity, new clinical events, or new important information became available. Combinations of several drugs were used at the discretion of the attending oncologist or based on the consensus of molecular tumor board recommendation, which was in line with the philosophy of a multiple-hit strategy (3). In a number of cases, patients may have also received surgery or radiation with curative or palliative intend as a part of standard and/or individualized treatment.

The following treatment approaches were evaluated: (i) METRO—low-dose metronomically administered chemotherapeutics (Azacitidin, Cyclophosphamide, Etoposide, Methotrexate, Paclitaxel, Temozolomide, Vinblastine, Vinorelbin) (ii) REPUR—repurposed drugs (Arsen trioxide, Tretinoin, Isotretinoin, Celecoxib, Fenofibrate, Fluvastatin, Metformin, Miltefostin, Propranolol, Thalidomide, Valproate) (iii) INHIB—tyrosine kinase inhibitors, mTOR inhibitors, or monoclonal antibodies (Axitinib, Bevacizumab, Cabozatinib, Denosumab, Erlotinib, Ibrutinib, Idelalisib, Ipilimumab, Nimotuzumab, Nivolumab, Obinutuzumab, Pazopanib, Pembrolizumab, Regorafenib, Sirolimus, Sorafenib, Sunitinib, Temsirolimus, Trametinib, Vemurafenib) (iv) SURG/RT—local interventions, such as surgery with at least partial resection and local radiation.

There was no explicit control group. Each treatment approach was compared to the rest of the sample, which did not comprise the evaluated treatment. It is essential to realize that the smallest unit to be processed by the models is not the whole patient but the patient-day unit due to the time-varying covariates. Therefore, even when all patients received any of the evaluated treatment during some part of their disease history, there were also periods (i.e., patient-days) without any such treatment at all in each of the patients. Specifically, periods with an evaluated treatment approach were compared to periods without a particular treatment approach. By the nature of the design, these control periods comprised periods with different treatment approaches other than the evaluated periods, periods without any of the evaluated treatments and the control periods came from both different (between-) and the same (within-comparison) patients. Thus, these periods formed a control background to which each evaluated treatment approach was compared. The control background was not exactly the same for each evaluated treatment. We hypothesized that the differences between control backgrounds were negligible compared to effects due to specific treatment that was evaluated due to random heterogeneity in the sample. This assumption was checked by comparing the control backgrounds.

TABLE 1 | Specification of survival models.

Variance corrected models	
Wei, Lin, and Weissfeld (WLW)	$h_{ik}(t) = h_{0k}(t)\, e^{x_{ik}\beta}$
Prentice, Williams, and Peterson (PWP)	$h_{ik}(t) = h_{0k}(t)\, e^{x_{ik}\beta}$
Andersen and Gill (AG)	$h_{ik}(t) = h_{0}(t)\, e^{x_{ik}\beta}$
Frailty models	
Conditional frailty	$h_{ik}(t) = u_i h_{0k}(t)\, e^{x_{ik}\beta}$
Shared frailty	$h_{ik}(t) = u_i h_{0}(t)\, e^{x_{ik}\beta}$
General joint model	
Recurrent event	$\left\{ r_{ik}(t) = u_i r_0(t)\, e^{x_{Rik}\beta_R} \right.$
Terminal event	$\left. \lambda_i(t) = u_i^{\alpha} \lambda_0(t)\, e^{x_{Ti}\beta_T} \right\}$

Where variance of u_i *var*$(u_i) = \theta$.

Statistical Methodology

Detailed parameterized data were recorded in a relational SQL-based database allowing for time-varying covariate data structure and enabling data retrieval in a format needed for creating risk sets based on specific survival models.

The effects of different treatment strategies in patients treated with individualized therapeutic approaches were evaluated using various extensions of Cox models (variance corrected or frailty models) or joint models to account for time varying treatments, repeated data, subject heterogeneity, event dependence, and informative censoring. A detailed explanation of all models used is given elsewhere (11–18). We encourage readers to review a brief summary of the method used, which is available in the **Supplementary Material**, to better appreciate the methodical background for interpretation. Specifications of the models used are given in **Table 1**. Treatment approaches were analyzed in multivariate models and adjusted for possible bias.

The events of interest were progressions or relapses, evaluated by common RECIST criteria, deaths, or a combined measure of event-free survival (EFS) depending on a specific model. Analyses were performed using R Core Team software (19) version 3.3.3, coxph (20) and frailtyPenal (21–23) functions.

Sample Size Justification

This study was a registry-based analysis where treatment allocations were not randomized and were not blinded to investigators as they followed the best clinical practice and best

TABLE 2 | Sample characteristics.

	Event rank 1 (baseline)	Event rank 2	Event rank 3*
	n = 70	*n* = 44	*n* = 17
Diagnoses, No. patients			
Soft tissue and other extraosseous sarcomas	24	16	4
CNS and miscellaneous intracranial and intraspinal neoplasms	22	12	4
Malignant bone tumors	9	8	5
Neuroblastoma and other peripheral nervous cell tumors	8	2	0
Hepatic tumors	3	2	0
Malignant melanomas	2	2	2
Lymphomas and reticuloendothelial neoplasms	1	1	1
Renal tumors	1	1	1
Demographics			
M/F, *N*	36/34	22/22	7/10
Age; mean ± *SD*, years	7.2 ± 5.6	7.5 ± 5.7	7.6 ± 4.7
Personalized (biologically guided) approach, N	17	24	9
Treatment approaches (empirical/targeted period), *N*			
METRO	35/15	13/15	5/7
REPUR	20/10	9/11	6/7
INHIB	25/15	13/19	7/7
SURG/RT	57/14	16/11	6/7
Events, *N* (%)			
Progression/relapses	46 (66%)	16 (36%)	5 (30%)
Deaths	4 (6%)	13 (30%)	3 (18%)
Overall survival; median, years		7.2	
Follow-up; median (min—max), months		26 (2–141)	

**Comprises 4 patients with a fourth event.*

patient interest, thus, no sample size analysis was performed in advance. We considered a rule of thumb of at least 10 events per variable (24) for the classical Cox model to be valid when building our models. Although we consider the commonly accepted significance level $\alpha = 5\%$ for interpretation of our results we may also consider the trends and effects of clinical relevance.

RESULTS

A total of 70 patients (36 males and 34 females, mean age 7.2 ± 5.6 years) were enrolled in the analysis. Sample characteristics are summarized in **Table 2**. Patients on the individualized treatment approach were followed for a median of 26 months. During this time, the patients experienced 67 recurrent events in total (relapses or progressions) and 20 terminal events (deaths). A biologically guided (personalized) approach was applied in 36 patients. A substantially lower number of patients was available for the evaluation of each subsequent event. The third event group comprised four patients with even a fourth event. Individual treatment schedules are schematically given in **Figure 1**. **Figure 2** illustrates the drug combinations. These figures are intended to roughly illustrate the complexity of the treatment. **Figure 3** shows the findings of the biological examination of tumor tissues and specific targeted drugs selected in patients for whom the targeted management was applied. Other concomitant treatments given to these patients are not indicated in this scheme.

Overall Kaplan-Meier curves for recurrent and terminal events were calculated as interevent (or gap) times and are given in **Figure 4A**. An overall survival curve (OS) calculated as the total time elapsed from an initial diagnosis was also plotted for comparison. All three recurrent events seem close to each other suggesting no major differences in survival times. On the other hand, there is improvement indicated in time to death beyond surviving a second year compared to previous events. The overall median survival time from the initial diagnosis was 7.2 years.

Effects estimates of bias-adjusted models are displayed in **Figures 4B–D**. The only strong observed covariate (rendering bias if omitted) associated with outcome was calendar time, which is not surprising due to the long study period covered. Therefore, we adjusted all models for this covariate. **Figure 4B** shows the model results, where treatment effects were modeled and shown separately for the empirical and the personalized period and represents a pragmatic view. It is obvious that treatments were more effective when given during the empirical period. Most beneficial effects on EFS were metronomically given low-dose classical chemotherapeutics. No obvious treatment benefit was noted in the personalized period for either of the treatments. Local treatment was shown to be beneficial for prolonging survival during the terminal event, which could be identified only using joint models.

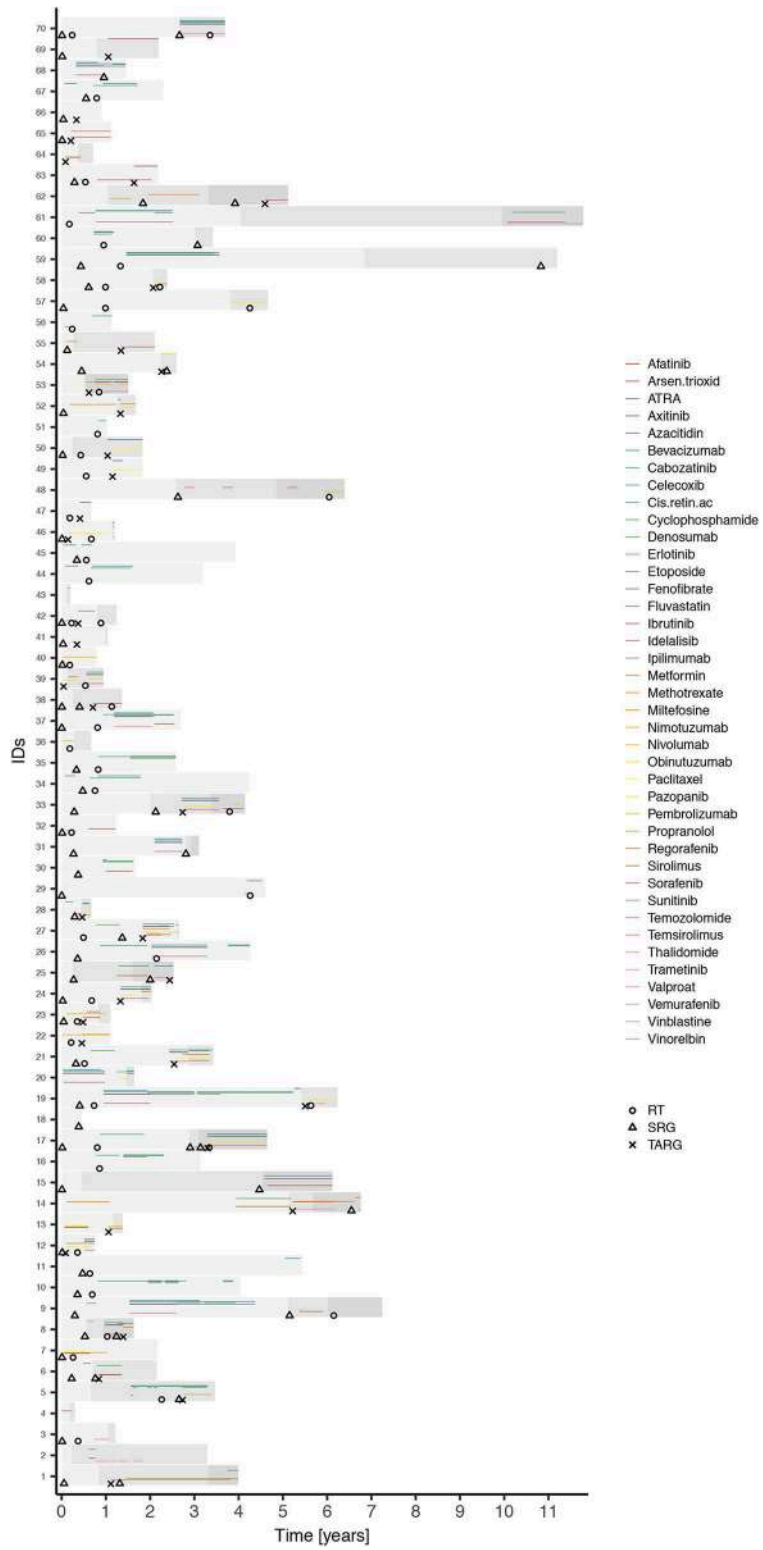

FIGURE 1 | Schematic overview of individual treatment plans. Figure schematically shows the treatment plans of individual patients. Three shades of gray bars represent periods to the first, second, and third event, respectively, within a patient. Circles, triangles, and crosses indicate irradiation (RT), surgery (SRG), and biologically guided approach commencement (TARG), respectively. Rainbow-like set of active agents is presented to illustrate the complexity of treatment plans in patients with individualized therapeutic approaches. Multiple combinations of different drugs commencing at different time points and changing within an individual patient create unique cases rather than similar groups.

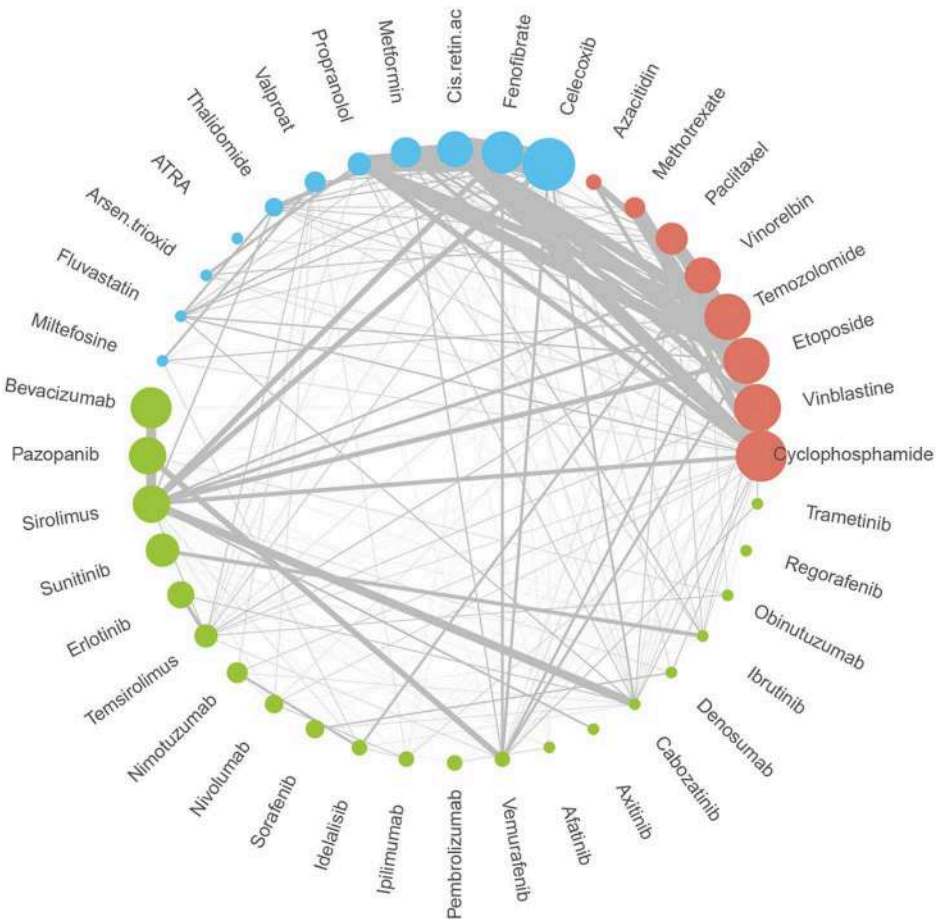

FIGURE 2 | Drugs and combinations utilized during individualized treatment. Circle size is proportional to the number of patients receiving the drug during any phase of the treatment. Line thickness is proportional to patient-days using a specific combination of a drug in the sample during the treatment.

The models shown in **Figure 4C** were adjusted for empirical/personalized periods, and the estimates represent pooled quasi-randomized treatment effects. Based on this analysis, we can see that all three drug groups are beneficial, with the most evident effect on EFS for metronomically given low dose chemotherapeutics. Repurposed drug or inhibitor effects on EFS were close to significance border. On the other hand, the results showed a significant and strong beneficial effect on overall survival during the terminal event. The beneficial effect of local treatment was noted only with respect to overall survival without affecting EFS or recurrences.

Figure 4D shows estimates of the personalized approach itself, i.e., effect of potentially guiding biological information, showing no benefit on EFS.

Finally, we evaluated all treatment strategies in multivariate models. The final models generated are given in **Table 3**. A conditional frailty model for combined outcome (EFS) was used as the most appropriate. Metronomically given low-dose chemotherapy was the only significantly beneficial treatment that halved the risk (HR 0.45, $p = 0.005$) with respect to EFS. To evaluate jointly modeled relapses and deaths, general frailty model was used. Metronomically given chemotherapy remained the only significantly beneficial effect on relapses (HR 0.46, $p = 0.017$) in this model. However, repurposed drugs or inhibitors/antibodies significantly improved survival (HR 0.15, $p = 0.004$) during the terminal event (death) and the local treatment (HR 0.16, $p = 0.001$) also improved survival during the terminal event. Notably, the size of the metronomic treatment effect on deaths was similar to that on EFS or relapses but did not reach conventional statistical significance because the number of deaths was markedly lower than the number of repeated events. This effect is also evident from wide confidence limits in **Figures 4B–D** for that particular model (general joint frailty model).

DISCUSSION

The evaluation of individualized therapies in children with high-risk cancer is difficult when using traditional approaches, such as large single-agent/approach RCTs. No matter how grateful we are for such clear evidence of treatment benefit, performing RCTs require international collaboration, and is redeemed by a time-consuming process. Based on recent experience, it may take 12 years to yield a single conclusion (25). In most pediatric cancer cases, traditional large population-based approaches may

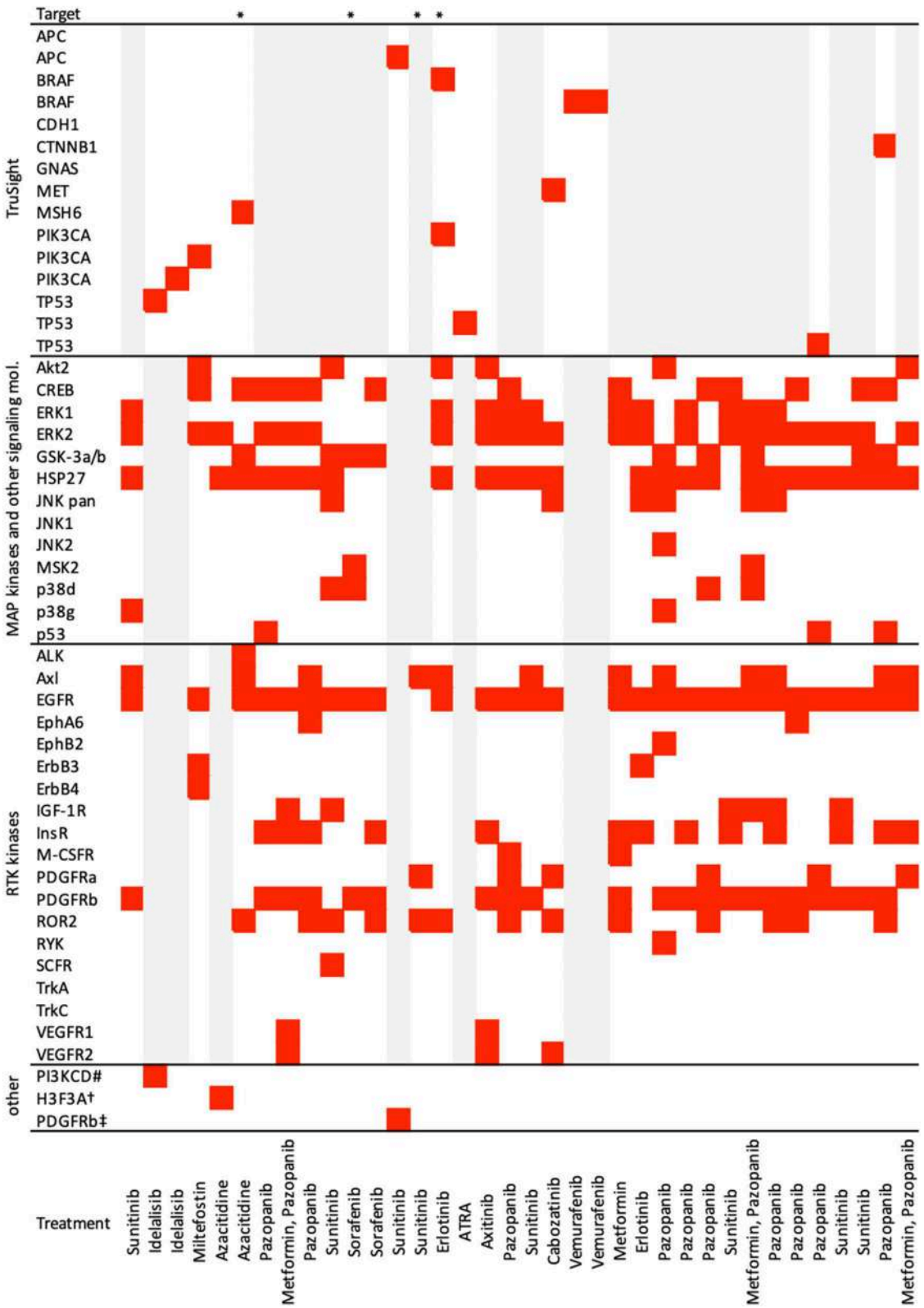

FIGURE 3 | Results of biological examinations and treatment summary. Figure shows findings of biological tissue examination and drugs selected in patients on targeted (TARG) management. Other concomitant medications are not indicated here. *Treatment classified as targeted retrospectively, sensitivity analysis performed; #germinal mutation, c.935C>G, Sanger seq.; †c.83A>T/p.K28M, Whole exome sequencing; ‡immunohistochemistry; gray bars—not done.

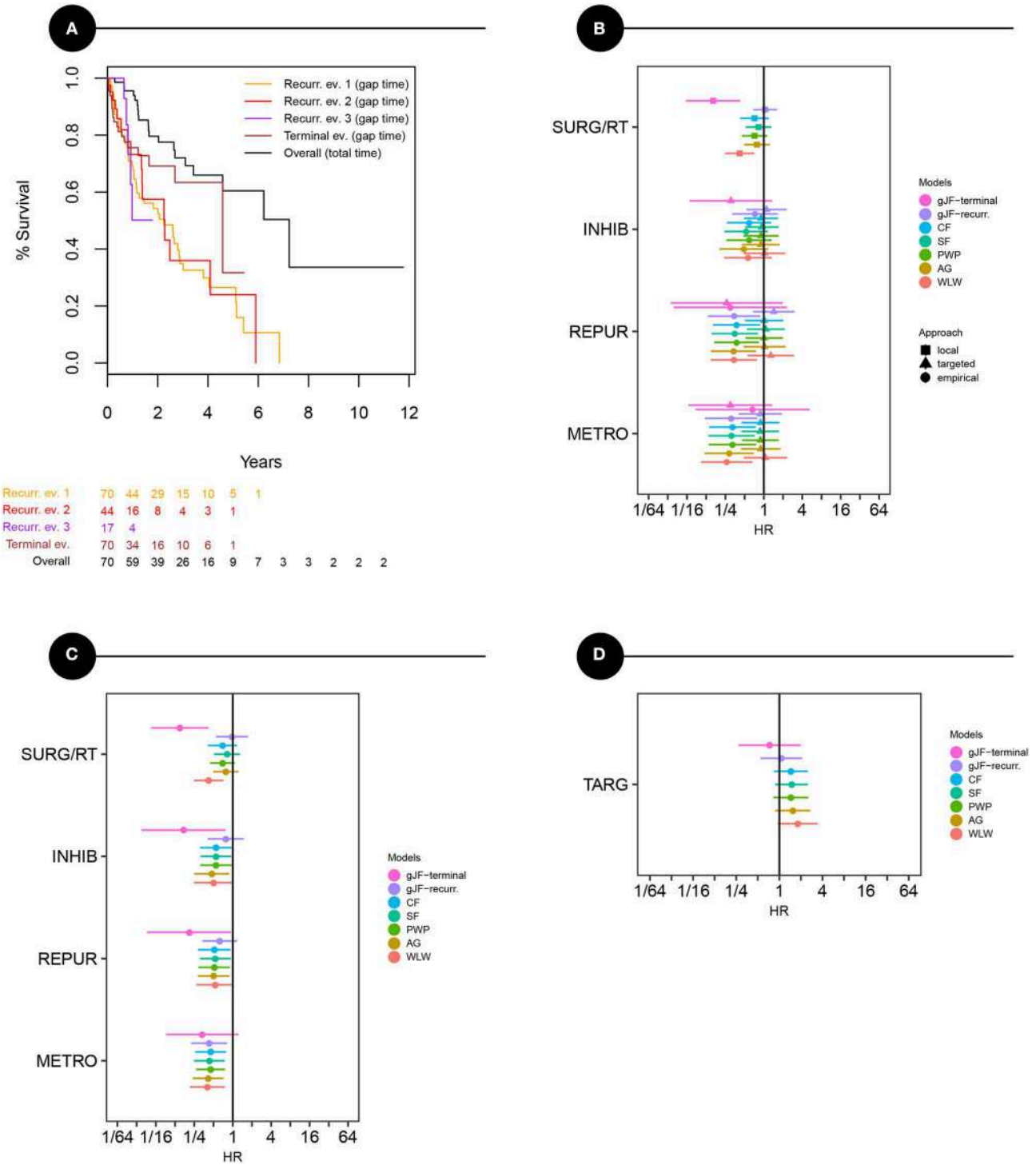

FIGURE 4 | Survival models of specific events and treatment effect estimates overview. **(A)** Kaplan-Maier curves representing survival times for each recurrent event (yellow, red, purple lines) and terminal event (brown line) as interevent (gap) times, and overall survival curve (black). **(B–D)** Effects estimates and confidence limits of different treatment modalities in bias-adjusted models: **(B)** pragmatic view representing raw effects of treatment groups separately in targeted and non-targeted period, **(C)** conditional, quasi-randomized view (adjusted for targeted/non-targeted period) representing a pooled treatment effects across periods, **(D)** effect of targeted (biologically guided) management itself. Models: marginal – Wei, Lin, and Weissfeld, AG – Andersen and Gill, PWP-GT – Prentice, Williams, and Peterson model in gap time, SF – shared frailty, CF – conditional frailty, gJF – general joint frailty model with effect for recurrent (recur) and terminal (term) event. METRO – metronomically given low-dose chemotherapeutics, REPUR – repurposed drugs, INHIB – signal pathway inhibitors/mTOR inhibitors/antibodies, SURG/RT – local treatment (surgery and/or irradiation). To the left from the midline favors treatment (survival improvement).

not be possible at all and contradict the driving philosophy of personalized medicine. Lindsey and Lambert wrote an excellent examination of the marginal (population-based) vs. conditional (patient-centered) inferences (26) which may help understand the limitations of classical population-based trials.

This was a pragmatic observational study dealing with real-world data, where various aspects of the complex data were addressed using appropriate statistical tools. These techniques have already been described long ago and applied in various research areas outside medicine (14). As shown in simulation studies (15, 27) for situations where event dependence and heterogeneity arise simultaneously from the same data, the conditional frailty model appears to be the most appropriate. However, in our study, we could not observe any substantial difference in treatment effects for conditional frailty models. This finding suggests that unmeasured heterogeneity between patients or event order did not substantially affect our models. Nevertheless, we still recommend using stratified and/or frailty models, at least as a part of the analysis process because it might become an important factor with different data and, more importantly, these models enable conditional (patient-centered) inferences. In general, similar effects were observed using different Cox-extension models or frailty models. The joint frailty models, however, showed different effects for recurrent and terminal events, as was obvious for repurposed drugs and inhibitors as well as local treatments. Such a fact, if ignored in conventional analysis, might lead to incorrect conclusions.

A similar EFS curve found for different ranks of events (**Figure 4A**) is an interesting finding. This suggests that regardless of the treatment strategy selected in the individualized scenario, the times to subsequent events were roughly similar without shortened survival that would be normally anticipated in the course of progressive malignant disease. This similar event-rank risk may also explain the small importance of rank stratification in the models in our data.

The efficacy of metronomically given low-dose chemotherapy, particularly cyclophosphamide, or vinblastine, has already been described (28–30). Here, we were able to identify their favorable effects in a customized observational pragmatic setting. A number of mechanisms of action are considered responsible for the efficacy of metronomic therapies. Antineoplastic, immunomodulatory, antiangiogenic, and tumor microenvironmental activity are reported most often (2).

Our results suggest similar effects of repurposed drugs and various signal pathway inhibitors or antibodies. Their beneficial effect on overall survival during the last (terminal) event was evident while we could not conclude that for recurrences. This results suggests that patients may live longer even though the disease itself does not regress when evaluated using conventional imaging studies and RECIST criteria. These observations are also complemented by our clinical experience in the number of patients who repeatedly reported improved well-being while on the medication, although we had no objective evidence of disease burden reduction or the patients even slowly progressed. The mechanism of action of numerous repurposed drugs or kinase inhibitors is far from cytotoxic, and stable disease may reflect only their different functional impact in cancer treatment. We face different mechanisms of action with new drugs that result in different disease behaviors. It thus raises the question of whether classical response criteria are optimal for personalized medicine.

TABLE 3 | Parameter estimates of final multivariate models.

Model	Treatment	HR	*p*
Conditional frailty (EFS combined)	METRO	0.45	0.005
General joint frailty (relapses)	METRO	0.46	0.017
General joint frailty (deaths)	REPUR/INHIB	0.15	0.004
	SURG/RT	0.16	0.001

Final bias-adjusted models from multivariate analysis represented by the most appropriate model (conditional frailty model for EFS and general joint frailty model for joint modeling of relapses and deaths).

Similar but stronger observations were found for local control of the disease. Local treatment did not influence the natural course of disease (reflected by recurrences) but may significantly improve survival. Providing additional time with relatively good quality of life may be an acceptable goal to refractory patients and, more importantly, may open a window of opportunity for other treatment modalities such as targeted therapies and immune therapies.

Utilizing the available knowledge arising from tissue analyses for biological guidance of the treatment we had at the time of early implementation of targeted therapies (in the present analysis) did not prove beneficial. The biological analyses were limited to kinase phosphorylation status and/or TruSight® Illumina NGS panel in only a few patients. Although these technologies may be useful in certain cases (31), they may not necessarily be sufficient for most analyzed patients. Several candidate alterations could be identified in most patients, but this fact does not warrant that an effective targeted therapy had to be utilized. The relevance and actionability of detected alteration are an issue (32). Specifically, if either only limited biological information is available or a detected alteration is assumed principal or driving in tumorigenesis but is actually not, it is not surprising that guidance of the targeted therapy having been based on such insufficient or irrelevant evidence was not beneficial. On the other hand, no effective drug can be available at all for a real driving alteration identified. We may also hypothesize that alterations mainly found among kinase phosphorylation profiles only indicated broad dysregulation of signal pathways. Several targeting agents might have been necessary in such situations to prove effective. Combined therapy is potentially more effective as is in accordance with multiple-hit philosophy (3) but also challenging due to unknown toxicity and interactions of novel agents. Molecular oncology board recommendations were based on very limited information compared to the currently utilized technologies, which include modern whole genome/exome sequencing and transcription analyses. A better understanding and correct interpretation of multi-omics data might provide more promising results in the near future.

The most surprising fact, however, was that treatment was more beneficial when given during the empirical period. There might be residual bias due to a combination of small factors that could not be accounted for in a more complex multivariate model and summed up to form more and less

risk periods and possibly being responsible for these results in part. However, we think that this observation could be explained through Bayesian reasoning as follows. Tumor board recommendations are based on various information, such as published data (prior evidence) and biological evaluation (new data). A new recommendation is then synthetized (posterior information). Philosophy of personalized medicine guides to base the evidence mainly on individual biological data. However, if based on limited or irrelevant information, it might divert our focus from, e.g., robust published evidence, although population-based, to less reliable or irrelevant individual data. Thus, the effect could be viewed as overweighting less reliable new data over underweighted prior robust evidence. Therefore, we strongly encourage the use of population-based evidence together with highly personalized approaches and comprehensive biological evaluation. Encouraging results of "personalized drugs" used on empirical grounds offers possibilities for patients in whom no target could be found.

There are several limitations that need to be discussed. This study was an observational, comparative-effectiveness study in which various sources of bias may have been introduced. Indication bias or unbalanced groups may be the most important factors. The long period covered in the analysis might have introduced inconsistencies in treatment indication strategies resulting in mentioned unbalances or bias. On the other hand, various factors were accounted for through the statistical tools used. Specifically, we believe that random effects in frailty models, event rank stratification and adjustment to calendar time in multivariate models could address most of the bias. Another question was the expected treatment effect onset and its duration after treatment initiation and discontinuation. We did not presume any specific time pattern of the treatment effects. Different coding of time-varying factors in the models could answer such specific questions. Furthermore, the interpretation of the results in the observational comparative setting needs to be adapted to the study design and in-house protocols. For example, we should regard the effects of the evaluated therapies in the context of concomitant or alternative treatment options being or having been given to our patients. Similarly, drug interactions or comedication effects could not be addressed because protocol-based same combinations or, on the other hand, individual single-cases of drug combinations arise. Thus, we cannot answer questions, such as which drug was most effective in which situation. However, the aim of the analysis was not the efficacy of a single drug but rather the treatment principle/modality under an individualized approach. There was no explicit control group in our data set, but we hypothesized that the sample itself rendered comparable control backgrounds to which the specific evaluated therapy of interest was compared. This assumption was also checked using the models.

We did not specifically address toxicity in this study. However, individualized management of a patient comprises standard assessment of toxicity and adjusting the treatment appropriately, and most patients were managed on an outpatient basis only.

CONCLUSIONS

Comparative patient series analysis provides institutional-level evidence for individualization of treatment in children with high-risk malignancies. Targeted treatment based on limited biological information is not beneficial for patients, which stresses the need for comprehensive multi-omics biological studies. Low-dose metronomic chemotherapy or local control of the disease may be a more rational option where targeted treatment cannot be justified by robust evidence and comprehensive information regarding tumor and the host biology. On the other hand, "targeted drugs" may be given empirically with a realistic benefit expectation when based on a robust rationale.

DATA AVAILABILITY

The datasets for this study will not be made publicly available because general provision of data is not in accordance with our institutional policy. We handle data of rare entities that may be at risk of identification even when anonymized. A journal representative may be invited for control purposes and the data sets may be temporarily provided on site and under the supervision of the institution.

ETHICS STATEMENT

All subjects or their legal guardians gave written informed consent in accordance with the Declaration of Helsinki. The study was approved by the Institutional review board of University hospital Brno.

AUTHOR CONTRIBUTIONS

MK designed the study, designed and created the registry SQL database, performed statistical analyses, and wrote the manuscript. KP evaluated patient records, performed data registry, and wrote the manuscript. ZK and TM evaluated patient records and performed data registry. JN, RV, JB, OH, and MJ performed biological samples analyses. GK and DV supervised and wrote the manuscript. JS conceived and supervised the project and wrote the manuscript.

ACKNOWLEDGMENTS

This study was supported by projects No. 16-34083A and No. 16-33209A from the Ministry of Healthcare of the Czech Republic, by project No. LQ1605 from the National Program of Sustainability II (MEYS CR), by project No. LM15089 (MEYS BBMRI-CZ), and project No. MUNI/A/1586/2018 from Masaryk University, Brno, Czech Republic, and by project MH CZ - DRO (FNBr, 65269705).

SUPPLEMENTARY MATERIAL

The Supplementary Material for this article can be found online at: https://www.frontiersin.org/articles/10.3389/fonc.2019.00644/full#supplementary-material

REFERENCES

1. Steliarova-Foucher E, Stiller C, Kaatsch P, Berrino F, Coebergh JW, Lacour B, et al. Geographical patterns and time trends of cancer incidence and survival among children and adolescents in Europe since the 1970s (the ACCIS project): an epidemiological study. *Lancet*. (2004) 364:2097–105. doi: 10.1016/S0140-6736(04)17550-8
2. Pasquier E, Kavallaris M, Andre N. Metronomic chemotherapy: new rationale for new directions. *Nat Rev Clin Oncol.* (2010) 7:455–65. doi: 10.1038/nrclinonc.2010.82
3. Zapletalova D, André N, Deak L, Kyr M, Bajciova V, Mudry P, et al. Metronomic chemotherapy with the COMBAT regimen in advanced pediatric malignancies: a multicenter experience. *Oncology*. (2012) 82:249–60. doi: 10.1159/000336483
4. Steppan DA, Pratilas CA, Loeb DM. Targeted therapy for soft tissue sarcomas in adolescents and young adults. *Adolesc Health Med Ther*. (2017) 8:41–55. doi: 10.2147/AHMT.S70377
5. Mendelsohn J. A national cancer clinical trials system for targeted therapies. *Sci Transl Med.* (2011) 3:75cm8. doi: 10.1126/scitranslmed.3001716
6. Skovlund E, Leufkens HGM, Smyth JF. The use of real-world data in cancer drug development. *Eur J Cancer*. (2018) 101:69–76. doi: 10.1016/j.ejca.2018.06.036
7. Korn EL, McShane LM, Freidlin B. Statistical challenges in the evaluation of treatments for small patient populations. *Sci Transl Med.* (2013) 5:178sr3. doi: 10.1126/scitranslmed.3004018
8. Couzin-Frankel J. Medical research. Clinical trials get practical. *Science*. (2015) 348:382. doi: 10.1126/science.348.6233.382
9. Conway PH, Clancy C. Comparative-effectiveness research-implications of the Federal Coordinating Council's report. *N Engl J Med*. (2009) 361:328–30. doi: 10.1056/NEJMp0905631
10. Sox HC, Goodman SN. The methods of comparative effectiveness research. *Annu Rev Public Health*. (2012) 33:425–45. doi: 10.1146/annurev-publhealth-031811-124610
11. Wei LJ, Lin DY, Weissfeld L. Regression analysis of multivariate incomplete failure time data by modeling marginal distributions. *J Am Stat Assoc*. (1989) 84:1065–73. doi: 10.1080/01621459.1989.10478873
12. Andersen PK, Gill RD. Cox's regression model for counting processes: a large sample study. *Ann Stat*. (1982) 10:1100–20. doi: 10.1214/aos/1176345976
13. Prentice RL, Williams BJ, Peterson AV. On the regression analysis of multivariate failure time data. *Biometrika*. (1981) 68:373–79. doi: 10.1093/biomet/68.2.373
14. Box-Steffensmeier JM, Zorn C. Duration models for repeated events. *J Polit*. (2002) 64:1069–96. doi: 10.1111/1468-2508.00163
15. Box-Steffensmeier JM, De Boef S, Joyce K. Event dependence and heterogeneity in duration models: the conditional frailty model. *Polit Anal.* (2007) 15:237–56. doi: 10.1093/pan/mpm013
16. Box-Steffensmeier JM, De Boef S. Repeated events survival models: the conditional frailty model. *Stat Med*. (2006) 25:3518–33. doi: 10.1002/sim.2434
17. Liu L, Wolfe RA, Huang X. Shared frailty models for recurrent events and a terminal event. *Biometrics*. (2004) 60:747–56. doi: 10.1111/j.0006-341X.2004.00225.x
18. Król A, Mauguen A, Mazroui Y, Laurent A, Michiels S, Rondeau V. Tutorial in joint modeling and prediction: a statistical software for correlated longitudinal outcomes, recurrent events and a terminal event. *J Stat Softw*. (2017) 81:1–52. doi: 10.18637/jss.v081.i03
19. R Core Team. *R: A Language and Environment for Statistical Computing*. Vienna: R Foundation for Statistical Computing (2017). Available online at: https://www.R-project.org/ (accessed July 9, 2019).
20. Therneau TM, Lumley T. *Survival: Survival Analysis*. R package version 2.41.3 (2017). Available online at: http://cran.r-project.org/web/packages/survival/ (accessed July 9, 2019).
21. Rondeau V, Mazroui Y, Gonzalez JR. frailtypack: an R package for the analysis of correlated survival data with frailty models using penalized likelihood estimation or parametrical estimation. *J Stat Softw*. (2012) 47:1–28. doi: 10.18637/jss.v047.i04
22. Rondeau V, Gonzalez JR. frailtypack: a computer program for the analysis of correlated failure time data using penalized likelihood estimation. *Comput Methods Programs Biomed*. (2005) 80:154–64. doi: 10.1016/j.cmpb.2005.06.010
23. Rondeau V, Gonzalez JR, Mazroui Y, Mauguen A, Krol A, Diakite A, et al. *Frailtypack: General Frailty Models Shared, Joint and Nested Frailty Models With Prediction*. R package version 2.11.1 (2017). Available online at: https://cran.r-project.org/web/packages/frailtypack/index.html (accessed July 9, 2019).
24. Peduzzi P, Concato J, Feinstein AR, Holford TR. Importance of events per independent variable in proportional hazards regression analysis. II. Accuracy and precision of regression estimates. *J Clin Epidemiol.* (1995) 48:1503–10. doi: 10.1016/0895-4356(95)00048-8
25. Bisogno G, De Salvo GL, Bergeron C, Jenney M, Merks JHM, Minard-Colin V, et al. Maintenance chemotherapy extends life for children with a rare cancer – first treatment advance for this cancer in 30 years. *Presented on 3rd June 2018, ASCO Annual Meeting*. Chicago, IL (2018).
26. Lindsey JK, Lambert P. On the appropriateness of marginal models for repeated measurements in clinical trials. *Stat Med*. (1998) 17:447–69.
27. Navarro A, Casanovas G, Alvarado S, Moriña D. Analyzing recurrent events when the history of previous episodes is unknown or not taken into account: proceed with caution. *Gac Sanit*. (2017) 31:227–34. doi: 10.1016/j.gaceta.2016.09.004
28. Stempak D, Gammon J, Halton J, Moghrabi A, Koren G, Baruchel S. A pilot pharmacokinetic and antiangiogenic biomarker study of celecoxib and low-dose metronomic vinblastine or cyclophosphamide in pediatric recurrent solid tumors. *J Pediatr Hematol Oncol*. (2006) 28:720–8. doi: 10.1097/01.mph.0000243657.64056.c3
29. Young SD, Whissell M, Noble JC, Cano PO, Lopez PG, Germond CJ. Phase II clinical trial results involving treatment with low-dose daily oral cyclophosphamide, weekly vinblastine, and rofecoxib in patients with advanced solid tumors. *Clin Cancer Res*. (2006) 12:3092–8. doi: 10.1158/1078-0432.CCR-05-2255
30. Ali AM, El-Sayed MI. Metronomic chemotherapy and radiotherapy as salvage treatment in refractory or relapsed pediatric solid tumours. *Curr Oncol.* (2016) 23:e253–9. doi: 10.3747/co.23.2873
31. Mudry P, Slaby O, Neradil J, Soukalova J, Melicharkova K, Rohleder O. Case report: rapid and durable response to PDGFR targeted therapy in a child with refractory multiple infantile myofibromatosis and a heterozygous germline mutation of the PDGFRB gene. *BMC Cancer*. (2017) 17:119. doi: 10.1186/s12885-017-3115-x
32. Kurnit KC, Dumbrava EEI, Litzenburger BC, Khotskaya YB, Johnson A, Yap TA, et al. Precision oncology decision support: current approaches and strategies for the future. *Clin Cancer Res*. (2018) 24:2719–31. doi: 10.1158/1078-0432.CCR-17-2494

Conflict of Interest Statement: GK was employed by CSTS Health Care Inc., Toronto, Ontario, Canada.

The remaining authors declare that the research was conducted in the absence of any commercial or financial relationships that could be construed as a potential conflict of interest.

frontiers in Oncology

METHODS
published: 20 September 2019
doi: 10.3389/fonc.2019.00930

Phospho-Protein Arrays as Effective Tools for Screening Possible Targets for Kinase Inhibitors and Their Use in Precision Pediatric Oncology

Jakub Neradil[1,2], *Michal Kyr*[2], *Kristyna Polaskova*[2], *Leos Kren*[3], *Petra Macigova*[1,2], *Jan Skoda*[1,2], *Jaroslav Sterba*[2] *and Renata Veselska*[1,2]*

[1] Laboratory of Tumor Biology, Department of Experimental Biology, Faculty of Science, Masaryk University, Brno, Czechia,
[2] Department of Pediatric Oncology, Faculty of Medicine, University Hospital Brno, Masaryk University, Brno, Czechia,
[3] Department of Pathology, Faculty of Medicine, University Hospital Brno, Masaryk University, Brno, Czechia

OPEN ACCESS

Edited by:
Suzie Chen,
Rutgers University, The State University of New Jersey, United States

Reviewed by:
Min Hee Kang,
Texas Tech University Health Sciences Center, United States
Vijay Pandey,
Tsinghua-Berkeley Shenzhen Institute, China

***Correspondence:**
Renata Veselska
veselska@sci.muni.cz

Specialty section:
This article was submitted to Cancer Molecular Targets and Therapeutics, a section of the journal Frontiers in Oncology

Received: 29 June 2019
Accepted: 05 September 2019
Published: 20 September 2019

Citation:
Neradil J, Kyr M, Polaskova K, Kren L, Macigova P, Skoda J, Sterba J and Veselska R (2019) Phospho-Protein Arrays as Effective Tools for Screening Possible Targets for Kinase Inhibitors and Their Use in Precision Pediatric Oncology. Front. Oncol. 9:930. doi: 10.3389/fonc.2019.00930

The specific targeting of signal transduction by low-molecular-weight inhibitors or monoclonal antibodies represents a very promising personalized treatment strategy in pediatric oncology. In this study, we present the successful and clinically relevant use of commercially available phospho-protein arrays for analyses of the phosphorylation profiles of a broad spectrum of receptor tyrosine kinases and their downstream signaling proteins in tumor tissue samples. Although these arrays were made for research purposes on human biological samples, they have already been used by several authors to profile various tumor types. Our study performed a systematic analysis of the advantages and pitfalls of the use of this method for personalized clinical medicine. In certain clinical cases and their series, we demonstrated the important aspects of data processing and evaluation, the use of phospho-protein arrays for single sample and serial sample analyses, and the validation of obtained results by immunohistochemistry, as well as the possibilities of this method for the hierarchical clustering of pediatric solid tumors. Our results clearly show that phospho-protein arrays are apparently useful for the clinical consideration of druggable molecular targets within a specific tumor. Thus, their potential validation for diagnostic purposes may substantially improve the personalized approach in the treatment of relapsed or refractory solid tumors.

Keywords: phospho-protein arrays, receptor tyrosin kinases, signal transduction, low-molecular-weight inhibitors, pediatric solid tumors, phosphorylation profiling

INTRODUCTION

Current curative treatment regimens for high-risk pediatric solid tumors consist of surgery, sometimes radiotherapy (to achieve adequate local control) and different intensive chemotherapeutic schedules, with a highly limited role of targeted agents thus far. Despite this multimodal approach, the rate of survival in patients suffering from refractory or relapsed solid tumors is still disappointing, and treatment is accompanied by many early and late side effects. This finding supports the need for more effective therapeutic approaches that are based on the principle of personalized medicine (1).

The personalized treatment of malignant diseases is defined as evidence-based, individualized medicine that delivers the right care to the right cancer patient at the right time (2). This personalized approach leads to measurable improvements in patient outcomes and thus to a rational distribution of health care costs (3). Therefore, such molecular individualized medicine has recently prevailed in traditional "one size fits all" medicine (2).

One very promising strategy involves the specific targeting of signal transduction by small molecule inhibitors or monoclonal antibodies; some of these medications have recently been tested in phase I and phase II clinical trials (4, 5). However, the basic step for this personalized approach includes the precise characterization of the individual tumor regarding the receptor tyrosine kinase (RTK) pattern—both the expression and phosphorylation correlating with activation—as well as of downstream signaling pathways. In the majority of published studies on this topic, total protein expression levels were usually considered, mostly on archival formalin-fixed paraffin-embedded (FFPE) tumor samples (6–8).

Nevertheless, a specific screening approach for activated, i.e., phosphorylated, RTKs and/or downstream signaling molecules should provide more accurate data concerning the dependency of tumor cells on a particular pathway and may provide a better guide for treatment choice (4, 9). In this article, we report the experimental use of commercially available phospho-protein arrays designed for the rapid screening of phosphorylated RTKs and other signaling molecules in several types of pediatric solid tumors. Although these arrays were made for research purposes on human biological samples, they have already been used for the characterization of certain tumors in adults (10, 11) and sporadically for the characterization of pediatric tumors (12–14). Nevertheless, no systematic analysis of the advantages and pitfalls of the possible use of this method for personalized clinical medicine is available. Thus, we hope that our results on the experimental use of this method may help validate its potential for clinical practice.

TABLE 1 | Overview of patients and their samples included in this study.

Sample No.	Sample type	Patient age range (months)	Tumor histology
1	Primary tumor	85–90	Malignant perivascular epitheliod cell tumor (PEComa)
2a	Primary tumor	185–190	Anaplastic ependymoma
2b	Relapsed primary tumor	215–220	
3	Relapsed primary tumor	35–40	Anaplastic ependymoma
4	Primary tumor	0–5	Infantile myofibromatosis
5	Primary tumor	20–25	Fibrodysplasia ossificans proggressiva
6	Lung metastasis	200–2005	Osteosarcoma
7	Primary tumor	95–100	Osteosarcoma
8a	Primary tumor	35–40	Alveolar rhabdomyosarcoma
8b	Relapsed primary tumor	45–50	
8c	Lymph node metastasis	45–50	
8d	Lymph node metastasis	80–85	
9	Primary tumor	20–25	Neuroblastoma
10	Primary tumor	30–35	Neuroblastoma
11	Orbital metastasis	15–20	Neuroblastoma
12	Hip metastasis	60–65	Neuroblastoma
13	Mediastinal metastasis	125–130	Neuroblastoma
14	Relapsed primary tumor	185–190	Pilocytic astrocytoma
15	Relapsed primary tumor	60–65	Pilocytic astrocytoma
16	Primary tumor	10–15	Pilomyxoid astrocytoma
17	Primary tumor	180–185	Glioblastoma
18	Relapsed primary tumor	140–145	Glioblastoma
19	Spinal cord metastasis	240–245	Medulloblastoma

MATERIALS AND METHODS

Tumor Samples

Tumor samples obtained from patients suffering from various types of relapsed or refractory pediatric solid tumors were included in this study. Written informed consent on the use of these samples and corresponding clinical data for research purposes were obtained from each patient or from the patient's parents/guardians. The Research Ethics Committee of the School of Medicine, Masaryk University (Brno, Czech Republic) approved the study protocol (certificate No. 29/2015). A description of the individual patients included in this study is given in **Table 1**. After surgery, the excised tumor tissue was examined macroscopically by pathologist and cut into two parts: one of them was designated for further microscopic examinations, and the second one was immediately frozen in liquid nitrogen. These frozen tumor samples were then processed for analyses using phospho-protein arrays. For immunohistochemistry (IHC) analyses, FFPE tumor samples were retrieved from files of the Department of Pathology, University Hospital Brno, Czech Republic.

Phospho-Protein Array Analysis

The relative phosphorylation levels of the selected target molecules involved in signal transduction pathways in human cells were analyzed using two types of commercially available phospho-protein arrays (R&D Systems, Minneapolis, MN, USA). The Proteome Profiler™ Human Phospho-RTK Array Kit (R&D Systems, Cat. No. ARY001B) was designed for the parallel detection of the activities of 49 RTKs (**Supplementary Table 1**), and the Proteome Profiler™ Human Phospho-MAPK Array Kit (R&D Systems, Cat. No. ARY002B) was designed for the parallel detection of 26 downstream signaling molecules, including 9 MAPKs (**Supplementary Table 2**). Deeply frozen tumor tissue samples were cut with a scalpel in 400 μl of appropriate lysis buffer on ice. Lysis Buffer 17 and Lysis Buffer 6 (both R&D Systems) were used for Phospho-RTK and Phospho-MAPK array kit, respectively. After complete homogenization,

TABLE 2 | Overview of antibodies used in this study.

Antigen	Type/host	Cat. No. (all Abcam)	Dilution	Positive control
EGFR (total)	Monoclonal/Rb	ab52894	1:200	Endometrial carcinoma
EGFR (anti-pTyr^{1092})	Monoclonal/Rb	ab40815	1:400	Papillary carcinoma of thyroid glad
PDGFRβ (total)	Monoclonal/Rb	ab32570	1:100	Breast and spleen
PDGFRβ (anti-pTyr^{751})	Polyclonal/Rb	ab51046	1:100	Brain
InsRβ (total)	Polyclonal/Rb	ab5500	1:200	Breast carcinoma
InsRβ (anti-pTyr^{1185})	Polyclonal/Rb	ab203278	1:150	Lung
Akt1/2/3 (total)	Monoclonal/Rb	ab32505	1:100	Prostate carcinoma
Akt1/2/3 (anti-pSer^{473})	Monoclonal/Rb	ab81283	1:50	Cervical carcinoma
ERK1/2 (total)	Monoclonal/Mo	ab54230	1:100	Stomach
ERK1/2 (anti-pThr^{202}/pTyr^{204}//pThr^{185}/pTyr^{187})	Monoclonal/Mo	ab50011	1:100	Brain

the whole suspension was centrifuged for 5 min at 14,000 g. The supernatants were used as whole-tissue lysates and then processed according to the manufacturer's protocol. The levels of phosphorylation were quantified using ImageJ software (15). The detailed procedure of data acquisition and processing is described below in the relevant part of the Results.

Immunohistochemical Analysis

Representative sections from relevant FFPE tumor samples were analyzed by IHC to determine the total and phosphorylated levels of the protein of interest. All of the antibodies used in this protocol are described in **Table 2**. The 4-μm-thick sections from FFPE blocks were deparaffinized with pure xylene for 3 × 5 min, washed in 96% alcohol for 3 × 5 min and then rinsed with distilled water. In the next step, endogenous peroxidase was inactivated by 3% H_2O_2 in methanol for 10 min, and the samples were washed in distilled water. Antigen retrieval was then performed by incubation in citrate buffer (pH 6.0) at 98°C for 20 min followed by cooling for 20 min and rinsing with PBS for 3 × 5 min. The incubation with primary antibodies was performed in a wet chamber at room temperature for 1 h, and samples were then rinsed with PBS for 3 × 5 min. The EnVision+System streptavidin-biotin peroxidase detection system (Dako, Glostrup, Denmark) was used according to the manufacturer's protocol in the wet chamber at room temperature for 45 min followed by washing in PBS and visualization using 3,3'diaminobenzidine as a substrate (Sigma-Aldrich, St. Louis, MO, USA). Nuclei were counterstained with Gill's hematoxylin for 1 min followed by bluing in water for 2–3 min for optimal results. Finally, the samples were dehydrated in a series of upconcentrated ethanol baths, cleared in xylene and mounted onto Entelan™ slides (Entelan Microscopy, Karlsruhe, Germany). Positive and negative controls were evaluated in each IHC run. Positive controls for each protein are listed in **Table 2**. Negative controls consisted of slides run without the primary antibodies. An Olympus BX45 microscope (Olympus Optical, Tokyo, Japan) equipped with an Olympus DP50 digital camera was used for the evaluation of IHC staining and to capture the micrographs. Olympus Viewfinder Lite™ software was used to process the images.

Statistical Analysis

Hierarchical clustering was used for multidimensional kinase phosphorylation data analysis to identify possible characteristic patterns of the kinase phosphorylation status for different diagnostic groups. Data preprocessing was performed as follows. Digitalized density levels were logarithmically transformed, and normalization and scaling of the data matrix were performed to enable comparison among samples. After filtering significantly different kinases, supervised clustering was applied. Hierarchical clustering using a Ward method with correlation distance metrics was performed. Data are presented using heatmap plots. Analyses were performed using R 3.4.3 (16) with gplots (17).

RESULTS

Although the phospho-protein arrays employed in this study were designed and produced by the manufacturer for research purposes only, our experimental results showed that they may also be successfully used for the rapid screening of active signal transducers as potential therapeutic targets in tumor tissue samples obtained from individual patients. Furthermore, we also showed that these arrays are also very suitable for comparative analyses of respective phospho-protein profiles among and/or within different tumor types, as described below in detail. Nevertheless, the use of phospho-protein arrays for these purposes encompasses several important aspects that must be carefully considered in the view of the correct interpretation of obtained results.

Data Acquisition and Processing

The phospho-protein arrays used in our experiments are based on analysis of tissue samples on nitrocellulose membranes, where specific antibodies against selected kinases are spotted in duplicate. In addition to these antibodies, each membrane contains three positive reference double spots and one negative control containing PBS only, which is also spotted in duplicate (**Figures 1A,E**). Tissue lysates are applied to this membrane, and both phosphorylated and unphosphorylated proteins are bound to the respective antibodies at an equimolar ratio.

In the phospho-RTK array, the phosphorylated proteins are distinguished only by a pan-anti-phospho-tyrosine antibody

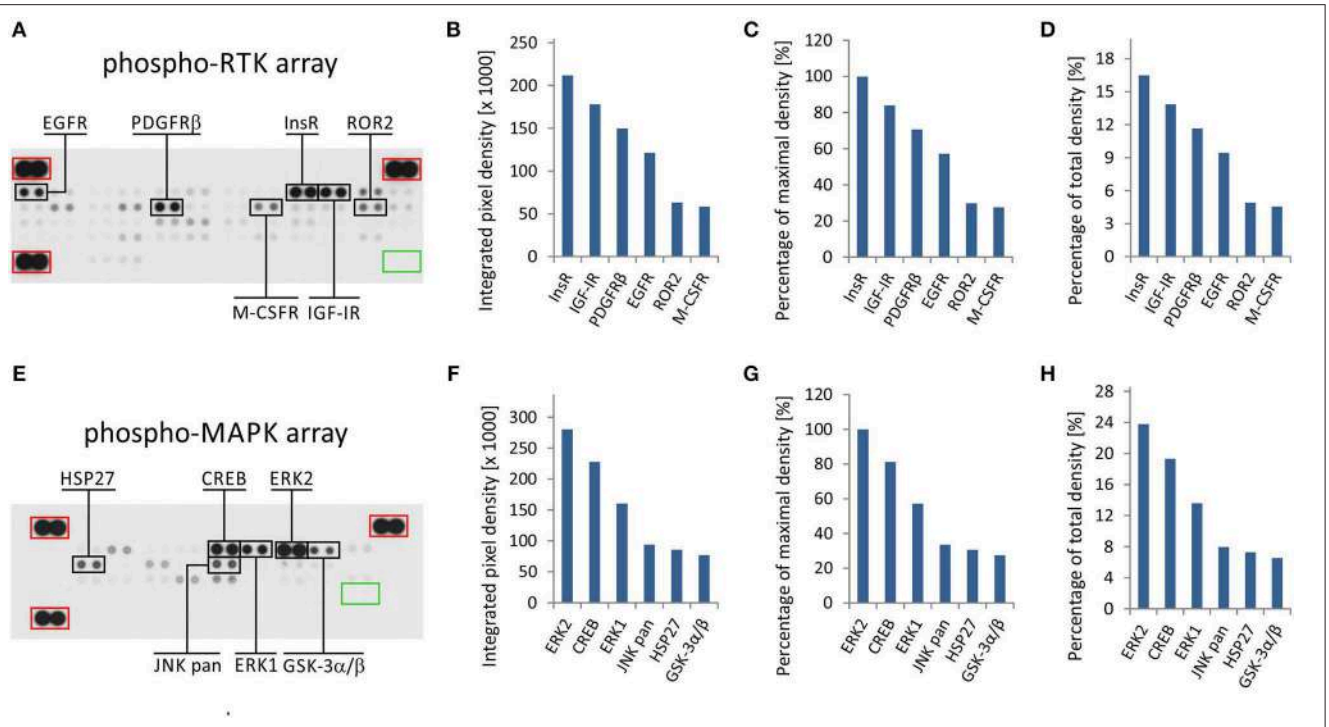

FIGURE 1 | One sample analysis of phospho-RTK and phospho-MAPK array. The array images are shown for both arrays **(A,E)**, and the six most phosphorylated proteins are marked in black rectangles. Positive reference double spots are marked in red rectangles; area of negative control spots is marked in green rectangle. The most phosphorylated RTKs **(B–D)** and MAPKs or other downstream signaling molecules **(F–H)** are displayed according to intensity of phosphorylation. Absolute values of integrated pixel density **(B,F)** of different kinases are displayed also as a percentage of the maximal pixel density **(C,G)** or as a percentage of the total sum of pixel density **(D,H)** (y-axis).

conjugated with horseradish peroxidase. This allows us to detect all phosphorylated tyrosines that are predominantly located on the cytoplasmic part of the RTK molecule and thus reflect the overall activity of the receptor in question.

In the phospho-MAPK array, a mixture of biotinylated anti-phospho-kinase antibodies followed by streptavidin conjugated with horseradish peroxidase is used to distinguish between phosphorylated and unphosphorylated proteins. Each individual antibody in this antibody mixture is designed to detect a specific phosphorylation site (or sites) of each particular signaling protein included in the array. A table containing the overview of phosphorylation sites for all detected proteins is given in the manufacturer's manual.

Finally, the luminescence induced by the addition of a chemiluminescent substrate is captured on X-ray film in both arrays (**Figures 1A,E**). As described in our previous studies, the levels of phosphorylation were quantified using ImageJ software (15) and subsequently normalized to the positive control spots (18). Although the experimental use of a phospho-protein array is usually based on the comparison of acquired data with a reference cell line (18) or with untreated control cells (19), the employment of these arrays in clinical practice apparently requires a different approach.

We presumed that highly phosphorylated proteins, as detected by these arrays, are highly activated within the tumor tissue and thus represent the most suitable targets for treatment with available small-molecule inhibitors or monoclonal antibodies (20). To evaluate the results of one sample analysis, it is possible to use the absolute values of integrated density as obtained by the employment of image analysis software (**Figures 1B,F**). Alternatively, the data can be normalized to the maximal integrated density achieved in each individual array, i.e., the highest value indicates 100% phosphorylation (**Figures 1C,G**). The third method by which to process the obtained data is recommended by ImageJ software documentation (15): the integrated densities of each kinase are displayed as a percentage of the total sum of density (**Figures 1D,H**). The resulting phosphorylation profiles obtained by these three processing modes are identical to each other, and they show the same differences in the phosphorylation of kinases included in the respective array (**Figures 1B–D,F–H**).

From the clinical viewpoint, the results described above (**Figure 1**) are those obtained by the analysis of tumor tissue obtained from patient No. 1 (**Table 1**). This sample was obtained by surgical resection of the tumor mass from the supravesical space. According to the results from molecular biology analyses, including these phospho-profiles, the patient was treated with low-molecular-weight inhibitors (everolimus and sunitinib), and complete remission was achieved.

The results from RTK phospho-protein arrays showed that two members of the insulin receptor family (InsR and IGF-1R) displayed the highest phosphorylation. Slightly reduced positivity was also observed for PDGFRβ and EGFR (**Figures 1A–D**). The analysis of MAPKs revealed the high phosphorylation of ERK1 and ERK2 on activation loop residues Thr^{202}/Tyr^{204} and Thr^{185}/Tyr^{187}, respectively. Among the other downstream signaling molecules, CREB was substantially phosphorylated on residue Ser^{133}. Lower but still detectable levels of phosphorylation were found for JNK kinases on Thr^{183}/Tyr^{185} and Thr^{221}/Tyr^{223}, for Hsp27 (also known as HSPB1) on Ser^{78}/Ser^{82} residues, and for GSK-3 kinases on Ser^{9}/Ser^{21} (**Figures 1E–H**).

Verification of Druggable Targets in Tumor Tissue

The main advantage of the use of phospho-protein arrays for the identification of active signal transducers within tumor tissue is the promptness of such a screening method and the relatively high number of signaling molecules covered by these arrays. Nevertheless, as these arrays are still available for experimental purposes only and not for routine laboratory diagnostics, the results obtained from these arrays should be verified by other independent methods.

Thus, we employed a standard IHC method for the independent detection of active signal transducers as already identified by the phospho-protein array. As an example of this approach, the results from both types of phospho-protein arrays were compared with results from the IHC analysis of paired FFPE samples from the same biopsies in a group of 6 patients: patients No. 2–7 (**Table 1**) were included in this part of the study.

For RTKs, the levels of phospho-EGFR, phospho-PDGFRβ, and phospho-InsR were compared with the presence of these phosphorylated RTKs as identified using specific anti-phospho antibodies (**Table 2**) against these three selected target molecules (**Figure 2**).

To verify EGFR phosphorylation, a specific anti-phospho-EGFR antibody against phosphorylated Tyr^{1092}, which is equivalent to Tyr^{1068} of mature EGFR, was used. All analyzed samples showed relatively high levels of phosphorylation as detected using both phospho-arrays, with ∼60–100% of maximal density, and the immunoreactivity was predominantly medium

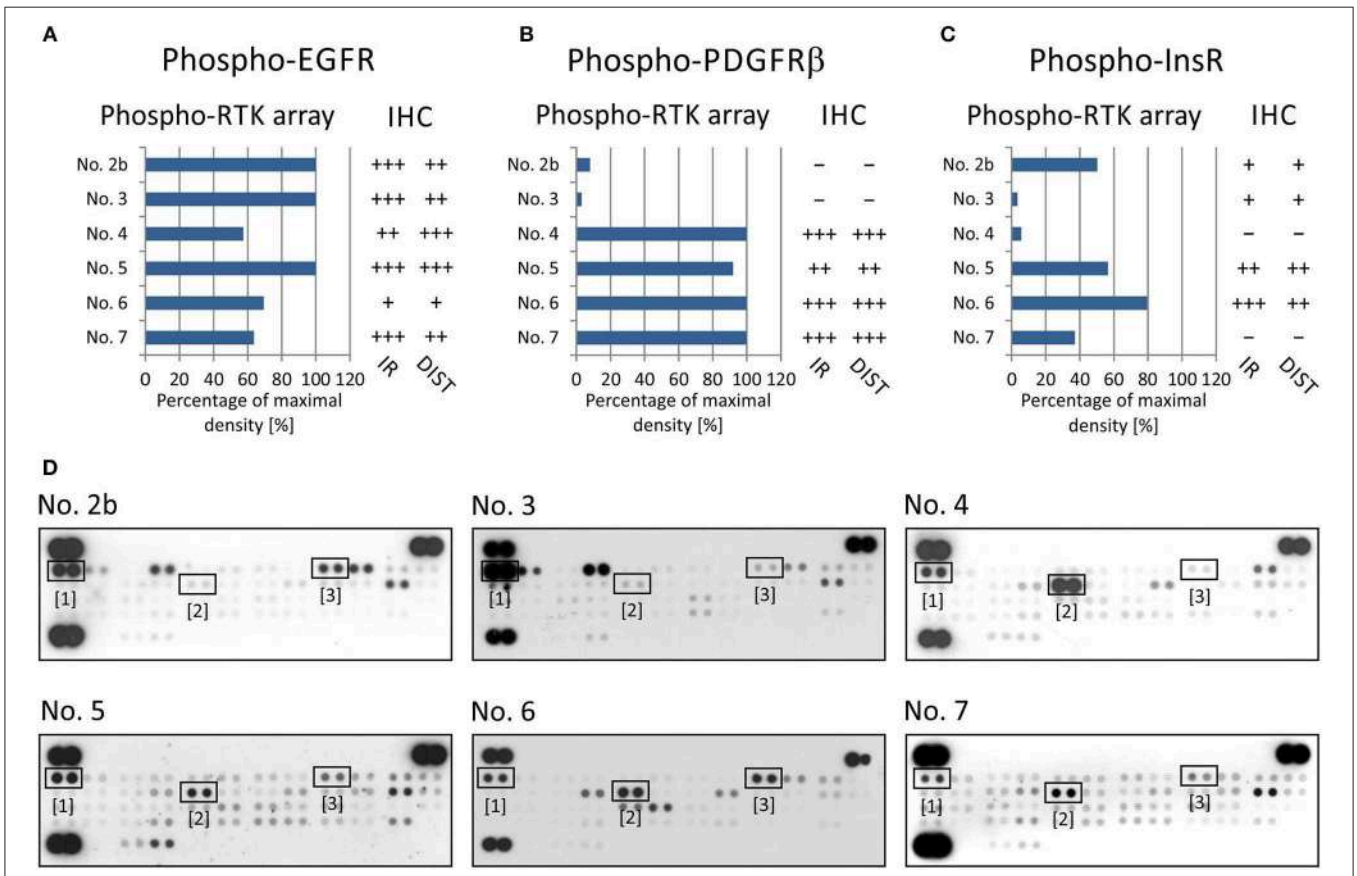

FIGURE 2 | Comparison of immunohistochemical and phospho-protein array analysis in determination of phosphorylated EGFR **(A)**, PDGFRβ **(B)**, and InsR **(C)**. Evaluation of phospho-protein array: values are displayed as a percentage of the maximal pixel density of every single sample. Evaluation of IHC: intensity of immunoreactivity (IR); –, very weak; +, weak; ++, medium; + + +, strong; distribution of immunostaining (DIST); –, non-detectable; +, focal; ++, regional; + + +, diffuse. The images of phospho-RTK arrays **(D)** with marked phosphorylated EGFR (1), PDGFRβ (2), and InsR (3) proteins.

to strong except in sample No. 6 (**Figure 2A**). The anti-phospho-PDGFRβ antibody against phosphorylated Tyr^{751} also showed a very good match with PDGFRβ phosphorylation as detected by the phospho-protein array in all six samples (**Figures 2B,D**): strong or medium immunoreactivity corresponded to the highest density from the phospho-protein arrays and vice versa; and very weak immunoreactivity was in accordance with very low phosphorylation—up to 10% of maximal density—in sample Nos. 2 and 3 (**Figures 2B,D**). The anti-InsR antibody against phosphorylated Tyr^{1185} in the beta chain of the InsR molecule showed strong or medium positivity in the same tumor tissues in which at least 50% of maximal density was detected by the phospho-array (**Figures 2C,D**). Nevertheless, for InsR activities up to 50% of maximal density, accordance with the IHC results was not obvious (**Figures 2C,D**).

To evaluate the two most prominent downstream signaling pathways, i.e., PI3K/AKT and RAS/RAF/MEK/ERK, antibodies designed to detect both phosphorylated forms of ERK kinase and all three phosphorylated forms of AKT kinase, respectively, were chosen. The phosphorylation of AKT kinases in FFPE tumor samples was evaluated using an anti-AKT1 antibody that detects phosphorylation at Ser^{473} within the C-terminus. Due to the high degree of similarity to the corresponding regions in the AKT2 and AKT3 molecules, this antibody may cross-react with these isoforms at Ser^{474} and Ser^{472}, respectively. The phospho-protein array can detect the relative phosphorylation of all three AKT isoforms at the same phospho-sites as the antibody employed for IHC. Anyway, the phosphorylation of AKT2 reached only ∼50% of the maximal density in sample Nos. 4, 5, and 6 (**Figures 3A,C**). The relative phosphorylation of AKT1 and AKT3 was close to the detection limit of this array in all tested samples, and the IHC method also showed very poor results for phosphorylated AKT1/2/3 molecules (**Figures 3A,C**). The anti-ERK1/2 antibody was designed against the epitopes with the same phospho-sites as those detected by the phospho-array. All FFPE samples showed strong immunoreactivity for ERK1/2, with diffuse or regional

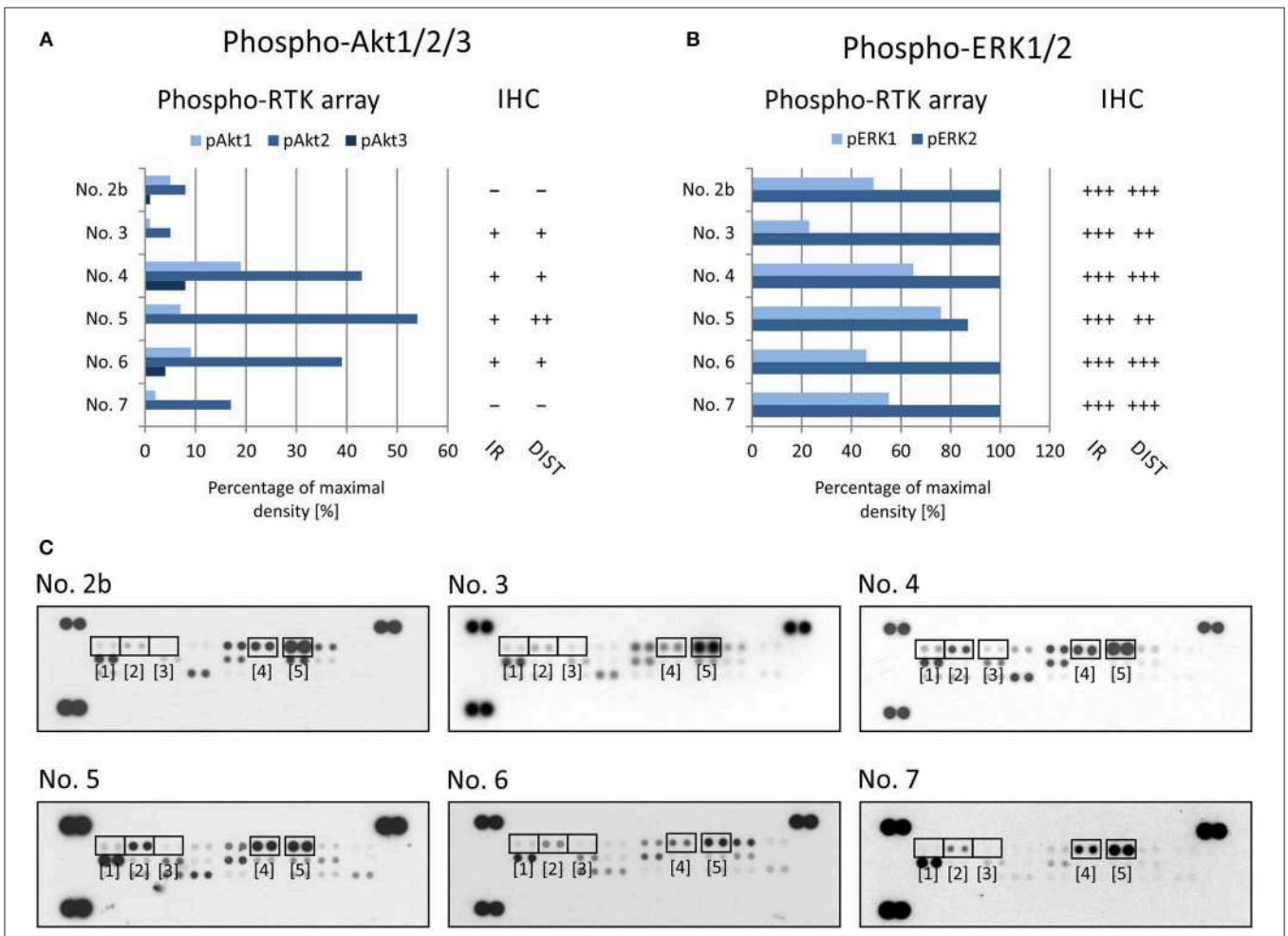

FIGURE 3 | Comparison of immunohistochemical and phospho-protein array analysis in determination of phosphorylated ERK1/2 **(A)** and Akt1/2/3 **(B)**. Evaluation of phospho-protein array: values are displayed as a percentage of the maximal pixel density of every single sample. Evaluation of IHC: intensity of immunoreactivity (IR); –, very weak; +, weak; ++, medium; + + +, strong; distribution of immunostaining (DIST); –, non-detectable; +, focal; ++, regional; + + +, diffuse. The images of phospho-MAPK arrays **(C)** with marked phosphorylated AKT1 (1), AKT1 (2), AKT1 (3), ERK1 (4), and ERK2 (5) proteins.

positivity, and these results were in accordance with the very high relative phosphorylation of ERK2 as detected by the phospho-protein array (**Figures 3B,C**).

Taken together, these results indicate that the IHC method using compatible anti-phospho antibodies can serve as a useful tool for final detection or rather confirmation of the phosphorylation of the possible therapeutic target previously identified in the tumor tissue by rapid screening using phospho-protein arrays.

Example of Serial Sample Analysis During Clinical Progression of the Disease

As described above, the analysis of one individual tumor sample provides us with information concerning the phosphorylation profile of RTKs and/or downstream signaling molecules just at the time of tissue sample acquisition. A typical clinical reason for a one sample analysis is the rapid screening of suitable (and druggable) targets for personalized treatment during the phase of initial diagnostics. Nevertheless, especially in cases of refractory or relapsed tumors, we are also able to analyze and compare a series of tumor samples taken from the same patient at different phases of the disease.

Here, we describe the employment of phospho-protein arrays in the profiling of cell signaling pathways in four serial tumor samples taken from a child suffering from PAX3/FKHR-positive alveolar rhabdomyosarcoma of the ala of nose. The child was diagnosed at the age of 19 months, staged as T1aN1M0 and classified into a very-high-risk group (IRS st. IIIa) according to the European Pediatric Soft Tissue Sarcoma Study Group (EpSSG). First, complete remission was achieved after 3 cycles of chemotherapy (EpSSG RMS2005 protocol) and adjuvant radiotherapy; however, the tumor relapsed after 16 months. Second, complete remission was achieved after 6 cycles of chemotherapy (vincristine, irinotecan, and temozolomide). The patient was treated with individualized metronomic chemotherapy, but metastatic relapse was diagnosed 3 months later. Despite intensive individualized therapy, the child died within 7 months. The complete overview of this case is given (**Figure 4A**).

Step-by-step, we analyzed using both phospho-protein arrays the samples taken from the primary tumor before the treatment using both phospho-protein arrays, from the relapsed primary tumor and from two metastatic lymph nodes at different times during the disease (**Table 1**, **Figure 4A**). Changes in the phospho-profiles of RTKs (**Figure 4B**) are described in the context of personalized therapy with small molecule inhibitors used in this patient; the phospho-profiles of downstream signaling pathways (**Figure 4C**), as well as examples of target validation by IHC (**Figures 4D,E**), are also given.

Based on the obtained data, specific small molecule inhibitors were incorporated into the treatment protocol. Although pazopanib showed partial effect in terms of RTK activity, the subsequent treatment with erlotinib and sunitinib markedly diminished the activities of the target RTKs in the tumor tissue (**Figure 4B**). Unfortunately, despite this very clear response at the molecular level, no encouraging effects of this targeted therapy were observed at the clinical level, probably because of the advanced stage of metastatic disease. Nevertheless, this case markedly illustrates the importance and usefulness of the rapid screening of the possible molecular targets for personalized therapy.

Multidimensional Analysis of Kinase Profiles in Specific Tumor Types

In addition to the individual and serial sample analyses described above, information regarding the phosphorylation profiles as obtained by the phospho-protein arrays can also be used for the hierarchical clustering of selected tumor samples. Here, we demonstrate the performance of such a classical multidimensional analysis using supervised hierarchical clustering on a small cohort ($n = 12$) of 5 neuroblastoma and 7 central nervous system (CNS) tumor samples: 3 astrocytomas, 2 glioblastomas, 1 ependymoma, and 1 medulloblastoma. The patients' detailed information is given in **Table 1**. This analysis performed on the data from the RTK phospho-protein arrays showed two distinct clusters of strongly and weakly phosphorylated RTK kinases in neuroblastoma and CNS tumors (**Figure 5A**). In contrast, even supervised clustering based on the data from the MAPK phospho-protein arrays did not result in distinct clusters of diagnostic groups in the same cohort (**Figure 5B**).

DISCUSSION

An antibody array is one of the simplest methods for measuring the relative levels of expression or phosphorylation of several proteins in a single sample. In this study, we present the successful and clinically relevant use of the Human Phospho-RTK Array Kit and the Human Phospho-MAPK Array Kit (both by R&D Systems) for the analyses of the phosphorylation profiles of a broad spectrum of RTKs and their downstream signaling proteins.

According to the manufacturer's instructions, the analysis of raw data obtained from these arrays includes determining the average signal of the pair of duplicate spots and subtracting the background signal. However, the subsequent analysis of these data is neither unified nor standardized and thus depends on the researcher's choice.

The results of one sample analysis can be presented as a specific profile with differently phosphorylated proteins, in which high levels of the detected signal, i.e., high density of spots in the phospho-protein arrays, correspond to high phosphorylation. Consequently, these highly phosphorylated signaling molecules can be considered potential therapeutic targets for low-molecular-weight kinase inhibitors or monoclonal antibodies. Moreover, the stability of phosphorylation profiles of frozen samples throughout long-term storing was proven (**Supplementary Figure 1**). The utility of commercially available phospho-protein arrays has already been demonstrated in other studies on various types of human solid tumors in adults (10, 11, 21–23).

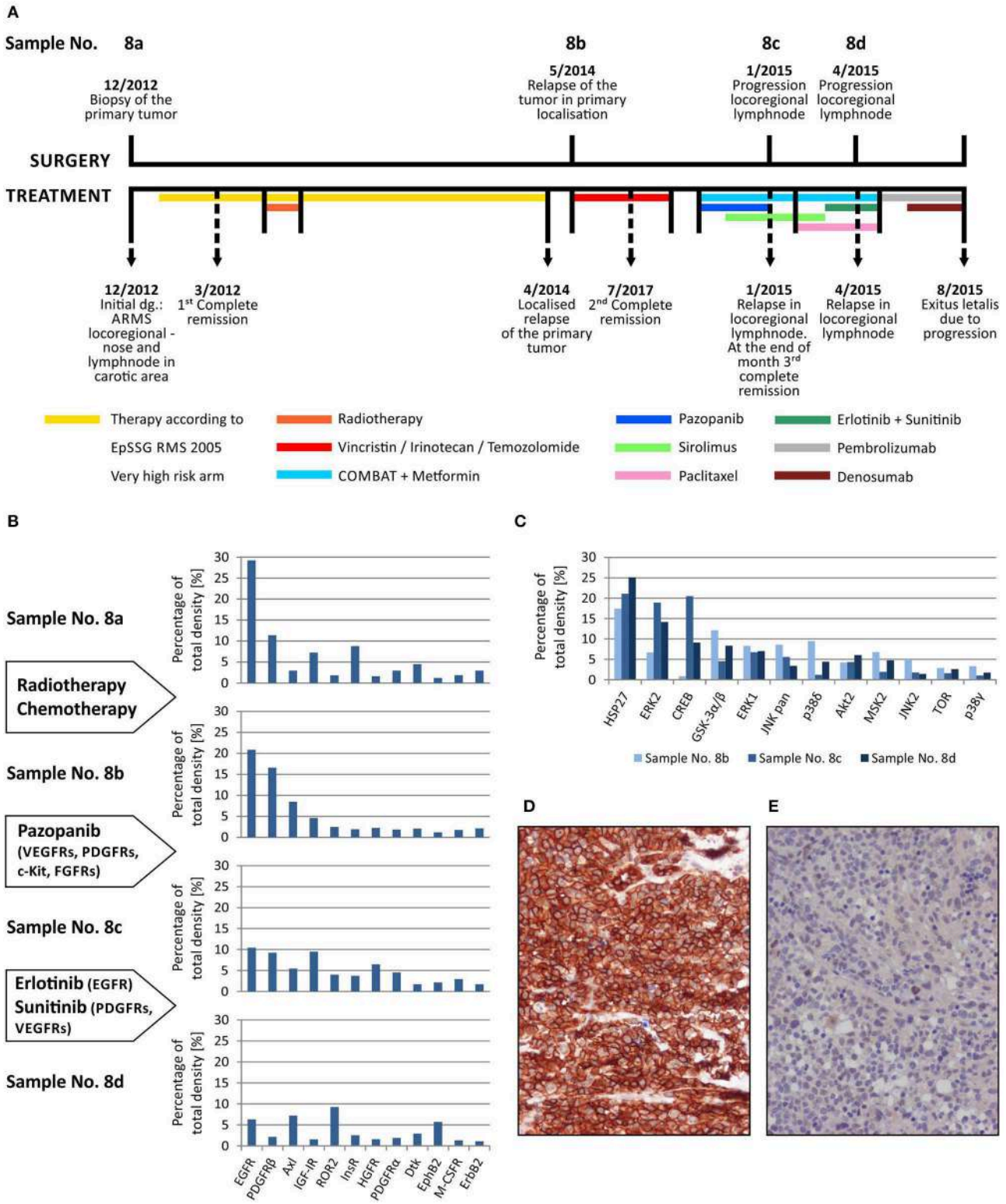

FIGURE 4 | Sequential analysis of phospho-protein arrays during individualized therapy of alveolar rhabdomyosarcoma. Timeline of patient's surgical and medical treatment **(A)**. Changes in the phospho-RTKs profiles of samples obtained during therapy **(B)**. Changes in the phospho-MAPKs profiles of samples obtained during therapy **(C)**. Immunohistochemical detection of phospho-EGFR in sample No. 8b **(D)** and phospho-PDGFRβ in sample No. 8d **(E)**.

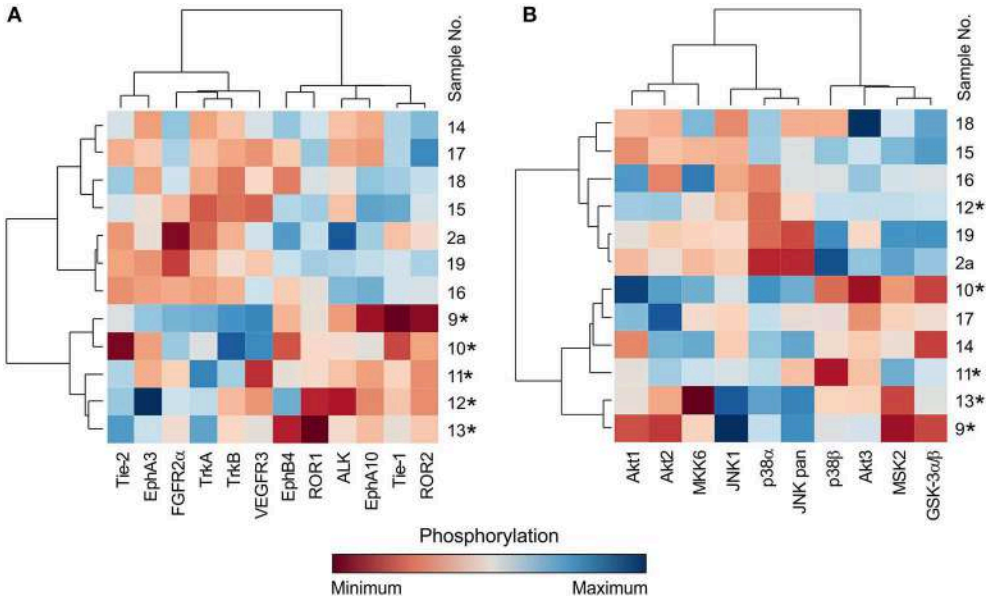

FIGURE 5 | Cluster analysis of phospho-RTK **(A)** and phospho-MAPK **(B)** array data. Samples were obtained from patients with neuroblastoma (marked with star) and different types of brain tumors. Filter $p < 0.05$ significance.

This experimental approach was also successfully used by our team in describing molecular targets and the subsequent effective treatment of several pediatric malignancies, such as Maffucci syndrome, which is characterized by multiple hemangiomas and enchondromas with a tendency to progress into malignancy (12), infantile myofibromatosis, in which PDGFR beta hyperphosphorylation is detected (13), or fibrodysplasia ossificans progressiva (14).

In addition to these individual cases, in this article, we summarize our experience with determining kinase phosphorylation profiles for single sample (**Figures 1**, **2**) and serial sample (**Figure 4**) analyses. The promising clinical response of patient No. 1 to sunitinib administration and the changes in serial kinase profiles after treatment with targeted low-molecular weight inhibitors (**Figure 4**) are other positive examples of the rational use of this experimental approach as a rapid screening method for the identification of druggable targets, which is a key part of personalized therapy. Nevertheless, as this method is not certified for diagnostic purposes, it is of high importance to employ another validation method to confirm the data from phospho-protein arrays independently.

Our data from the IHC validation showed good consistency in the levels of the phosphorylated forms of all three selected RTKs, i.e., phospho-EGFR, phospho-PDGFRβ, and phospho-InsR, as determined independently by IHC and the phospho-protein array (**Figure 2**). Similarly, data on the downstream signal transducers ERK and AKT showed moderate accordance (**Figure 3**), although the pan-phospho-ERK and pan-phospho-AKT antibodies were used for IHC detection, whereas isoform-specific antibodies against ERK1/2 or AKT1/2/3 were spotted onto the MAPK phospho-protein array. The same strategy, i.e., the validation of phosphorylated signal transducers as suitable targets by IHC, was successfully used for personalized treatment with low-molecular-weight inhibitors in malignant mesothelioma (24).

The most interesting finding from our study is the example of a cluster analysis performed in a cohort of 12 patients suffering from neuroblastomas or CNS tumors. In general, for the graphical presentation of results on differences among individual samples and their clusters, a heat map is the best choice (**Figure 5**). For the heat map display, data normalization is required, and the values range from −3 to 3 (23, 25). The same approach was used, and the hierarchical clustering of data from the MAPK phospho-protein arrays showed no distinct clusters for these tumor types (**Figure 5B**), whereas the same clustering method revealed significantly different patterns of the selected 12 RTKs in neuroblastomas and in the group of CNS tumors (**Figure 5A**). These interesting data will be reanalyzed in our forthcoming study on a large cohort of patients with neurogenic tumors; however, these results suggest another useful approach to employ the phospho-protein arrays in personalized therapy.

As apparent from all results presented in the current study as well as those from previously published data obtained by the same type of phospho-protein arrays, the key step in the use of these arrays for the identification of druggable molecular targets is the manner of data processing and interpretation. Comparative analyses of phosphorylation profiles in various tumor tissue samples are typically used in these studies: the analysis of 20 glioma cell lines and 14 tissue samples of primary glioblastoma multiforme can be used as an example (26). The categorization of achieved data into several groups according to the signal intensity is also a frequently used approach (21, 22, 27). Some of these groups are distinguished by different levels of positive signals, and the last one is considered negative. The

definition of a particular group can be described by specific categorization terms such as "strongly activated," "moderately activated," "activated to a lower extent," and "poorly activated" (22) or by a grading system similar to the IHC evaluation (27). A simplified binary view is able to distinguish positive or negative signals only, and thus activated and non-activated proteins can be described by this approach (10, 11, 24). In the first of these studies, all intensity values of the probes and the local background of the probes were $\log_2$ transformed (to obtain a more symmetrical distribution) and subtracted. In the next step, the mean of all obtained values was calculated for the individual array, and only the probes with values higher than the mean plus standard deviation (SD) were considered significantly activated (10). In the second study, the cut-off level for activated proteins was calculated as triple that of the highest negative control (24). In the last study, the cut-off level was not described (11).

In conclusion, our study showed the usefulness of phospho-protein arrays for the personalized treatment of patients suffering from relapsed/refractory solid tumors. From the clinical point of view, these arrays are especially suitable for the rapid screening of targets for treatment with low-molecular-weight inhibitors or monoclonal antibodies, although they can also be used for deep analyses of the differences in phosphorylation profiles among selected tumor types. These phospho-protein arrays are available for research use only, and they are not designated for *in vitro* diagnostic purposes. However, their apparent usefulness in the clinical consideration of druggable molecular targets within a specific tumor brings forward a demand for their validation also for diagnostic purposes.

DATA AVAILABILITY STATEMENT

The datasets generated for this study are available on request to the corresponding author.

ETHICS STATEMENT

This study was reviewed and approved by The Research Ethics Committee of the School of Medicine, Masaryk University (Brno, Czech Republic). Written informed consent was obtained from the minor(s)' legal guardian/next of kin for use of the biological samples and corresponding clinical data for research purposes, as well as for the publication of any potentially identifiable images or data included in this article.

AUTHOR CONTRIBUTIONS

JN, JSt, and RV designed the study. KP and JSt provided tumor samples and relevant clinical data. JN and PM performed phospho-protein arrays. LK performed immunohistochemical analyses. MK performed statistical analyses. JN and RV composed the manuscript. MK and JSk participated in data analyses and manuscript preparation. All authors reviewed and approved the final version of the manuscript.

FUNDING

This study was supported by project No. 16-34083A from the Ministry of Healthcare of the Czech Republic.

ACKNOWLEDGMENTS

The authors thank Lenka Zlamalikova and Kvetoslava Liskova for their technical assistance.

SUPPLEMENTARY MATERIAL

The Supplementary Material for this article can be found online at: https://www.frontiersin.org/articles/10.3389/fonc.2019.00930/full#supplementary-material

REFERENCES

1. Forrest SJ, Geoerger B, Janeway KA. Precision medicine in pediatric oncology. *Curr Opin Pediatr.* (2018) 30:17–24. doi: 10.1097/MOP.0000000000000570
2. Kalia M. Personalized oncology: recent advances and future challenges. *Metabolism.* (2013) 62:S11–4. doi: 10.1016/j.metabol.2012.08.016
3. Jackson SE, Chester JD. Personalised cancer medicine. *Int J Cancer.* (2015) 137:262–6. doi: 10.1002/ijc.28940
4. Fleuren ED, Versleijen-Jonkers YM, Heskamp S, van Herpen CM, Oyen WJ, van der Graaf WT, et al. Theranostic applications of antibodies in oncology. *Mol Oncol.* (2014) 8:799–812. doi: 10.1016/j.molonc.2014.03.010
5. Kalia M. Biomarkers for personalized oncology: recent advances and future challenges. *Metabolism.* (2015) 64:S16–21. doi: 10.1016/j.metabol.2014.10.027
6. Cossu-Rocca P, Contini M, Uras MG, Muroni MR, Pili F, Carru C, et al. Tyrosine kinase receptor status in endometrial stromal sarcoma: an immunohistochemical and genetic-molecular analysis. *Int J Gynecol Pathol.* (2012) 31:570–9. doi: 10.1097/PGP.0b013e31824fe289
7. Corbo V, Beghelli S, Bersani S, Antonello D, Talamini G, Brunelli M, et al. Pancreatic endocrine tumours: mutational and immunohistochemical survey of protein kinases reveals alterations in targetable kinases in cancer cell lines and rare primaries. *Ann Oncol.* (2012) 23:127–34. doi: 10.1093/annonc/mdr048
8. Matsumura Y, Umemura S, Ishii G, Tsuta K, Matsumoto S, Aokage K, et al. Expression profiling of receptor tyrosine kinases in high-grade neuroendocrine carcinoma of the lung: a comparative analysis with adenocarcinoma and squamous cell carcinoma. *J Cancer Res Clin Oncol.* (2015) 141:2159–70. doi: 10.1007/s00432-015-1989-z
9. Sun X, Song Q, He L, Yan L, Liu J, Zhang Q, et al. Receptor tyrosine kinase phosphorylation pattern-based multidrug combination is an effective approach for personalized cancer treatment. *Mol Cancer Ther.* (2016) 15:2508–20. doi: 10.1158/1535-7163.MCT-15-0735
10. Dewaele B, Floris G, Finalet-Ferreiro J, Fletcher CD, Coindre JM, Guillou L, et al. Coactivated platelet-derived growth factor receptor {alpha} and epidermal growth factor receptor are potential therapeutic targets in intimal sarcoma. *Cancer Res.* (2010) 70:7304–14. doi: 10.1158/0008-5472.CAN-10-1543
11. Montero JC, Esparís-Ogando A, Re-Louhau MF, Seoane S, Abad M, Calero R, et al. Active kinase profiling, genetic and pharmacological data define mTOR as an important common target in triple-negative breast cancer. *Oncogene.* (2014) 33:148–56. doi: 10.1038/onc.2012.572
12. Melicharkova K, Neradil J, Mudry P, Zitterbart K, Obermannova R, Skotakova J, et al. Profile of activation of tyrosine kinases and MAP kinases in therapy of maffucci syndrome. *Klin Onkol.* (2015) 28:2S47–51. doi: 10.14735/amko20152S47
13. Mudry P, Slaby O, Neradil J, Soukalova J, Melicharkova K, Rohleder O, et al. Case report: rapid and durable response to PDGFR targeted

therapy in a child with refractory multiple infantile myofibromatosis and a heterozygous germline mutation of the PDGFRB gene. *BMC Cancer.* (2017) 17:119. doi: 10.1186/s12885-017-3115-x
14. Rohleder O, Mudry P, Neradil J, Noskova H, Slaby O, Sterba J. et al., Early clinical observations on the use of imatinibmesylate in FOP: a report of seven cases. *Bone.* (2018) 116:171. doi: 10.1016/j.bone.2018.08.003
15. Schneider CA, Rasband WS, Eliceiri KW. NIH Image to ImageJ: 25 years of image analysis. *Nat Methods.* (2012) 9:671–5. doi: 10.1038/nmeth.2089
16. R Core Team. *R: A Language and Environment for Statistical Computing.* Vienna: R Foundation for Statistical Computing (2017). Available online at: https://www.r-project.org/ (accessed September 12, 2019).
17. Warnes GR, Bolker B, Bonebakker L, Gentleman R, Liaw WHA, Lumley T, et al. *Gplots: Various R Programming Tools for Plotting Data. R Package Version 3.0.1.* (2016). Available online at: https://cran.r-project.org/web/packages/gplots/index.html (accessed September 12, 2019).
18. Skoda J, Neradil J, Zitterbart K, Sterba J, Veselska R. EGFR signaling in the HGG-02 glioblastoma cell line with an unusual loss of EGFR gene copy. *Oncol Rep.* (2014) 31:480–7. doi: 10.3892/or.2013.2864
19. Patwardhan PP, Musi E, Schwartz GK. Preclinical evaluation of nintedanib, a triple angiokinase inhibitor, in soft-tissue sarcoma: potential therapeutic implication for synovial sarcoma. *Mol Cancer Ther.* (2018) 17:2329–40. doi: 10.1158/1535-7163.MCT-18-0319
20. Regad T. Targeting RTK signaling pathways in cancer. *Cancers.* (2015) 7:1758–84. doi: 10.3390/cancers7030860
21. Stacchiotti S, Tamborini E, Marrari A, Brich S, Rota SA, Orsenigo M, et al. Response to sunitinib malate in advanced alveolar soft part sarcoma. *Clin Cancer Res.* (2009) 15:1096–104. doi: 10.1158/1078-0432.CCR-08-2050
22. Stacchiotti S, Negri T, Palassini E, Conca E, Gronchi A, Morosi C, et al. Sunitinib malate and figitumumab in solitary fibrous tumor: patterns and molecular bases of tumor response. *Mol Cancer Ther.* (2010) 9:1286–97. doi: 10.1158/1535-7163.MCT-09-1205
23. Guo T, Lee SS, Ng WH, Zhu Y, Gan CS, Zhu J, et al. Global molecular dysfunctions in gastric cancer revealed by an integrated analysis of the phosphoproteome and transcriptome. *Cell Mol Life Sci.* (2011) 68:1983–2002. doi: 10.1007/s00018-010-0545-x
24. Kawaguchi K, Murakami H, Taniguchi T, Fujii M, Kawata S, Fukui T, et al. Combined inhibition of MET and EGFR suppresses proliferation of malignant mesothelioma cells. *Carcinogenesis.* (2009) 30:1097–105. doi: 10.1093/carcin/bgp097
25. Lee H, Bennett AM. Receptor protein tyrosine phosphatase-receptor tyrosine kinase substrate screen identifies EphA2 as a target for LAR in cell migration. *Mol Cell Biol.* (2013) 33:1430–41. doi: 10.1128/MCB.01708-12
26. Stommel JM, Kimmelman AC, Ying H, Nabioullin R, Ponugoti AH, Wiedemeyer R, et al. Coactivation of receptor tyrosine kinases affects the response of tumor cells to targeted therapies. *Science.* (2007) 318:287–90. doi: 10.1126/science.1142946
27. Zhang YX, van Oosterwijk JG, Sicinska E, Moss S, Remillard SP, van Wezel T, et al. Functional profiling of receptor tyrosine kinases and downstream signaling in human chondrosarcomas identifies pathways for rational targeted therapy. *Clin Cancer Res.* (2013) 19:3796–807. doi: 10.1158/1078-0432.CCR-12-3647

Conflict of Interest: The authors declare that the research was conducted in the absence of any commercial or financial relationships that could be construed as a potential conflict of interest.

frontiers in Oncology

ORIGINAL RESEARCH
published: 25 October 2019
doi: 10.3389/fonc.2019.01063

Coagulation FXIII-A Protein Expression Defines Three Novel Sub-populations in Pediatric B-Cell Progenitor Acute Lymphoblastic Leukemia Characterized by Distinct Gene Expression Signatures

Katalin Gyurina[1], Bettina Kárai[2], Anikó Ujfalusi[2], Zsuzsanna Hevessy[2], Gábor Barna[3], Pál Jáksó[4], Gyöngyi Pálfi-Mészáros[5], Szilárd Póliska[6], Beáta Scholtz[6], János Kappelmayer[2], Gábor Zahuczky[5†] and Csongor Kiss[1*†]*

[1] Department of Pediatrics, University of Debrecen, Debrecen, Hungary, [2] Department of Laboratory of Medicine, University of Debrecen, Debrecen, Hungary, [3] 1st Department of Pathology and Experimental Cancer Research, Semmelweis University, Budapest, Hungary, [4] Department of Pathology, University of Pécs, Pécs, Hungary, [5] UD GenoMed Medical Genomic Technologies Ltd., Debrecen, Hungary, [6] Genomic Medicine and Bioinformatic Core Facility, Department of Biochemistry and Molecular Biology, Faculty of Medicine, University of Debrecen, Debrecen, Hungary

Background: Leukemic B-cell precursor (BCP) lymphoblasts were identified as a novel expression site for coagulation factor XIII subunit A (FXIII-A). Flow cytometry (FC) revealed three distinct expression patterns, i.e., FXIII-A negative, FXIII-A dim, and FXIII-A bright subgroups. The FXIII-A negative subgroup was significantly associated with the "B-other" genetic category and had an unfavorable disease outcome.

Methods: RNA was extracted from bone marrow lymphoblasts of 42 pediatric patients with BCP-acute lymphoblastic leukemia (ALL). FXIII-A expression was determined by multiparameter FC. Genetic diagnosis was based on conventional cytogenetic method and fluorescence *in situ* hybridization. Affymetrix GeneChip Human Primeview array was used to analyze global expression pattern of 28,869 well-annotated genes. Microarray data were analyzed by Genespring GX14.9.1 software. Gene Ontology analysis was performed using Cytoscape 3.4.0 software with ClueGO application. Selected differentially expressed genes were validated by RT-Q-PCR.

Results: We demonstrated, for the first time, the general expression of *F13A1* gene in pediatric BCP-ALL samples. The intensity of *F13A1* expression corresponded to the FXIII-A protein expression subgroups which defined three characteristic and distinct gene expression signatures detected by Affymetrix oligonucleotide microarrays. Relative gene expression intensity of *ANGPTL2*, *EHMT1 FOXO1, HAP1, NUCKS1*, *NUP43, PIK3CG, RAPGEF5*, *SEMA6A, SPIN1, TRH,* and *WASF2* followed the pattern of change in the intensity of the expression of the *F13A1* gene. Common enhancer elements of these genes revealed by *in silico* analysis suggest that common transcription factors may regulate the expression of these genes in a similar fashion. *PLAC8* was downregulated in the FXIII-A bright subgroup. Gene expression signature of the FXIII-A negative subgroup

OPEN ACCESS

Edited by:
Jaroslav Sterba,
Masaryk University, Czechia

Reviewed by:
Min Hee Kang,
Texas Tech University Health Sciences Center, United States
Justin Vareecal Joseph,
Aarhus University, Denmark

***Correspondence:**
Gábor Zahuczky
zahu@ud-genomed.hu
Csongor Kiss
kisscs@med.unideb.hu

[†]These authors have contributed equally to this work

Specialty section:
This article was submitted to Cancer Molecular Targets and Therapeutics, a section of the journal Frontiers in Oncology

Received: 19 July 2019
Accepted: 30 September 2019
Published: 25 October 2019

Citation:
Gyurina K, Kárai B, Ujfalusi A, Hevessy Z, Barna G, Jáksó P, Pálfi-Mészáros G, Póliska S, Scholtz B, Kappelmayer J, Zahuczky G and Kiss C (2019) Coagulation FXIII-A Protein Expression Defines Three Novel Sub-populations in Pediatric B-Cell Progenitor Acute Lymphoblastic Leukemia Characterized by Distinct Gene Expression Signatures. Front. Oncol. 9:1063. doi: 10.3389/fonc.2019.01063

showed an overlap with the signature of "B-other" samples. *DFFA, GIGYF1, GIGYF2*, and *INTS3* were upregulated and *CD3G* was downregulated in the "B-other" subgroup. Validated genes proved biologically and clinically relevant. We described differential expression of genes not shown previously to be associated with pediatric BCP-ALL.

Conclusions: Gene expression signature according to FXIII-A protein expression status defined three novel subgroups of pediatric BCP-ALL. Multiparameter FC appears to be an easy-to-use and affordable method to help in selecting FXIII-A negative patients who require a more elaborate and expensive molecular genetic investigation to design precision treatment.

Keywords: pediatric BCP-ALL, FXIII-A, *F13A1*, gene expression signature, B-other genotype, oligonucleotide microarray, RT-Q-PCR

INTRODUCTION

According to current knowledge, acute lymphoblastic leukemia (ALL) can be best characterized by an integrated set of clinical, pathological, morphologic, immunophenotypic, and genetic properties. Detailed characterization of the neoplastic clones of children with ALL allowed the development of highly effective risk-tailored therapies. Introduction of advanced diagnostic tools helped in identifying an increasing number of molecular targets and may contribute to the application of personalized treatment offering cure for each individual patient. Recurrent genetic aberrations represent the basis of the classification of ALL according to the 4th edition of the WHO Classification of Tumors of Hematopoietic and Lymphoid Tissues in 2008, and its 2016 revision (1, 2). Gene expression profiling by oligonucleotide microarray was shown to contribute to conventional and molecular cytogenetics by improving diagnostic accuracy and prognostic relevance as well as by defining new entities. The "B-other" genetic subgroup, i.e., BCP-ALL cases without established recurrent genetic abnormalities exhibits alterations to be revealed by advanced genomic technologies. Within "B-other" ALL, Philadelphia-like (Ph-like) or *BCR-ABL1*-like ALL, a provisional entity of the 2016 revision of the WHO classification, has been defined based on gene expression signature similar to Ph-positive/*BCR-ABL1*-positive ALL and characteristically distinct from the rest of BCP-ALL cases ("non-B-other") (3–6). Recently, fourteen B-cell precursor (BCP)-ALL subgroups were defined by analyzing a large sample set of an international study using RNA-sequencing. The study revealed six new subgroups in addition to previously identified ones demonstrating the diagnostic utility and prognostic power of gene expression studies in pediatric BCP-ALL (7).

Our group identified BCP-ALL blasts as a new expression site for coagulation factor XIII subunit A (FXIII-A). In contrast to the BCP-ALL blasts, neither normal bone marrow B-cell progenitors, nor mature B-cells, both normal and leukemic once, nor T-lymphoblasts/lymphocytes express FXIII-A (8). We observed three characteristic expression patterns by flow cytometry (FC): FXIII-A negative, FXIII-A dim, and FXIII-A bright lymphoblasts with about two thirds of pediatric BCP-ALL patients representing FXIII-A positive (FXIII-A dim and bright) cases. According to our retrospective clinical investigation, patients with FXIII-A negative lymphoblasts had significantly worse event-free and overall survival than patients with FXIII-A positive lymphoblasts. Moreover, the "B-other" genetic subtype was significantly more frequent within the FXIII-A negative than in the FXIII-A positive subgroup (9). The prognostic importance of FXIII-A expression by FC was confirmed and further specified in a recently concluded prospective study suggesting a favorable prognostic effect of the FXIII-A dim expression pattern within the FXIII-A positive subgroup (unpublished results). Here we present results, for the first time, on gene expression signatures associated with the three characteristic FXIII-A protein expression patterns. In addition, we investigated overlaps between the gene expression profile of the FXIII-A negative protein expression subgroup with the gene expression profile of the "B-other" subgroup.

MATERIALS AND METHODS

Patients

Samples were collected from pediatric patients with BCP-ALL treated in four Hungarian Pediatric Hematology and Oncology Departments (University of Debrecen, Debrecen; Semmelweis University, Budapest; University of Pécs, Pécs; BAZ Country Hospital and University Teaching Hospital, Miskolc) between September 1, 2015 and August 31, 2018. Patients were treated according to BFM ALL-IC 2009 clinical trial (EuDraCT No: 2010-019722-13). Patients with *BCR-ABL1* rearrangement [$t_{(9,22)}$] were excluded, since they were not treated according to BFM ALL-IC 2009 protocol. Quantitatively and qualitatively suitable RNA was separated from 42 patients with FXIII-A negative (14), FXIII-A dim (21), and FXIII-A bright (7) BCP-ALL.

Excess bone marrow (BM) samples were collected after signed informed consent obtained from study participants and their legal caregivers. The study was approved by the Scientific Research Ethical Committee ("TUKEB") of the Medical Research Council of Hungary: No. 43033-1/2014/EUK(423/2014) and was carried out according to the Code of Ethics of the World Medical Association and the ethical standards of the 2000 Revision of the Helsinki Declaration.

Immunophenotype Analysis

The FXIII-A expression pattern was determined by multiparameter FC analysis as published before (9). Bone marrow samples were examined for the following antibody combination: cytoplasmic FXIII-A(FITC)–CD10(PE)–CD45(PerCP-Cy5.5)–CD19(APC)–CD19(PECY7). CD19, CD45 markers were purchased from Becton Dickinson Biosciences (San Jose, CA, USA), CD10 marker were purchased from DAKO (Glostrup, Denmark), CD19(PECY7) marker were purchased from Sony Biotechnology (San Jose, CA, USA). Generation and fluorescent isotihocyanate (FITC) labeling of mouse monoclonal antibody against FXIII-A was carried out as previously described (10). One-hundred thousand events were acquired with the help of FacsCanto-II (Becton Dickinson Biosciences, San Jose, CA, USA) and Navios (Beckman Coulter, Brea, CA, USA) flow cytometers. According to the intensity of FXIII-A expression, patients were assigned to three groups: BCP-ALL with FXIII-A negative blasts (<20% FXIII-A positive lymphoblasts; FXIII-A negative group), BCP-ALL with moderate FXIII-A expression (20–79% FXIII-A positive lymphoblasts; FXIII-A dim group), and BCP-ALL with strong FXIII-A expression (≥80% FXIII-A positive lymphoblasts; FXIII-A bright group). To determine FXIII-A expression of leukemic cells, normal residual lymphocytes served as a negative control.

FC data were analyzed by FACSDiva (Becton Dickinson, Franklin Lakes, NJ, USA) or Kaluza (Beckman Coulter, Brea, CA, USA) softwares. Flow cytometers were subjected to daily performance checks, using Cytometer Setup and Tracking (Becton Dickinson, Franklin Lakes, NJ, USA) or Flow Check Pro (Beckman Coulter, Brea, CA, USA) fluorescent microbeads.

Genetic Investigations

Cytogenetic analysis was performed on unstimulated 24 h cultures of BM according to standard protocol. Fluorescence *in situ* hybridization (FISH) was carried out on cells from the same BM samples using commercially available probe sets (*BCR-ABL, ETV6-RUNX1, KMT2A)*. Patients with $t_{(12,21)}$/*ETV6/RUNX1* or high hyperdiploidy (51–65 chromosome number) were considered as low-risk group. The high-risk group consisted of patients with *KMT2A* rearrangements, iAMP21, complex karyotype, near haploidy (chromosome number 23–29), and low hypodiploidy (chromosome number <45). Patients with $t_{(1,19)}$, and all other genetic subgroups not fitting in the low- and high-risk categories, including the "B-other" subgroup were considered as intermediate-risk group (6, 11).

RNA Preparation

Excess BM samples from BCP-ALL patients were collected into PAXgene Blood RNA Plastic Tube (PreAnaltyX, Hombrechtikon, Switzerland). Total cellular RNA was isolated using PAXgene Blood miRNA Kit (PreAnalityX) according to conventional protocol. Qualitative and quantitative analyses of RNA were performed using Agilent Bioanalyzer (Agilent Technologies, La Jolla, CA, USA). Samples with an RNA Integrity number above 8.0 were used in MicroArray analysis.

Microarray Analysis

Affymetrix GeneChip Human Primeview array (Affymetrix, Santa Clara, CA, USA) was used to analyze global expression pattern of 28,869 well-annotated genes. 3'IVT Expression Kit (Affymetrix) and GeneChip WT Terminal Labeling and Control Kit (Affymetrix) were used for amplifying and labeling 250 ng of RNA samples. Samples were hybridized at 45°C for 16 h and then standard washing protocol was performed using GeneChip Fluidics Station 450 (Affymetrix) and the arrays were scanned on GeneChip Scanner 7G (Affymetrix) procedure. Data of this study have been deposited in NCBI's Gene Expression Omnibus and are accessible through GEO Series accession number GSE134480 (https://www.ncbi.nlm.nih.gov/geo/query/acc.cgi?acc=GSE134480).

Gene Ontology Analysis

Gene Ontology (GO) analysis was performed using Cytoscape 3.4.0 software (cytoscape.org) with ClueGO application. The settings were the following: GO biological process and GO immune system process. For statistical analysis two-sided hypergeometric test and Benjamini-Hochberg FDR were used. Significantly enriched GO categories were considered to p-value <0.05 and κ score <0.4.

Real Time Quantitative Polymerase Chain Reaction (RT-Q-PCR) Validation of Microarray Data

For RT-Q-PCR validation of microarray data pre-designed, factory-loaded 384-well TaqMan low-density array (ThermoFisher Scientific, Waltham, MA, USA) was used to determine the level of expression of selected genes using technical duplicates. Genes for validation were selected based on fold-changes (with fold-changes >2.0 cut-off) between any of the pre-defined subgroups and based on putative biological and clinical relevance of gene functions as defined by GO analysis data (**Table 1**). RT-Q-PCR expression levels of target genes were normalized to the mean of *B2M*, *GAPDH*, and *GUSB* reference genes. Normalized gene expression values were calculated based on the ΔC_t method, where relative expression equals $2^{-\Delta Ct}$, where ΔC_t represents the threshold cycle (C_t) of the target minus that of the mean of reference genes.

In silico Investigation of Validated DE Genes

Interactions of validated genes and *F13A1* gene were investigated using STRING v11. (12) and GeneHancer (13) databases. STRING v11 database contains putative protein-protein interactions predicted on a well-defined score system. GeneHancer portrays 285 000 integrated candidate enhancers and subsequently links enhancers to genes.

Statistical Analysis

Microarray data were analyzed by Genespring GX14.9.1 software (Agilent Technologies, La Jolla, CA, USA). To identify statistically significant genes, we used volcano plot analysis. The resulting scatterplot showed statistical significance (p-value) vs. magnitude of change (fold-change).

TABLE 1 | Genes selected for validation by RT-Q-PCR based either on gene expression fold-changes detected by Affymetrix Microarray (in bold characters) or based on selected GO annotations.

Genes selected for validation	Fold changes detected by Affymetrix MicroArray			GO annotations
	FXIII-A negative/FXIII-A dim	FXIII-A negative/FXIII-A bright	FXIII-A bright/FXIII-A dim	
WASF2	**0.94**	**0.50**	**0.53**	**Angiogenesis**
BCL2L1	0.79	0.60	0.75	Apoptosis regulation
CASP2	0.90	0.79	0.88	Apoptosis regulation
DFFA	0.33	0.39	1.19	Apoptosis regulation
PAK2	1.91	1.07	0.56	Apoptosis regulation
PIK3CG	1.58	1.62	1.03	Apoptosis regulation
PKN2	1.43	1.26	0.88	Apoptosis regulation
SEMA6A	**1.06**	**2.38**	**2.23**	**Apoptotic process**
CLSTN1	**0.51**	**0.45**	**0.88**	**Calcium ion binding**
IL7R	1.03	0.98	0.94	Cell differentiation
PLAC8	1.30	1.33	1.02	Cell differentiation
RORA	0.92	1.01	1.10	Cell differentiation
NUCKS1	**1.56**	**1.41**	**0.90**	**Cell differentiation**
TRH	**2.05**	**1.64**	**0.80**	**Cell-cell signaling**
FOXO1	1.53	1.28	0.84	Cellular response to glucocorticoid stimulus
CX3CR1	0.83	1.63	1.97	Chemokine receptor activity
EHMT1*	1.18	1.22	1.03	Chromatin modification
ING5*	0.97	1.25	1.29	Chromatin modification
JMJD1C	0.97	0.67	0.69	Chromatin modification
WAC	1.24	1.50	1.21	Chromatin modification
SART3	5.90	2.55	0.43	Chromatin modification
MDM2*	**1.28**	**1.14**	**0.89**	**Identical protein binding**
GIGYF1	3.84	5.07	1.32	Insulin-like growth factor receptor signaling pathway
GIGYF2	1.08	1.06	0.98	Insulin-like growth factor receptor signaling pathway
TAOK1	**4.60**	**2.67**	**0.58**	**Kinase activity**
SPIN1	**1.28**	**1.27**	**0.99**	**Methylated histone binding**
MAP4	**1.29**	**1.19**	**0.92**	**Microtubule binding**
AKAP13	1.14	1.16	1.02	Nuclear export
KHDRBS1	1.66	1.21	0.73	Nuclear export
MAGOH	1.35	1.25	0.92	Nuclear export
NUP43*	1.12	1.00	0.89	Nuclear export
ZC3H11A	**12.64**	**3.37**	**0.27**	**Nuclear export**
POLDIP3	1.60	1.48	0.92	Nuclear export
SRSF5	1.14	1.28	1.12	Nuclear export
FGFR1OP	7.20	2.50	0.35	Nuclear export
HAP1	1.07	0.86	0.80	Post-transcriptional regulation of gene expression
F13A1	**1.86**	**1.60**	**0.86**	**Protein-glutamine gamma-glutamyltransferase activity**
CCL5	1.16	1.12	0.97	Protein homodimerization
CD3G	0.80	0.65	0.81	Protein heterodimerization
RAPGEF5	**1.35**	**1.22**	**0.90**	**Ras signaling pathway**
ANGPTL2	**16.94**	**2.89**	**0.17**	**Signaling receptor binding**
DHX36	0.83	0.80	0.96	Translation regulation
INTS3	17.71	3.41	0.19	Translation regulation
RC3H1	0.69	0.46	0.67	Translation regulation
SECISBP2L	1.45	1.54	1.06	Translation regulation

For definition of the three different FXIII-A expression groups see text.

*Genes marked in * have also been listed under the GO term: peptidyl-lysine modification (GO:0018205).*

TABLE 2 | Clinical and pathological characterization of patiens with BCP-ALL.

Patient ID code	Sex	Age (years)	Initial WBC (G/L)	Ratio of FXIII-A positive cells (%)	Genetic category	Outcome (dead/alive)
cALL_RNS_13	M	8	3.9	10.9	iAMP21	Dead
cALL_RNS_14	M	11	19	1.4	B-other	Dead
cALL_RNS_15	M	3	5.9	5.1	B-other	Alive
cALL_RNS_16	M	2	23.38	0.9	Hyperdiploid	Dead
cALL_RNS_17	F	4	25.9	1.7	B-other	Alive
cALL_RNS_26	M	0	8.33	2	Hyperdiploid	Alive
cALL_RNS_33	F	12	22.6	5	B-other	Alive
cALL_RNS_34	F	13	98.8	13	B-other	Alive
cALL_RNS_35	M	2	10.45	1.8	ETV6/RUNX1	Alive
cALL_RNS_36	F	1	11.03	4	TCF3/PBX1	Alive
cALL_RNS_53	M	2	5.51	11.4	B-other	Dead
cALL_RNS_54	F	3	18.33	8.4	B-other	Dead
cALL_RNS_18	M	2	5.9	1.1	Hyperdiploid	Alive
cALL_RNS_19	M	3	15.9	10.6	KMT2A	Alive
cALL_RNS_45	F	1	11.37	28.8	B-other	Dead
cALL_RNS_46	F	1	5.71	32.6	ETV6/RUNX1	Dead
cALL_RNS_47	M	0	377	23	KMT2A	Alive
cALL_RNS_58	F	4	12.14	41	Hyperdiploid	Alive
cALL_RNS_59	F	3	4.4	48.9	Hyperdiploid	Alive
cALL_RNS_60	M	6	3.31	34.6	Hyperdiploid	Alive
cALL_RNS_61	M	4	8.9	52	ETV6/RUNX1	Alive
cALL_RNS_62	F	2	21.91	71.9	Hyperdiploid	Alive
cALL_RNS_63	M	3	3.62	45	ETV6/RUNX1	Alive
cALL_RNS_64	F	2	5.3	71.9	ETV6/RUNX1	Alive
cALL_RNS_44	M	8	19.73	76.8	Hyperdiploid	Alive
cALL_RNS_50	M	3	7.28	59.6	B-other	Alive
cALL_RNS_52	F	3	83.69	58	B-other	Alive
cALL_RNS_55	F	2	12.34	56	Hyperdiploid	Dead
cALL_RNS_56	M	12	10.5	24.9	B-other	Dead
cALL_RNS_57	F	7	1.33	35.6	Hyperdiploid	Alive
cALL_RNS_51	F	16	12.38	25	B-other	Alive
cALL_RNS_49	M	2	14.5	22.4	B-other	Alive
cALL_RNS_02	F	10	6.51	95	B-other	Dead
cALL_RNS_03	F	15	5.64	72.5	Hyperdiploid	Alive
cALL_RNS_04	F	5	5.1	69	ETV6/RUNX1	Alive
cALL_RNS_01	F	1	222.8	85	B-other	Dead
cALL_RNS_05	F	12	19.54	95	ETV6/RUNX1	Alive
cALL_RNS_06	F	16	48.55	94	KMT2A	Alive
cALL_RNS_07	F	5	61.6	88	ETV6/RUNX1	Alive
cALL_RNS_08	F	2	2.72	91	Hyperdiploid	Alive
cALL_RNS_09	F	4	8.12	82.3	ETV6/RUNX1	Alive
cALL_RNS_37	M	16	20.1	98.9	Hyperdiploid	Alive

Affymetrix data files were imported using the Robust Multi-Array Average algorithm and median normalization was performed. To identify differentially expressed genes between pre-defined data sets, statistical analysis was performed using ANOVA with Tukey *post-hoc* test (14) and moderated *T*-test, Benjamini-Hochberg False Discovery Rate was used for multiple testing corrections, p-value <0.05 was considered as significant difference.

RESULTS

Characterization of Samples of Children With BCP-ALL

RNA samples obtained from 42 pediatric patients with BCP-ALL were used for gene expression profiling investigations (**Table 2**). Cytoplasmic expression pattern of FXIII-A by FC successfully divided patients into three categories: patients with

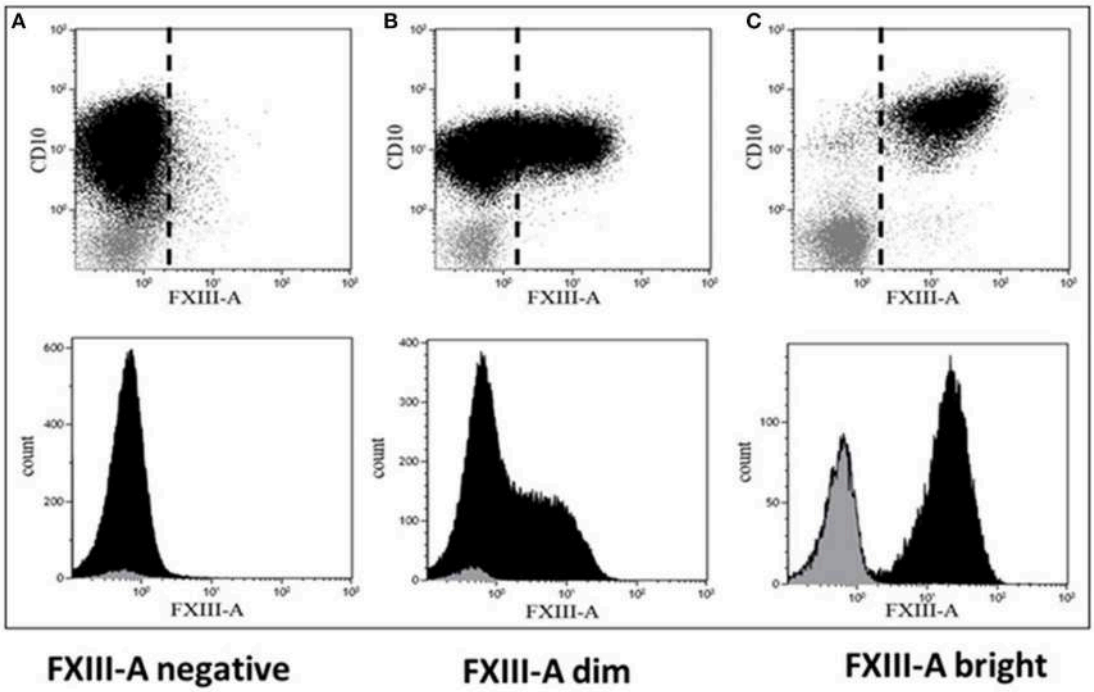

FIGURE 1 | Representative dot plots and histograms of leukemic lymphoblasts. There are three different patterns of cytoplasmic FXIII-A expression in terms of positivity of leukemic lymphoblasts: **(A)** negative expression pattern below 20%, **(B)** dim expression pattern between 20 and 80%, and **(C)** bright expression pattern ≥80% of leukemic lymphoblasts (black) with a FXIII-A staining exceeding the intensity of negative controls, i.e., residual normal lymphocytes (gray). Based on FXIII-A expression intensity of normal residual lymphocytes, the threshold of positivity is marked by the dashed line on the respective dot-plots (upper quadrants). The intensity of the FXIII-A expression increased continuously, as the histogram of lymphoblasts with dim expression pattern shows (**B**, lower quadrant), which excludes the existence of a distinct FXIII-A negative and a FXIII-A bright sub-population.

FXIII-A negative, FXIII-A dim and FXIII-A bright BCP-ALL. Representative FC dot plots and histograms are shown in **Figure 1**. Regarding genetic categories, 27 patients had recurrent genetic abnormalities and 15 patients were assigned to the "B-other" subgroup: 7/12 FXIII-A negative patients, 6/21 FXIII-A dim patients, and 2/7 FXIII-A bright patients.

Gene Expression Profiles of BCP-ALL Samples

Differentially expressed (DE) genes were identified using two distinctive features: FXIII-A protein expression determined by FC and "B-other" status. DE genes were screened by volcano plot filtering. There were 26 genes found when comparing the FXIII-A negative with the FXIII-A bright subgroup. The FXIII-A dim vs. bright comparison resulted in 155 DE genes and there were 88 DE genes identified between the FXIII-A negative and dim subgroups. With the exception of one to two outliers within the respective groups, heat map analysis exhibited three different patterns of gene expression for each, FXIII-A negative, FXIII-A dim, and FXIII-A bright subgroup. Importantly, FXIII-A negative and bright samples clustered close together and were well-separated from the FXIII-A dim subgroup (**Figure 2**).

Comparing the gene expression signature of the "B-other" subgroup with the rest of patient samples, the so called "non-B-other" group, 142 DE genes were found after filtering to 1.5-fold-change. Heat map analysis clearly showed two distinct sub-populations: gene expression signature of the "B-other" subgroup differed characteristically from the gene expression signature of the "non-B-other" subgroup (**Figure 3**). Then we investigated how DE genes, characteristic for "B-other" status, were related to DE genes of subgroups according to FXIII-A expression pattern. We found 32 DE genes expressing exclusively in the FXIII-A negative and "B-other" group vs. FXIII-A negative and the "non-B-other" group. Heat map analysis confirmed that, with the exception of one outlier, gene expression profile characterizing FXIII-A negative samples overlapped with gene expression profile characterizing samples of the "B-other" subgroup (**Figure 4**).

Functional Characterization of Differentially Expressed Genes in the BCP-ALL Subgroups

Identification of enriched functional categories according to the FXIII-A protein expression pattern, DE genes were categorized into 156 GO processes. Nevertheless, most of them, in particular those with the strongest statistical *p*-values, were related to epigenetic and/or gene expression regulatory processes such as histone modification, chromatin organization, RNA destabilization, post-transcriptional regulation of gene expression, etc., or other regulatory and cellular processes, such

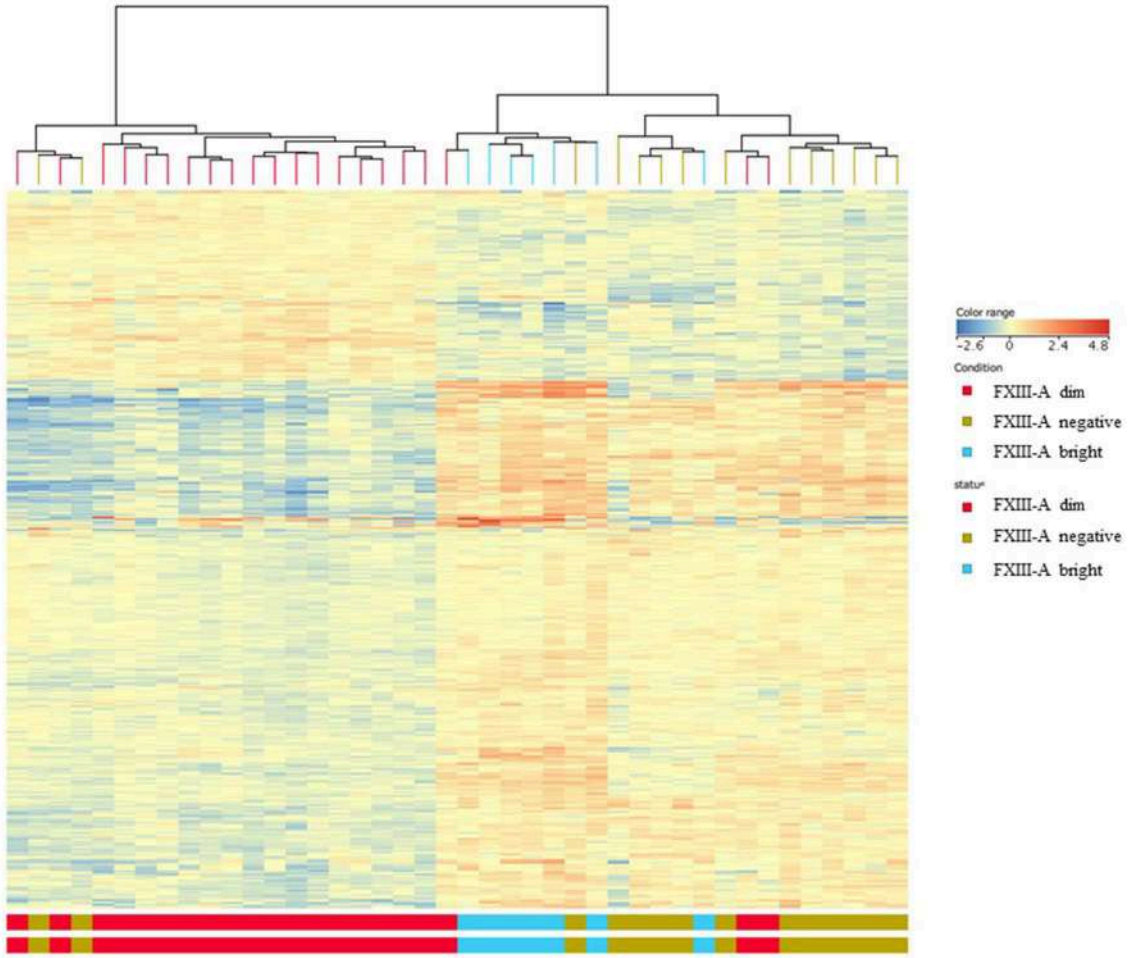

FIGURE 2 | Gene expression signatures according to FXIII-A protein expression; heat map analysis. With the exception of one to two outliers within the respective groups, heat map analysis exhibited three different patterns of gene expression for each, FXIII-A negative (green color), FXIII-A dim (red color), and FXIII-A bright (blue color) subgroups.

as apoptosis and morphogenesis (**Supplementary Table 1**). In addition, we identified biological processes resulting in peptidyl-lysine modification, which are in relation with the known physiological function of FXIII-A catalyzing the formation of γ-glutamyl-ε-lysyl amide crosslinks between fibrin monomers to form an insoluble clot (**Supplementary Table 1**).

In the "B-other" status comparison of DE genes with a fold-change >2.0, much less GO processes were identified than according to the FXIII-A status comparison. Genes involved in lymphocyte and T-cell apoptotic processes (*CCL5, CD3G, IL7R, PLAC8*) were over-presented, as well as two others, *CX3CR1*, *RORA*, corresponding to macrophage migration. When decreasing the filtering threshold to fold-change >1.5, additional biological processes proved significant represented by the following genes, *BCL10, CX3CR1, GNLY, PTPRC, STK4, TNFSF10, ATP2B1, DNAJC3, PLAC8, THRA, MAPKBP1, PER1, RORA, USP32, CCL5, GNG2, PLCB3, BCL10, CCL5, CD3G, IL7R* (**Supplementary Table 2**).

Validation of Global Transcriptomics Data

From the oligonucleotide microarray results of DE genes, either according to FXIII-A expression status or according to "B-other" genetic status we selected 45 genes for validation by RT-Q-PCR. Selection of 13/45 genes was based on fold change results, whereas an additional 32/45 genes were selected according to enriched functional categories of potential interest as defined by the GO analysis (**Table 1**). We were not able to detect transcripts of *RORA* by RT-Q-PCR which might have a technical reason.

FXIII-A Expression-Based Results

Expression of *F13A1* gene was detected and readily validated by RT-Q-PCR in every sample. Intensity of gene expression; however, was characteristically different among samples of the three different FXIII-A protein expression subgroups with an increasing intensity in terms of relative fold-changes measured

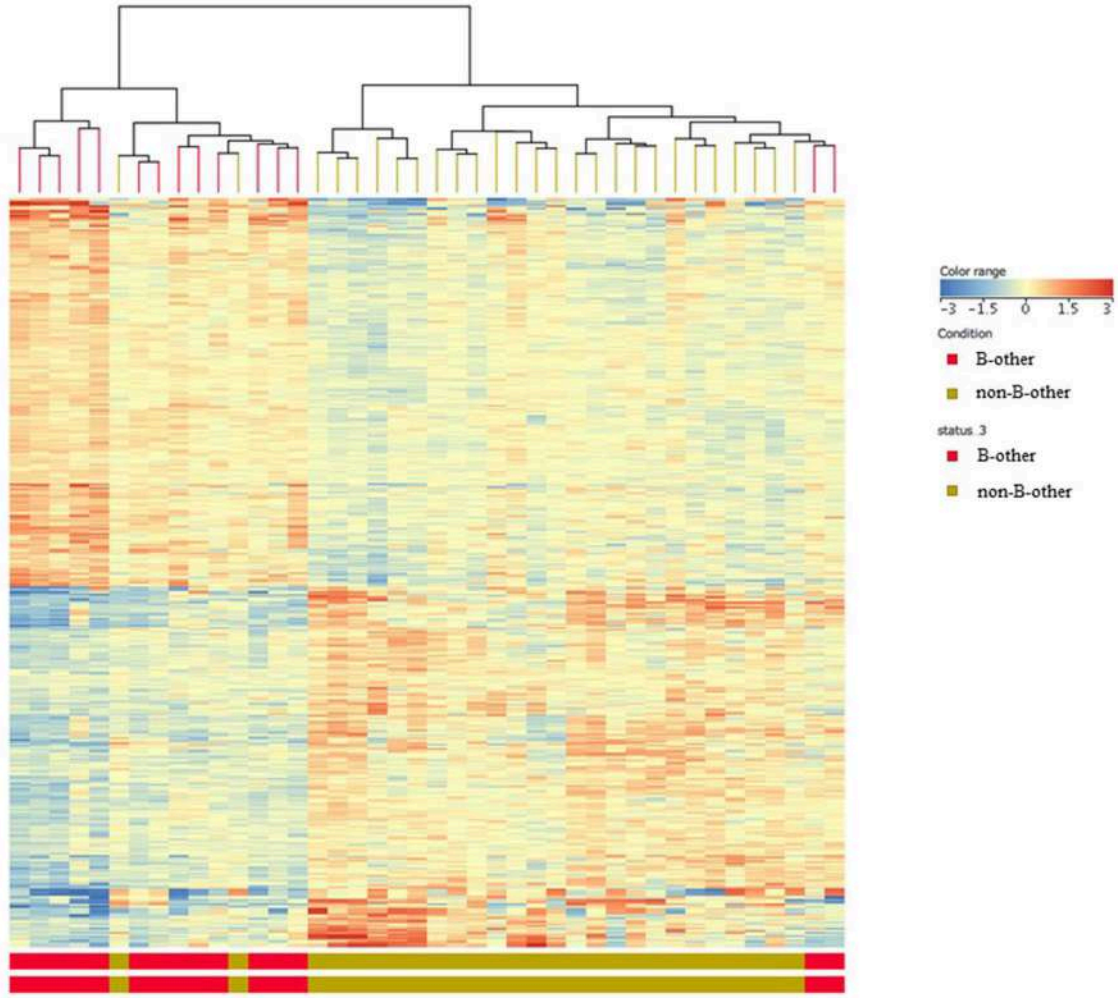

FIGURE 3 | Gene expression signatures according to "B-other" status; heat map analysis. Heat map analysis clearly showed two distinct sub-populations: gene expression signature of the "B-other" subgroup (red color) differed characteristically from the gene expression signature of the rest of samples, the "non-B-other" subgroup (green color).

by RT-Q-PCR from the FXIII-A negative, through dim to bright subgroups (**Figure 5**).

Similarly, most of the genes (8/13 $p < 0.05$, 9/13 $p < 0.10$) from the group selected on the basis of highest fold changes between any two groups among FXIII-A negative, dim and bright groups according to the microarray results were validated by RT-Q-PCR. Of the 25 genes selected on basis of functional significance according to GO analysis, four genes could be validated. Within the GO group of translation regulation there were 2/6 with $p < 0.05$, and 3/6 with $p < 0.10$ (**Table 3**) genes that could be validated, providing a considerably better ratio than it was found in the subgroups of apoptosis regulation (0/3), chromatin modification (1/5), and nuclear export (0/5) (**Tables 1**, **3**). Generally, fold-changes were enhanced in RT-Q-PCR compared to microarray data (**Supplementary Table 3**). *PLAC8* and *HAP1* represent impressive examples. DE of *PLAC8*, a placenta-specific gene of unrevealed function, was not found significant by microarray but turned out significant upon validation. *HAP1,* a member of the translation regulation GO group, exhibited a very slight overexpression by microarray and it proved much stronger by RT-Q-PCR.

Considering individual normalized gene expression values, in most of the cases, there was a clear trend of a continuous increase from FXIII-A negative through dim to bright subgroups that was endogenously validated by the *F13A1* relative expression. *ANGPTL2*, *NUCKS1*, *RAPGEF5*, and *SEMA6A* followed this trend (**Figure 5**). Relative fold-changes were similar whether determined by microarray measurements or RT-Q-PCR. In case of *FOXO1*, *HAP1*, and *TRH,* separation of the bright subgroup from the other two subgroups seemed more prominent and showed a relatively higher fold-change value as determined by RT-Q-PCR than compared to the microarray results. With the exception of *PLAC8,* validated DE genes were downregulated

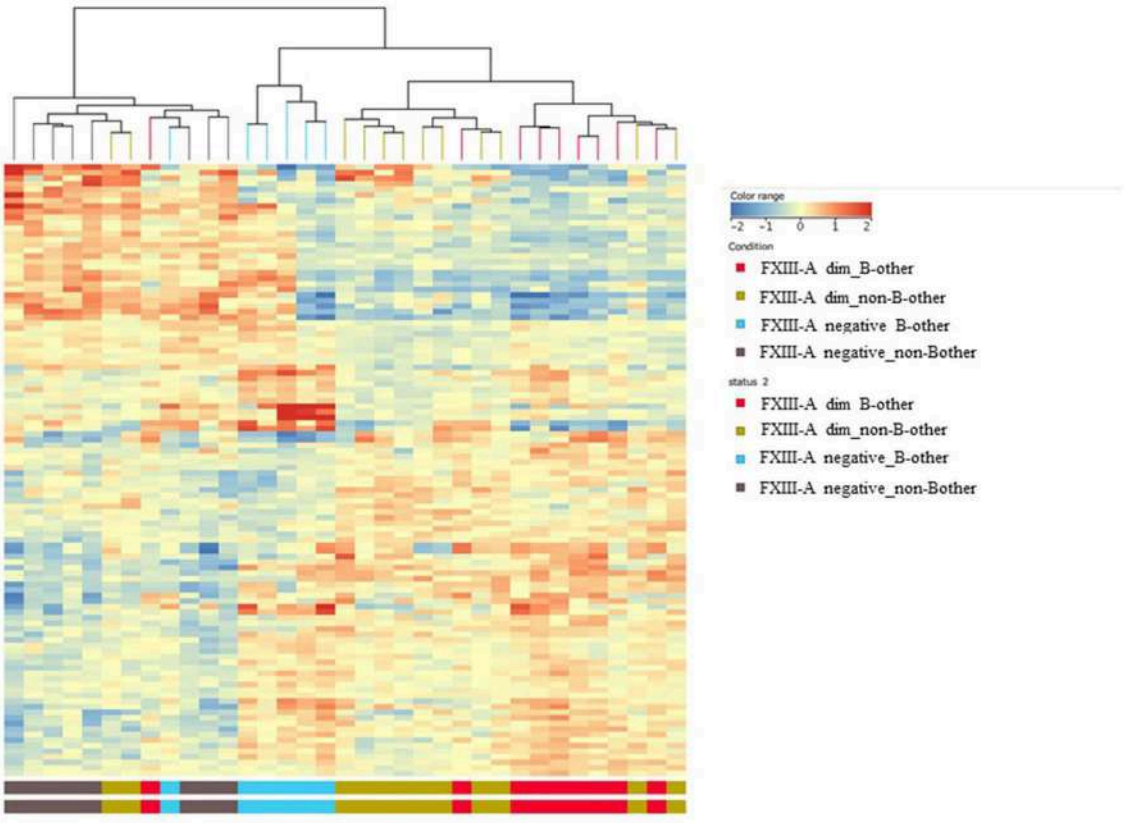

FIGURE 4 | Overlap between the gene expression signatures of FXIII-A negative and "B-other" samples; heat map analysis. Heat map analysis confirmed that, except for two outliers, gene expression profile characterizing FXIII-A negative samples overlapped with gene expression profile characterizing samples of the "B-other" subgroup.

in the FXIII-A negative subgroup compared to the two other subgroups (**Supplementary Table 3**).

Potential interactions could not be revealed between the protein products of validated genes and FXIII-A using STRING v11 functional protein association networks database. Nevertheless, we could identify a FXIII-A dependent expression of *FOXO1*. Using GeneHancer database we could *in silico* identify enhancers that might have roles in the parallel upregulation of *F13A1* and validated genes. Transcription factor binding sites of *ATF7*, *POLR2A*, *RAD21*, *SMARCA5* gene products were identified for all of the 14 genes shown in **Table 3**.

"B-OTHER" STATUS-BASED RESULTS

For the "B-other" status-based validation, DE genes related to biological processes (macrophage migration, lymphocyte apoptotic process, T cell apoptotic process, and their regulation), were selected for validation, as GO analysis results were less diverse than in the case of FXIII-A expression-based GO annotations (**Supplementary Table 1**). We were able to validate the differential expression of five genes by RT-Q-PCR. *DFFA, GIGYF1, GIGYF2*, and *INTS3* were overexpressed in "B-other" vs. "non-B-other" samples and in turn, *CD3G* exhibited a relatively lower expression in the "B-other" vs. "non-B-other" samples (**Figure 6**). *RORA, IL7R, CCL5, PLAC8, CX3CR* genes, selected for validation based on their functions and fold-changes detected by microarray, could not be validated.

DISCUSSION

FXIII-A is a useful marker of acute myeloid leukemia (AML) of the monocyte and megakaryocyte lineages (31–34). However, its expression in BCP-ALL blasts was an unexpected finding, since, in contrast to the normal myeloid counterparts of AML blasts, normal B-lymphocytes and their precursors do not express FXIII-A (8). Intracellular expression of FXIII-A protein can be consistently demonstrated in about two thirds of pediatric BCP-ALL samples by FC. Interestingly, the FXIII-A negative status was shown to be significantly associated with the "B-other" genetic subtype and patients with FXIII-A negative BCP-ALL had a significantly worse disease outcome than patients with FXIII-A positive lymphoblasts (9). These facts together suggested that pathological expression of FXIII-A in leukemic BCP blasts may define one or more sub-populations according to the FXIII-A expression pattern by FC.

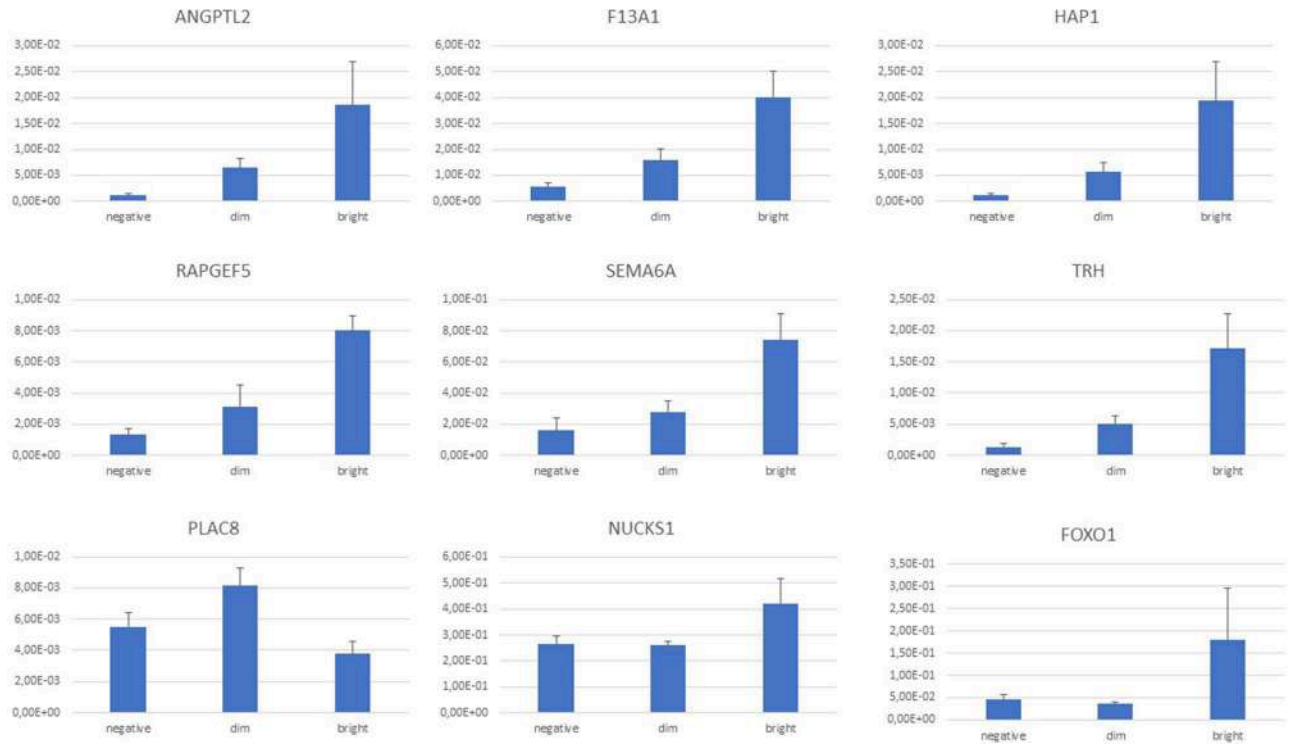

FIGURE 5 | Normalized gene expression values by RT-Q-PCR according to FXIII-A protein expression status; graph diagram. There was a continuous increase in normalized gene expression levels from FXIII-A negative through dim to bright subgroups that was endogenously validated by the *F13A1* differential expression within the three FXIII-A protein expression groups. *ANGPTL2, NUCKS1, RAPGEF5*, and *SEMA6A* followed this trend. Based on the intensity of the differential expression, separation of *FOXO1, HAP1*, and *TRH* genes of the FXIII-A bright subgroup were more prominent. *PLAC8* expression was most intensive in the FXIII-A dim subgroup.

Little is known on the transcriptional regulation of the *F13A1* gene. Molecular investigations of myeloid leukemia cell lines revealed the presence of binding sites for ubiquitous (NF-1 and SP-1) and myeloid enriched (MZF-1-like protein, GATA-1, and Ets-1) transcription factors in the promoter region of the gene (35). Interestingly, transcription factor binding sites for SP-1, GATA-1, and Ets-1 could not be confirmed by the ENCODE ChIP-seq datasets (data not shown) (36). A more recent study demonstrated that FXIII-A was synergistically regulated by IL-4 and dexamethasone in alternatively activated macrophages and these regulatory molecules are relevant for both normal and leukemic BCPs as well (37). However, transcriptional regulation of the *F13A1* gene in leukemic lymphoblasts has not yet been studied.

Therefore, we decided to investigate the gene expression profile of BCP lymphoblasts according to their FXIII-A expression status. Preliminary results of an ongoing prospective, multi-centric clinical study performed by our group suggested the clinical relevance of the sub-populations characterized by the FXIII-A expression pattern, since patients with FXIII-A dim but not bright lymphoblasts had a better disease outcome than patients with FXIII-A negative lymphoblasts (unpublished preliminary results). Accordingly, we investigated the global gene expression signature of three sample sets.

We have revealed that the three groups according to FXIII-A expression pattern had unique gene expression signatures which were characteristically different from each other. GO analysis of data resulted in a number of biologically relevant enriched functional categories. Identification of biological processes resulting in peptidyl-lysine modification supported the clinical relevance of our findings. FXIII-A is an enzyme catalyzing the formation of γ-glutamyl-ε-lysyl amide crosslinks. In addition to its well-known role in the formation of stable fibrin clot, FXIII-A participates also in much less characterized intracellular regulatory processes including differentiation of monocyte/macrophages, osteoblast, and osteoclast (38). In platelets, FXIII-A has been shown to crosslink cytoskeletal proteins (39). Should FXIII-A participate in similar processes in leukemic BCP lymphoblast, intracellular FXIII-A activity might contribute to autophagy and apoptosis of FXIII-A expressing lymphoblast. Moreover, the product of four genes validated in our cohort, *EHMT1*, *ING5*, *MDM2*, *NUP43* were shown to methylate and acetylate lysyl groups of intranuclear and intracellular proteins, among others, p53, and that way they can regulate survival of neoplastic cells (25).

In addition, we showed that gene expression pattern of the FXIII-A negative subgroup overlapped with the gene expression profile of the "B-other" genetic subgroup. However, our results indicated that the FXIII-A expression status was a more powerful determinant of gene expression profile than the "B-other" status.

Fourteen genes were validated according to the FXIII-A expression status. Importantly, we were able to detect the

TABLE 3 | Relative expression, enriched functional categories according to GO annotations and clinical relevance of validated genes accordig to FXIII-A protein expression patterns.

Gene	Normalized fold-change by RT-Q-PCR				GO annotations	Clinical relevance in leukemia and cancer	References
	P-value*	FXIII-A negative	FXIII-A dim	FXIII-A bright			
ANGPTL2	0.0061	1.10E-03	6.47E-03	1.87E-02	Signaling receptor binding	*ETV6* target gene in pediatric ALL	(15)
EHMT1	0.0401	4.79E-02	5.55E-02	8.89E-02	Chromatin modification	Transcriptional coactivator involved in glucocorticoid-induced cell death	(16)
F13A1	0.0013	5.58E-03	1.61E-02	4.02E-02	Protein-glutamine gamma-glutamzltransferase activitz	See article	
FOXO1	0.0371	4.69E-02	3.56E-02	1.80E-01	Cellular response to glucocorticoid stimulus	Key gene of the *AKT/FOXO1* pathway involved in apoptosis regulation of ALL blasts	(17–19)
HAP1	0.0016	1.10E-03	5.69E-03	1.94E-02	Post-transcriptional regulation of gene expression	Negative asparaginase-resistance biomarker in ALL	(20)
NUCKS1	0.0182	2.67E-01	2.59E-01	4.21E-01	Cell differentation	Downregulated in VCR-resistant ALL blasts	(21)
NUP43	0.0424	1.03E-02	1.17E-02	1.47E-02	Nuclear export	W/o proven function in cancer	
PIK3CG	0.0037	1.15E-01	1.24E-01	1.84E-01	Apoptosis regulation	*PIK3/AKT* pathwayplays key regulatory role in BCP-ALL	(22, 23)
PLAC8	0.0362	5.51E-03	8.20E-03	3.79E-03	Cell differentiation	Gene of unknown function, activated in various types of mammalian and human cancer	(24, 25)
RAPGEF5	0.0192	1.36E-03	3.14E-03	8.01E-03	RAS signal pathway	Abnormal expression involved in papillary thyroid cancer	(26)
SEMA6A	0.0019	1.61E-02	2.78E-02	7.43E-02	Apoptotic process	Overexpressed in *ETV6/RUNX1* ALL	(27)
SPIN1	0.0077	1.35E-01	1.68E-01	2.76E-01	Chromatin organization	Downregulation induces p53 activation in human cancer cells	(28)
TRH	0.0002	1.36E-03	5.09E-03	1.72E-02	Cell-cell signaling	Deregulation implicated in breast cancer	(29)
WASF2	0.0002	1.11E-01	1.55E-01	2.95E-01	Angiogenesis	Recurrent *WASF2/FGR* fusions are involved in suamous cell cancer, cystadenocarcinoma, and melanoma	(30)

**P-value of annova analysis comparing the FXIII-A negative, FXIII-A dim, FXIII-A bright groups.*

expression of *F13A1* gene in each individual sample, and the intensity of *F13A1* expression increased in parallel with the increasing protein expression of FXIII-A among the three subgroups. Of the 14 genes, *ANGPTL2, EHMT1 FOXO1, HAP1, NUCKS1*, *PIK3CG, RAPGEF5*, *SEMA6A, SPIN1, TRH*, and *WASF2* have biologically and clinically relevant functions in GO terms, and appear to have a role in leukemia and other forms of cancer (**Table 3**). *NUP43* has not yet been shown to be associated with any forms of human cancer in contrast to other members of the *NUP* gene family (40). *PLAC8* which is a trophoblast lineage marker physiologically, was most intensively expressed in the FXIII-A dim subgroup. This gene has been shown to be aberrantly activated in various types of cancer arising in mammals and mammalian cancer cell lines, but not in any subtype of human ALL (24, 25). Based on *in silico* investigations we were not able to reveal a direct link between DE genes as related to the three different FXIII-A expression groups and the regulation of *F13A1* gene. Common enhancer elements of the validated DE genes and the *F13A1* make likely that common transcription factors may regulate the expression of these genes in a similar fashion.

Validated DE genes of the "B-other" subgroup overlapping with the gene expression profile of the FXIII-A negative subgroup suggested the definition of a different sub-population from the *BCR-ABL1*-like/Ph-like B-ALL subgroup discovered originally by oligonucleotide microarrays (4, 5). Evaluating the microarray results, we identified 14 DE genes in our "B-other" subgroup (*ANXA5, ARL4C, CD34, IFNGR1, MAGT1, MAPKBP1, MAP3K2, ME3, OSBPL8, PAPOLA, PTPRC, SUZ12, TACC1, TEMPO*) overlapping with DE genes in the "B-other" subgroup defined by Den Boer et al. (5). However, all the DE genes within our "B-other" group differed from class-defining

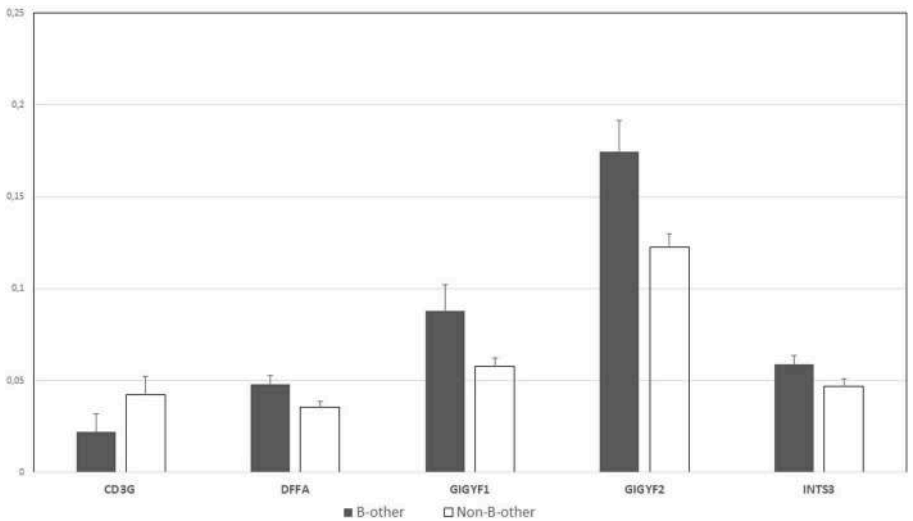

FIGURE 6 | Normalized gene expression values by RT-Q-PCR according to the "B-other" status; graph diagram. *DFFA, GIGYF1, GIGYF2* and *INTS3* genes were overexpressed in "B-other" vs. "non-B-other" samples and in turn, *CD3G* exhibited a relatively lower expression in the "B-other" vs. "non-B-other" samples.

genes of the so called "novel" ALL subtype introduced by Yeoh et al. (3) implying that they specify a different subtype. Each validated gene in this category, i.e., *CD3G, DFFA, GIGYF1, GIGYF2*, and *INTS3* were shown to play a role in neoplastic processes, including leukemia (41–45). However, none of these genes were published previously to be associated with pediatric BCP-ALL.

The small sample size and the low number of validated genes due to restricted budget represent an important limitation of the present study. The small number of patients involved in this investigation would make a clinical outcome analysis unreliable, even if statistically significant. Nevertheless, there was a substantially larger ratio of children who died due to their disease in the FXIII-A negative group: 5/14 children (36%), than in the FXIII-A dim group: 5/21 (24%) and in the FXIII-A bright group: 1/7 (14%). To investigate the clinical significance of FXIII-A expression in children with BCP-ALL we have started a pilot study of the ongoing BFM ALL-IC 2009 clinical trial with the participation of the Hungarian, Polish and Slovak national study groups. Preliminary analysis of this pilot study confirmed the unfavorable outcome of patients with FXIII-A negative BCP-ALL (results to be published upon completion of the pilot study). Similarly, an exact relationship between gene expression signature of FXIII-A negative samples and "B-other" samples, including *BCR-ABL1*-like/Ph-like signature, can be defined by investigating a larger number of samples from children with BCP-ALL.

In conclusion, we were the first to demonstrate the general expression of *F13A1* gene in pediatric BCP-ALL samples. The intensity of *F13A1* expression corresponded to the expression of FXIII-A protein, determined by FC in these samples. Three well-defined categories of FXIII-A protein expression: FXIII-A negative, FXIII-A dim, and FXIII-A bright subgroups defined characteristic and distinct gene expression signatures detected by Affymetrix oligonucleotide microarrays. Gene expression signature of the FXIII-A negative subgroup showed an overlap with that of the subgroup with "B-other" genetics. Validated genes proved biologically and clinically relevant. We described differential expression of genes not shown previously to be associated with pediatric BCP-ALL. Protein products of the newly identified genes may offer therapeutic targets for precision treatment of BCP-ALL. Multiparameter FC appears to be an easy-to-use and affordable method to assist in selecting pediatric patients with FXIII-A negative BCP-ALL who require a more elaborate and expensive molecular genetic investigation to design individualized therapeutic protocols.

DATA AVAILABILITY STATEMENT

The datasets generated for this study can be found in the NCBI's Gene Expression Omnibus and are accessible through GEO Series accession number GSE134480 (https://www.ncbi.nlm.nih.gov/geo/query/acc.cgi?acc=GSE134480).

ETHICS STATEMENT

The studies involving human participants were reviewed and approved by Scientific Research Ethical Committee (TUKEB) of the Medical Research Council of Hungary: No. 43033-1/2014/EUK(423/2014). Written informed consent to participate in this study was provided by the participants' legal guardian/next of kin.

AUTHOR CONTRIBUTIONS

CK: conceptualization, funding acquisition, project administration, and supervision. KG, BK, SP, and GZ: data curation. KG, BK, AU, ZH, GZ, and CK: formal analysis. KG, BK, GB, PJ, AU, and GP-M: investigation. CK, AU, ZH, BS, JK,

and GZ: methodology. KG, AU, JK, and GZ: resources. BK, ZH, SP, JK, and GZ: software. ZH, JK, GZ, and CK: validation. KG, BK, and GZ: visualization. GZ and CK: writing—original draft. KG, BK, AU, GB, PJ, GP-M, SP, BS, JK, GZ, and CK: writing—reviewer and editing.

FUNDING

This work was supported by the Hungarian National Scientific Research fund OTKA K108885 grant (Principal investigator CK), by the Junior Research Grant of the Hungarian Pediatric Hematology-Oncology Group, No.: 06/MGYH-MGYGYT/2018 (KG), and by the Leukémiás Gyermekekért Foundation.

ACKNOWLEDGMENTS

Patients were diagnosed and treated and BM samples and clinical data provided by Dr. Imre Gáspár, Prof. Gábor Kovács, Assoc. Prof. Judit Müller, Dr. Miklós Petrás, Dr. Réka Simon, Assoc. Prof. István Szegedi, and Dr. Ágnes Vojczek.

SUPPLEMENTARY MATERIAL

The Supplementary Material for this article can be found online at: https://www.frontiersin.org/articles/10.3389/fonc.2019.01063/full#supplementary-material

REFERENCES

1. Campo E, Swerdlow SH, Harris NL, Pileri S, Stein H, Jaffe ES. The 2008 WHO classification of lymphoid neoplasms and beyond: evolving concepts and practical applications. *Blood*. (2011) 117:5019–32. doi: 10.1182/blood-2011-01-293050
2. Arber DA, Orazi A, Hasserjian R, Thiele J, Borowitz MJ, Le Beau MM, et al. The 2016 revision to the World Health Organization classification of myeloid neoplasms and acute leukemia. *Blood*. (2016) 127:2391–405. doi: 10.1182/blood-2016-03-643544
3. Yeoh EJ, Ross ME, Shurtleff SA, Williams WK, Patel D, Mahfouz R, et al. Classification, subtype discovery, and prediction of outcome in pediatric acute lymphoblastic leukemia by gene expression profiling. *Cancer Cell*. (2002) 1:133–43. doi: 10.1016/S1535-6108(02)00032-6
4. Mullighan CG, Su X, Zhang J, Radtke I, Phillips LAA, Miller CB, et al. Deletion of IKZF1 and prognosis in acute lymphoblastic leukemia. *N Engl J Med*. (2009) 360:470–80. doi: 10.1056/NEJMc090454
5. Den Boer ML, van Slegtenhorst M, De Menezes RX, Cheok MH, Buijs-Gladdines JG, Peters ST, et al. A subtype of childhood acute lymphoblastic leukaemia with poor treatment outcome: a genome-wide classification study. *Lancet Oncol*. (2009) 10:125–34. doi: 10.1016/S1470-2045(08)70339-5
6. Moorman AV. New and emerging prognostic and predictive genetic biomarkers in B-cell precursor acutelymphoblastic leukemia. *Haematologica*. (2016) 101:407–16. doi: 10.3324/haematol.2015.141101
7. Li JF, Dai YT, Lilljebjörn H, Shen SH, Cui BW, Bai L, et al. Transcriptional landscape of B cell precursor acute lymphoblastic leukemia based on an international study of 1,223 cases. *Proc Natl Acad Sci USA*. (2018) 115:E11711–20. doi: 10.1073/pnas.1814397115
8. Kiss F, Hevessy Z, Veszprémi A, Katona E, Kiss C, Vereb G, et al. Leukemic lymphoblasts, a novel expression site of coagulation factor XIII subunit A. *Thromb Haemost*. (2006) 96:176–82. doi: 10.1160/TH06-05-0270
9. Kárai B, Hevessy Z, Szánthó E, Csáthy L, Ujfalusi A, Gyurina K, et al. Expression of coagulation factor XIII subunit A correlates with outcome in childhood acute lymphoblastic leukemia. *Pathol Oncol Res*. (2018) 24:345–52. doi: 10.1007/s12253-017-0236-0
10. Katona EE, Ajzner E, Tóth K, Kárpáti L, Muszbek L. Enzyme-linked immunosorbent assay for the determination of blood coagulation factor XIIIA subunit in plasma and in cell lysates. *J Immunol Methods*. (2001) 258:127–35. doi: 10.1016/S0022-1759(01)00479-3
11. Inaba H, Greaves M, Mullighan CG. Acute lymphoblastic leukaemia. *Lancet*. (2013) 381:1943–55. doi: 10.1016/S0140-6736(12)62187-4
12. Szklarczyk D, Gable AL, Lyon D, Junge A, Wyder S, Huerta-Cepas J, et al. STRING v11: protein-protein association networks with increased coverage, supporting functional discovery in genome-wide experimental datasets. *Nucleic Acids Res*. (2019) 47:D607–13. doi: 10.1093/nar/gky1131
13. Fishilevich S, Nudel R, Rappaport N, Hadar R, Plaschkes I, Iny Stein T, et al. GeneHancer: genome-wide integration of enhancers and target genes in GeneCards. *Database*. (2017) 2017:1–17. doi: 10.1093/database/bax028
14. Kim HY. Statistical notes for clinical researchers: A one-way repeated measures ANOVA for data with repeated observations. *Restor Dent Endod*. (2015) 40:91–5. doi: 10.5395/rde.2015.40.1.91
15. Neveu B, Spinella JF, Richer C, Lagacé K, Cassart P, Lajoie M, et al. CLIC5: a novel ETV6 target gene in childhood acute lymphoblastic leukemia. *Haematologica*. (2016) 101:1534–43. doi: 10.3324/haematol.2016.149740
16. Poulard C, Kim HN, Fang M, Kruth K, Gagnieux C, Gerke DS, et al. Relapse-associated AURKB blunts the glucocorticoid sensitivity of B cell acute lymphoblastic leukemia. *Proc Natl Acad Sci USA*. (2019) 116:3052–061. doi: 10.1073/pnas.1816254116
17. Wang F, Demir S, Gehringer F, Osswald CD, Seyfried F, Enzenmüller S, et al. Tight regulation of FOXO1 is essential for maintenance of B-cell precursor acute lymphoblastic leukemia. *Blood*. (2018) 131:2929–42. doi: 10.1182/blood-2017-10-813576
18. Han J, Jin R, Zhang M, Guo Q, Zhou F. Ikaros 6 protects acute lymphoblastic leukemia cells against daunorubicin-induced apoptosis by activating the Akt-FoxO1 pathway. *J Leukoc Biol*. (2017) 101:675–81. doi: 10.1189/jlb.2A0116-040RR
19. Köhrer S, Havranek O, Seyfried F, Hurtz C, Coffey GP, Kim E, et al. Pre-BCR signaling in precursor B-cell acute lymphoblastic leukemia regulates PI3K/AKT, FOXO1and MYC, and can be targeted by SYK inhibition. *Leukemia*. (2016) 30:1246–54. doi: 10.1038/leu.2016.9
20. Lee JK, Kang S, Wang X, Rosales JL, Gao X, Byun HG, et al. HAP1 loss confers l-asparaginase resistance in ALL by downregulating the calpain-1-Bid-caspase-3/12 pathway. *Blood*. (2019) 133:2222–32. doi: 10.1182/blood-2018-12-890236
21. Akbari Moqadam F, Lange-Turenhout EA, Ariës IM, Pieters R, den Boer ML. MiR-125b, miR-100 and miR-99a co-regulate vincristine resistance in childhood acute lymphoblastic leukemia. *Leuk Res*. (2013) 37:1315–21. doi: 10.1016/j.leukres.2013.06.027
22. Sanchez VE, Nichols C, Kim HN, Gang EJ, Kim YM. Targeting PI3K signaling in acute lymphoblastic leukemia. *Int J Mol Sci*. (2019) 20:E412. doi: 10.3390/ijms20020412
23. Archer MC. Role of sp transcription factors in the regulation of cancer cell metabolism. *Genes Cancer*. (2011) 2:712–9. doi: 10.1177/1947601911423029
24. Grate LR. Many accurate small-discriminatory feature subsetsexist in microarray transcript data: biomarker discovery. *BMC Bioinformatics*. (2005) 6:97. doi: 10.1186/1471-2105-6-97
25. Cabreira-Cagliari C, Dias NC, Bohn B, Fagundes DGDS, Margis-Pinheiro M, Bodanese-Zanettini MH, et al. Revising the PLAC8 gene family: from a central role in differentiation, proliferation, and apoptosis in mammals to a multifunctional role in plants. *Genome*. (2018) 61:857–65. doi: 10.1139/gen-2018-0035
26. Liu W, Zhao J, Jin M, Zhou M. circRAPGEF5 contributes to papillary thyroid proliferation and metastasis by regulation miR-198/FGFR1. *Mol Ther Nucleic Acids*. (2019) 14:609–16. doi: 10.1016/j.omtn.2019.01.003
27. Gandemer V, Rio AG, de Tayrac M, Sibut V, Mottier S, Ly Sunnaram B, et al. Five distinct biological processes and 14 differentially expressed genes

characterize TEL/AML1-positive leukemia. *BMC Genomics*. (2007) 8:385. doi: 10.1186/1471-2164-8-385
28. Fang Z, Cao B, Liao JM, Deng J, Plummer KD, Liao P, et al. SPIN1 promotes tumorigenesis by blocking the uL18 (universal large ribosomal subunit protein 18)-MDM2-p53 pathway in human cancer. *ELife Sci*. (2018) 7:e31275. doi: 10.7554/eLife.31275
29. Frölich E, Wahl R. The forgotten effects of thyreotropin-releasing hormone: metabolic functions and medical applications. *Front Neuroendocrinol*. (2019) 52:29–43. doi: 10.1016/j.yfrne.2018.06.006
30. Stransky N, Cerami E, Schalm S, Kim JL, Lengauer C. The landscape of kinase fusions in cancer. *Nat Commun*. 5:4846. doi: 10.1038/ncomms5846
31. Invernizzi R, De Fazio P, Iannone AM, Zambelli LM, Rastaldi MP, Ippoliti G, et al. Immunocytochemical detection of fac- tor XIII A–subunit in acute leukemia. *Leuk Res*. (1992) 16:829–36. doi: 10.1016/0145-2126(92)90163-2
32. Kappelmayer J, Simon A, Katona E, Szanto A, Nagy L, Kiss A, et al. Coagulation factor XIII-A. A flow cytometric intracellular marker in the classification of acute myeloid leukemias. *Thromb Haemost*. (2005) 94:454–9. doi: 10.1160/TH05-03-0206
33. Kiss F, Simon A, Csáthy L, Hevessy Z, Katona E, Kiss C, et al. A coagulation factor becomes useful in the study of acute leukemias: studies with blood coagulation factor XIII. *Cytometry A*. (2008) 73:194–201. doi: 10.1002/cyto.a.20485
34. Kida M, Souri M, Yamamoto M, Saito H, Ichinose A. Transcriptional regulation of cell type-specific expression of the TATA-less A subunit gene for human coagulation factor XIII. *J Biol Chem*. (1999) 274:6138–47. doi: 10.1074/jbc.274.10.6138
35. Gratchev A, Kzhyshkowska J, Utikal J, Goerdt S. Interleukin-4 and dexamethasone counterregulate extracellular matrix remodelling and phagocytosis in type-2 macrophages. *Scand J Immunol*. (2005) 61:10–7. doi: 10.1111/j.0300-9475.2005.01524.x
36. ENCODE Project Consortium. A user's guide to the encyclopedia of DNA elements (ENCODE). *PLoS Biol*. (2011) 9:e1001046. doi: 10.1371/journal.pbio.1001046
37. Mitchell JL, Mutch NJ. Let's cross-link: diverse functions of the promiscuous cellular transglutaminase factor XIII-A. *J Thromb Haemost*. (2019) 17:19–30. doi: 10.1111/jth.14348
38. Richardson VR, Cordell P, Standeven KF, Carter AM. Substrates of factor XIII-A: roles in thrombosis and wound healing. *Clin Sci*. (2013) 3:123–37. doi: 10.1042/CS20120233
39. Huang J, Dorsey J, Chuikov S, Pérez-Burgos L, Zhang X, Jenuwein T, et al. G9a and Glp methylate lysine 373 in the tumor suppressor p53. *J of Biol Chem*. (2010) 285:9636–41. doi: 10.1074/jbc.M109.062588
40. Nofrini V, Di Giacomo D, Mecucci C. Nucleoporin genes in human disease. *Eur J Human Genet*. (2016) 24:1388–95. doi: 10.1038/ejhg.2016.25
41. Zamani-Ahmadmahmudi M, Najafi A, Nassiri SM. Detection of critical genes associated with Overall Survival (OS) and Progression-Free Survival (PFS) in reconstructed canine B-cell lymphoma Gene Regulatory Network (GRN). *Cancer Invest*. (2016) 34:70–9. doi: 10.3109/07357907.2015.1114120
42. Yi B, Zhang M, Schwartz-Albiez R, Cao Y. Mechanisms of the apoptosis induced by CD176 antibody in human leukemic cells. *Int J Oncol*. (2011) 38:1565–73. doi: 10.3892/ijo.2011.992
43. Ajiro M, Nishidate T, Katagiri T, Nakamura Y. Critical involvement of RQCD1 in the EGFR-Akt pathway in mammary carcinogenesis. *Int J Oncol*. (2010) 37:1085–93. doi: 10.3892/ijo_00000760
44. Christen F, Hoyer K, Yoshida K, Hou HA, Waldhueter N, Heuser M, et al. Genomic landscape and clonal evolution of acute myeloid leukemia with t(8;21): an international study on 331 patients. *Blood*. (2019) 133:1140–51. doi: 10.1182/blood-2018-05-852822
45. Federico A, Rienzo M, Abbondanza C, Costa V, Ciccodicola A, Casamassimi A. Pan-cancer mutational and transcriptional analysis of the integrator complex. *Int J Mol Sci*. (2017) 18:E936. doi: 10.3390/ijms18050936

Conflict of Interest: The authors declare that the research was conducted in the absence of any commercial or financial relationships that could be construed as a potential conflict of interest.

frontiers in Oncology

ORIGINAL RESEARCH
published: 25 October 2019
doi: 10.3389/fonc.2019.01034

Dendritic Cell-Based Immunotherapy in Advanced Sarcoma and Neuroblastoma Pediatric Patients: Anti-cancer Treatment Preceding Monocyte Harvest Impairs the Immunostimulatory and Antigen-Presenting Behavior of DCs and Manufacturing Process Outcome

Eva Hlavackova[1,2†], Katerina Pilatova[1,3†], Dasa Cerna[2], Iveta Selingerova[3], Peter Mudry[2], Pavel Mazanek[2], Lenka Fedorova[1,3], Jana Merhautova[1], Lucie Jureckova[1], Lukas Semerad[4], Rita Pacasova[5], Lucie Flajsarova[1], Lenka Souckova[1,2], Regina Demlova[1], Jaroslav Sterba[1,2], Dalibor Valik[1,3] and Lenka Zdrazilova-Dubska[1,3]*

[1] Department of Pharmacology, Faculty of Medicine, Masaryk University, Brno, Czechia, [2] Department of Pediatric Oncology, University Hospital and Faculty of Medicine, Masaryk University, Brno, Czechia, [3] Regional Centre for Applied Molecular Oncology, Masaryk Memorial Cancer Institute, Brno, Czechia, [4] Department of Internal Medicine-Hematology and Oncology, University Hospital and Medical Faculty, Masaryk University, Brno, Czechia, [5] Transfusion and Tissue Department, University Hospital Brno, Brno, Czechia

Despite efforts to develop novel treatment strategies, refractory and relapsing sarcoma, and high-risk neuroblastoma continue to have poor prognoses and limited overall survival. Monocyte-derived dendritic cell (DC)-based anti-cancer immunotherapy represents a promising treatment modality in these neoplasias. A DC-based anti-cancer vaccine was evaluated for safety in an academic phase-I/II clinical trial for children, adolescents, and young adults with progressive, recurrent, or primarily metastatic high-risk tumors, mainly sarcomas and neuroblastomas. The DC vaccine was loaded with self-tumor antigens obtained from patient tumor tissue. DC vaccine quality was assessed in terms of DC yield, viability, immunophenotype, production of IL-12 and IL-10, and stimulation of allogenic donor T-cells and autologous T-cells in allo-MLR and auto-MLR, respectively. Here, we show that the outcome of the manufacture of DC-based vaccine is highly variable in terms of both DC yield and DC immunostimulatory properties. In 30% of cases, manufacturing resulted in a product that failed to meet medicinal product specifications and therefore was not released for administration to a patient. Focusing on the isolation of monocytes and the pharmacotherapy preceding monocyte harvest, we show that isolation of monocytes by elutriation is not superior to adherence on plastic in terms of DC yield, viability, or immunostimulatory capacity. Trial patients having undergone monocyte-interfering pharmacotherapy prior to monocyte harvest was associated with an impaired DC-based immunotherapy product outcome.

OPEN ACCESS

Edited by:
Christina Annunziata, National Cancer Institute (NCI), United States

Reviewed by:
Daniel Green, Kite Pharma, United States
Oladapo Yeku, Massachusetts General Hospital Cancer Center, United States

***Correspondence:**
Lenka Zdrazilova-Dubska
dubska@mou.cz

† These authors have contributed equally to this work and are listed in alphabetical order

Specialty section:
This article was submitted to Cancer Molecular Targets and Therapeutics, a section of the journal Frontiers in Oncology

Received: *19 July 2019*
Accepted: *24 September 2019*
Published: *25 October 2019*

Citation:
Hlavackova E, Pilatova K, Cerna D, Selingerova I, Mudry P, Mazanek P, Fedorova L, Merhautova J, Jureckova L, Semerad L, Pacasova R, Flajsarova L, Souckova L, Demlova R, Sterba J, Valik D and Zdrazilova-Dubska L (2019) Dendritic Cell-Based Immunotherapy in Advanced Sarcoma and Neuroblastoma Pediatric Patients: Anti-cancer Treatment Preceding Monocyte Harvest Impairs the Immunostimulatory and Antigen-Presenting Behavior of DCs and Manufacturing Process Outcome. Front. Oncol. 9:1034. doi: 10.3389/fonc.2019.01034

Certain combinations of anti-cancer treatment resulted in a similar pattern of inadequate DC parameters, namely, a combination of temozolomide with irinotecan was associated with DCs showing poor maturation and decreased immunostimulatory features, and a combination of pazopanib, topotecan, and MTD-based cyclophosphamide was associated with poor monocyte differentiation and decreased DC immunostimulatory parameters. Searching for a surrogate marker predicting an adverse outcome of DC manufacture in the peripheral blood complete blood count prior to monocyte harvest, we observed an association between an increased number of immature granulocytes in peripheral blood and decreased potency of the DC-based product as quantified by allo-MLR. We conclude that the DC-manufacturing yield and the immunostimulatory quality of anti-cancer DC-based vaccines generated from the monocytes of patients were not influenced by the monocyte isolation modality but were detrimentally affected by the specific combination of anti-cancer agents used prior to monocyte harvest.

Keywords: dendritic cells, anti-cancer medications, sarcoma, neuroblastoma, cell-based medicinal products, investigator-initiated clinical trial, manufacturing outcome variability

INTRODUCTION

Several progressive and relapsing malignancies in pediatric patients have dismal life prognosis. Refractory neuroblastoma and refractory or metastatic sarcoma have an especially poor prognosis, with no consistently curative treatments available. Oberlin et al. (1) published a meta-analysis of North American and European studies on primary metastatic sarcomas and well-defined risk factors that—where two or more are present at presentation—distribute patients into a subgroup with only a 14% event-free and overall survival probability at 3 years from diagnosis. Patients over 10 years of age with limb primary or "other site" primary tumors with the alveolar subtype of rhabdomyosarcoma, bone marrow or bone involvements, and more than three metastatic sites are defined as having markers for a worse prognosis (1). Similar results were published in a study of relapsed rhabdomyosarsomas, with the prognosis for survival being < 10% at 5 years (2). In high-risk neuroblastoma, survival after relapse is poor, and the usual life expectancy is < 6 months. Based on our experience, patients with neuroblastomas with a high MIBG score after induction therapy have very poor 2-year survival (3). High-risk rhabdomyosarcomas are treated according to several globally accepted protocols with a combination of chemotherapy, surgery, and radiotherapy. Chemotherapy regimens consist of the alkylating agent ifosfamide or cyclophosphamide and vinca alkaloids combined with either etoposide or doxorubicin and actinomycin D. The cytotoxic chemotherapy regimens for relapsed and refractory neuroblastoma typically use a combination of camptothecins, topotecan, and irinotecan with agents such as cyclophosphamide and temozolomide, and achieve objective tumor responses but poor long-term outcomes. For such poor-prognosis patients, treatments with innovative and metronomic therapies (e.g., COMBAT, METRO) (4, 5), cell-based immunotherapies (6, 7), and novel molecularly targeted agents (8) are justified and are also effective in many cases, although their long-term effect has yet to be demonstrated.

DCs are essential antigen-presenting cells for the initiation, maintenance, and regulation of immune response (9). Active cancer immunotherapy directs the immune system to attack tumor cells by targeting tumor-associated antigens. We manufacture a fully personalized monocyte-derived dendritic cell-based vaccine that was evaluated in the investigator-initiated clinical trial "Combined antitumor therapy with *ex vivo* manipulated dendritic cells producing interleukin-12 in children, adolescents, and young adults with progressive, recurrent, or primarily metastatic high-risk tumors" (EudraCT number 2014-003388-39). The primary endpoint of the trial was an assessment of safety by analysis of the frequency of occurrence of AESI (adverse events of special interest). Vaccines that meet quality control (QC) requirements are registered for use and applied intradermally every 2–4 weeks for up to 35 doses.

Dendritic cell-based medical products are mostly manufactured through derivation from monocytes. Autologous monocytes are readily accessible and can be obtained from peripheral blood in sufficient amounts to prepare 10^7-10^8 DCs. Monocytes arise from hematological precursors in bone marrow, with a maturation time of 50–60 h (10), and enter the bloodstream for several days until their recruitment into tissues, where they possess the property to mature into tissue macrophages (11). Specifically, the classical CD14++ CD16– subpopulation representing 80–95% of circulating monocytes has a 1-day lifespan in circulation, the intermediate CD14+ CD16+ subpopulation (2–8% of circulating monocytes) has a 4-day lifespan, and the non-classical CD14+ CD16++ subpopulation (2–11% of circulating monocytes) has a 7-day lifespan in circulation (12–14). Monocyte count and function are influenced by various anti-cancer agents. Nevertheless, the published data on the impact of particular anti-cancer agents on the development and function of monocytes are scarce in comparison with those on hematologic toxicity

toward neutrophils and lymphocytes. As most anti-cancer agents target DNA, they interfere with dividing cells including hematopoetic cells. Also, tyrosine kinase inhibitors (regorafenib, sunitinib, sorafenib) are associated with adverse events including hematological toxicities (15). Regorafenib hematological toxicity has been explained by the TK inhibition of FMS like tyrosine kinase 3 (FLT-3) and stem cell factor (c-KIT ligand), which represent hematopoietic growth receptors (15, 16). Reduction in the circulating monocyte count after sunitinib has been shown (17). Monocytes are also highly sensitive to the methylating agent temozolomide (TMZ) (18, 19). Cisplatin and carboplatin have been shown to alter monocyte differentiation to favor the generation of IL-10-producing M2 macrophages (20).

Various chemotherapeutics affect cell differentiation and the antigen presentation of DCs when treated *in vitro* during the differentiation process (21). Data are lacking on the potential *in vivo* impact of hematotoxic agents on the properties of medicinal products from monocyte-derived DCs. During the manufacture of DC-based anti-cancer immunotherapy under stringent GMP-compliant conditions, we experienced highly variable final product parameters in terms of both DC yield and immunostimulatory properties, and we hypothesized that hematotoxic anti-cancer therapy preceding monocyte harvest may influence the quality of DC-based medicinal products. The issue of the effect of pharmacotherapy on the quality of human monocyte-derived DCs cannot be reliably assessed in mimicked conditions by *in vitro* pretreatment of monocytes by anti-cancer agents. Thus, data addressing this issue can only be gathered retrospectively from real-life clinical conditions, such as our clinical trial, though with a limited number of patients included. Here, the Phase-I/II clinical trial protocol designed for heavily pre-treated cancer patients with heterogenic anti-cancer therapeutic protocols allows us to observe and analyze the effect of pharmacotherapy on the quality and presumably also on the anti-cancer action of *ex vivo*-manufactured DCs.

Therefore, our primary aims were to analyze the impact of (i) cytotoxic and targeted anti-cancer therapy preceding monocyte harvest and (ii) variability in the complete blood count on the quality of DC-based anti-cancer immunotherapy in high-risk sarcoma and neuroblastoma patients, representing the two main diagnoses in the DC clinical trial. A secondary aim was to reveal whether monocyte isolation by elutriation is superior to the isolation of monocytes through their adherence to plastic cultivation flasks.

METHODS

Patients and Clinical Trial

Clinical Trial Eligibility and Allowed Medication

Patient eligibility/inclusion criteria for the clinical trial included being 1–25 years old male/female with histologically confirmed refractory, relapsing, or primarily metastatic high-risk tumors and having a performance status (Karnofsky or Lansky score) $\geq$ 50 and a life expectancy of longer than 10 weeks. Patients had to be clinically eligible for the surgical procedure to harvest tumor tissue for histological verification and tumor antigen extraction. Female patients had to have had a negative pregnancy test. All patients had to have adequate bone marrow, kidney, liver, and heart function, defined as absolute neutrophil count (ANC) $\geq 0.75 \times 10^9$/L, thrombocytes $\geq 75 \times 10^9$/L, hemoglobin 80 g/L, estimated glomerular filtration rate (eGFR) $\geq$ 70 mL/min/1.73 m^2, serum creatinine $\leq$ 1.5-fold the upper limit for the appropriate age, bilirubin $\leq$ 1.5-fold the upper limit for the appropriate age, AST and ALT $\leq$ 2.5-fold the upper limit for the appropriate age, ejection fraction $\geq$ 50%, and fractional shortening $\geq$ 27% as assessed by echocardiography. In the case of bone marrow infiltration, the allowable ANC was $\geq 0.5 \times 10^9$/L and blood platelets 40×10^9/L. In case of liver metastases, AST and ALT had to be $\leq$ 5-fold the upper limit for the appropriate age. The exclusion criteria were as follows: seropositivity to HIV1,2, *Treponema pallidum*, hepatitis B or C, known hypersensitivity to the study medication, autoimmune disease that was not adequately treated, uncontrolled psychiatric disease, or uncontrolled hypertension defined as systolic and diastolic blood pressure over the 95th percentile for the appropriate age and height (patients $\leq$ 17 years old) or $\geq$ 160/90 mmHg or diastolic blood pressure $\geq$ 90 mmHg (patients $\geq$ 17 years old). Patients previously treated with dendritic cells or participating in another clinical trial during the 30 days before enrollment were not eligible to enter this clinical trial.

The allowed medication prior to monocyte harvest (leukapheresis) was as follows: metronomic chemotherapy, immune checkpoint inhibitors, and anti-CD20 antibodies were allowed as concomitant medication for any time before leukapheresis. Monoclonal antibodies (except anti-CD20), high-dose chemotherapy, and high-dose corticoids had to have been withdrawn at least 3 weeks prior to leukapheresis with the exception of corticoid treatment of brain edema, which was allowed. Since November 2017, an amendment has been made to the procedure for monocyte harvest, and tyrosine kinase inhibitors have to be withdrawn according to their half-life: drugs with a short half-life of 3–14 h must be withdrawn at least 2 days before leukapheresis (axitinib, dabrafenib, dasatinib, ibrutinib, idelalisib, nintedanib, ruxolitinib, and trametinib), drugs with a medium half-life of 15–35 h at least 7 days before leukapheresis (alectinib, bosutinib, lapatinib, lenvatinib, nilotinib, osimertinib, pazopanib, ponatinib, regorafenib, and non-TKI everolimus), and drugs with a long half-life of 36–60 h at least 12 days before leukapheresis (afatinib, ceritinib, erlotinib, gefitinib, imatinib, cabozantinib, crizotinib, sorafenib, sunitinib, vemurafenib, and non-TKI temsirolimus). Myelopoietic growth factors have to be withdrawn at least 7 days before leukapheresis/monocyte harvest.

Evaluation of Preceding and Concomitant Therapy

A precise analysis was performed of preceding and/or concomitant therapy 60 days before monocyte harvest for clinical trial subjects with neuroblastoma and sarcoma diagnoses. Data were mined from the clinical trial electronic case report form and the subjects' medical records. We particularly focused on therapeutic agents with a potential impact on the generation of DCs from monocytes and on DC immunostimulatory properties. These agents and the reports on their role in monocyte biology are summarized in **Supplementary Table 1**.

DC Manufacture and Quality Control

Dendritic cell vaccine manufacture encompassed two phases—(i) preparation of tumor lysate as a source of the patient's tumor antigens and (ii) preparation of monocyte-derived DCs and their loading with tumor lysate. Quality control tests evaluated safety (negativity for pathogens), identity (cell immunophenotype), viability, and functions (cytokine production, stimulation of T-cells). The flow and decision tree of the manufacturing process is shown in **Supplementary Figure 1**.

Self-Tumor Antigen Extraction

Tumor lysate was prepared from the tumor tissue obtained from the patient during curative surgery or extended biopsy. In Clean Rooms, necrotic areas and connective tissue were removed from the tumor tissue with a surgical scalpel, keeping the specimen immersed in buffered solution. The remaining tissue was sliced into fragments of about 0.5 mm with a scalpel and forceps and then further crushed with the back of a syringe. Each suspension of tumor fragments and cells in HBSS was lysed through repeated (5 times) freezing in liquid nitrogen and thawing at 37°C. The crude tumor lysate was centrifuged at 450 g/7 min/4°C to remove particulate components. The tumor lysate was released for DC manufacture if the following criteria were met: (i) presence of viable tumor cells reported by a histopathologist, (ii) protein concentration, and (iii) microbiological sterility.

Peripheral Mononuclear Cell Collection

Monocytes were harvested as part of the mononuclear white blood cell (WBC) fraction. Mononuclear cells were collected from the peripheral blood of the patient using the Terumo BCT Spectra Optia Apheresis System. For collection, we used either an intermittent or continuous leukapheresis system. Due to its superior collection efficacy and easier procedure settings, we have preferred the continuous leukapheresis system since April 2018. A citrate dextrose solution, solution A (ACD-A), was used as an anticoagulant. In patients with a body weight of < 20 kg, anticoagulation with heparin was used to prevent citrate toxicity. The requirement for the minimal WBC count was 3×10^9/L before the initiation of leukapheresis. To prevent risk of bleeding or ischemic complications during and after the procedure, hemoglobin of at least 80 g/L and platelets of at least 30×10^9/L were required. In case of a patient with a body weight of < 20 kg, the leukapheresis set was pre-filled with donor erythrocytes. The aim of the leukapheresis was to obtain 60–80 mL of concentrate of mononuclear cells with a content of at least 0.5×10^9 monocytes. Subsequent addition of 5% human albumin to the minimum required volume of 80 mL for further processing was allowed.

DC Manufacture in Clean Rooms

The numbers of WBCs, B-cells and T-cells, monocytes, and granulocytes in the leukapheretic product were evaluated using a hematology analyzer (XT-4000i, Sysmex) and flow cytometer (FC-500, Beckman Coulter) with staining for CD3 (clone UCHT1, Beckman Coulter) and CD19 (clone J3-119, Beckman Coulter). Monocytes for DC manufacture were separated from the leukapheresis product by either elutriation or adherence to a plastic surface. During elutriation (using an Elutra cell separator, Gambro BCT), blood cells were separated on the basis of sedimentation velocity into six fractions, where the last fraction rich in monocytes was used for DC manufacture. Contaminating cells after elutriation were mainly granulocytes with similar sedimentation velocity to monocytes. Five hundred million monocytes adhered for 2–4 h in three 175-cm^2 tissue culture flasks with 35 mL of CellGenix® GMP DC Medium at 37°C/5% CO_2 and were then washed with HBSS and processed further. Monocytes seeded from the elutriation product or attached by plastic adherence were then cultivated in three 175-cm^2 tissue culture flasks with 70 mL of CellGenix® GMP DC medium supplemented with GM-CSF (1000 U/mL, CellGenix®) and IL-4 (320 U/mL, CellGenix®) at 37°C/5% CO_2/6 days. On day 3, a fresh 70 mL of medium supplemented with the same concentration of GM-CSF and IL-4 was added to the culture. On day 6, immature DCs were exposed to autologous tumor lysate antigens (10 μg/mL) with added keyhole limpet haemocyanin (KLH, 1 μg/mL), IL-4 (320 U/mL), and GM-CSF (1000 U/mL) at 37°C/5% CO_2/for 1.5–2 h. Maturation was induced by lipopolysaccharide (200 U/mL) and interferon-γ (50 ng/mL) for an additional 6 h at 37°C/5% CO_2. Finally, cells were collected using accutase (Accutase®, Corning), counted in a Bürker cell chamber and frozen in aliquots of 2×10^6 DCs in 100 μL of freezing medium CryoStor® CS2 at -80°C. All doses of the DC-based investigational medical product (IMP) named "MyDendrix®" were stored at -150°C until administration to the patient.

Quality Control of DC-Based Investigational Medicinal Product

DC characteristics were evaluated as a part of the quality control process of IMP from an aliquot of manufactured DC from each batch. The cryotube with DC was removed from a deep freezing box (-150°C) into a laminar flow box, quickly and gently thawed in hand while avoiding shaking, 1 mL of cold (2–8°C) DC medium (CellGenix® GMP-grade) was slowly added to the thawed DCs, and the DC suspension was transferred into 2 mL of cold DC medium. The DC suspension was handled at room temperature and processed immediately. DCs (8×10^5 cells) were seeded into 1 well of a 6-well culture plate for sensitive adherent cells (Sarstedt, TC Plate 6-well, Cell+, growth area 8.87 cm^2) and cultured in 3 mL of DC medium for 2 days (37°C/5% CO_2) to obtain (i) medium containing cytokines produced by DCs during cultivation and (ii) mature DCs for phenotypic evaluation after 2 days of post-thaw cultivation. A 0.5 mL volume of medium containing DC-produced cytokines was collected after 23–25 h upon DC seeding and was centrifuged (10 min/410 g/4°C), and the supernatant was stored at -25°C for no longer than 30 days prior to analysis. For immunophenotypic evaluation of mature DCs, both detached and adherent DCs were harvested 47–49 h after DC seeding. The culture medium was collected and pooled with DCs harvested by accutase (0.5 mL/well 8.87 cm^2/37°C) and centrifuged (5 min/410 g/20°C). The pellet was resuspended in 800 μL HBSS with 0.25% human albumin (Grifols) and processed immediately for immunophenotypic evaluation. Viability quantification was

performed by propidium iodide (PI) exclusion assay. Briefly, 10^5 DCs were stained with 10 μL of 1% PI in HBSS followed by immediate flow cytometric (Cytomics FC500) analysis of PI-positive events (= non-viable cells). The immunophenotype of DCs was evaluated in post-thaw DCs and in post-cultivation mature DCs. For the detection of each surface molecule, 0.5 × 10^5 DCs were incubated for 20 min in the dark with the following antibodies: CD80-PC7 (clone MAB104, 10 μL), CD83-FITC (clone HB15e, 10 μL), CD86-PE (clone HA5.2B7, 10 μL), CD197-PE (clone G043H7, 10 μL), HLA-DR-PC5 (clone Immu357, 10 μL), CD14-PE (clone RMO52, 10 μL), or isotype controls IgG-PC5 (clone 679.1Mc7, 10 μL), IgG-PC7 (clone 679.1Mc7, 10 μL), IgG2a-FITC (clone 7T4-1F5, 10 μL), or IgG2a-PE (7T4-1F5, 10 μL), all from Beckman Coulter. Flow cytometric analysis was performed using a Cytomics FC500 with CXP software by manual gating on individual parameters, and the discrimination by appropriate isotype control was used to gate and quantify positive events. The concentrations of IL-12 and IL-10 in the DC culture medium were measured by flow cytometric bead assay (BD Biosciences) using internal quality controls (Quantikine® Immunoassay Control Group 1, R&D Systems). Absolute production of IL-12 or IL-10 per 10^6 DC and the IL-12/IL-10 ratio were calculated. The allogenic (allo) and autologous (auto) stimulatory properties of DCs were examined by mixed lymphocyte reaction (MLR). In allo-MLR, the target cells were the peripheral blood mononuclear cells (PBMCs) obtained from pooled buffy coats from healthy donors. In auto-MLR, the target cells were the patient's lymphocytes separated by centrifugation in a density gradient using Histopaque-1077 (SigmaAldrich, density 1,077 g/mL) from the leukapheresis product obtained for DC manufacture. These pre-vaccination lymphocytes were cryopreserved using CryoStor CS5 medium (BioLife solutions) at -150°C and thawed prior to auto-MLR seeding. A sample of 10^7 target lymphocytes were stained with 250 μL 10 μM carboxyfluorescein succidimidyl ester (CFSE, SigmaAldrich) and seeded into a sterile 96-well culture plate (Sarstedt, TC Plate 96-well, Suspension, F) at 10^5 cells/well in 200 μL of complete X-vivo 10 medium (Lonza) containing 5% inactivated human male AB serum (SigmaAldrich) for the following: (i) 10^4 DC/well in 10:1 target:effector MLR, (ii) positive control (PC) with phytohemagglutinin (PHA, SigmaAldrich) at a final concentration of 10 μg/mL, or (iii) negative control (NC) with complete X-vivo medium only. MLR experiments were seeded in triplicate and cultured for 6 days at 37°C/5% CO_2. 2 × 10^4 cells from each well were stained with CD3-PC7 (clone UCHT1, 10 μL/test, Beckmann Coulter) for flow cytometric detection of CFSE fluorescence on CD3+ T cells. Discrimination for dividing cells was set up using NC. T-cell proliferation was calculated as follows: [(average % of dividing T-cells in 10:1 MLR) – (average % of dividing T-cells in NC)] × 100/[(average % of dividing T-cells in PC) – (average % of dividing T-cells in NC)].

Statistical Analysis

The Spearman correlation coefficient with a significance test was used to measure the strength of the relationship between patient CBC prior to leukapheresis, the parameters of the leukapheresis product, the DC yield, and the quality control parameters. Differences in parameter values between groups were assessed by the non-parametric Mann-Whitney or Kruskal-Wallis test. Hierarchical clustering analyses were performed using the complete linkage method with the distance based on the Spearman correlation coefficient. The Spearman correlation distance was used for clustering of batches, and the absolute Spearman correlation distance was used for clustering DC parameters. For clustering analyses, DC parameters were centered and scaled (Z-score of parameters). $P < 0.05$ were considered statistically significant. All statistical analyses were performed with R 3.5.3 software (22).

RESULTS

Clinical Trial Accrual and Course

As of May 2019, 47 subjects were enrolled in the clinical trial, and the manufacturing process of DC-based vaccine was performed in 31 cases. Of these 31, the most common diagnoses were sarcoma, with 19 cases (61%), and high-risk neuroblastoma, with 4 cases (**Table 1**). In this group of 23 patients, we performed analysis of the manufacturing issues presented here. Sarcomas were specifically: seven Ewing sarcomas (36% of sarcoma pts), five (26%) osteosarcoma, two (11%) alveolar rhabdomyosarcoma, two (11%) embryonal rhabdomyosarcoma, and three (16%) synovial sarcoma (**Table 1**). The median enrollment age of the clinical trial was 14 years; 15 years for sarcoma patients and 5 years for neuroblastoma patients (**Table 1**). All 23 study subjects, i.e., 19 with sarcoma and four with neuroblastoma, underwent initial surgery to obtain tumor tissue for the tumor lysate-manufacturing process, and tumor lysates were manufactured without any tumor antigen extraction failure. Monocyte harvest and the subsequent manufacturing of DC-based IMP were performed for all 23 subjects. Out of the 23, 16 DC-based IMPs successfully passed through the manufacturing process and met the quality control criteria for administration to the patients. DC-based IMPs from seven subjects (six sarcoma, one neuroblastoma) were not manufactured or failed to pass quality control due to inadequate immunostimulatory properties (**Table 1**). The basic patient characteristics are described in **Table 1**, and the detailed clinical course is summarized in **Supplementary Table 2**.

Dendritic Cell Manufacturing, Its Yield, and DC Quality Including Immunostimulatory Properties

We achieved DC yields ranging from 0 to 43.6%, with a mean of 17.2% and an s.d. of 12.7% in this specific cohort. A DC yield equal to 0 represented a manufacturing process that was unsuccessful, with all DCs detached from the flasks. The quality control parameters involved microbial sterility and *Mycoplasma* spp. negativity, the viability and phenotype of thawed DCs, the phenotype of thawed DCs after 2-day cultivation, the production of IL-12 and IL-10 during 24-h cultivation of thawed DCs, and 6-day allo-MLR and auto-MLR. All batches of DCs fulfilled the microbiological criteria of QC and the criteria

TABLE 1 | DC-based vaccine-manufacturing outcome, basic patient characteristics, therapy preceding monocyte harvest.

Primary diagnosis	Date of study enrollment/Age in years at study enrollment/Pt No	Treatment line prior to monocyte harvest/Treatment and its duration/Date of monocyte harvest	DC-based vaccine-manufacturing outcome
EWING SARCOMA			
Ewing sarcoma of the mandible	09/2015; 14; KDO-0101	2nd; VCR/Irino + pazopanib, 09/2015–04/2016; 01/2016	Passed QC
Localized Ewing sarcoma of the left femur	02/2016; 12; KDO-0109	3rd; ARST08P1 + sunitinib, 03/2016–06/2016; 03/2016	Did not pass QC
Localized Ewing sarcoma of the left distal humerus	02/2016; 12; KDO-0111	2nd; AEWS1031 + pazopanib, 02/2016–08/2016; 05/2016	Did not pass QC
Localized Ewing sarcoma of the spine C5-Th2, extradural, and intraspinal involvement	08/2016; 24; KDO-0118	2nd; AEWS1031, 08/2016–02/2017, 2 cycles VTC, 2 cycles VCR/Irino; 01/2017	Passed QC
Ewing sarcoma of the pelvis	12/2016; 14; KDO-0121	1st; Euro Ewing 2008, 11/2016–05/2017; 06/2017	Did not pass QC
Ewing sarcoma of the left proximal tibia	12/2016; 15; KDO-0122	2nd; VTC cycles, 01/2017–05/2017; 03/2017	Did not pass QC
Localized Ewing sarcoma of the left tibia	08/2018; 22; KDO-0144	2nd; 2x TMZ/Irino, 08/2018–10/2018; 10/2018	Did not pass QC
OSTEOSARCOMA			
Localized high-grade osteosarcoma of the right distal femur	09/2015; 10; KDO-0102	4th; VCR/Irino + pazopanib; 12/2015	Passed QC
High grade osteoblastic osteosarcoma of the left distal femur	10/2016; 8; KDO-0120	1st; AOST 0331, 10/2016–07/2017; 03/2017	Not manufactured
Localized osteoblastic osteosarcoma of the right proximal tibia	01/2017; 18; KDO-0124	3rd; AOST 1321 + VBL + CPM, 02/2017–10/2017; 3/2017	Passed QC
Localized osteosarcoma of the right proximal femur	02/2018; 25; KDO-0133	2nd; COMBAT III, 04/2018–12/2018; 04/2018	Passed QC
High-grade osteoblastic osteosarcoma of the left distal femur	05/2018; 22; KDO-0139	2nd; AOST0331 – cycle IE 07/2018; 09/2018	Passed QC
ALVEOLAR RHABDOMYOSARCOMA			
Alveolar rhabdomyosarcoma of the right calf	10/2015; 14; KDO-0103	2nd; ARST 0921 + TEM, 11/2015–01/2016; 12/2015	Passed QC
Alveolar rhabomyosarcoma, primum ignotum	10/2016; 12; KDO-0119	1st; ARST08P1 + TEM, 10/2016–05/2018; 04/2017	Passed QC
EMBRYONAL RHABDOMYOSARCOMA			
Embryonal rhabomyosarcoma of the pelvis	09/2017; 18; KDO-0131	1st; EpSSG RMS 2005, 09/2017–06/2018; 01/2017	Passed QC
Localized embryonal rhabomyosarcoma of the pelvis	07/2018; 15; KDO-0143	3rd; - rEECur - Topo/CYC, 08/2018–12/2018; 09/2018	Passed QC

(Continued)

TABLE 1 | Continued

Primary diagnosis	Date of study enrollment/Age in years at study enrollment/Pt No	Treatment line prior to monocyte harvest/Treatment and its duration/Date of monocyte harvest	DC-based vaccine-manufacturing outcome
SYNOVIALOSARCOMA			
Synovial sarcoma of the left thigh	04/2016; 14; KDO-0114	1st followed by COMBAT III 05/2015–12/2016; 12/2016	Passed QC
Localized synovial sarcoma of the neck	04/2018; 17; KDO-0137	2nd; Modified COMBAT III from 04/2018 + pazopanib from 08/2018; 06/2018	Passed QC
Localized synovial sarcoma of the left calf	06/2018; 21; KDO-0141	2nd; COMBAT III modified, 08/2018–02/2019; 10/2018	Passed QC
NEUROBLASTOMA			
Neuroblastoma in the retroperitoneum	04/2016; 12; KDO-0115	2nd; METRO-NB2012, 05/2016–10/2016; 07/2016	Passed QC
High-risk neuroblastoma in the left glandula suprarenalis	02/2018; 4; KDO-0135	1st followed by dinutuximab + retinoic acid, 11/2018–02/2019; 02/2019	Passed QC
Neuroblastoma in the right retroperitoneum	07/2018; 3; KDO-0142	2nd; ANBL 1221 - 3 cycles TMZ/Irino + dinutuximab, 08/2018–11/2018; 08/2018	Did not pass QC
Neuroblastoma in the right glandula suprarenalis	10/2018; 6; KDO-0147	4th; METRO-NB2012, 05/2017–12/2018; 11/2018	Passed QC

CPM, cyclophosphamide; Irino, irinotecan; TEM, temsirolimus; TMZ, temozolomide; Topo, topotecan; VBL, vinblastine; VCR, vincristine; IE, ifosfamide etoposid; VTC, vincristine, topotecan, cyclophosphamide; Pt. No., patient number; QC, quality control. Chemotherapy protocols: AEWS1031 (Ewing sarcoma)—vincristine, doxorubcin, cyclophosphamide, ifosfamide, etoposide; AOST0331 (osteosarcoma)—cisplatin, doxorubicine, methotrexate; AOST1321 (osteosarcoma)—denosumab; ARST0921 (refractory or relapsed rhabdomyosarcoma)—bevacizumab, vinorelbine, cyclophosphamide and temsirolimus; ARST1321 (non-rhabdomyosarcoma soft tissue sarcomas)—ifosfamide, doxorubicin, pazopanib; COMBAT III (metronomic)—celecoxib, etoposide, temozolomide, fenofibrate, ergocalciferol, bevacizumab, vinorelbine, cis-retinoic acid; EpSSG RMS 2005 (rhabdomyosarcoma)—ifosfamide, vincristine, actinomycin, doxorubicin; Euro Ewing (Ewing sarcoma)—vincristine, ifosfamide, doxorubicin, etoposide, actinomycin, cyclophosphamide; METRO-NBL2012 (metronomic treatment for neuroblastoma)—etoposide, celecoxib, propranolol, cyclophosphamide, vinblastine; rEECur protocol (relapsed soft tissue sarcoma)—topotecan, cyclophosphamide, irinotecan, temozolomide. Details on anti-cancer therapy dosing are summarized in ***Supplementary Table 2****.*

of viability, ranging from 85 to 100% with a mean of 95%. Their variability in phenotype and immunostimulatory property is shown in **Supplementary Table 3**. The mean phenotype of the manufactured DCs immediately after thawing for selected parameters was as follows: CD8019 (range: 2–86%), CD86 91% (76–100%), CD83 21% (0–86%), CD14 20% (1–69%), and CD197 90% (73–99%). The mean phenotype of thawed DCs after 2-day cultivation for selected parameters was as follows: CD80 77% (range: 25–97%), CD86 99% (95–100%), CD83 61% (12–89%), and MHC II 93% (63–100%). Mean cytokine production was as follows: IL-12 8,327 pg/10^6 DC (range: 9–80,824 pg/10^6 DC), IL-10 280 pg/10^6 DC (6–1,731 pg/10^6 DC), and IL-12/IL-10 ratio 35 (1–246). The mean *in vitro* proliferation of T-cells stimulated by manufactured DCs was 67% (29–98%) in allo-MLR and 9% (−3–37%) in auto-MLR. Due to inappropriate results for the immunostimulatory parameters of QC (phenotype, cytokine production, MLR), six out of 22 (27%) of the manufactured batches of DCs were not released for use in the clinical trial. The parameter values of the manufactured batches of DCs are shown in **Supplementary Table 3**.

Isolation of Monocytes by Adherence vs. Elutriation and Its Impact on Manufacturing Process Yield and the Immunostimulatory Parameters of DCs

Isolation of monocytes for DC manufacture was performed by elutriation in 14 cases and by plastic adherence in nine (39%) cases based on the real-world situation. Until March 2017, we performed elutriation of the leukapheresis product in all cases (11 cases: KDO-0101, -0102, -0103, -0109, -0111, -0114, -0115, -0118, -0120, -0122, -0124). Between April and September 2018, we performed elutriation in cases KDO-0121, -0137, and -0139, and adherence to plastic in cases KDO-0133, -0142, and -0144 due to there being > 10% neutrophils in the leukapheresis product or technical issues with the Elutra device for KDO-0119 and -0131. After October 2018, we isolated monocytes exclusively by adherence to the plastic surface in all cases: KDO-0135, -0141, -0144, and -0147.

Addressing the issue of whether the elutriation process is superior to adherence to plastic retrospectively, we compared the proportions of batches passing QC and their DC yield and phenotypic and immunostimulatory properties under the

two methods. Adherence to plastic resulted in two (22%) batches not being released, and elutriation resulted in five (36%) batches not being released (four did not pass QC and one was not manufactured). The OR (odds ratio) for passing QC in the plastic-adherence modality was 1.94 (95% CI: 0.29–13.19). The DC yield, viability, phenotype, and immunostimulatory properties (IL-12, IL-10, the IL-12/IL-10 ratio, allo-MLR, auto-MLR) in adherence to plastic vs. elutriation are summarized in **Figure 1**. A statistically significant difference was observed between QC results and monocyte isolation modality for the following post-thaw parameters (i) DC expression of CD86 on day 0 that was higher in the manufacturing process with plastic adherence, and (ii) borderline significant expression of CD14 on day 0 that was higher with elutriation. The values of both parameters were in favor of adherence to plastic. It is of note here that the subgroup with isolation of monocytes by the adherence to plastic was not biased by including a higher proportion of cases without potentially monocyte-interfering pharmacotherapy ("m" vs. "0" as described later; $p = 0.643$). Thus, we conclude that the isolation of monocytes by adherence to plastic is comparable to a manufacturing process with monocyte elutriation.

Parameters of CBC Prior to Monocyte Harvest, and Parameters of the Leukapheresis Product and Their Impact on Manufacturing Process Yield and the Immunostimulatory Properties of DCs

With the aim of identifying the CBC parameters (shown for each batch in **Supplementary Table 3**) associated with adequate DC characteristics and thus predicting whether the DC-manufacturing process would pass QC, we analyzed CBC prior to monocyte harvest in the context of batches that fail to pass QC and DC yield, phenotype, and immunostimulatory properties. The presence of immature granulocytes in CBC was associated with unsuccessful manufacturing ($p = 0.046$). DC yield was not associated with any single parameter of CBC. Expression of CD14 on manufactured cells was negatively correlated with relative lymphocyte count in CBC ($p = 0.001$) (**Figure 2**). The level of allogenic MLR was negatively associated with both the presence of immature granulocytes ($p = 0.010$) and NRBC ($p = 0.018$)

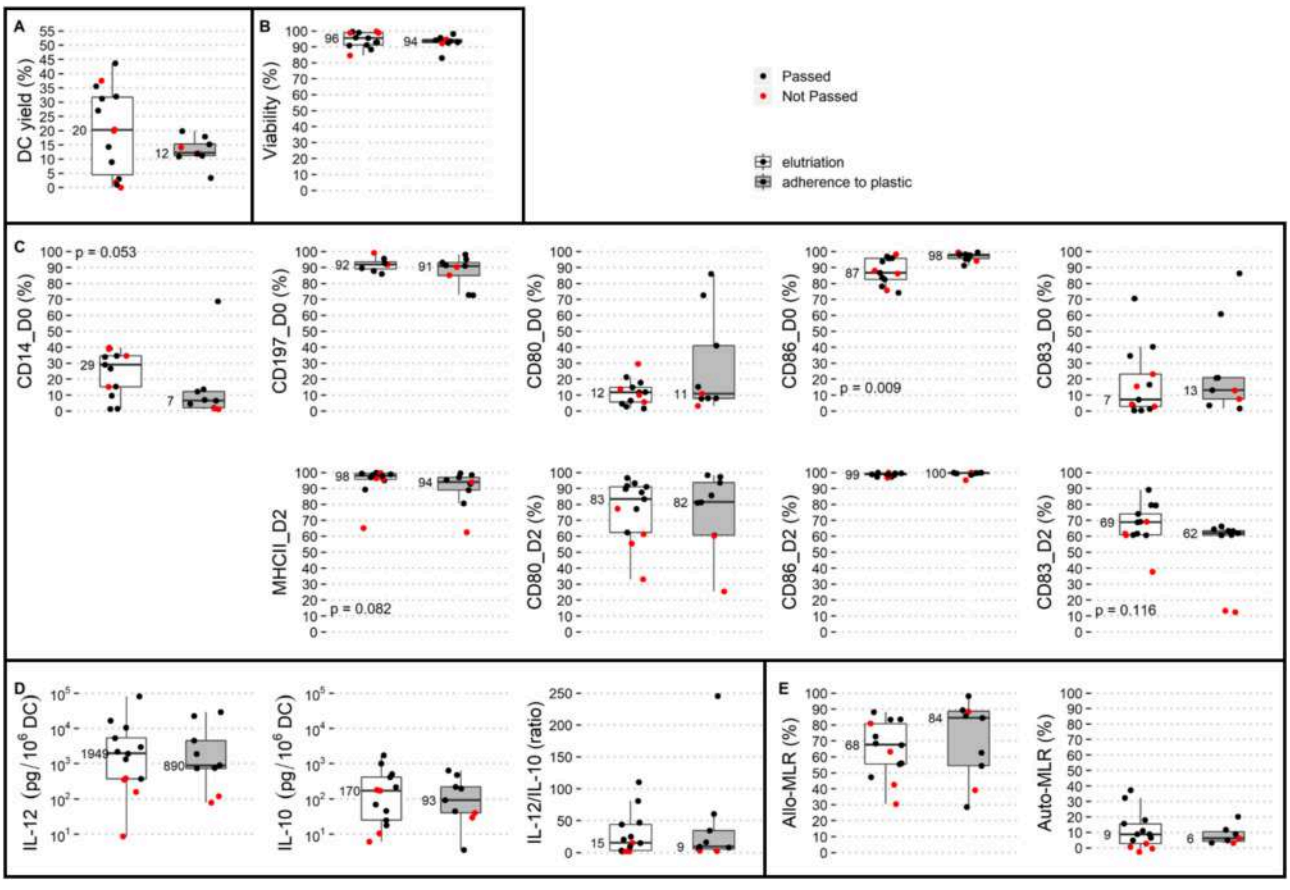

FIGURE 1 | Comparison of two monocyte isolation modalities with respect to dendritic cell (DC) production. Elutriation (white box plots) and adherence to plastic (gray box plots) were compared based on QC parameters: **(A)** DC yield, and post-thaw: **(B)** viability, **(C)** DC phenotype on day 0: CD14, CD197, CD80, CD86, and CD83 and on day 2: MHC II, CD80, CD86, and CD83, and immunostimulatory properties presented by **(D)** IL-12 production, IL-10 production, and IL-12/IL-10 production ratio, **(E)** allo-MLR and auto-MLR. Median values are shown for each parameter for each monocyte isolation modality. Black dots show QC results of manufactured DCs that passed quality control, and red dots show results of manufactured DCs that did not pass quality control.

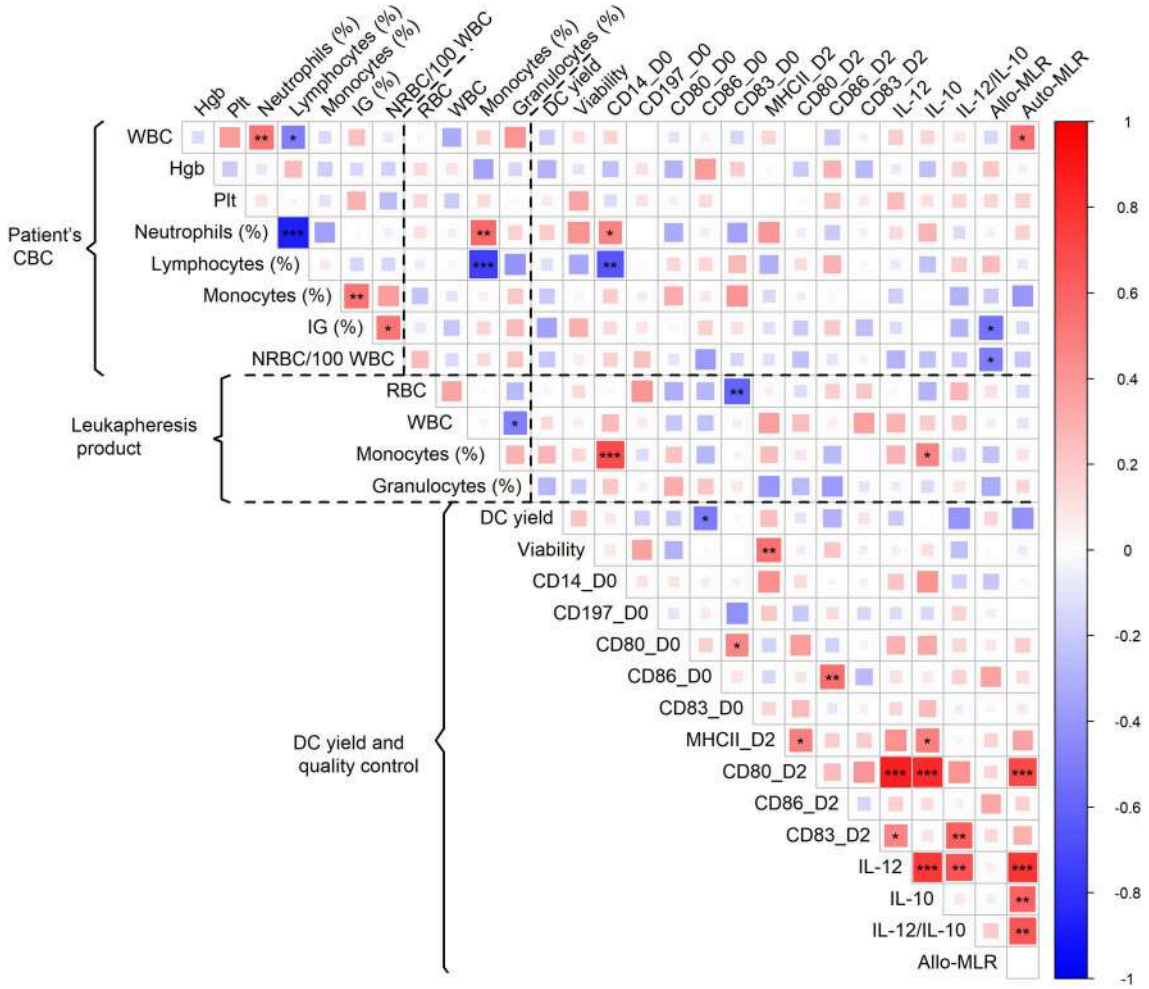

FIGURE 2 | Association of patient CBC prior to monocyte harvest and parameters of leukapheresis product with DC yield and quality control. Red color represents a positive correlation and blue color a negative correlation; strength of relationship is represented by size of square and intensity of color—larger squares with intense color have a stronger association; $^{*}p < 0.05$, $^{**}p < 0.01$, $^{***}p < 0.001$.

in pre-leukapheresis CBC (**Figure 2**). The level of autologous MLR was positively associated with absolute leukocyte count ($p = 0.016$) (**Figure 2**). Similarly, a high proportion of monocytes ($p < 0.001$) and low proportion of T-cells ($p = 0.001$) in the leukapheresis product were associated with increased expression of CD14 on manufactured cells (**Figure 2**). A high proportion of monocytes in the leukapheresis product was associated with increased production of IL-10 by manufactured cells ($p = 0.027$) (**Figure 2**).

Therapy Preceding and/or Concomitant With Monocyte Harvest and Its Association With Manufacturing Process Yield and the Immunostimulatory Properties of DCs

The patient history of anti-cancer treatment and the outcome of DC manufacture were evaluated for an association between DC parameters and lines of therapy classified as 1st, 2nd, and 3rd or subsequent lines that were followed by monocyte harvest for DCs. The history of anti-cancer treatment had no observed impact on the quality of manufactured DCs (**Supplementary Figure 2**). Pharmacotherapeutics 60 days prior to and/or concomitant to monocyte harvest were classified into two groups and designated as follows (i) "m" ($n = 17$) for administration of therapy potentially interfering with monocyte viability and/or differentiation, namely TKI, mTOR inhibitors, chemotherapy in cell biology-interfering doses, i.e., MTD-based dose, anti-RANKL mAb, retinoic acid, and/or G-CSF (**Supplementary Table 1**) < 60 days prior to monocyte harvest, (ii) "0" ($n = 6$) for metronomic therapy/chemotherapy or no potentially monocyte-interfering therapy concomitantly or < 60 days prior to monocyte harvest. All batches from the "0" category passed QC, whereas seven out of 17 (41%) monocyte-derived DCs from the "m" category failed to be released for patient administration. The OR for passing QC in category "0" was 9.3 (95% CI: 0.5–191). DC yield, DC immunophenotype on day 0 and day 2, and production of IL-10 did not differ between

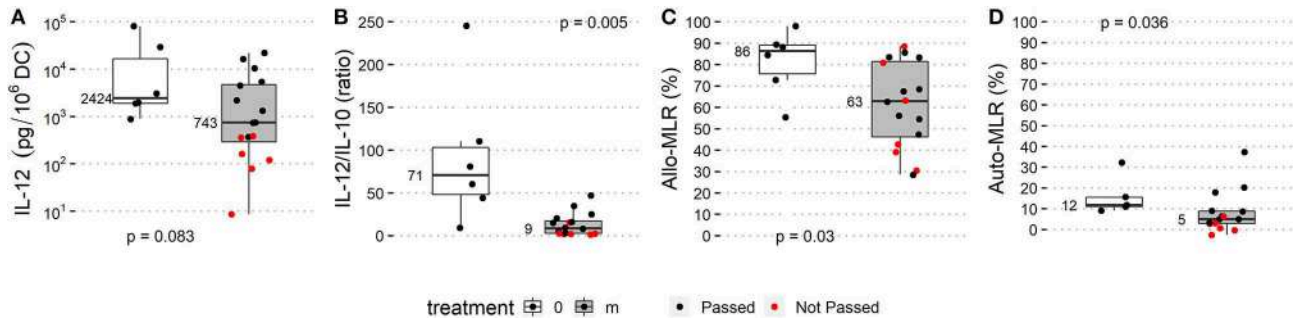

FIGURE 3 | Treatment prior to monocyte harvest and immunostimulatory properties of manufactured DCs. Manufacturing subgroup from monocytes harvested after MTD-based therapy potentially interfering with monocyte biology (listed in **Supplementary Table 1**; "m" treatment, gray box plots) and manufacturing subgroup from monocytes from untreated patients or after non-interfering treatment ("0" treatment, white box plots) were compared based on QC parameters: **(A)** IL-12 production, **(B)** IL-12/IL-10 production ratio, **(C)** allo-MLR and **(D)** auto-MLR. Median values are shown for each parameter for each treatment subgroup. Black dots show QC results of manufactured DCs that passed quality control, and red dots show results of manufactured DCs that did not pass quality control.

the "0" and "m" categories (**Supplementary Figure 3**). Median IL-12 production was 2,424 pg/10^6 DCs in the "0" category and 743 pg/10^6 DCs in category "m" ($p = 0.083$). The median IL-12/IL-10 ratio was 71 in the "0" category and 9 in the "m" category ($p = 0.002$). The median T-cell proliferation in allo-MLR was 86% in the "0" category and 63% in the "m" category ($p = 0.027$), and the in auto-MLR was 12% in the category "0" and 5% in category "m" ($p = 0.036$) (**Figure 3**).

In the analyzed study cohort, therapeutic regimens were heterogenic, with patients often treated with a combination of various compounds prior to monocyte harvest, and thus further categorization into single agent-defined subgroups and their analysis were impossible. Therefore, we performed cluster analysis of DC parameters in the context of therapy prior to monocyte harvest (**Figure 4**). Here we observed a cluster defined mainly by a superior IL-12/IL-10 ratio but low DC yield comprising batches KDO-0133 without any anti-cancer treatment, KDO-0137 treated with metronomic modified COMBAT with celecoxib, fenofibrate, low-dose cyclophosphamide, and low-dose vinblastine, and KDO-0115 treated with metronomic therapy with low-dose vinblastine, celecoxib, low-dose cyclophosphamide, and propranolol (see **Supplementary Table 2** for details on the treatment schedule and dosing). Furthermore, we observed a very similar pattern in DC properties in two batches, KDO-0142 and KDO-0144, that were manufactured from monocytes obtained from patients treated with temozolomide and irinotecan. These batches exhibited robust monocyte differentiation, as represented by their low CD14 expression, but failed to produce IL-12 or an immunostimulatory phenotype when matured, as represented by CD80 on post-cultivation DCs on day 2, and therefore did not meet the QC criteria. A pattern of relatively low DC yield, high production of IL-12, and notable monocyte differentiation and DC immunostimulatory phenotype and function was observed for batches KDO-0147, generated from monocytes from patients treated with celecoxib, and KDO-0141, from patients pretreated with combined metronomic therapy with low-dose vinblastine, low-dose etoposide, celecoxib, cholecalciferol, and fenofibrate. Batches KDO-0103 and KDO-0122 similarly exhibited poor yield, poor monocyte differentiation, a rather low IL-12/IL-10 ratio, and very low immunostimulatory functions toward donor T-cells. Monocytes from both batches were pretreated with an MTD-based combination of topoisomerase inhibitor and alkylating agent, with last administration from day 21 to 17, namely etoposide and ifosfamide in KDO-0103 and topotecan and cyclophosphamide in KDO-0122. This was followed in both cases by 9 days of administration of G-CSF filgrastim up to 7 days prior to monocyte harvest. High DC yield and viability but low markers of differentiation, immunostimulatory phenotype and IL-12/IL-10 ratio were similarly observed for batches KDO-0111 and KDO-0109 treated with topotecan, cyclophosphamide, and pazopanib. Based on features such as good DC yield and viability but low monocyte differentiation and a below-average IL-12/IL-10 ratio, these two batches clustered with KDO-0139 (treated with etoposide, ifosfamide, and filgrastim), KDO-0121 (etoposide, ifosfamide, and filgrastim), KDO-0118 (irinotecan and sunitinib), and KDO-0119 (cyclophosphamide, temsirolimus, and filgrastim). Notably, monocytes affected by retinoic acid (KDO-0135) or anti-RANKL denosumab (KDO-0124) produced DCs of average quality. In summary, monocyte-interfering MTD-based treatment of the clinical trial patients prior to monocyte harvest was associated with an impaired DC-based immunotherapy manufacturing process outcome. Certain combinations of anti-cancer treatments elicited a similar pattern of inadequate DC parameters. Namely, a combination of temozolomide and irinotecan was associated with poor DC maturation and immunostimulatory features, and a combination of pazopanib, topotecan, and MTD-based cyclophosphamide was associated with poor DC differentiation maturation and immunostimulatory parameters.

DISCUSSION

Here we show that despite strict adherence to the validated manufacturing protocol, the outcome of the manufacture of

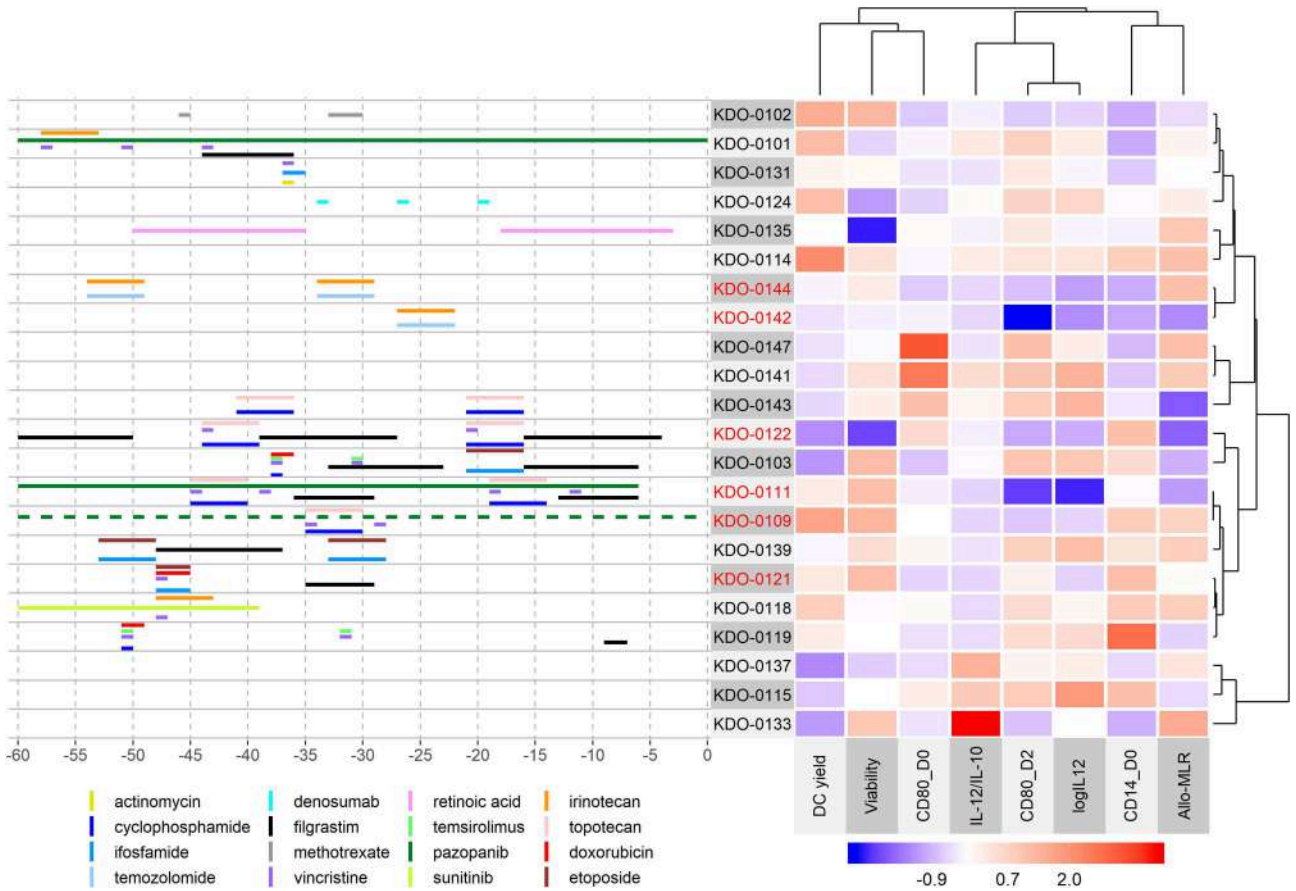

FIGURE 4 | Cluster analysis of DC parameters in the context of therapy prior to monocyte harvest. The heatmap on the right shows the immunostimulatory properties of manufactured DCs centered and scaled in the column direction (Z-score of parameters). Clusters are based on correlations. For clustering of DC parameters, but not batches, an equal meaning to positive and negative correlations was considered, and therefore strongly correlated parameters in the positive or negative manner clustered together. The left panel shows the treatment administered within 60 days of monocyte harvest. The day of the mononuclear harvest was set as day 0. An interactive version of the left panel with a detailed description of treatment including dosing is provided in **Supplementary Material 1**. Metronomic doses of chemotherapeutic drugs and supportive therapy such as vitamins and probiotics are not shown here but are summarized in **Supplementary Table 2**. Batches that did not pass quality control are indicated in red.

the medicinal product with monocyte-derived DCs is highly variable in terms of both DC yield and immunostimulatory properties. Moreover, in 30% of cases, manufacture of DC-based immunotherapy for advanced sarcoma and high-risk neuroblastoma patients resulted in a product that did not meet the specifications for the medicinal product and therefore was not released for application. This product failure rate was higher than in published studies (23, 24). Thus, in an attempt to improve the manufacturing process, to predict DC-manufacturing outcome, and, subsequently, to avoid laborious and costly DC manufacture that would not meet QC specifications, we addressed key variables in the manufacturing process. Namely, we focused on the issues of (i) monocyte isolation from the mononuclear leukapheresis product, (ii) parameters of the patient's CBC prior to monocyte harvest and parameters of the leukapheresis product, and (iii) anti-cancer therapy preceding monocyte harvest that may interfere with the ability of monocytes to differentiate into immunostimulatory DCs.

Regarding the method of monocyte isolation, we assessed whether monocyte extraction by a simple method of adherence to a plastic surface is comparable to the elaborate method of elutriation. During elutriation, monocytes can be contaminated with granulocytes with a similar sedimentation velocity to monocytes. Based on this observation, we validated the DC-manufacturing process with isolation of monocytes by adherence to plastic (25) to avoid contaminants that may interfere with DC differentiation by altering the levels of pro-differentiation cytokines and/or the formation of a suppressing microenvironment through generating decay products during cultivation. By comparative analysis of DC yield and immunostimulatory properties from the manufacturing processes of isolation of monocytes by elutriation vs. adherence to plastic, we conclude that the adherence method is comparable to the elutriation method. The method of adherence to plastic is simple in terms of the equipment, material, and manufacturing steps required and therefore is less costly, less prone to errors,

and more GMP-friendly than the elutriation process. In healthy adult volunteers, monocyte-derived DC yield with monocyte elutriation has been shown to be superior to adherence to plastic (26); this was not observed under our manufacturing conditions of heavily pretreated pediatric sarcoma and neuroblastoma patients.

With regards to the pharmacotherapy preceding monocyte harvest, we observed that therapy with agents interfering with the biology of monocytes 60 days prior to monocyte harvest was associated with reduced production of IL-12 and deficient functional immunostimulatory properties of the manufactured DC-based vaccine and subsequently often resulted in QC failure. It is of note here that failures in DC production occurred more often prior to the implementation of stricter criteria for non-allowed pharmacotherapy preceding monocyte harvest. Specifically, we observed impaired monocyte differentiation and, subsequently, inadequate immunostimulatory features in monocytes pretreated with a combination of an MTD-based dose of the alkylating agent cyclophosphamide, topoisomerase I inhibitor topotecan, and TKI pazopanib. We have previously shown that TKI pazopanib *in vitro* impairs the immunostimulatory properties of monocytes, including up-regulation of the immunoinhibitory surface molecule ILT-3 and decreased capability to up-regulate MHC II in response to LPS (27). Interestingly, however, pretreatment of monocytes *in vivo* with pazopanib without any other immediate treatment (KDO-0101) did not result in attenuated DC vaccine quality. Topotecan has been shown to partially activate monocyte-derived DCs but to prevent the full maturation of DCs stimulated with a cocktail of proinflammatory mediators (28). A different pattern was observed for DCs from cases treated with a combination of the alkylating agent temozolomide (TMZ) and the topoisomerase I inhibitor irinotecan (iri), and we observed monocyte differentiation but not DC immunostimulatory properties, resulting in a medicinal product that did not pass QC and was not administered. It is of note that one case was a sarcoma and one a neuroblastoma patient. Moreover, we also observed a similar pattern of poor DC parameters in a case of synovialosarcoma with TMZ/iri therapy in a cohort of patients outside this clinical trial. It has been shown that monocytes are particularly sensitive to the methylating agent temozolomide, undergoing apoptosis, while monocyte-derived DCs and macrophages are resistant to TMZ (19). Briegert and Kaina and Bauer et al. showed that monocytes accumulated single-strand DNA breaks due to failure of the re-ligation step in base excision repair and showed a lack of DNA repair protein expression (18, 19). Following TMZ treatment, monocytes demonstrated an unbalanced expression of DNA repair proteins, impairing base excision repair and the accumulation of double-stranded breaks (18, 19). *In vitro* studies of TMZ/iri cytotoxicity to neuroblastoma cells have revealed single- or double-stranded DNA damage to be mostly due to SN-38 (the active metabolite of irinotecan) and to be further enhanced through the addition of TMZ (29). Thus, we hypothesize that DNA damage caused by the combination of irinotecan and TMZ in the context of particular hypersensitivity of monocytes to temozolomide may underlie the unfavorable effect of anti-cancer therapy with TMZ/iri on the monocyte-derived immunostimulatory DC-manufacturing process. Monocytes from a patient treated with methotrexate, doxorubicin, and cisplatin failed to produce viable dendritic cells, but monocytes from another patient treated with methotrexate did not fail to produce DC vaccine. Methotrexate has reportedly inducedl apoptosis, reduced viability, induced differentiation, and reduced inflammatory properties of monocytes (30–33), and we may speculate, although based on anecdotal observation, that if combined with cisplatin, thereby shifting monocyte differentiation into an immunosuppressive phenotype (20), methotrexate may result in failure of monocyte-derived DC generation.

Regarding the composition of pre-leukapheresis CBC and the derived leukapheresis product and the outcome of DC manufacture, we observed that three interconnected features, i.e., (i) a low relative lymphocyte count, (ii) a high relative neutrophil count in CBC, and (iii) a high proportion of monocytes in the leukapheresis product, were associated with unfavorably high expression of CD14 on the manufactured cell product. Moreover, the presence of an increased number of immature granulocytes was associated with decreased potency of the DC-based product as quantified by allo-MLR. These observations may be underlain by emergency myelopoesis stimulated by G-CSF, which leads to a quantitative and qualitative change in all circulating myeloid cell types including neutrophils, monocytes, and myeloid-derived suppressor cells (34, 35). While fostering granulocyte effector functions, G-CSF also seems to promote immunosuppressive and tolerogenic properties in monocytes and monocyte-derived cells including increased production of IL-10 (36–39). In this context, it is of note that six out of seven cases treated with G-CSF within 60 days prior to monocyte harvest exhibited donor T-cell stimulation below the average and that the level of T-cell stimulation decreased with the intensity of G-CSF prior to monocyte harvest. Although the effect of G-CSF treatment on the DC-manufacturing process in our study cannot be dissected from the effect of preceding chemotherapy and targeted therapy, the tentative interpretation is that stimulation of myelopoesis with growth factors of granulocytes may have a rather negative impact on the outcome of the DC-based vaccine-manufacturing process.

Here, we show that treatment of patients with certain anti-cancer agents in MTD-based doses prior to monocyte harvest often leads to failure of manufacture of the immunostimulatory DC-based vaccine. We propose that the optimal time for monocyte harvest for generating DCs is prior to a cell-interfering treatment. With respect to the DC-manufacturing workflow, this would mean, in a majority of cancer patients, the implementation of DC manufacture from cryopreserved monocytes. Several studies have investigated the effect of cryopreservation on monocyte differentiation into DCs, but results have been conflicting. Some studies observed cryopreservation to have no effect on monocyte-derived DC production (40, 41). On the other hand, Silveira et al. showed that, when compared to fresh monocytes, cryopreserved monocytes exhibited impaired differentiation into dendritic cells, with lower rates of maturation and cytokine production in response to LPS and lower lymphocyte proliferation in allo-MLR (42). Thus, the cryopreservation of monocytes for

DC generation may decrease the quality of manufactured DCs, and the level of this decrease needs to be specified for a particular manufacturing protocol. In case of a minor drop in DC maturation and immunostimulatory parameters and function due to the cryopreservation of monocytes, this manufacturing modality should be considered, as it would allow harvesting of therapy-naïve monocytes and avoid a potentially detrimental effect of certain anti-cancer and supportive treatment on the quality of DC-based anti-cancer immunotherapy.

Another issue in the context of the concurrence of anti-cancer treatment and monocyte-derived DC manufacture is the length of the pharmacotherapy-free period prior to monocyte harvest. From our real-life experience gained on this study group, we conclude that a 30-day interval without treatment is not sufficient for the combination of temozolomide and irinotecan to sufficiently wash out the monocyte biology-interfering effect of this combination. However, the issue of a safe therapy-free window is not likely to be addressable through the establishment of a wash-out period for a particular drug. The fitness of monocytes and their capacity to differentiate and mature into DCs with high antigen-presenting effect is a matter of their biological function in the context of iatrogenic affection, which is complexly shaped by the need for immediate treatments, their combinations, their cumulative doses, and the long-term history of treatment. Therefore, identifying a marker revealed from a patient's peripheral blood that predicts the outcome of DC-generation would help to avoid an unproductive anti-cancer DC-manufacturing process. Here we show that a high monocyte count in CBC is not predictive of an efficacious outcome for DC generation. Nevertheless, we find that the presence of immature granulocytes in CBC may predict decreased immunostimulation elicited by DCs and, subsequently, unsuccessful preparation of DC-based IMP. However, closer evaluation of monocyte function prior to their collection for DC generation may be considered. A surrogate marker for the immunostimulatory capacity of monocytes may be evaluated in (i) their phenotype, e.g., the level of HLA-DR or ILT-3 expression on monocytes or the proportion of particular monocyte subsets according to CD14 and CD16 expression, or (ii) their ability to produce pro-inflammatory cytokines upon TLR stimulation (27).

In summary, monocytes represent a key starting material for anti-cancer DC-based vaccine manufacture. Therefore, monocyte conditions have an impact on the manufacturing yield, the differentiation into DCs, and the level of maturation and subsequent immunostimulatory functions. For DC manufacture from heavily pretreated pediatric patients with high-risk sarcomas and neuroblastoma, we conclude that the manufacturing yield and immunostimulatory quality of anti-cancer DC-based vaccine generated from patient's monocytes were not influenced by the monocyte isolation modality but were detrimentally affected by certain combinations of anti-cancer agents. Thus, the combination of chemotherapy or targeted therapy with DC-based immunotherapy needs to be scheduled not only with respect to the likely beneficial role of anti-cancer agents on the immunogenicity of tumor antigens for both *in vitro* DC generation via induction of immunogenic cell death and *in vivo* for effector response of DC-activated T-cells but also with respect to optimal monocyte immunostimulatory functions. Finally, these findings may also have implications for the general pharmacology of anticancer treatment. As our model of *ex vivo*-activated DC preparation generally parallels the *in vivo* differentiation pathways of monocytes to the antigen-presenting cells, we may imply that drug combinations at doses used clinically may result in an impairment of patient DCs and possibly immune competence in general. In conclusion, these findings may stimulate further research on dose and mechanism-of-action-based drug combination in patient-centered trials to optimize the treatment modalities currently available in clinical oncology.

DATA AVAILABILITY STATEMENT

All datasets generated for this study are included in the manuscript/**Supplementary Files**.

ETHICS STATEMENT

The studies involving human participants were reviewed and approved by Ethics Committee, University Hospital Brno. Written informed consent to participate in this study was provided by the participants' legal guardian/next of kin.

AUTHOR CONTRIBUTIONS

EH contributed to the trial design, contributed to the study design, participated in clinical data acquisition and analysis, contributed to Supplementary Material preparation, and drafted the manuscript. KP supervised IMP manufacture, contributed to laboratory data acquisition and analysis, contributed to data interpretation, and drafted the manuscript. DC participated in clinical data acquisition, contributed to Supplementary Material preparation, and revised the manuscript. IS performed statistical analysis, contributed to figure preparation and data interpretation, and drafted the manuscript. PMu contributed to the trial design, performed patient enrollment and treatment, contributed to data interpretation, and drafted the manuscript. PMa contributed to the trial design, participated in patient treatment, and drafted the manuscript. LFe contributed to laboratory data acquisition and analysis, contributed to Supplementary Material preparation, and drafted the manuscript. JM contributed to the trial design and drafted the manuscript. LJ participated in IMP manufacturing and revised the manuscript. LSe contributed to IMP manufacturing—monocyte harvest and drafted the manuscript. RP contributed to IMP manufacturing—starting material harvest and revised the manuscript. LFl contributed to IMP manufacturing—certification and revised the manuscript. LSo contributed to the trial design and revised the manuscript. RD, JS, and DV contributed to the trial design, contributed to data interpretation, and revised the manuscript. LZ-D conceived the study design, designed and supervised laboratory data acquisition and analysis, contributed to data analysis and interpretation, and drafted and finalized the manuscript.

FUNDING

This work was supported by the Czech Ministry of Education, Youth and Sport via Large infrastructure CZECRIN (LM2015090) and RECAMO (LO1413), by the European Regional Development Fund—project CZECRIN_4PATIENTY (Reg. No. CZ.02.1.01/0.0/0.0/16_013/0001826), and by the Czech Ministry of Health via DRO 00209805.

SUPPLEMENTARY MATERIAL

The Supplementary Material for this article can be found online at: https://www.frontiersin.org/articles/10.3389/fonc.2019.01034/full#supplementary-material

Supplementary Figure 1 | Decision tree for DC-IMP manufacturing workflow including in-process and quality controls.

Supplementary Figure 2 | Number of anti-cancer therapy lines preceding monocyte harvest were compared based on QC parameters: **(A)** DC yield, and post-thaw: **(B)** viability, **(C)** DC phenotype on day 0: CD14, CD197, CD80, CD86, CD83 and on day 2: MHC II, CD80, CD86, CD83 and immunostimulatory properties presented by **(D)** IL-12 production, IL-10 production and IL-12/IL-10 production ratio, **(E)** allo-MLR and auto-MLR.

Supplementary Figure 3 | Manufacturing subgroup from monocytes harvested after MTD-based therapy potentially interfering with monocyte biology and manufacturing subgroup from monocytes from untreated patients or after non-interfering treatment compared based on QC parameters: **(A)** DC yield, and post-thaw: **(B)** viability, **(C)** DC phenotype on day 0: CD14, CD197, CD80, CD86, CD83 and on day 2: MHC II, CD80, CD86, CD83 and immunostimulatory properties presented by **(D)** IL-12 production, IL-10 production and IL-12/IL-10 production ratio, **(E)** allo-MLR and auto-MLR.

Supplementary Table 1 | Monocyte biology-interfering medications.

Supplementary Table 2 | Study patient characteristics, disease course, and therapy.

Supplementary Table 3 | Source data: CBC parameters, manufacturing details, and QC parameters.

Supplementary Material 1 | html. Interactive—medications 60 days prior to monocyte harvest.

REFERENCES

1. Oberlin O, Rey A, Lyden E, Bisogno G, Stevens MC, Meyer WH, et al. Prognostic factors in metastatic rhabdomyosarcomas: results of a pooled analysis from United States and European cooperative groups. *J Clin Oncol.* (2008) 26:2384–9. doi: 10.1200/JCO.2007.14.7207
2. Pappo AS, Anderson JR, Crist WM, Wharam MD, Breitfeld PP, Hawkins D, et al. Survival after relapse in children and adolescents with rhabdomyosarcoma: a report from the Intergroup Rhabdomyosarcoma Study Group. *J Clin Oncol.* (1999) 17:3487–93. doi: 10.1200/JCO.1999.17.11.3487
3. Sharp SE, Trout AT, Weiss BD, Gelfand MJ. MIBG in neuroblastoma diagnostic imaging and therapy. *Radiographics.* (2016) 36:258–78. doi: 10.1148/rg.2016150099
4. Zapletalova D, Andre N, Deak L, Kyr M, Bajciova V, Mudry P, et al. Metronomic chemotherapy with the COMBAT regimen in advanced pediatric malignancies: a multicenter experience. *Oncology.* (2012) 82:249–60. doi: 10.1159/000336483
5. Berthold F, Homberg M, Proleskovskaya I, Mazanek P, Belogurova M, Ernst A, et al. Metronomic therapy has low toxicity and is as effective as current standard treatment for recurrent high-risk neuroblastoma. *Pediatr Hematol Oncol.* (2017) 34:308–19. doi: 10.1080/08880018.2017.1373314
6. Krishnadas DK, Shusterman S, Bai F, Diller L, Sullivan JE, Cheerva AC, et al. A phase I trial combining decitabine/dendritic cell vaccine targeting MAGE-A1, MAGE-A3 and NY-ESO-1 for children with relapsed or therapy-refractory neuroblastoma and sarcoma. *Cancer Immunol Immunother.* (2015) 64:1251–60. doi: 10.1007/s00262-015-1731-3
7. Merchant MS, Bernstein D, Amoako M, Baird K, Fleisher TA, Morre M, et al. Adjuvant immunotherapy to improve outcome in high-risk pediatric sarcomas. *Clin Cancer Res.* (2016) 22:3182–91. doi: 10.1158/1078-0432.CCR-15-2550
8. Klement GL, Arkun K, Valik D, Roffidal T, Hashemi A, Klement C, et al. Future paradigms for precision oncology. *Oncotarget.* (2016) 7:46813–31. doi: 10.18632/oncotarget.9488
9. Rossi M, Young JW. Human dendritic cells: potent antigen-presenting cells at the crossroads of innate and adaptive immunity. *J Immunol.* (2005) 175:1373–81. doi: 10.4049/jimmunol.175.3.1373
10. Hoffman R, Benz EJ Jr, Shattil S, Furie B, Cohen H. *Hematology: Basic Principles and Practice.* Churchill Livingstone (2005).
11. Jakubzick CV, Randolph GJ, Henson PM. Monocyte differentiation and antigen-presenting functions. *Nat Rev Immunol.* (2017) 17:349–62. doi: 10.1038/nri.2017.28
12. Boyette LB, Macedo C, Hadi K, Elinoff BD, Walters JT, Ramaswami B, et al. Phenotype, function, and differentiation potential of human monocyte subsets. *PLoS ONE.* (2017) 12:e0176460. doi: 10.1371/journal.pone.0176460
13. Patel AA, Zhang Y, Fullerton JN, Boelen L, Rongvaux A, Maini AA, et al. The fate and lifespan of human monocyte subsets in steady state and systemic inflammation. *J Exp Med.* (2017) 214:1913–23. doi: 10.1084/jem.20170355
14. Sampath P, Moideen K, Ranganathan UD, Bethunaickan R. Monocyte subsets: phenotypes and function in tuberculosis infection. *Front Immunol.* (2018) 9:1726. doi: 10.3389/fimmu.2018.01726
15. Zhou JX, Feng LJ, Zhang X. Risk of severe hematologic toxicities in cancer patients treated with PARP inhibitors: a meta-analysis of randomized controlled trials. *Drug Des Devel Ther.* (2017) 11:3009–17. doi: 10.2147/DDDT.S147726
16. Rusten LS, Lyman SD, Veiby OP, Jacobsen SE. The FLT3 ligand is a direct and potent stimulator of the growth of primitive and committed human CD34+ bone marrow progenitor cells *in vitro*. *Blood.* (1996) 87:1317–25.
17. Kao J, Timmins J, Ozao-Choy J, Packer S. Effects of combined sunitinib and extracranial stereotactic radiotherapy on bone marrow hematopoiesis. *Oncol Lett.* (2016) 12:2139–44. doi: 10.3892/ol.2016.4851
18. Briegert M, Kaina B. Human monocytes, but not dendritic cells derived from them, are defective in base excision repair and hypersensitive to methylating agents. *Cancer Res.* (2007) 67:26–31. doi: 10.1158/0008-5472.CAN-06-3712
19. Bauer M, Goldstein M, Heylmann D, Kaina B. Human monocytes undergo excessive apoptosis following temozolomide activating the ATM/ATR pathway while dendritic cells and macrophages are resistant. *PLoS ONE.* (2012) 7:e39956. doi: 10.1371/journal.pone.0039956
20. Dijkgraaf EM, Heusinkveld M, Tummers B, Vogelpoel LT, Goedemans R, Jha V, et al. Chemotherapy alters monocyte differentiation to favor generation of cancer-supporting M2 macrophages in the tumor microenvironment. *Cancer Res.* (2013) 73:2480–92. doi: 10.1158/0008-5472.CAN-12-3542
21. Hu J, Kinn J, Zirakzadeh AA, Sherif A, Norstedt G, Wikstrom AC, et al. The effects of chemotherapeutic drugs on human monocyte-derived dendritic cell differentiation and antigen presentation. *Clin Exp Immunol.* (2013) 172:490–9. doi: 10.1111/cei.12060
22. R Core Team. *R: A Language and Environment for Statistical Computing.* R Foundation for Statistical Computing, Vienna (2019).
23. Ge C, Li R, Song H, Geng T, Yang J, Tan Q, et al. Phase I clinical trial of a novel autologous modified-DC vaccine in patients with resected NSCLC. *BMC Cancer.* (2017) 17:884. doi: 10.1186/s12885-017-3859-3
24. Rodriguez J, Castanon E, Perez-Gracia JL, Rodriguez I, Viudez A, Alfaro C, et al. A randomized phase II clinical trial of dendritic cell vaccination

following complete resection of colon cancer liver metastasis. *J Immunother Cancer.* (2018) 6:96. doi: 10.1186/s40425-018-0405-z
25. Repnik U, Knezevic M, Jeras M. Simple and cost-effective isolation of monocytes from buffy coats. *J Immunol Methods.* (2003) 278:283–92. doi: 10.1016/S0022-1759(03)00231-X
26. Dohnal AM, Graffi S, Witt V, Eichstill C, Wagner D, Ul-Haq S, et al. Comparative evaluation of techniques for the manufacturing of dendritic cell-based cancer vaccines. *J Cell Mol Med.* (2009) 13:125–35. doi: 10.1111/j.1582-4934.2008.00304.x
27. Zdrazilova Dubska L, Fedorova L, Pilatova K, Mudry P, Hlavackova E, Matoulkova E, et al. TKI pazopanib impaires immunostimulatory properties of monocytes: implication for monocyte-derived DC-based anti-cancer vaccine preparation. *Ann Oncol.* (2016) 27:18P. doi: 10.1093/annonc/mdw525.18
28. Trojandt S, Knies D, Pektor S, Ritz S, Mailander V, Grabbe S, et al. The chemotherapeutic agent topotecan differentially modulates the phenotype and function of dendritic cells. *Cancer Immunol Immunother.* (2013) 62:1315–26. doi: 10.1007/s00262-013-1431-9
29. Cai W, Maldonado NV, Cui W, Harutyunyan N, Ji L, Sposto R, et al. Activity of irinotecan and temozolomide in the presence of O6-methylguanine-DNA methyltransferase inhibition in neuroblastoma pre-clinical models. *Br J Cancer.* (2010) 103:1369–79. doi: 10.1038/sj.bjc.6605927
30. Seitz M, Zwicker M, Loetscher P. Effects of methotrexate on differentiation of monocytes and production of cytokine inhibitors by monocytes. *Arthritis Rheum.* (1998) 41:2032–8. doi: 10.1002/1529-0131(199811)41:11<2032::AID-ART19>3.0.CO;2-J
31. Cutolo M, Sulli A, Craviotto C, Felli L, Pizzorni C, Seriolo B, et al. Antiproliferative-antiinflammatory effects of methotrexate and sex hormones on cultured differentiating myeloid monocytic cells (THP-1). *Ann N Y Acad Sci.* (2002) 966:232–7. doi: 10.1111/j.1749-6632.2002.tb04220.x
32. Moller B, Kukoc-Zivojnov N, Okamgba S, Kessler U, Puccetti E, Ottmann OG, et al. Folinic acid antagonizes methotrexate-induced differentiation of monocyte progenitors. *Rheumatol Int.* (2002) 22:60–7. doi: 10.1007/s00296-002-0188-9
33. Perpetuo IP, Caetano-Lopes J, Rodrigues AM, Campanilho-Marques R, Ponte C, Canhao H, et al. Methotrexate and low-dose prednisolone downregulate osteoclast function by decreasing receptor activator of nuclear factor-kappabeta expression in monocytes from patients with early rheumatoid arthritis. *RMD Open.* (2017) 3:e000365. doi: 10.1136/rmdopen-2016-000365
34. Manz MG, Boettcher S. Emergency granulopoiesis. *Nat Rev Immunol.* (2014) 14:302–14. doi: 10.1038/nri3660
35. Pilatova K, Bencsikova B, Demlova R, Valik D, Zdrazilova-Dubska L. Myeloid-derived suppressor cells (MDSCs) in patients with solid tumors: considerations for granulocyte colony-stimulating factor treatment. *Cancer Immunol Immunother.* (2018) 67:1919–29. doi: 10.1007/s00262-018-2166-4
36. Hartung T, Docke WD, Gantner F, Krieger G, Sauer A, Stevens P, et al. Effect of granulocyte colony-stimulating factor treatment on *ex vivo* blood cytokine response in human volunteers. *Blood.* (1995) 85:2482–9.
37. Mielcarek M, Graf L, Johnson G, Torok-Storb B. Production of interleukin-10 by granulocyte colony-stimulating factor-mobilized blood products: a mechanism for monocyte-mediated suppression of T-cell proliferation. *Blood.* (1998) 92:215–22.
38. Boneberg EM, Hareng L, Gantner F, Wendel A, Hartung T. Human monocytes express functional receptors for granulocyte colony-stimulating factor that mediate suppression of monokines and interferon-gamma. *Blood.* (2000) 95:270–6.
39. Saito M, Kiyokawa N, Taguchi T, Suzuki K, Sekino T, Mimori K, et al. Granulocyte colony-stimulating factor directly affects human monocytes and modulates cytokine secretion. *Exp Hematol.* (2002) 30:1115–23. doi: 10.1016/S0301-472X(02)00889-5
40. Hori S, Heike Y, Takei M, Maruyama M, Inoue Y, Lee JJ, et al. Freeze-thawing procedures have no influence on the phenotypic and functional development of dendritic cells generated from peripheral blood CD14+ monocytes. *J Immunother.* (2004) 27:27–35. doi: 10.1097/00002371-200401000-00003
41. Ghanekar SA, Bhatia S, Ruitenberg JJ, Dela Rosa C, Disis ML, Maino VC, et al. Phenotype and *in vitro* function of mature MDDC generated from cryopreserved PBMC of cancer patients are equivalent to those from healthy donors. *J Immune Based Ther Vaccines.* (2007) 5:7. doi: 10.1186/1476-8518-5-7
42. Silveira GF, Wowk PF, Machado AM, Duarte Dos Santos CN, Bordignon J. Immature dendritic cells generated from cryopreserved human monocytes show impaired ability to respond to LPS and to induce allogeneic lymphocyte proliferation. *PLoS ONE.* (2013) 8:e71291. doi: 10.1371/journal.pone.0071291

Conflict of Interest: The authors declare that the research was conducted in the absence of any commercial or financial relationships that could be construed as a potential conflict of interest.

frontiers in Oncology

CLINICAL TRIAL
published: 14 November 2019
doi: 10.3389/fonc.2019.01169

Assessment of Immune Response Following Dendritic Cell-Based Immunotherapy in Pediatric Patients With Relapsing Sarcoma

Lenka Fedorova[1,2,3], *Peter Mudry*[4], *Katerina Pilatova*[1,2,3], *Iveta Selingerova*[3], *Jana Merhautova*[1], *Zdenek Rehak*[2,5], *Dalibor Valik*[1,2,3], *Eva Hlavackova*[4], *Dasa Cerna*[4], *Lucie Faberova*[4], *Pavel Mazanek*[4], *Zdenek Pavelka*[4], *Regina Demlova*[1,3], *Jaroslav Sterba*[1,4,6] *and Lenka Zdrazilova-Dubska*[1,2,3]*

[1] Department of Pharmacology, Faculty of Medicine, Masaryk University, Brno, Czechia, [2] Department of Laboratory Medicine, Masaryk Memorial Cancer Institute, Brno, Czechia, [3] Regional Centre for Applied Molecular Oncology, Masaryk Memorial Cancer Institute, Brno, Czechia, [4] Department of Pediatric Oncology, University Hospital and Faculty of Medicine, Masaryk University, Brno, Czechia, [5] Department of Nuclear Medicine, Masaryk Memorial Cancer Institute, Brno, Czechia, [6] International Clinical Research Center, St. Anne's University Hospital, Brno, Czechia

OPEN ACCESS

Edited by:
Andrew Zloza, Rush University Medical Center, United States

Reviewed by:
Pierpaolo Correale, Azienda Ospedaliera 'Bianchi-Melacrino-Morelli', Italy
Simone Anfossi, University of Texas MD Anderson Cancer Center, United States
Praveen Bommareddy, Rutgers, The State University of New Jersey, United States

***Correspondence:**
Lenka Zdrazilova-Dubska
dubska@mou.cz

Specialty section:
This article was submitted to Cancer Molecular Targets and Therapeutics, a section of the journal Frontiers in Oncology

Received: *18 June 2019*
Accepted: *18 October 2019*
Published: *14 November 2019*

Citation:
Fedorova L, Mudry P, Pilatova K, Selingerova I, Merhautova J, Rehak Z, Valik D, Hlavackova E, Cerna D, Faberova L, Mazanek P, Pavelka Z, Demlova R, Sterba J and Zdrazilova-Dubska L (2019) Assessment of Immune Response Following Dendritic Cell-Based Immunotherapy in Pediatric Patients With Relapsing Sarcoma. Front. Oncol. 9:1169. doi: 10.3389/fonc.2019.01169

Monocyte-derived dendritic cell (DC)-based vaccines loaded with tumor self-antigens represent a novel approach in anticancer therapy. We evaluated DC-based anticancer immunotherapy (ITx) in an academic Phase I/II clinical trial for children, adolescent, and young adults with progressive, recurrent, or primarily metastatic high-risk tumors. The primary endpoint was safety of intradermal administration of manufactured DCs. Here, we focused on relapsing high-risk sarcoma subgroup representing a major diagnosis in DC clinical trial. As a part of peripheral blood immunomonitoring, we evaluated quantitative association between basic cell-based immune parameters. Furthermore, we describe the pattern of these parameters and their time-dependent variations during the DC vaccination in the peripheral blood immunograms. The peripheral blood immunograms revealed distinct patterns in particular patients in the study group. As a functional testing, we evaluated immune response of patient T-cells to the tumor antigens presented by DCs in the autoMLR proliferation assay. This analysis was performed with T-cells obtained prior to DC ITx initiation and with T-cells collected after the fifth dose of DCs, demonstrating that the anticancer DC-based vaccine stimulates a preexisting immune response against self-tumor antigens. Finally, we present clinical and immunological findings in a Ewing's sarcoma patient with an interesting clinical course. Prior to DC therapy, we observed prevailing CD8+ T-cell stimulation and low immunosuppressive monocytic myeloid-derived suppressor cells (M-MDSC) and regulatory T-cells (Tregs). This patient was subsequently treated with 19 doses of DCs and experienced substantial regression of metastatic lesions after second disease relapse and was further rechallenged with DCs. In this patient, functional *ex vivo* testing of autologous T-cell activation by manufactured

DC medicinal product during the course of DC ITx revealed that personalized anticancer DC-based vaccine stimulates a preexisting immune response against self-tumor antigens and that the T-cell reactivity persisted for the period without DC treatment and was further boosted by DC rechallenge.

Trial Registration Number: EudraCT 2014-003388-39.

Keywords: dendritic cells, anticancer immunotherapy, dendritic-cell (DC)-based vaccine, pediatric sarcoma, academic clinical trials, immunomonitoring, personalized medicine

INTRODUCTION

Patients with relapsed or refractory Ewing's sarcoma have a very poor prognosis. No substantial improvement has been achieved in the therapy of sarcoma patients in the last two decades despite research, and long-term survival is still <25%. Immunotherapeutic approaches including antigen-presenting cell-based vaccines have been employed as single agent or as part of combination strategies having been substantiated by a report on immunogenicity of Ewing's sarcoma with specific translocation resulting in EWS/FLI1 fusion. Following dendritic cell (DC) vaccine with untreated autologous lymphocytes, 39% of patients had measurable immune response against a neopeptide derived from the fusion gene (1). Promising results were reported after CD25+ regulatory T-cell depletion of an autologous lymphocyte infusion product augmented with interleukin (IL)-7, where immune reconstitution correlated with an improved survival of 63% in Ewing's sarcoma and rhabdomyosarcoma (2). Immunocompetent CD8+ T lymphocytes were observed within the tumor microenvironment of metastases after DC immunotherapy (ITx) but without direct cytotoxic efficacy probably due to expression of PD-1 on lymphocytes and PD-L1 on tumor cells (3). Such immune suppression could be bypassed using recently developed anti-PD-1 and anti-PD-L1 agents, demonstrating improved survival in several malignancies, including anecdotal cases of sarcomas (4, 5).

Proper antigen presentation has a key role in directing the immune system to attack tumor cells by targeting tumor-associated antigens. We manufacture fully personalized monocyte-derived DC-based vaccines that are evaluated in an academic investigator-initiated clinical trial for children, adolescents, and young adults with progressive, recurrent, or primarily metastatic high-risk tumors (EudraCT 2014-003388-39). As a part of clinical and research evaluation of patients, we performed DC characterization, peripheral blood immunomonitoring during DC treatment, and *ex vivo* assessment of T-cell cytotoxic function pre- and post-DC treatment. During peripheral blood immunomonitoring, we quantified circulating immune cells to evaluate both positive and negative players in cancer surveillance and eradication. We focused on absolute lymphocyte count (ALC) and neutrophil-to-lymphocyte ratio (NLR). Both parameters are associated with the number of lymphocytes as key players in the immune response to tumors. Additionally, NLR reflects the number of neutrophils that is a negative prognostic factor often related to paraneoplastic immune response. The peripheral blood lymphocyte compartment contains conventional αβ TCR+ T-cells, B-cells, natural killer (NK) cells, and also minor specific effector and regulatory cell types, including regulatory T-cells (Tregs), CD56+ CD3+ NKT-like cells (6), γδ T-cells (7), and monocytic myeloid-derived suppressor cells (M-MDSCs). These immune cell subsets constitute the actual clinical immunomonitoring, and their characteristics are reviewed in **Supplementary Material 1**.

This study focuses on high-risk sarcoma patients representing a major diagnosis in this clinical trial. First, we evaluated quantitative association between basic cell-based immune parameters. Next, we described patterns of these parameters and their time changes during the DC vaccination course in the peripheral blood immunograms. As a functional testing, we evaluated immune response of patient T-cells to the tumor antigens presented by DCs in autoMLR proliferation assay. This analysis was performed with T-cells obtained prior to DC ITx initiation and with T-cells collected after administration of the fifth dose of DCs. Finally, we presented clinical and immunological findings from DC-based ITx after relapse in the case of the Ewing's sarcoma patient.

METHODS

Clinical Trial Design and Methodology

This nonrandomized, open-label, academic, investigator-initiated, phase I/II clinical trial (EudraCT No. 2014-003388-39) was performed at a single center in Czechia in accordance with the principles of the Declaration of Helsinki and Good Clinical Practice. The protocol was approved by the local ethics committee at the site and by the designated authority of Czechia (the State Institute for Drug Control).

Patients eligible for the clinical trial were children, adolescents, and young adults (1–25 years old) with histologically confirmed refractory, relapsing, or primarily metastatic high-risk tumors; Karnofsky or Lansky score ≥50; life expectancy longer than 10 weeks; and adequate function of bone marrow, kidney, liver, and heart defined as absolute neutrophil count (ANC) ≥0.75 × 10^3/μl, thrombocytes ≥75 × 10^3/μl, hemoglobin 80 g/l, estimated glomerular filtration rate (eGFR) ≥70 ml/min/1.73 m^2, serum creatinine ≤1.5-fold upper limit for the appropriate age, bilirubin ≤1.5-fold upper limit for the appropriate age,

AST and ALT ≤2.5-fold upper limit for the appropriate age, ejection fraction ≥50%, and fractional shortening ≥27% assessed by echocardiography. In the case of bone marrow infiltration, ANC had to be $\geq 0.5 \times 10^3/\mu l$ and thrombocytes $\geq 40 \times 10^3/\mu l$. In the case of liver metastases, AST and ALT must have been ≤5-fold upper limit for the appropriate age. Patients must not have had severe ongoing toxicity resulting from any previous treatment. Radiotherapy (RTx), myelosuppressive, and immunosuppressive treatment must have been withdrawn at least 3 weeks before tumor tissue harvesting; the only exception is corticoid treatment of brain edema that was allowed. Myelopoietic growth factors must have been withdrawn at least 7 days before tumor tissue harvesting. Targeted therapy must have been withdrawn at least 7 days for tyrosine kinase inhibitors (TKI) or at least 3-fold half-life of the drug (upper limit 6 weeks) before tumor tissue harvesting. The time interval between autologous transplantation and tumor tissue harvest must have been ≥12 weeks and in the case of allogeneic transplantation ≥26 weeks. Patients with seropositivity to HIV1, HIV2, *Treponema pallidum*, hepatitis B or C, known hypersensitivity to the study medication, an autoimmune disease that was not adequately treated, uncontrolled psychiatric disease, or uncontrolled hypertension were not eligible. Allowed medication prior to monocyte harvest (leukapheresis) was as follows: metronomic chemotherapy (CTx), immune checkpoint inhibitors, and anti-CD20 antibodies are allowed as concomitant medication for any time before leukapheresis. Monoclonal antibodies (except anti-CD20), high-dose CTx, and high-dose corticoids must have been withdrawn at least 3 weeks prior to leukapheresis with the exception of corticoid treatment of brain edema, which was allowed. Since November 2017, amendment of the procedure for monocyte harvest was made, and TKI must have been withdrawn according to their half-life: drugs with short half-life of 3–14 h at least 2 days before leukapheresis (axitinib, dabrafenib, dasatinib, ibrutinib, idelalisib, nintedanib, ruxolitinib, trametinib), drugs with medium half-life of 15–35 h at least 7 days before leukapheresis [alectinib, bosutinib, lapatinib, lenvatinib, nilotinib, osimertinib, pazopanib, ponatinib, regorafenib, and non-tyrosine kinase inhibitor (non-TKI) everolimus], and drugs with long half-life of 36–60 h at least 12 days before leukapheresis (afatinib, ceritinib, erlotinib, gefitinib, imatinib, cabozantinib, crizotinib, sorafenib, sunitinib, vemurafenib, and non-TKI temsirolimus). Myelopoietic growth factors must have been withdrawn at least 7 days before leukapheresis/monocyte harvest. Patients previously treated with DCs were not allowed to enter the trial.

The primary endpoint of the trial was assessment of safety by analysis of incidence of adverse events of special interest (AESI; i.e., allergic reactions grade ≥3, acute or subacute autoimmune organ toxicity symptoms manifesting up to 30 days after administration of the vaccine, injection site reactions grade ≥4, infectious complications grade ≥3). The secondary safety endpoint was incidence of all adverse events assessed in relation to type, seriousness, and causality. Secondary efficacy endpoints were time to progression, overall survival, objective response to treatment at 12 and 24 months, and clinical benefit rate assessment at 6 and 12 months.

Investigational medicinal product (IMP) was administered as an add-on therapy to standard treatment. The dose of IMP contains 2×10^6 DCs in 100 μl of cryopreservation medium. DC-based IMP was administered intradermally every 3 ± 1 weeks, up to 35 doses, to a predefined site on the left or right arm near the axillary lymph node. The evening before administration and two evenings after application, topical imiquimod, toll-like receptor (TLR)-7 agonist, was applied on the injection site as an adjuvant. On the day of administration, the patient had to have adequate bone marrow function (defined in the same way as in the entry criteria described above) and was not allowed the following therapy: more than a week systemically administered corticosteroids except treatment for cerebral or spinal edema (single administration of corticoids due to premedication, treatment of allergic reaction, and substitution treatment in secondary hypocortisolism are allowed), anticoagulants in therapeutical dose (prophylactic doses of low-molecular-weight heparins were allowed), erythropoietin, pegylated granulocyte-stimulating growth factors or other growth factors except for filgrastim, RTx to sites and regional lymph nodes, except radiation for pain control, the interval between vaccine application, and administration of conventional CTx must have been more than 72 h. Complete blood count, biochemical analysis, and immunomonitoring were performed on every patient visit associated with administration of IMP.

DC Manufacturing and Quality Control

The DC-based vaccine, called MyDendrix, was manufactured under GMP in Clean rooms of the Department of Pharmacology, Faculty of Medicine, Masaryk University. Briefly, mononuclear cells were collected by leukapheresis, and then monocytes were separated by elutriation or adherence to a plastic surface. Harvested monocytes were cultivated with IL-4 and granulocyte-macrophage colony-stimulating factor (GM-CSF) and differentiated into DC. Immature DCs were subsequently exposed to autologous tumor lysate antigens. The preparation of tumor lysate from the patient's tumor obtained during curative surgery or extended biopsy preceded monocyte harvest. Maturation was induced by lipopolysaccharide and interferon-γ. Manufactured DCs were aliquoted into IMP doses, each containing 2×10^6 DCs based on reports (8, 9), cryopreserved in DMSO-containing medium, and stored at −150°C to −196°C. Quality control (QC) of DC-based IMP included viability, cell phenotype, production of IL-12 and IL-10, and stimulation of allogeneic and autologous T-cells to reflect the level of stimulatory properties of DCs. Details on DC-based IMP manufacturing were described in **Supplementary Material 2** (8, 10). DCs were stored frozen until the day of administration when a DC dose was shipped on dry ice for administration to a study patient, shortly thawed, and immediately injected intradermally to the patient.

Ex vivo Assessment of Prevaccination and Postvaccination T-Cells

Stimulatory properties of DCs were examined pre- and post-DC treatment by autologous mixed lymphocyte reaction (MLR). Pre-DC ITx lymphocytes were obtained during the manufacturing of

DCs of from the elutriation process or adherence of leukapheresis product obtained for separation of monocytes. The number of T-cells in the lymphocyte-rich fraction was quantified by flow cytometry: approximately 10^5 PBMCs were mixed with 10 µl of anti-CD45-PC7 (clone J33) and anti-CD3-FITC (clone UCHT1, both from Beckman Coulter), incubated 20 min in the dark, and analyzed on an FC500 flow cytometer (Beckman Coulter). PBMCs were aliquoted, cryopreserved in 1,000 µl of Cryostor CS5 (BioLife Solutions), frozen, stored at −150°C to −196°C, and thawed prior to auto-MLR seeding. For post-DC treatment assay, PBMCs were obtained from peripheral blood collected into K3EDTA tube (7 ml, Sarstedt) after application of at least five doses of DCs. Blood was layered onto Histopaque-1077® (Sigma-Aldrich, density 1,077 g/ml) and centrifuged (450 g, 30 min, 20°C, acceleration 3, brake 3). Fractions of mononuclear cells were collected and washed with Hank's Balanced Salt Solution (HBSS, Lonza). 10^7 PBMCs were cryopreserved in 1,000 µl Cryostor CS5 (BioLife solutions) and stored at −150°C. For pre- and post-DC treatment autoMLR, 10^7 target lymphocytes were stained with 250 µl 10 µM carboxyfluorescein succinimidyl ester (CFSE, Sigma-Aldrich) and seeded into sterile 96-well culture plate (Sarstedt, TC Plate 96-well, Suspension, F) at 10^5 cells/well in X-vivo 10 medium (Lonza) containing 5% inactivated human male AB serum (Sigma-Aldrich) at a 1:10 effector:target ratio (10^4 DC/well), positive control (PC) with phytohemagglutinin (PHA, Sigma-Aldrich) 1 mg/ml HBSS (final concentration 10 µg/ml in MLR), or negative control (NC) with complete X-vivo medium, final volume 200 µl/well. MLR experiments were seeded in triplicates and cultured for 6 days at 37°C/5% CO_2. Then 2×10^4 cells from each well were stained with CD3-PC7 (clone UCHT1, 10 µl/test, Beckman Coulter) for flow cytometric detection of CFSE fluorescence dilution on CD3+ T-cells. Discrimination for dividing cells was set up using the NC. T-cell proliferation was calculated as follows: [(average % of dividing T-cells in 10:1 MLR)−(average % of dividing T-cells in NC)] × 100/[(average % of dividing T-cells in PC)−(average % of dividing T-cells in NC)].

The medium from autoMLR was centrifuged, and pooled supernatant from triplicates was stored at −20°C until analysis. The concentration of interferon-gamma (IFN-γ), tumor necrosis factor alpha (TNF-α), and IL-17A was measured using a flow cytometric bead assay (BD Biosciences).

Peripheral Blood Immunomonitoring

Detailed peripheral blood immunomonitoring was performed at baseline (= before DC therapy initiation) and at each DC dose administration. The samples were collected on the day of vaccination just before the application of the vaccine. Blood was collected in a 7.5-ml S-Monovette® tube with K_3EDTA anticoagulant. Lymphocytes (ALC) and neutrophils (ANC) were measured using a Sysmex XN hematology analyzer. NLR was calculated as ANC/ALC. Immunophenotype was analyzed by multiparameter multicolor flow cytometer and software (Navios, Beckman Coulter). Diagnostic antibodies were purchased from Beckman Coulter, premixed in equal amounts in five cocktails, and stored in the dark at 2–8°C not longer than 7 days: 1/ CD14-PE (RMO52), CD15-KrO (80H5), CD11b-APC (Bear1), CD33-FITC (D3HL60.251), CD45-PB (J33), HLA-DR-PC5 (Immu357); 2/ CD3-FITC (UCHT1), CD4-PB (13B8.2), CD16-PC7 (3G8), CD56-PE (NKH-1); 3/ CD3-FITC (UCHT1), CD4-PB (13B8.2), CD27-AF750, CD45-KrO (J33), CD45RO-ECD (UCHL1), HLA-DR-PC5 (Immu357); 4/ TCR PAN γ/δ-FITC (IMMU510), TCR Vγ9-PC5 (IMMU360), TCR Vδ2-PB (IMMU 389), CD314-APC (ON72); 5/ CD3-FITC (UCHT1), CD4-PC7 (SFCI12T4D11), CD25-PC5 (B1.49.9), CD127-PE (R34.34). Blood (25 µl) was incubated with 10 µl of premixed antibody cocktail for 15 min in the dark at room temperature, hemolyzed by Versalyse® (Beckman Coulter) for 15 min and measured in five flow cytometric assays to detect: (1) M-MDSCs detected as CD45+ CD14+ CD11b+ CD33+ HLA-DR−, and their absolute count was calculated using the number of white blood cells (WBC) measured by the Sysmex XN hematology analyzer; (2) NK cells detected as CD3− CD56+ CD16+, NKT-like cells detected as CD56+CD3+; (3) circulating effector CD8+ T-cells were defined as CD3+ CD8+ CD27–, activated CD8+ T-cells were defined as CD8+ HLA-DR+; (4) γδ T-cell subsets classified as δ2+γ9−, δ2+γ9+, δ2−γ 9+, δ2−γ9− and evaluated for CD314; (5) Tregs defined as CD3+ CD4+ CD25+ CD127−/low+.

^{18}F-FDG PET/CT Scan

^{18}F-FDG PET/CT examination was performed using the hybrid scanner Biograph 64 HR+ (Siemens Erlangen, Germany). CT scan was provided in low-dose CT (25 mAs eff/120 kV). The patient had standard preparation prior to examination, including

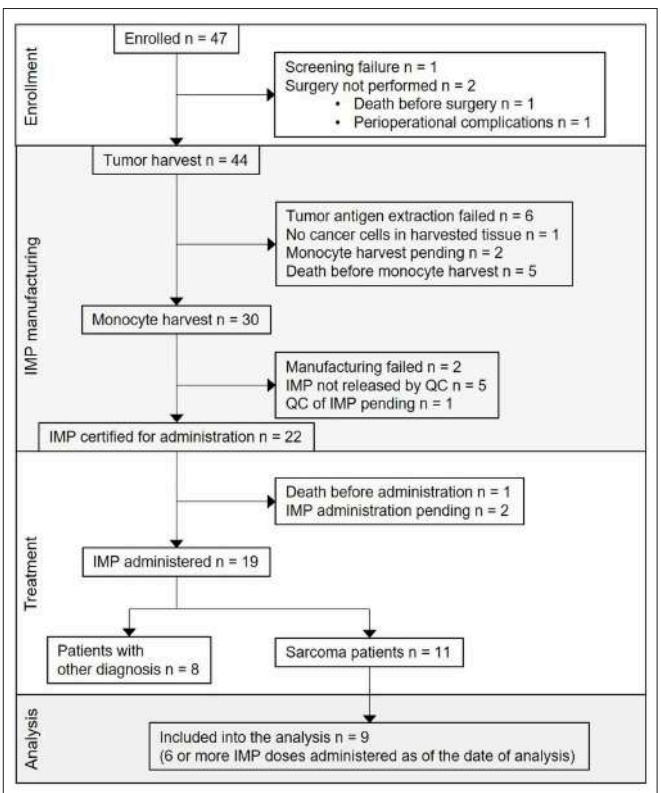

FIGURE 1 | Flow diagram for DC-based immunotherapy trial and study group definition. CONSORT flow diagram showing participant flow through each stage of the trial [enrollment, DC-based investigational medicinal product (IMP) manufacturing, treatment] and the analysis of sarcoma patients study group.

restriction of physical activity for 12 h, fasting for at least 6 h, capillary glycemia lower than 10 mmol/l (180 mg/dl) prior to ^{18}F-FDG administration and peroral hydration with 500–1,000 ml of plain water. ^{18}F-FDG was administered at a dose of 262 MBq in study 7/2017 and at a dose of 260 MBq in 1/2018. After an *in vivo* accumulation time of 60 min, whole-body scanning from the proximal third of thighs to the vertex of the skull was performed in both studies. All images were iteratively reconstructed and corrected for attenuation. ^{18}F-FDG uptake was assessed visually and also semi-quantitatively in the defined region of interest with calculation of target-to-liver ratios. A target-to-liver ratio higher than 1.0 was considered positive in all evaluated regions.

Statistical Analysis

Spearman correlation coefficient with significance test was used to measure the strength of the relationship between baseline circulating immune parameters. Graphic visualization of immunograms was performed using radar plot. Non-parametric Wilcoxon test for paired samples was used for analysis of pre- and post-treatment T-cell stimulation. *P*-values <0.05 were considered statistically significant. All statistical analyses were performed with R 3.5.3 software (11).

RESULTS

Clinical Trial Progress With Focus on Sarcoma Patients

The first subject was enrolled in September 2015. As of May 2019, the clinical trial was still ongoing, but with the accrual suspended. From the overall 47 enrolled patients, 25 (53%) were sarcoma patients. Screening failure occurred in one subject, and tumor harvest was not performed in two subjects. Tumor was harvested in 44 subjects; among them, the harvested tissue contained no cancer cells in one subject, tumor antigen extraction failure presenting as low concentration of protein in tumor lysate in six subjects, participation in the trial ended in five subjects due to disease progression and/or death, monocyte harvest has been pending in two subjects, monocyte harvest and subsequent manufacturing of DC-based IMP was performed in 30 subjects. Of the 30, manufacturing failed in two subjects, IMP did not pass quality control specifications in five subjects (four of them are sarcoma patients) (10), and 22 DC-based IMPs were released for administration to the patients. Of the 22, one subject died before IMP administration, administration has been pending in two sarcoma patients until the completion of high-dose CTx, and DC vaccine was administered to 19 subjects, including 11 sarcoma patients. Of these 11, nine patients received at least six doses of DC-based IMP as of March 2019 and were analyzed in presented immunomonitoring study (**Figure 1**). The age of sarcoma patients in the study group ranged from 10 to 24 years at the DC ITx initiation (**Table 1**). Stage of the disease in the study group at the DC ITx initiation was as follows: one (11%) in complete remission, three (33%) subjects in partial remission, one (11%) with stable disease, four (44%) with progressive disease (**Table 1**). Detail clinical course

TABLE 1 | Baseline patient characteristics and peripheral blood immune cell levels at dendritic cell (DC) therapy initiation.

Subject no./ sex	Primary diagnosis (primary localization)	Stage of the disease and PS at DC ITx init.	Age at DC ITx init.	Baseline cell-based immune parameters at DC ITx initiation									
				ALC* 10^6/ml	Eff. CD8+ %	Act. CD8+ %	NK* %	NKT-like* %	GD %* %	Tregs* %	M-MDSC count* 10^6/ml	NLR* Ratio
KDO-0101/F	Ewing sarcoma (mandible)	2nd CR Karnofsky 100	15 years	**1.9**	73.8	34.8	1.6↓	**4.9**	**2.9**	**5.9**	**0.07**	0.8↓
KDO-0102/F	Osteosarcoma (right distal femur)	PD Lansky 80	10 years	1.3↓	58.9	21.5	**4.6**	**1.9**	**4.6**	2.9↓	**0.07**	**1.2**
KDO-0114/M	Synovial sarcoma (left thigh)	PD Karnofsky 80	15 years	0.2↓	34.3	72.0	0.5↓	**2.9**	1.1↓	**12.0**	0.63↑	19.9↑
KDO-0118/F	Ewing sarcoma (spine C5-Th2)	PR Karnofsky 100	24 years	0.6↓	31.3	11.6	**8.1**	**2.2**	**3.2**	**4.5**	0.25↑	5.2↑
KDO-0119/F	Alveolar rhabdomyo-sarcoma (primum ignotum)	PR Karnofsky 80	13 years	0.6↓	25.1	10.8	**5.8**	**4.6**	**2.6**	**13.4**	**0.24**	**2.7**
KDO-0124/F	Osteosarcoma (right proximal tibia)	2nd mts relapse Karnofsky 100	19 years	0.8↓	73	21.9	**6.4**	**1.5**	**6**	2.9↓	**0.04**	**1.6**
KDO-0131/M	Embryonal rhabdomyosarcoma (pelvis)	PR Karnofsky 70	19 years	0.6↓	94.9	60.5	3.5↓	**14.8**	**3.1**	3.0↓	**0.00**	**1.7**
KDO-0133/M	Osteosarcoma (right proximal femur)	PD Karnofsky 100	24 years	0.9↓	49.1	2.7	**6.5**	**1.5**	**2.8**	3.0↓	0.26↑	**2.9**
KDO-0139/F	Osteosarcoma (left distal femur)	SD Karnofsky 90	22 years	0.5↓	14.73	37.9	4.9↓	**1.2**	0.6↓	**7.9**	0.42↑	10.7↑

*Cell-based immune parameters and their age-specific reference range (*if available): ALC, absolute lymphocyte count (reference range[1] 10 – 16 years 1.4–4.2 × 10^6/ml, >16 years 1.2–4.1 × 10^6/ml); NLR, neutrophil-to-lymphocyte ratio (reference range[2] 1–3); Eff CD8+, circulating effector cytotoxic T-cells (CD27-/CD8+, % of CD8+ T-cells); Act CD8+, activated cytotoxic T-cells (HLA-DR+/CD8+; % of CD8+ T-cells); NK cells, natural killers (reference range[1] 10–16 years 4–51% of lymphocytes, >16 years 5–49% of lymphocytes); NKT-like, circulating CD3+CD56+ cells (reference range[1] 10–16 years 0.64–15% of lymphocytes, >16 years 1–18% of lymphocytes); GD-T, gamma-delta T-cells (reference range[1] 10–16 years 2–17% of lymphocytes, >16 years 0.8–11% of lymphocytes); Treg, regulatory T-cells (reference range[1] 10–16 years 4–20% of CD4+ T-cells, >16 years 4–17% of CD4+ T-cells); M-MDSC, monocytic myeloid-derived suppressor cells (reference range[3] 0–0.24 × 10^6/ml). Numbers in bold refer to the values within the reference range, ↑–above the upper limit of the reference range, ↓–bellow the lower limit of the reference range. [1]Reference range originated from Schatorje et al. (12), [2]Estimated from reference ranges for relative differential cell blood count (13), [3]Own reference value, source group described in Pilatova et al. (13), init., initiation; F, female; M, male.*

of disease in nine sarcoma study patients is summarized in **Supplementary Material 3**.

No immune or infection-related AESIs were reported for all 15 evaluated subjects receiving DC ITx by the date of analysis.

Peripheral Blood Immunomonitoring of DC-Treated Sarcoma Patients

First, we evaluated the possible association of cell-based immune parameters in sarcoma patients before DC ITx and during DC treatment, up to six doses of DCs (**Figure 2**). Based on positive and negative correlations, immune parameters clustered *de facto* into two groups with inverse relation; a group consisting of ALC, proportion of effector cytotoxic T-cells among all T-cells, proportion of CD56+ CD3+ NKT-like cells among lymphocytes, proportion of γδ T-cells among lymphocytes, and an inversely correlated group with neutrophil-to-lymphocyte ratio (NLR), proportion of regulatory T-cells among CD4+ cells, number of M-MDSC, proportion of activated HLA-DR+ CD8+ cells among CD8+ cells, and proportion of CD56+ CD16+ CD3− NK cells among lymphocytes (**Figure 2**).

Baseline circulating immune parameters in nine sarcoma patients are shown in **Table 1**. At baseline, eight of nine patients had lymphopenia with mean ALC of 0.81 × 10^6/ml (**Table 1**). An exception was patient KDO-0101 (ALC 1.9 × 10^6/ml) with Ewing's sarcoma whose clinical course and laboratory findings are described later. The proportion of NK cells was low in six of nine patients (median 4.9%, min. 0.5%, max. 8.1%). The proportion of NKT-like cells among lymphocytes was predominantly low (median 2.2%), except for expanded NKT-like cells (14.8% of lymphocytes) in patient KDO-0131. γδ T-cells were low in six of nine patients (median 2.9%, min. 0.6%, max. 6.0%). Based on observed positive and negative association between particular cell-based immune markers, we constructed peripheral blood immunograms with putative anticancer effectors in upper part of an immunogram (namely, total lymphocytes, effector cytotoxic T-cells, CD56+ CD3+ NKT-like cells, γδ T-cells), and on the other hand, cancer-promoting or immunosuppressive actors (namely, NLR, M-MDSC, Tregs) and related factors (activated T-cells and NK cells) in the lower part of an immunogram (**Figure 3**). In peripheral blood immunograms, we presented baseline values of cell-based immune markers and their level after doses 1, 3, and 6 of ITx with DCs (**Figure 3**). The peripheral blood immunograms revealed distinct patterns in particular patients in the study group. For instance, we observed "immune-activated" pattern with patient KDO-0101 with Ewing's sarcoma who started DC ITx in the second complete remission, ALC was not decreased, effector cytotoxic T-cells represented the majority of circulating T-cells, and NLR and M-MDSC count were low. On the other hand, case KDO-0114 with progressing synovial sarcoma appeared to have an "immune-suppressive pattern" with high NLR, M-MDSC count, Tregs, and low ALC, proportion of effector cytotoxic T-cells, as well as NKT-like and γδ T-cells. Regarding time-dependent variations over the DC vaccination course, we did not observe any consistent trend in the dose-dependent change of levels of evaluated immune system parameters.

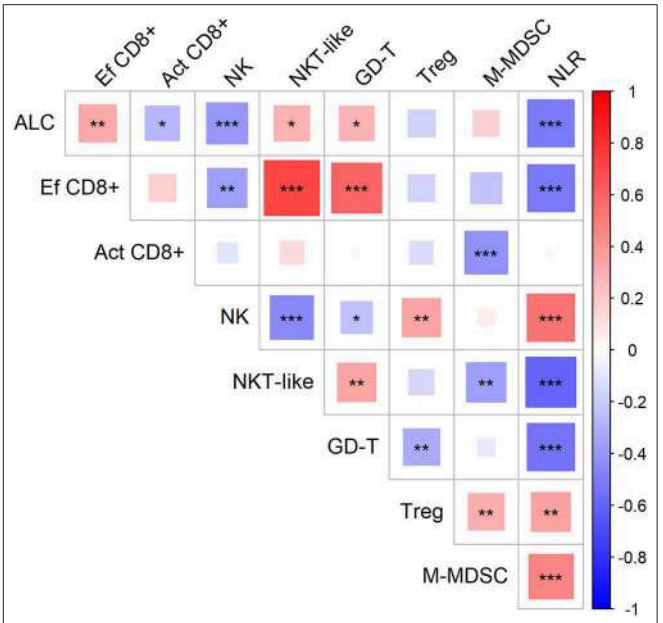

FIGURE 2 | Association of circulating immune markers during the course (from baseline to the sixth dose) of therapy with dendritic cells (DCs) in sarcoma study group. Red—positive correlation, blue—negative correlation; strength of relationship is represented by size of the square and intensity of the color, larger squares with intensified color have stronger relationship; $^*p < 0.05$, $^{**}p < 0.01$, $^{***}p < 0.001$; ALC, absolute lymphocyte count (10^6/ml); NLR, neutrophil-to-lymphocyte ratio; Ef CD8+, circulating effector cytotoxic T-cells (% of CD27− of CD8+ T-cells); Act CD8+, activated cytotoxic T-cells (% of HLA-DR+ of CD8+ T-cells); NK, circulating NK-cells (% of lymphocytes); NKT-like, circulating NKT-like cells (% of lymphocytes); GD-T, γδ T-cells (% of lymphocytes); Treg, regulatory T-cells (% of CD4+ T-cells); M-MDSC, monocytic myeloid-derived supressor cells (10^6/ml).

Patient T-Cells *in vitro* Stimulation by DCs Before and After DC Vaccination

The stimulation of sarcoma patient T-cells was examined by MLR proliferation assay with DCs from manufactured IMP and autologous T-cells obtained before DC ITx (pre-DC) and after at least five doses of DCs (post-DC) (**Figure 4**). The level of auto-MLR ranged from 0.5 to 18% (median 7.7%) with T-cells collected before DC ITx and from 4.9 to 28.4% (median 14.6%) with T-cells obtained after DC vaccination. Paired data with both pre-DC and post-DC were available for five cases, and all exhibited an increase in the T-cell stimulation after DC ITx. We observed the lowest post-DC increase in autologous T-cell stimulation by self-tumor antigens in cases KDO-0114, KDO-0124, and KDO-0133 who started DC treatment in disease progression. On the other hand, the highest increase in the T-cell stimulation with post-DC T-cells was exhibited by patient KDO-0101 who started DC ITx in complete remission of Ewing's sarcoma and remained at least up to ninth dose of DCs in complete remission. This case is described in more detail.

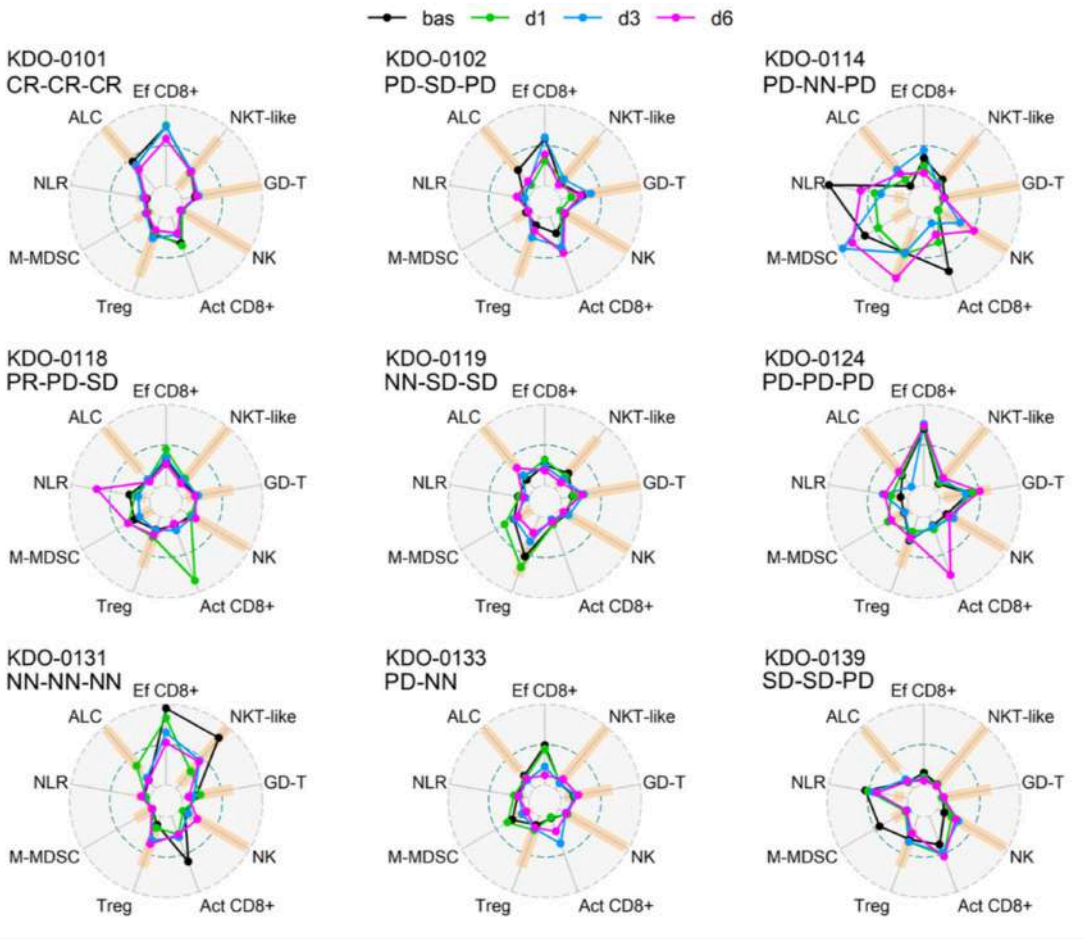

FIGURE 3 | Peripheral blood immunograms of dendritic cell (DC)-treated sarcoma patients. Nine circulating immune parameters are radially arranged with reference ranges shown in orange. Parameters are scaled according to numbers achieved within the entire study group of nine patients. Outer circle (OC, gray dashed) represents the upper limit of the reference range for ALC, NK cells, NKT-like cells, GD T-cells, maximum number reached for the particular marker for Tregs, M-MDSC, and NLR or 100% for Ef CD8+ and Act CD8+; small inner circle (IC, gray dashed) represents zero level; middle circle (MC, pacific blue dashed) represents 50% of OC level. Particular levels are listed for each parameter as follows. ALC, absolute lymphocyte count (reference range[1] 10–16 years 1.4–4.2 × 10^6/ml, >16 years 1.2–4.1 × 10^6/ml; OC: 4.2 10^6/ml); NLR, neutrophil-to-lymphocyte ratio (reference range[2] 1–3; OC 19.9); Ef CD8+, circulating effector cytotoxic T-cells (CD27−/CD8+; % of CD8+ T-cells) (OC: 100%); Act CD8+, activated cytotoxic T-cells (HLA-DR+/CD8+; % of CD8+ T-cells) (OC 100%), NK cells (reference range[1] 10–16 years 4–51% of lymphocytes, >16 years 5–49% of lymphocytes; OC: 51% of lymphocytes); NKT-like, circulating CD3+CD56+ NKT-like cells (reference range[1] 10–16 years 0.64–15% of lymphocytes, >16 years 1–18% of lymphocytes, OC 18% of lymphocytes); GD-T, γδ T-cells (reference range[1] 10–16 years 2–17% of lymphocytes, >16 years 0.8–11% of lymphocytes; OC: 17% of lymphocytes); Treg, regulatory T-cells (reference range[1] 10–16 years 4–20% of CD4+ T-cells, >16 years 4–17% of CD4+ T-cells; OC: 25.3% of CD4+ T-cells); M-MDSC, monocytic myeloid-derived suppressor cells (reference range[3] 0–0.24 × 10^6/ml; OC: 0.98 × 10^6/ml). Baseline levels prior to DC ITx initiation are shown in black and levels at doses d1, d3, d6 are shown in shades of blue. Clinical outcome is shown for each subject at DC ITx initiation, at dose 5, at dose 9. Clinical outcome is abbreviated as follows: CR, complete response; PD, progressive disease; SD, stable disease; NN, non-CR/non-PD; NA, not available. [1]Reference range originated from Schatorje et al. (12). [2]Estimated from reference ranges for relative differential cell blood count. [3]Our user-defined reference value, source group described in Pilatova et al. (13).

DC-Based Therapy After Relapse in a Ewing's Sarcoma Patient: Treatment Course and Outcome

A girl, born 2001, was diagnosed with primary disseminated EWS/FLI-1 positive Ewing sarcoma with a primary tumor in the mandible and skull metastases in December 2011. The patient was treated by protocol EuroEwing 2008, 6x VIDE: vincristine (1.5 mg/m^2/day; day 1), ifosfamide (3,000 mg/m^2/day; days 1, 2, 3), doxorubicin (20 mg/m^2/day; days 1, 2, 3), etoposide (15 mg/m^2/day; days 1, 2, 3), 1× VAC: vincristine (1.5 mg/m^2/day; day 1), actinomycin (0.75 mg/m^2/day; days 1, 2), cyclophosphamide (1,500 mg/m^2/day; day 1) from 12/2011 to 10/2012. Surgery was performed in June 2012 with partial resection of primary tumor. Radical resection was not possible due to mutilation. High-dose (HD) CTx treosulphan/melphalan with autologous peripheral blood stem cell transplantation (APBSC) followed in July 2012. Then, the patient underwent RTx of the mandible and parietal bone from September 2012 to November 2012 (34 Gy + 45 Gy), and CTx continued by

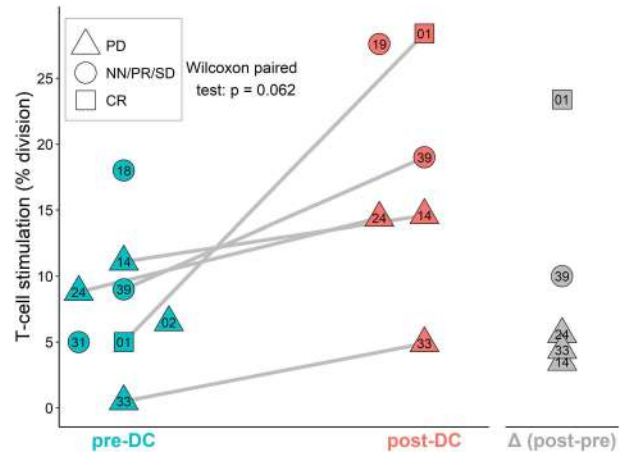

FIGURE 4 | AutoMLR with patients' pre-dendritic cell (DC) and post-DC T-cells stimulated by DC-based investigational medicinal product (IMP). The stimulation is expressed as the percentage of dividing autologous T-cells after incubation with DCs. Pre-DC (blue) refers to the stimulation of patients' T-cells obtained prior to DC-based ITx initiation. Post-DC (red) refers to the stimulation of patients' T-cells obtained after the fifth dose of DC vaccine. The difference (post-DC)−(pre-DC) is shown in gray. The shape of symbols refers to a stage of the disease; PD, progressive disease; CR, complete remission; NN, non-CR/non-PD; PR, partial remission; SD, stable disease. Two-digit numbers refer to the last digits in patients' number (e.g., 01 = KDO-0101, etc.). A pair of pre-DC and post-DC autoMLR in the same patient is linked by a gray line.

protocol EuroEwing 2008 with 7× VAC from October 2012 to May 2013. The first complete remission was achieved and lasted until May 2015 when the first relapse occurred in the skull. The patient was enrolled in the DC clinical trial, and the surgically removed tumor from the skull was used as a source of tumor antigens. In the second-line CTx, the patient received vincristine (1.5 mg/m^2/day; 5 days block), irinotecan (50 mg/m^2/day; 5 days block), and pazopanib (200 mg/daily). Monocytes were harvested in January 2016, and 35 doses of DC-based medicinal product were manufactured. One week after monocyte separation, palliative RTx on lesions in the skull was started and was performed from January 2016 to February 2016 with a total dose 41 Gy. Subsequently, after recovery from HD CTx and RTx, experimental DC-based ITx (on a biweekly basis) with immunomodulation *via* low-dose cyclophosphamide (26 mg/m^2/day) started in August 2016. The patient received 19 doses of DCs until the second relapse in 7/2017 with multiple metastases in the skull, pelvis (**Figures 5A,B**), and lesions in liver. FDG PET positivity without CT scan correlates was noted in the spinal column. Third-line CTx with topotecan (0.75 mg/m^2; 5 days block), cyclophosphamide (250 mg/m^2; 5 days block), and zoledronate (4 mg/4 weeks) with concomitant RTx was initiated. Evaluation of response showed stable disease. After three cycles, CTx was stopped due to hematological toxicity. Surprisingly, during the subsequent 4 months without treatment, substantial regression of metastases was noted both on PET/CT scan in 1/2018 (**Figures 5C,D**) and upon clinical examination of palpable metastases. Fourth-line maintenance metronomic CTx with low-dose vinblastine (3 mg/m^2/day) and continuing zoledronate (4 mg/dose/4 weeks) was started with rechallenge with DC-based vaccines from the original manufacturing from March 2018 to August 2018. Unfortunately, the partial regression was temporary, and slow continuing progressive disease led to the death of the patient in November 2018.

DC-Based Therapy After Relapse in a Ewing's Sarcoma Patient: *Ex vivo* Prevaccination and Postvaccination T-Cell Response and Peripheral Blood Immunomonitoring

Pre-DC treatment T-cell response evaluated by autoMLR as a part of DC quality control resulted in a mean of 5% T-cell division. Post-DC (after the fifth dose) autoMLR exhibited 28% T-cell division (**Figure 6A** blue). Production of cytokines (IFN-γ, TNF-α, IL-17A) during auto-MLR mildly increased in post-DC compared to pre-DC evaluation (**Figure 6B** blue). AutoMLR with T-cells collected before restart of DC treatment in February 2018 (after the third-line Ctx with topotecan, cyclophosphamide, and zoledronate with RT and an additional 4 months with no antitumor treatment) exhibited 22% T-cell division and, upon the fifth "rechallenge" dose, 40% T-cell division was observed (**Figure 6A** red). IFNγ production during autoMLR substantially increased after the fifth dose of DC rechallenge (**Figure 6B** red). The variations of circulating immune markers exhibited only minor changes at the beginning of both lines of therapy with DCs (**Figure 6C**). Levels of circulating immune markers at each dose of both lines of DC-based therapy are shown in **Supplementary Material 4**. At DC rechallenge, an increase in the proportion of circulating effector CD8+ cells and an increase in the proportion of γδ T-cells compared to the initiation of first-line DCs was observed (**Figure 6C**). In this patient, γδ T-cells were predominantly Vγ9-Vδ2- prior to DC ITx initiation (baseline 39%). Vγ9+Vδ2+ T-cells represented 33% of γδ T-cells, and their proportion decreased during DC Itx, and this γδ subset was almost depleted from circulation after third-line CTx (**Figure 6D**). In contrast to the Vγ9+Vδ2+ subset, Vγ9-Vδ2- T-cells were predominantly CD314(NKG2D)+ (**Supplementary Material 4**).

DISCUSSION

The primary endpoint of the clinical trial investigating anticancer therapy with DCs was the evaluation of treatment safety with interim result from 15 patients of no immune- or infection-related adverse events. Moreover, to gain more information from DC-treated patients, we performed immunomonitoring at baseline and at each DC dose. Collected data will be evaluated in the context of clinical outcomes after completion of the trial.

Here we show that an ALC was positively associated with the proportion of effector CD8+ cytotoxic T-cells out of total T-cells that is reflected by an inversion of the CD4:CD8 ratio and proportion of effector cells CD8+ among total CD8+ cytotoxic T-cells. The proportion of effector CD8+ cytotoxic

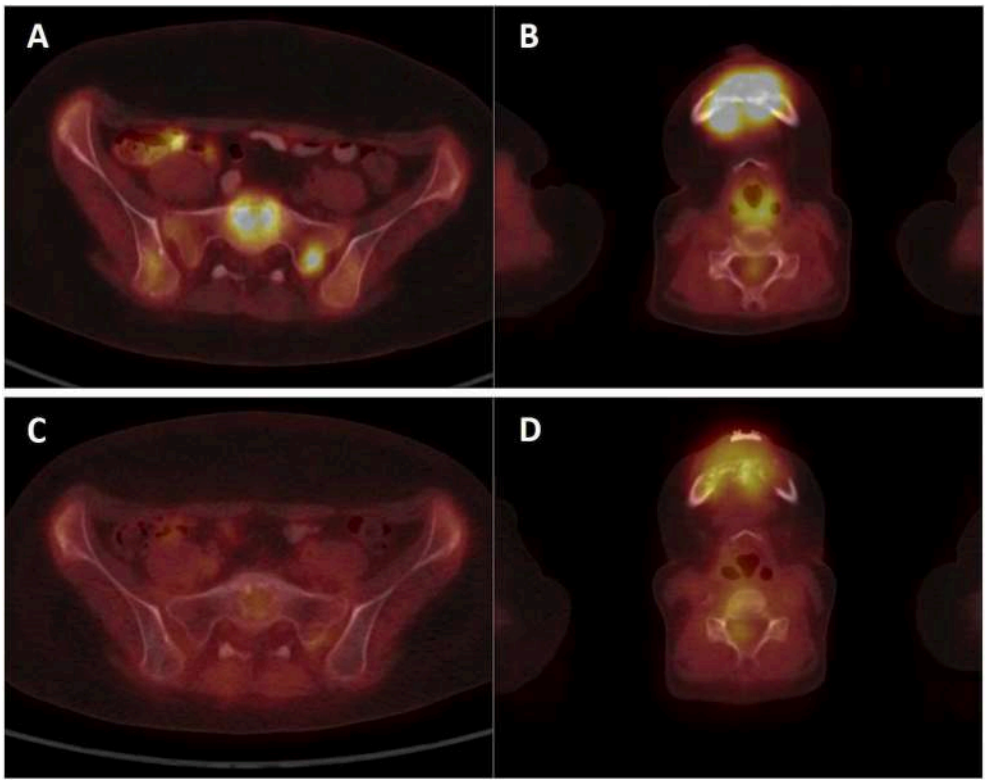

FIGURE 5 | PET/CT imaging of patient KDO-0101. **(A,B)** Examination of patient at second relapse in July 2017 showed ^{18}F-FDG-positive osteolytic lesions in the skeleton **(A)** sacrum, sacral base with a target-to-liver ratio of 2.74 and sacral left lateral mass with a target-to-liver ratio of 2.39 **(B)** mandible with a target-to-liver ratio of 4.88. **(C,D)** Control ^{18}FDG-PET/CT examination in January 2018 showed a decrease or complete diminishment of ^{18}FDG accumulation **(C)** sacrum, sacral base with a target-to-liver ratio of 0.69, and sacral lateral mass with a target-to-liver ratio of 0.66 **(D)** mandible with a target-to-liver ratio of 1.47.

T-cells among total T-cells was further correlated with the proportion of NKT-like cells and γδ T-cells. Both of these non-classical lymphocyte subsets have been studied and described for their role in cancer surveillance (6, 14, 15). On the other hand, in the putative cancer-enhancing/immune-suppressive cluster, we observed an association between circulating M-MDSC and Tregs that might be explained by increase in Tregs induced by MDSC-derived immunosuppressive cytokines (16) as described previously in non-cancer settings (17, 18). NLR associated with M-MDSC and Tregs, which may reflect "emergency" myelopoiesis induced by tumor or by host-related conditions, that promotes production of not only classical myeloid cells such as neutrophils and monocytes but also myeloid-derived suppressor cells (19). In line with two inversely associated clusters of immune-based circulating biomarkers, we have previously shown a negative correlation between effector CD27− cytotoxic CD8+ T-cells and number of both CD33hi PMN-MDSCs and M-MDSC in pediatric cancer patients (19).

The current clinical trial was designed for patients with progressive, recurrent, or primarily metastatic high-risk tumors that are always heavily pretreated by prior multimodal anticancer therapy. Indeed, patients with measurable disease represented vast majority of cases enrolled to this clinical trial. Therefore, we may expect that patients evaluated in this clinical trial exhibit prior profound suppression of immune function. Indeed, the majority of sarcoma patients were lymphopenic. On peripheral blood immunograms, we showed distinct patterns of immune parameters such as prevailing CD8+ T-cell stimulation in patient KDO-0101 or marked immunosuppression in KDO-0114. However, observations from immunomonitoring and clinical course in the patient KDO-0101 are worth particular attention. In comparison to the rest of the study group, patient KDO-0101 exhibited a lymphocyte count within the reference range, a high proportion of effector T-cells, and low levels of all observed parameters associated with adverse disease outcome, namely, Treg count, M-MDSC count, and neutrophil-to-lymphocyte ratio. This DC-vaccinated patient experienced substantial regression of metastatic Ewing's sarcoma after the second relapse. In comparison to the initial DC vaccination, at DC rechallenge, a proportion of effector and activated DC increased, although ALC dropped. We also observed an increase in γδ T-cells, which may be attributable to therapy with zoledronic acid that was part of the third-line therapy prior to DC rechallenge. Zoledronic acid causes accumulation of isopentenyl pyrophosphates (IPP), leading to stimulation of γδ T-cells (20). γδ T-cells responding to zoledronic acid are Vγ9+Vδ2+ T-cells that sense IPP via Vδ2 TCR (20).

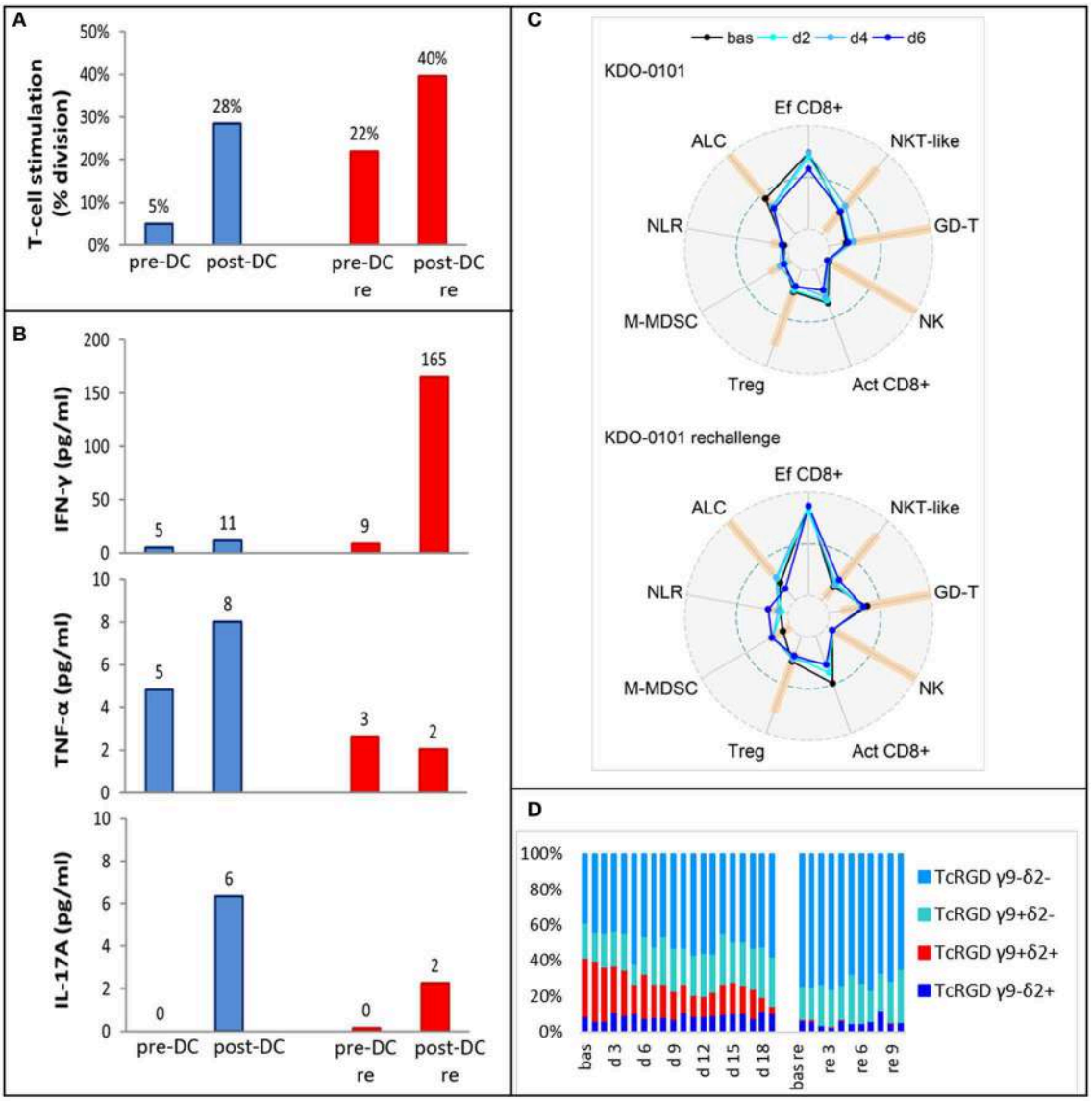

FIGURE 6 | *Ex vivo* functional and peripheral blood immunomonitoring of subject KDO-0101 during first dendritic cell (DC) immunotherapy and its rechallenge. **(A)** Stimulation of T-cells by DCs, reflected by the percentage of division T-cells. **(B)** Production of interferon-γ, tumor necrosis factor (TNF)-α, and interleukin (IL)-17A. **(A,B)** Pre- and post-DC treatment T-cell response was measured i/ (blue) before start of DC administration (pre-DC) and after the fifth dose (post-DC) ii/ (red) after 4 months with no antitumor treatment, before start of DC rechallenge (pre-DC re) and after the fifth rechallenege dose (post-DC re). **(C)** Peripheral blood immunogram from baseline (bas) through doses 2, 4, and 6 in the course of both DC treatment (upper) and DC rechallenge (lower). The layout of immunograms is described in **Figure 3**. **(D)** Four subtypes of gamma-delta TCR (Vγ9−Vδ2−, Vγ9+Vδ2−, Vγ9+Vδ2+, Vγ9−Vδ2+) in the course of both DC treatment from baseline to dose 19 and DC rechallenge from baseline to dose 10.

Interestingly, however, in this patient, we observed an increase in number of Vγ9−Vδ2− T cells and depletion of Vγ9+Vδ2+ T-cells. It is of note that only in two out of nine pediatric sarcoma patients (KDO-0118 and KDO-0139), the Vγ9+Vδ2+ subset represented a majority of circulating γδ T-cells. This is an unexpected observation in the context of reported findings (21) and of our observations in adult carcinoma patients (7) and patients treated and evaluated in the DC clinical trial with non-sarcoma cancers (data not shown).

The second relapse in subject KDO-0101 occurred during maintenance therapy with DC ITx. The observed temporary regression of metastases of the Ewing's sarcoma after second relapse may have been related to the immune response induced by previous DC treatment. Despite stable disease on the third-line CTx topotecan/cyclophosphamide, the patient exhibited partial response after concomitant RTx and DC vaccination only. Performance status of the patient was good over a long period of time, namely, Karnofsky index over 80%, despite

heavy metastatic involvement in skull, pelvic bones, spinal column, and liver. Performance status declined after 1 year of RTx, DCs ITx, and metronomic vinblastine and zoledronic acid. This unexpected observation suggests an opportunity to deliver such treatment to more patients. We observed substantial enhancement of T-cell reactivity toward DC-presented tumor antigens upon DC vaccination in patient KDO-0101 and to a lesser extent in four other sarcoma patients vaccinated with DCs and analyzed here. Thus, we confirmed that our anticancer DC-based vaccine stimulates a preexisting immune response against self-tumor antigens. Moreover, in the case of KDO-0101, functional *ex vivo* testing revealed that T-cell reactivity toward DC-presented self-tumor antigens persisted for a long period of time without DC treatment and was further boosted by DC rechallenge. In principle, the mechanism of action of anticancer DCs relies on stimulation of T-cell-mediated antitumor immune response targeting the presented cancer neoantigens. However, to date, the majority of patients treated with investigational DCs including the pediatric cancer patients in this clinical trial were end-stage or advanced cancer patients with extensive tumor mass and severely destroyed immune system. Limited clinical response achieved by DC-based ITx across numerous clinical trials can be attributed to both tumor-induced immunosuppression and, in heavily pretreated patients, also to anticancer therapy-induced immunosuppression. This is, nevertheless, supported by limited observational experience that enhancement of T-cell response to self-tumor antigens was related to the stage of the disease, that is, lower in cases with sarcomas in progression. It is thus crucial to overcome the immunosuppressive barrier to improve the efficacy of DC-based ITx as to have the antigen-presenting DC-based ITx combinable with cytokines, immune adjuvants, CTx, targeted therapy, and/or checkpoint inhibitors in order to boost T-cell effector functions and/or inhibit immune-suppressive pathways in the tumor mass (22). Ideally, selection of the right concomitant treatment to be combined with DC ITx shall be personalizable to target either particular immunosuppressive elements prevailing or particular immune effectors deficient in a particular patient, such as low-dose cyclophosphamide to deplete Tregs (23) or zoledronic acid to enhance γδ T-cells (24). In this context, immune-based biomarkers within the tumor microenvironment (if accessible) and/or systemic from peripheral blood could be exploited not only to provide an optimal ITx combination but also to select patients that would benefit from DC-based ITx. Regarding tumor-induced immunosuppression that is dependent on the tumor volume renders DC ITx less effective in patients with extensive tumor burden (25) and elicits higher tumor-specific immunologic response rates in the adjuvant compared to the metastatic setting (26). Thus, there is a rationale for the use of DC-based ITx earlier in the course of disease when tumor burden is still minimal; for example, in the adjuvant setting in patients at high risk of recurrence or in patients with minimal metastatic disease.

From our perspective beyond the study, anticancer DC vaccination could be more effective if appropriately personalized not only in terms of loading DC with self-tumor antigens but also in terms of (i) selection of the right patients that would benefit from ITx (such as patients with tumor with high mutational load), (ii) treatment at the right time when the disease and the level of immune suppression is minimal, and (iii) selection of right (possibly personalized) concomitant treatment that allows the optimal immunostimulation and anticancer activity of effector cells.

DATA AVAILABILITY STATEMENT

The datasets generated for this study are available on request to the corresponding author.

ETHICS STATEMENT

The studies involving human participants were reviewed and approved by Ethics Committee, University Hospital Brno. Written informed consent to participate in this study was provided by the participants' legal guardian/next of kin or by the adult participants. Written informed consent was obtained from the minor(s)' legal guardian/next of kin for the publication of any potentially identifiable images or data included in this article.

AUTHOR CONTRIBUTIONS

LFe contributed to the study design, performed laboratory data acquisition and analysis, prepared figures, tables, supplementary material, contributed to data interpretation, and drafted the manuscript. PMu contributed to the trial design, performed patient enrollment and treatment, contributed to data interpretation, and drafted the manuscript. KP supervised IMP manufacturing, contributed to laboratory data acquisition and analyses, supplementary material preparation, and drafted the manuscript. IS performed statistical analysis, contributed to figure preparation, data interpretation, and drafted the manuscript. JM contributed to the trial design, participated in clinical and manufacturing data analysis, and drafted the manuscript. ZR performed PET/CT data acquisition, contributed to figure preparation, data interpretation, and drafted the manuscript. DV and EH contributed to the trial design, data interpretation, and revised the manuscript. DC participated in clinical data acquisition, contributed to supplementary material preparation, and revised the manuscript. LFa participated in clinical data acquisition and revised the manuscript. PMa and ZP contributed to the trial design, participated in patient treatment, and revised the manuscript. RD and JS contributed to the trial design, contributed to data interpretation, and revised the manuscript. LZ-D conceived the study design, designed and supervised laboratory data acquisition and analysis, contributed to data analysis and interpretation, and drafted and finalized the manuscript.

FUNDING

This work was supported by Czech Ministry of Education, Youth and Sports via Large infrastructure CZECRIN (LM2015090)

and via National Sustainability Program I (RECAMO2020, LO1413), by Czech Ministry of Health via project No. NV18-03-00339 and DRO 00209805, and by European Regional Development Fund–project CZECRIN_4PATIENTY (Reg. No. CZ.02.1.01/0.0/0.0/16_013/0001826).

SUPPLEMENTARY MATERIAL

The Supplementary Material for this article can be found online at: https://www.frontiersin.org/articles/10.3389/fonc.2019.01169/full#supplementary-material

REFERENCES

1. Mackall CL, Rhee EH, Read EJ, Khuu HM, Leitman SF, Bernstein D, et al. A pilot study of consolidative immunotherapy in patients with high-risk pediatric sarcomas. *Clin Cancer Res.* (2008) 14:4850–8. doi: 10.1158/1078-0432.CCR-07-4065
2. Merchant MS, Bernstein D, Amoako M, Baird K, Fleisher TA, Morre M, et al. Adjuvant immunotherapy to improve outcome in high-risk pediatric sarcomas. *Clin Cancer Res.* (2016) 22:3182–91. doi: 10.1158/1078-0432.CCR-15-2550
3. Goldberg JM, Fisher DE, Demetri GD, Neuberg D, Allsop SA, Fonseca C, et al. Biologic activity of autologous, granulocyte-macrophage colony-stimulating factor secreting alveolar soft-part sarcoma and clear cell sarcoma vaccines. *Clin Cancer Res.* (2015) 21:3178–86. doi: 10.1158/1078-0432.CCR-14-2932
4. Lewin J, Davidson S, Anderson ND, Lau BY, Kelly J, Tabori U, et al. Response to immune checkpoint inhibition in two patients with alveolar soft-part sarcoma. *Cancer Immunol Res.* (2018) 6:1001–7. doi: 10.1158/2326-6066.CIR-18-0037
5. Thanindratarn P, Dean DC, Nelson SD, Hornicek FJ, Duan Z. Advances in immune checkpoint inhibitors for bone sarcoma therapy. *J Bone Oncol.* (2019) 15:100221. doi: 10.1016/j.jbo.2019.100221
6. Zdrazilova-Dubska L, Valik D, Budinska E, Frgala T, Bacikova L, Demlova R. NKT-like cells are expanded in solid tumour patients. *Klin Onkol.* (2012) 25 (suppl. 2):2S21–5. doi: 10.14735/amko20122S21
7. Cibulka M, Selingerova I, Fedorova L, Zdrazilova-Dubska L. Immunological aspects in oncology–circulating $\gamma\delta$ T-cells. *Klin Onkol.* (2015) 28 (Suppl. 2):2S60–8. doi: 10.14735/amko20152S60
8. Dohnal AM, Witt V, Hugel H, Holter W, Gadner H, Felzmann T. Phase I study of tumor Ag-loaded IL-12 secreting semi-mature DC for the treatment of pediatric cancer. *Cytotherapy*. (2007) 9:755–70. doi: 10.1080/14653240701589221
9. Aarntzen EH, Srinivas M, Bonetto F, Cruz LJ, Verdijk P, Schreibelt G, et al. Targeting of 111In-labeled dendritic cell human vaccines improved by reducing number of cells. *Clin Cancer Res.* (2013) 19:1525–33. doi: 10.1158/1078-0432.CCR-12-1879
10. Hlavackova E, Pilatova K, Cerna D, Selingerova I, Mudry P, Mazanek P, et al. Dendritic cell-based immunotherapy in advanced sarcoma and neuroblastoma pediatric patients: anti-cancer treatment preceding monocyte harvest impairs immunostimulatory and antigen-presenting behavior of DCs and manufacturing process outcome. *Front Oncol.* (2019) 9:1034. doi: 10.3389/fonc.2019.01034
11. R_Core_Team. *R: A Language and Environment for Statistical Computing*. Vienna: R Foundation for Statistical Computing (2019).
12. Schatorje EJ, Gemen EF, Driessen GJ, Leuvenink J, Van Hout RW, De Vries E. Paediatric reference values for the peripheral T cell compartment. *Scand J Immunol.* (2012) 75:436–44. doi: 10.1111/j.1365-3083.2012.02671.x
13. Pilatova K, Budinska E, Benscikova B, Nenutil R, Sefr R, Fedorova L, et al. Circulating myeloid suppressor cells and their role in tumour immunology. *Klin Onkol.* (2017) 30:s166–9.
14. Lu PH, Negrin RS. A novel population of expanded human CD3+CD56+ cells derived from T cells with potent *in vivo* antitumor activity in mice with severe combined immunodeficiency. *J Immunol.* (1994) 153:1687–96.
15. Kabelitz D, Kalyan S, Oberg HH, Wesch D. Human Vdelta2 versus non-Vdelta2 gammadelta T cells in antitumor immunity. *Oncoimmunology*. (2013) 2:e23304. doi: 10.4161/onci.23304
16. Vignali DA, Collison LW, Workman CJ. How regulatory T cells work. *Nat Rev Immunol.* (2008) 8:523–32. doi: 10.1038/nri2343
17. Sieminska I, Rutkowska-Zapala M, Bukowska-Strakova K, Gruca A, Szaflarska A, Kobylarz K, et al. The level of myeloid-derived suppressor cells positively correlates with regulatory T cells in the blood of children with transient hypogammaglobulinaemia of infancy. *Cent Eur J Immunol*. (2018) 43:413–20. doi: 10.5114/ceji.2018.81359
18. Pal S, Nandi M, Dey D, Chakraborty BC, Shil A, Ghosh S, et al. Myeloid-derived suppressor cells induce regulatory T cells in chronically HBV infected patients with high levels of hepatitis B surface antigen and persist after antiviral therapy. *Aliment Pharmacol Ther*. (2019) 49:1346–59. doi: 10.1111/apt.15226
19. Pilatova K, Bencsikova B, Demlova R, Valik D, Zdrazilova-Dubska L. Myeloid-derived suppressor cells (MDSCs) in patients with solid tumors: considerations for granulocyte colony-stimulating factor treatment. *Cancer Immunol Immunother*. (2018) 67:1919–29. doi: 10.1007/s00262-018-2166-4
20. Gober HJ, Kistowska M, Angman L, Jeno P, Mori L, De Libero G. Human T cell receptor gammadelta cells recognize endogenous mevalonate metabolites in tumor cells. *J Exp Med*. (2003) 197:163–8. doi: 10.1084/jem.20021500
21. Holtmeier W, Pfander M, Hennemann A, Zollner TM, Kaufmann R, Caspary WF. The TCR-delta repertoire in normal human skin is restricted and distinct from the TCR-delta repertoire in the peripheral blood. *J Invest Dermatol.* (2001) 116:275–80. doi: 10.1046/j.1523-1747.2001.01250.x
22. Bol KF, Schreibelt G, Gerritsen WR, De Vries IJ, Figdor CG. Dendritic cell-based immunotherapy: state of the art and beyond. *Clin Cancer Res.* (2016) 22:1897–906. doi: 10.1158/1078-0432.CCR-15-1399
23. Noordam L, Kaijen MEH, Bezemer K, Cornelissen R, Maat L, Hoogsteden HC, et al. Low-dose cyclophosphamide depletes circulating naive and activated regulatory T cells in malignant pleural mesothelioma patients synergistically treated with dendritic cell-based immunotherapy. *Oncoimmunology*. (2018) 7:e1474318. doi: 10.1080/2162402X.2018.1474318
24. Nada MH, Wang H, Workalemahu G, Tanaka Y, Morita CT. Enhancing adoptive cancer immunotherapy with Vgamma2Vdelta2 T cells through pulse zoledronate stimulation. *J Immunother Cancer*. (2017) 5:9. doi: 10.1186/s40425-017-0209-6
25. Gulley JL, Madan RA, Schlom J. Impact of tumour volume on the potential efficacy of therapeutic vaccines. *Curr Oncol.* (2011) 18:e150–7. doi: 10.3747/co.v18i3.783
26. Bol KF, Aarntzen EH, Hout FE, Schreibelt G, Creemers JH, Lesterhuis WJ, et al. Favorable overall survival in stage III melanoma patients after adjuvant dendritic cell vaccination. *Oncoimmunology*. (2016) 5:e1057673. doi: 10.1080/2162402X.2015.1057673

Conflict of Interest: The authors declare that the research was conducted in the absence of any commercial or financial relationships that could be construed as a potential conflict of interest.

frontiers in Oncology

ORIGINAL RESEARCH
published: 15 November 2019
doi: 10.3389/fonc.2019.01221

Comparative Analysis of Putative Prognostic and Predictive Markers in Neuroblastomas: High Expression of PBX1 Is Associated With a Poor Response to Induction Therapy

Renata Veselska[1,2,3], Marta Jezova[4], Michal Kyr[2,3], Pavel Mazanek[2], Petr Chlapek[1,3], Viera Dobrotkova[1,3] and Jaroslav Sterba[2,3]*

[1] Laboratory of Tumor Biology, Department of Experimental Biology, Faculty of Science, Masaryk University, Brno, Czechia, [2] Department of Pediatric Oncology, Faculty of Medicine, University Hospital Brno, Masaryk University, Brno, Czechia, [3] International Clinical Research Center, St. Anne's University Hospital Brno, Brno, Czechia, [4] Department of Pathology, Faculty of Medicine, University Hospital Brno, Masaryk University, Brno, Czechia

OPEN ACCESS

Edited by:
Ruth Plummer,
Newcastle University, United Kingdom

Reviewed by:
Deborah Anne Tweddle,
Newcastle University, United Kingdom
Justin Vareecal Joseph,
Aarhus University, Denmark

***Correspondence:**
Renata Veselska
veselska@sci.muni.cz

Specialty section:
This article was submitted to Cancer Molecular Targets and Therapeutics, a section of the journal Frontiers in Oncology

Received: 09 January 2019
Accepted: 25 October 2019
Published: 15 November 2019

Citation:
Veselska R, Jezova M, Kyr M, Mazanek P, Chlapek P, Dobrotkova V and Sterba J (2019) Comparative Analysis of Putative Prognostic and Predictive Markers in Neuroblastomas: High Expression of PBX1 Is Associated With a Poor Response to Induction Therapy. Front. Oncol. 9:1221. doi: 10.3389/fonc.2019.01221

The survival rate for patients with high-risk neuroblastomas remains poor despite new improvements in available therapeutic modalities. A detailed understanding of the mechanisms underlying clinical responses to multimodal treatment is one of the important aspects that may provide precision in the prediction of a patient's clinical outcome. Our study was designed as a detailed comparative analysis of five selected proteins (DDX39A, HMGA1, HOXC9, NF1, and PBX1) in one cohort of patients using the same methodical approaches. These proteins were already reported separately as related to the resistance or sensitivity to retinoids and as useful prognostic markers of survival probability. In the cohort of 19 patients suffering from high-risk neuroblastomas, we analyzed initial immunohistochemistry samples obtained by diagnostic biopsy and post-induction samples taken after the end of induction therapy. The expression of DDX39A, HMGA1, HOXC9, and NF1 showed varied patterns with almost no differences between responders and non-responders. Nevertheless, we found very interesting results for PBX1: non-responders had significantly higher expression levels of this protein in the initial tumor samples when compared with responders; this expression pattern changed inversely in the post-induction samples, and this change was also statistically significant. Moreover, our results from survival analyses reveal the prognostic value of PBX1, NF1, and HOXC9 expression in neuroblastoma tissue. In addition to the prognostic importance of PBX1, NF1, and HOXC9 proteins, our results demonstrated that PBX1 could be used for the prediction of the clinical response to induction chemotherapy in patients suffering from high-risk neuroblastoma.

Keywords: neuroblastoma, prognostic markers, predictive markers, PBX1, NF1, HOXC9, immunohistochemistry

INTRODUCTION

Neuroblastoma (NBL) is the most common extracranial solid tumor in children, accounting for 6–8% of all childhood cancers and more than 10% of pediatric cancer-related mortality. NBL is a complex and heterogeneous disease with several factors determining the clinical outcome, especially the age at diagnosis, stage of the disease (localized vs. metastasizing), and biological features of the tumor (MYCN copy number determined by fluorescence *in situ* hybridization, DNA content measured by flow cytometry, and tumor histology evaluated using the International NBL Pathology Classification system). Based upon these factors, NBL is classified into low-, intermediate-, or high-risk categories. The estimated risk category correlates with the clinical outcome of the disease: patients with low-risk or intermediate-risk NBL have a 5-year overall survival rate exceeding 90%, whereas this value is ∼40% for patients suffering from high-risk NBL (1, 2).

The stratification of patients into the risk categories described above represents a key step in choosing the right therapy for the right patient. Children with biologically favorable non-metastatic NBL generally require little or no cytotoxic therapy. In contrast, outcomes for patients with high-risk NBL remain poor despite new improvements of available therapeutic modalities, including biological therapy with differentiation inducers and immunotherapy with chimeric monoclonal antibodies (2–4).

Standard chemotherapy for high-risk NBL includes dose-dense or dose-intensive myeloablative regimens using alkylating agents, platinum compounds, topoisomerase-II inhibitors (doxorubicin, etoposide), and topoisomerase-I inhibitors (topotecan, irinotecan) followed by autologous hematopoietic stem cell transplantation (4, 5). At the end of this intensive multimodal treatment, the administration of retinoids in patients with minimal residual disease was shown to be effective and able to delay or prevent tumor relapse after myeloablative therapy (4, 6, 7). Nevertheless, even though retinoids are able to improve the survival of patients with high-risk NBL, ∼50% of these patients were resistant to this treatment or developed resistance during therapy (8).

A detailed understanding of the mechanisms underlying the response of NBL to multimodal treatment is one of the important aspects that may provide precision in the prediction of a patient's clinical outcome, especially within the group of high-risk NBL. In this regard, resistance or sensitivity to retinoids is one of the discussed aspects of this strategy (8). A number of potential molecular mechanisms of resistance to retinoid therapy have been described over the past decade (9). Detailed investigation of the mechanisms of resistance to retinoids led to the identification of several molecules that are discussed as possible predictive biomarkers of clinical response to the treatment with retinoids (10).

In various types of tumor cells, including NBL, several key mediators of retinoid action were recently identified: NF1, HOXC9, or PBX1 (11–13). Based on published results, these proteins can be successfully used for the identification of NBL cell lines showing resistance to retinoids under *in vitro* conditions. Interestingly, certain studies have suggested that some of these molecules could also be used as prognostic markers for estimating survival probability in clinical practice (11, 13, 14).

Nevertheless, the clinical outcome of patients suffering from high-risk NBL is influenced by many other factors, including simple resistance or sensitivity to retinoids administered at the end of the intensive multimodal treatment. To elucidate the actual usefulness of these putative markers in clinical practice, our present study aimed to thoroughly analyze five selected markers already reported to be related to retinoid action (10): DDX39A, HMGA1, HOXC9, NF1, and PBX1. We analyzed the expression of these proteins by immunohistochemistry (IHC) in one cohort of patients suffering from high-risk NBL who underwent intensive induction chemotherapy and were finally treated with retinoids. This unique design allowed us to compare the reliability of these markers for the prediction of therapeutic response if their expression is related to the same set of clinical data. Finally, we also performed survival probability analyses in relation to the expression of these five protein markers to evaluate their prognostic usefulness using the same cohort of patients.

MATERIALS AND METHODS

Tumor Samples

Nineteen samples of newly diagnosed, untreated, high-risk NBL (11 male patients, eight female patients; age range at the time of diagnosis, 19 months−12-years old) were included in this study. In addition to these samples from initial biopsies, we also analyzed an additional 12 samples taken from the same patients after intensive induction chemotherapy. Formalin-fixed, paraffin-embedded (FFPE) tumor samples were retrieved from the files of the Department of Pathology, University Hospital Brno, Czech Republic. Written informed consent was obtained from each participant or his/her legal guardian before entering into this study. The Research Ethics Committee of the School of Science, Masaryk University (Brno, Czech Republic) approved the study protocol.

Immunohistochemistry

Representative sections from archival FFPE tumor samples were selected by one experienced pathologist (MJ) and processed for IHC as described previously in detail (15). All antibodies used in this study are specified in **Table 1**. In each IHC experiment, positive and negative controls were also evaluated (**Supplementary Figure 1**): tissues used as positive controls are also described in **Table 1**, and negative controls were processed without the primary antibodies. For each of the evaluated protein markers, specific nuclear or cytoplasmic immunostaining (as specified in the **Table 1**) was considered positive. The slides were evaluated with an Olympus BX50 light microscope at ×200 magnification. At least five discrete foci of tumor tissue were analyzed per sample by the same experienced pathologist (MJ), and the average staining intensity and the percentage of antigen-positive cells were determined. The percentage of antigen-positive tumor cells (TC) was categorized into five levels: – (0% positive TC), +/– (1–10% positive TC), + (11–50% positive TC), ++ (51–80% positive TC), and + + + (81–100% positive TC). The intensity of immunostaining (immunoreactivity, IR) was

TABLE 1 | Antibodies and positive controls used in this study. N, nuclear staining; C, cytoplasmic staining.

Antigen	Type/Host	Clone	Manufacturer	Dilution	Positive control
DDX39A	Monoclonal/ rabbit	EPR13508	Abcam	1:150	Human testis (N)
HMGA1	Monoclonal/ rabbit	D1A7	Cell Signaling	1:500	Human colorectal cancer (N)
HOXC9	Polyclonal/ rabbit	–	Bioss	1:100	Human kidney (N, C)
NF1	Polyclonal/ rabbit	–	Santa Cruz Biotechnology	1:50	Human pancreas (C)
PBX1	Monoclonal/ mouse	4A2	LSBio	1:50	Human pancreas (N)

classified as none (0), weak (1), medium (2), or strong (3). Finally, the total immunoscores were calculated for individual antigens by multiplying the median percentage category of positive cells by their respective immunoreactivity as described previously (16) with possible immunoscore values ranging from 0 to 300.

Statistical Analysis

IR and the percentage of IHC-stained TC were analyzed separately on a semiquantitative ordinal scale for baseline tissue samples. Proportions of patients with particular immunoscores are shown in bar plots, and differences between responders and non-responders were tested using the chi-square test. Summary statistics and raw data are presented in combined dot and box plots for baseline tissue samples. Differences between responders and non-responders were tested using the Mann-Whitney test. Immunoscores were also calculated for tissue samples after induction therapy, and pre-posttreatment differences in immunoscores between responders and non-responders were evaluated using factor ANOVA and displayed in error bar plots. The clinical significance of immunoscores was evaluated using survival analysis. For statistical purposes, data were dichotomized into low- and high-expression groups based on the median values of each particular parameter. Kaplan–Meier curves were plotted for event-free survival (EFS) and overall survival (OS), and differences between low- and high-expression groups were tested using log-rank tests. Analyses were performed using R software version 3.5.1. (17), and alpha = 0.05 was considered significant. We report raw *p*-values without correction for multiple testing because all tests we made are reported. Corrected *p*-values may thus be computed using a method according to the reader's selection. Nevertheless, we rather discourage from routine performing usual corrections. Our results are prone to the risk of overcorrection due to correlated measures, already preselected set of putative markers, low power of tests (in general) for categorical data, and the purpose of the study. We are interested in any indicator of possible predictive and/or prognostic markers, and we would rather not inflate the type II error.

TABLE 2 | Clinical description of the patients included in this study.

Patient no.	Age range (months)	Tumor histology	INSS stage	MYCN status	Response to the induction therapy	Status
1	30–35	UH	3	Amp	Y	NED
2	30–35	UH	4	Neg	Y	NED
3	30–35	UH	4	Neg	N	DOD
4	40–45	UH	4	Neg	Y	NED
5	46–50	N/A	4	Neg	Y	NED
6	15–20	UH	2B	Amp	Y	NED
7	145–150	UH	4	Neg	Y	NED
8	30–35	UH	4	Amp	N	DOD
9	15–20	FH	4	Neg	N	NED
10	30–35	UH	4	Amp	N	AWD
11	10–15	UH	4	Neg	N	DOD
12	60–65	UH	4	Neg	Y	NED
13	20–25	UH	4	Amp	N	AWD
14	26–30	UH	4	Amp	N	NED
15	20–25	UH	4	Amp	Y	NED
16	40–45	N/A	4	N/A	Y	AWD
17	46–50	UH	4	Neg	N	AWD
18	26–30	UH	4	Amp	Y	DOD
19	100–105	UH	4	Neg	N	DOD

Age range at the time of diagnosis (in months). Tumor histology according INPC (Shimada system): UH, unfavorable histology; FH, favorable histology; N/A, not available. INSS stage according to the International Neuroblastoma Staging System Committee (INSS) system. Response to the induction therapy: Y, yes = responder (partial remission or better); N, no = non-responder (stable disease or worse). Status: NED, no evidence of disease; DOD, dead of disease; AWD, alive with disease.

RESULTS

Cohort Description and Expression Patterns of Evaluated Proteins

A cohort consisting of 19 patients suffering from high-risk NBL was included in this study: a detailed clinical description of these patients is given in the **Table 2**. All of them were treated according the same Children's Oncology Group ANBL 0532 protocol. In this cohort, we analyzed two sets of FFPE tumor samples using IHC: (i) initial samples obtained by a diagnostic biopsy (**Figure 1**) and (ii) post-induction samples taken after the end of induction therapy (**Figure 2**). Although all patients were originally chosen for this cohort according to the availability of both FFPE samples—initial and post-induction—some samples had to be omitted from the final analyses due to poor quality. The initial sample obtained from patient no. 5 and the post-induction samples from patients nos. 1, 2, 6, 8, 11, and 19 were excluded from this cohort. In total, 18 initial samples and 13 post-induction samples were ultimately included in the statistical analyses. Complete detailed results are given in the **Table 3**.

For analysis purposes, the patients were subdivided into two groups: responders achieving at least partial remission and non-responders with stable disease or worse outcome (**Figures 1**, **2**). The response definition is based on the International Neuroblastoma Risk Group response criteria,

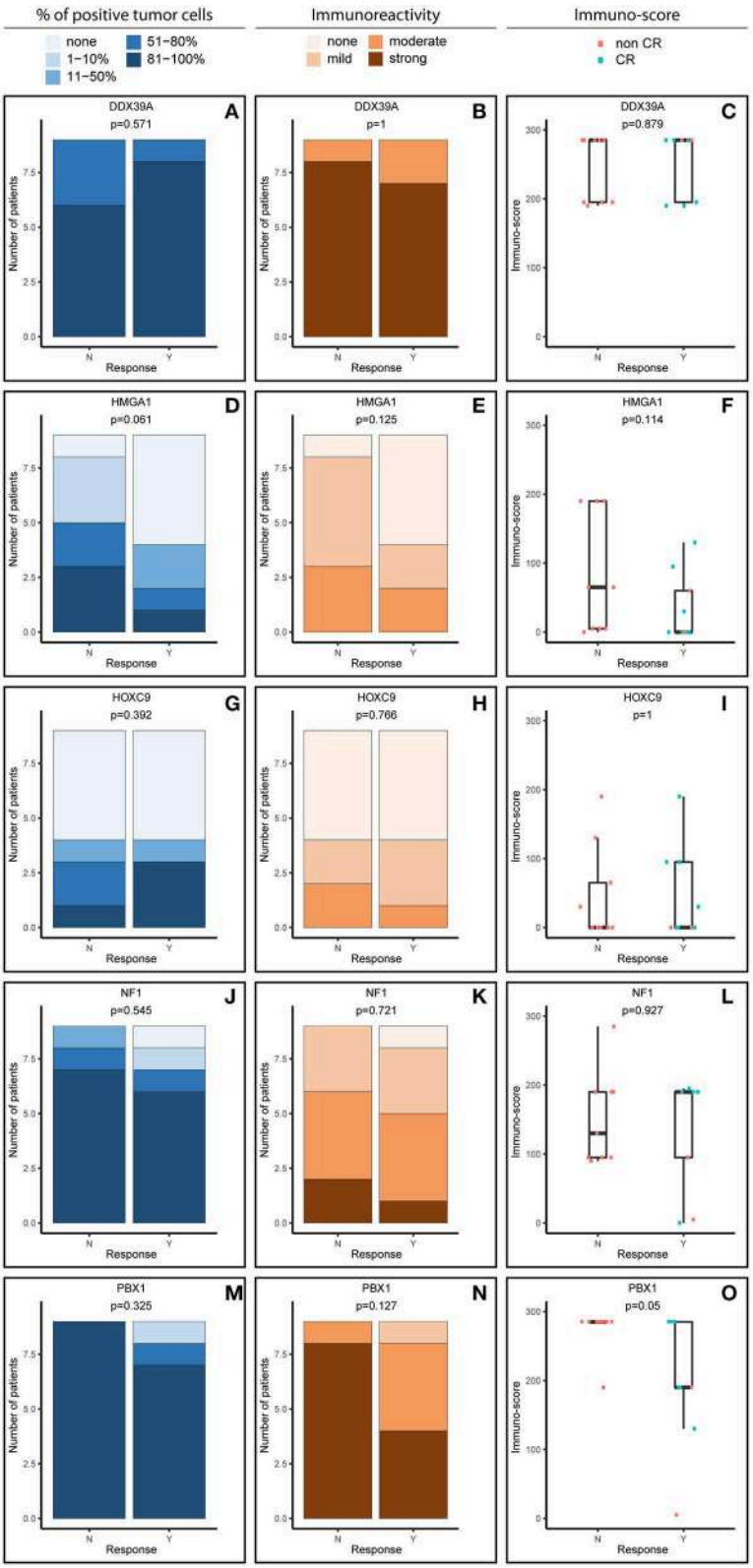

FIGURE 1 | Comparative immunohistochemistry (IHC) analysis of DDX39A **(A–C)**, HMGA1 **(D–F)**, HOXC9 **(G–I)**, NF1 **(J–L)**, and PBX1 **(M–O)** in the initial samples. Immunoscores were calculated for individual antigens by multiplying the median percentage category of positive cells by their respective immunoreactivity. N, non-responder; Y, responder. CR, complete remission.

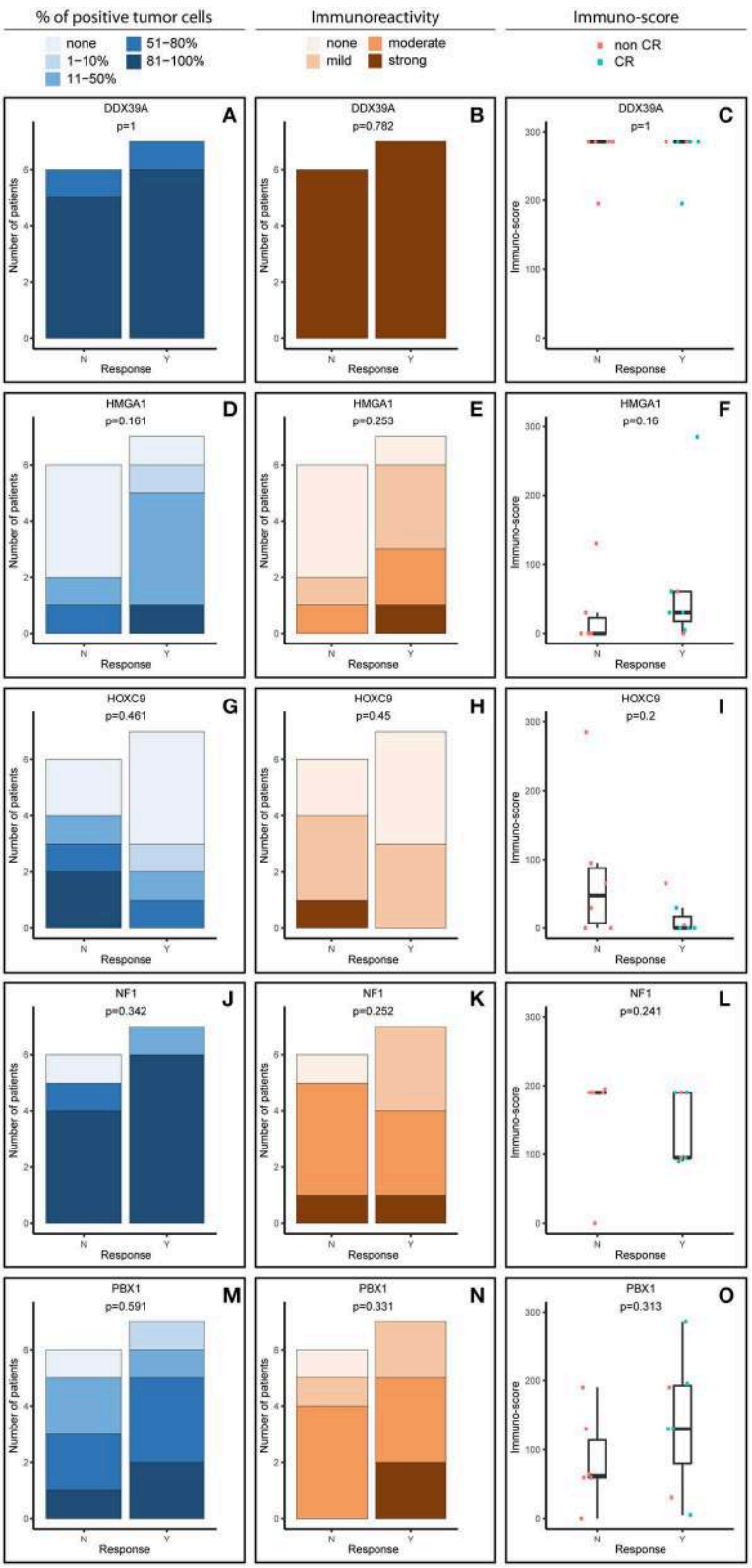

FIGURE 2 | Comparative immunohistochemistry (IHC) analysis of DDX39A **(A–C)**, HMGA1 **(D–F)**, HOXC9 **(G–I)**, NF1 **(J–L)**, and PBX1 **(M–O)** in the post-induction samples. Immunoscores were calculated for individual antigens by multiplying the median percentage category of positive cells by their respective immunoreactivity. N, non-responder; Y, responder. CR, complete remission.

TABLE 3 | Results of IHC analyses of DDX39A, HMGA1, HOXC9, NF1, and PBX1 expression.

Sample no.	Sample type	DDX39A		HMGA1		HOXC9		NF1		PBX1	
		% TC	IR	% TC	IR	% TC	IR	% TC	IR	% TC	IR
1a	I	+++	3	–	0	–	0	–	0	+++	3
2a	I	+++	2	–	0	–	0	+++	1	+++	2
3a	I	+++	3	+/–	1	++	1	+++	1	+++	3
3b	P	+++	3	–	0	–	0	+++	2	++	1
4a	I	+++	3	–	0	–	0	+++	1	+++	2
4b	P	+++	3	–	0	++	1	+++	2	+++	2
5a	P	+++	3	+++	3	–	0	+++	1	+/–	1
6a	I	+++	3	–	0	+++	2	+++	2	++	2
7a	I	++	3	+	1	+++	1	+++	2	+++	2
7b	P	+++	3	+/–	1	+	1	+	3	++	2
8a	I	+++	3	++	1	–	0	+++	2	+++	3
9a	I	+++	3	++	1	++	2	+++	1	+++	3
9b	P	+++	3	+	1	++	1	+++	2	++	2
10a	I	+++	3	+/–	1	+	1	+++	3	+++	3
10b	P	++	3	–	0	+	1	+++	2	+	2
11a	I	+++	2	+/–	1	–	0	+++	2	+++	3
12a	I	+++	2	–	0	+++	1	+++	2	+++	3
12b	P	+++	3	+	1	–	0	+++	2	++	3
13a	I	++	3	–	0	+++	2	++	2	+++	3
13b	P	+++	3	–	0	+++	1	++	3	+++	2
14a	I	++	3	+++	2	–	0	+++	1	+++	3
14b	P	+++	3	–	0	–	0	–	0	–	0
15a	I	+++	3	++	2	+	1	++	3	+++	3
15b	P	++	3	+	1	–	0	+++	1	++	2
16a	I	+++	3	+	2	–	0	+/–	1	+/–	1
16b	P	+++	3	+	2	+/–	1	+++	1	+	1
17a	I	++	3	+++	2	–	0	+	3	+++	2
17b	P	+++	3	++	2	+++	3	+++	2	+	2
18a	I	+++	3	+++	1	–	0	+++	2	+++	3
18b	P	+++	3	+	2	–	0	+++	2	+++	3
19a	I	+++	3	+++	2	–	0	+++	2	+++	3

The percentage of antigen-positive tumor cells (TC) was counted and categorized into five levels: – (0% positive TC), +/– (1–10% positive TC), + (11–50% positive TC), ++ (51–80% positive TC), and +++ (81–100% positive TC). The intensity of immunostaining (immunoreactivity, IR) was classified as none (0), weak (1), medium (2), or strong (3).

and it was evaluated as overall response, i.e., combination of primary tumor response and response of metastatic sites. For each sample and protein marker, the percentage of positive TC (**Figures 1A,D,G,J,M**, **2A,D,G,J,M**) as well as the IR (**Figures 1B,E,H,K,N**, **2B,E,H,K,N**) was evaluated. In the next step, immunoscore values were determined for each sample (**Figures 1C,F,I,L,O**, **2C,F,I,L,O**).

In general, we observed several obvious differences in the expression patterns among these five proteins in the initial samples. DDX39A (**Figures 1A–C**) and PBX1 (**Figures 1M–O**) exhibited the highest proportions of positive TC in the sample and the highest IR in both responders and non-responders, which also led to the highest immunoscore values. High proportions of NF1-positive tumor cells were also found, but the IR was almost moderate to mild for this protein (**Figures 1J–L**). Moderate to mild IR was also observed for HMGA1 (**Figures 1D–F**) and HOXC9 (**Figures 1G–I**), and the percentage of cells positive for these markers and their respective immunoscores were reduced compared with the previously mentioned proteins.

Analysis of Expression Patterns of Evaluated Proteins in Relation to the Response to Induction Chemotherapy

Although the analyzed markers exhibited varied expressions in the initial samples, nearly no significant changes were detected in responders and non-responders. Nevertheless, the most interesting result was found for PBX1: non-responders had significantly higher expression of this protein in the initial tumor samples (**Figure 1O**). Representative examples of IHC detection of evaluated protein markers in the initial samples for responders and non-responders are also provided (**Figure 3**).

The expression patterns of DDX39A, HMGA1, HOXC9, and NF1 proteins in the post-induction samples were very similar to those in the initial samples, as described above (**Figures 2A–L**). The only apparent difference was found for PBX1: both the proportion of PBX1-positive cells as well as the IR and subsequently immunoscore values were reduced (**Figures 2M–O**).

Furthermore, we also analyzed changes in the expression of these putative markers before and after induction chemotherapy according the response to treatment (**Figure 4**). Interestingly, the expression pattern of PBX1 changed inversely, and this change was also statistically significant (**Figure 4E**). A similar inverse expression pattern was also observed for HMGA1 (**Figure 4B**), but this trend was not significant.

Analysis of Expression Patterns of Evaluated Proteins in Relation to the Survival Probability

In addition to the analysis of their possible predictive values, we also performed a detailed evaluation of the expression of these five proteins in relation to the probability of OS and EFS (**Figure 5**). High expression of NF1 (**Figures 5G,H**) was significantly related to reduced OS ($p = 0.027$). Similarly, high expression of PBX1 (**Figures 5I,J**) was significantly related to reduced EFS ($p = 0.048$) and the same—although statistically insignificant—trend was also found for OS. In contrast, low HOXC9 expression (**Figures 5E,F**) is apparently associated with reduced OS; however, this difference remained insignificant ($p = 0.051$). The results of 3- and 5-year Kaplan–Meier survival estimates with 95% confidence limits in parentheses are summarized in **Table 4**.

Analysis of Expression Patterns of Evaluated Proteins and Survival Probability in Relation to the MYCN Status

Finally, we also perform the detailed analysis of the expression patterns among these five proteins in relation to the MYCN

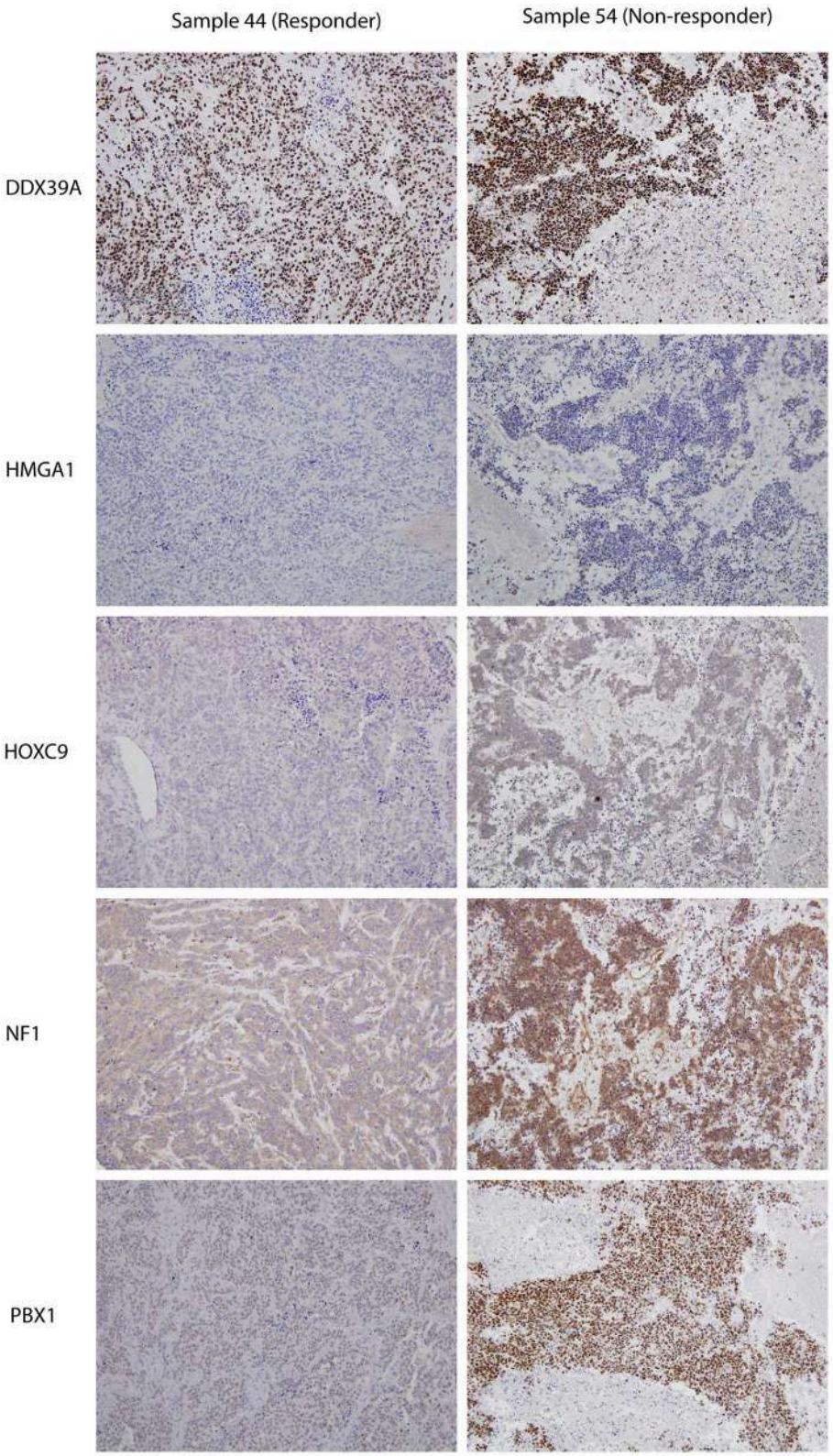

FIGURE 3 | Representative expressions of DDX39A, HMGA1, HOXC9, NF1, and PBX1 in responder (sample 7a) and non-responder (sample 10a) initial tumor samples. Original magnification, 200×.

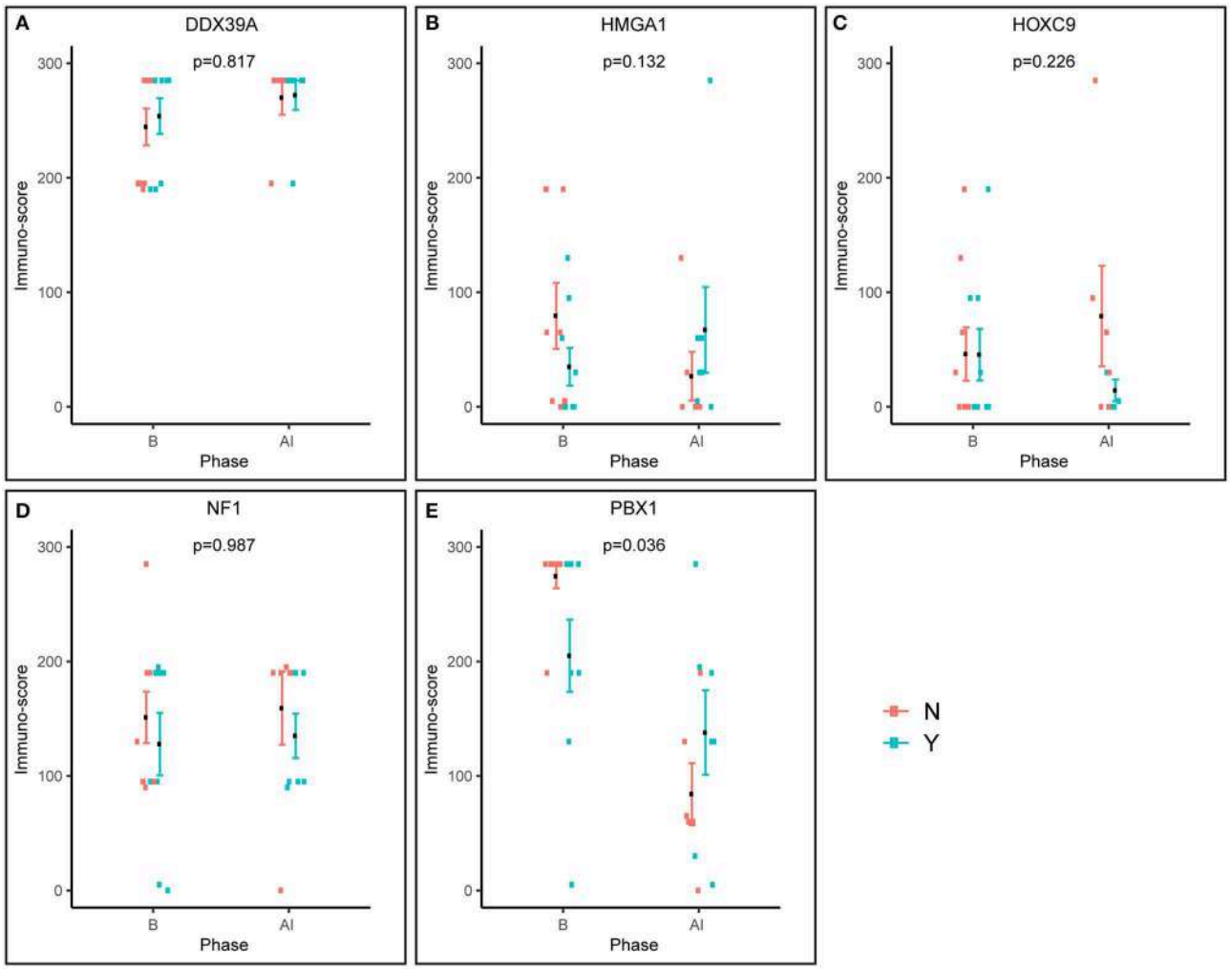

FIGURE 4 | Pre-posttreatment differences in immunoscores between responders and non-responders as evaluated using factor ANOVA. Phase: B, baseline (initial samples); AI, after induction (post-induction samples). N, non-responder; Y, responder.

status: both in the initial (**Supplementary Figure 2**) and post-induction (**Supplementary Figure 3**) samples; no significant difference was found. Surprisingly, the MYCN amplification was not related to reduced OS or EFS (**Supplementary Figure 4**) in our cohort of patients.

DISCUSSION

Although all five of these proteins were previously reported as related to the prognosis or to the resistance/sensitivity to retinoids in NBL, our results apparently show that their usefulness as predictive markers in "real-life scenario" is limited. This discrepancy with previously published studies can be caused by several important factors that should be considered during the interpretation of our results. First, our study compared five putative markers that were previously analyzed separately by different research groups. Second, our comparative analysis was performed using FFPE tumor samples, not using cell lines or frozen samples; this biological model allowed us to compare the actual amount of the protein in question in real tumor tissue. Third, we analyzed both samples taken during initial biopsies and samples taken from the same patients after multimodal induction chemotherapy; this was a key new approach for evaluating the possible use of analyzed proteins as predictive biomarkers in NBL. Finally, our experimental design based on the homogenous cohort of patients suffering solely from high-risk NBL was focused both on the prediction of the clinical response to multiagent chemotherapy and the estimation of survival probability using Kaplan–Meier analysis in relation to the same set of clinical data. In the next paragraphs, we will discuss these markers one by one in light of our findings in comparison with the previously published results.

ATP-dependent RNA helicase DDX39A, also known as URH49, is a paralog of DDX39B helicase with 90% amino acid identity (18). In NBL, its expression was reported as an independent unfavorable prognostic factor when analyzed in

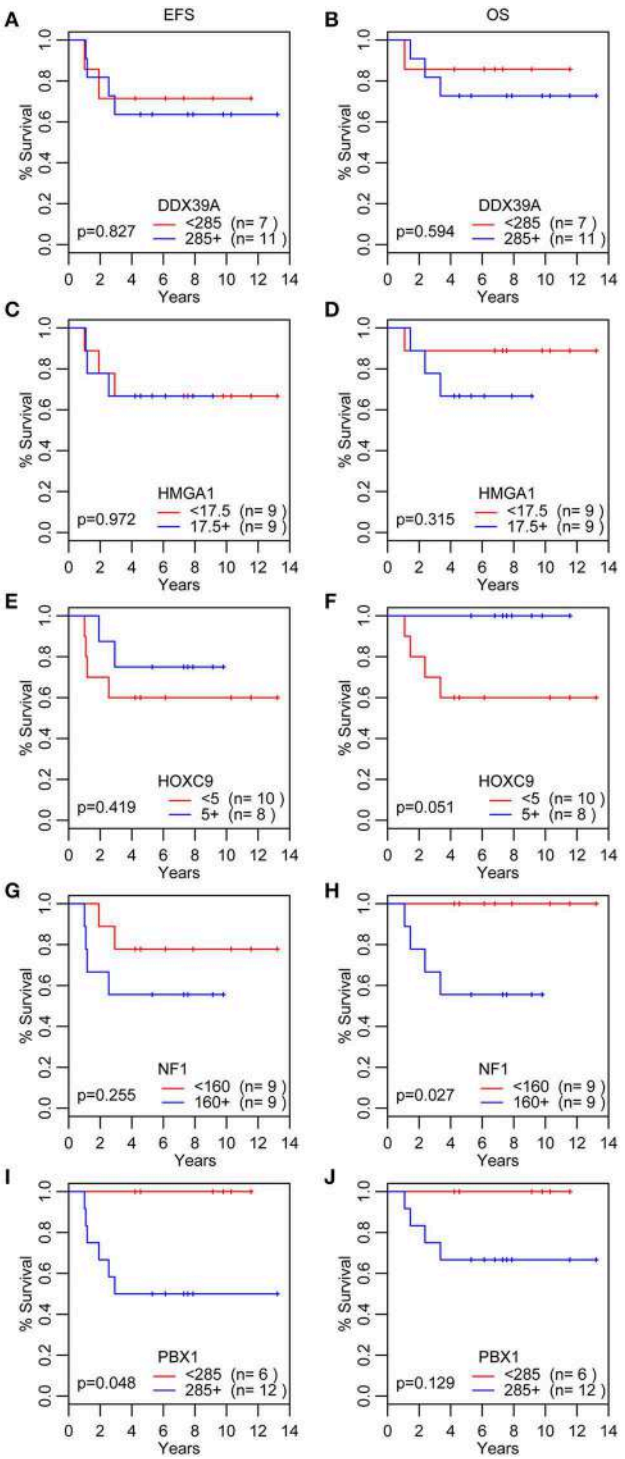

FIGURE 5 | Analyses of survival probability. Kaplan-Meier Q20 curves stratified by the median values of the immunoscore for each particular protein marker. A red line indicates low expression; a blue line indicates the high expression. OS, overall survival **(B,D,F,H,J)**; EFS, event-free survival **(A,C,E,G,I)**.

primary tumor samples using IHC. Nevertheless, this cohort of patients was not fully comparable to ours because the samples included in this study were taken from patients with NBL of

TABLE 4 | Overview of 3- and 5-year Kaplan–Meier survival estimates with 95% confidence limits in parentheses.

Parameter	Group	*N*	3-year survival (CI) %	5-year survival (CI) %
EFS				
Score DDX39A	<285	7	71.4 (44.7–100)%	71.4 (44.7–100)%
	285+	11	63.6 (40.7–99.5)%	63.6 (40.7–99.5)%
Score HMGA1	<17.5	9	66.7 (42–100)%	66.7 (42–100)%
	17.5+	9	66.7 (42-100)%	66.7 (42–100)%
Score HOXC9	<5	10	60 (36.2–99.5)%	60 (36.2–99.5)%
	5+	8	75 (50.3–100)%	75 (50.3–100)%
Score NF1	<160	9	77.8 (54.9–100)%	77.8 (54.9–100)%
	160+	9	55.6 (31–99.7)%	55.6 (31–99.7)%
Score PBX1	<285	6	NA	NA
	285+	12	50 (28.4–88)%	50 (28.4–88)%
OS				
Score DDX39A	<285	7	85.7 (63.3–100)%	85.7 (63.3–100)%
	285+	11	81.8 (61.9–100)%	72.7 (50.6–100)%
Score HMGA1	<17.5	9	88.9 (70.6–100)%	88.9 (70.6–100)%
	17.5+	9	77.8 (54.9–100)%	66.7 (42–100)%
Score HOXC9	<5	10	70 (46.7–100)%	60 (36.2–99.5)%
	5+	8	NA	NA
Score NF1	<160	9	NA	NA
	160+	9	66.7 (42–100)%	55.6 (31–99.7)%
Score PBX1	<285	6	NA	NA
	285+	12	75 (54.1–100)%	66.7 (44.7–99.5)%

Each score parameter was dichotomized based on the median value of the respective parameter (immunoscore). Cut-off values are indicated for each parameter. Survival cannot be estimated for groups with no events (indicated as NA). EFS, event-free survival, OS, overall survival.

unknown risk categories and evaluated according to MYCN status (19). Thus, the same and relatively high levels of DDX39A in both initial (**Figures 1A,B**) and post-induction (**Figures 2A,B**) biopsies independent of the clinical outcome (responders vs. non-responders), as observed in our study, are not in direct contradiction and can be explained by different experimental designs. In other words, high levels of DDX39A in high-risk NBL are not surprising *per se* because patients with this category of NBL have a worse prognosis when compared with patients with other NBL risk categories. Consequently, the high median value of the immunoscore used as cutoff for this analysis according to our unified methodology is apparently not suitable for discrimination of these patients with high-risk NBL into different survival probability categories. Similar to the published findings (19), high levels of DDX39 were associated with poor prognosis in gastrointestinal stromal tumors (20). In contrast, low levels of DDX39 were reported as a marker of poor prognosis for bladder carcinoma (21) and colorectal carcinoma (22).

The HOXC9 protein belongs to the homeobox (HOX) family of transcription factors, members of which play an important role in the mediation of retinoid action during the development of the nervous system (12). HOXC9 was reported as a key regulator in the induced differentiation of NBL cells (23, 24). Our data showed no significant change in HOXC9 expression in relation to the response to induction therapy in either initial (**Figures 1G,H**)

or post-induction (**Figures 2G,H**) biopsies. Unfortunately, no comparable data regarding HOXC9 and the therapeutic outcome have been published thus far. Nevertheless, high levels of HOXC9 were identified as markers associated with a better prognosis of survival in three different datasets obtained from NBL patients (14) and our results (**Figures 5E,F**) are in full accordance with these findings. Similar results were also previously reported for glioblastoma (25) and breast carcinoma (26).

A key role of neurofibromin 1 (NF1) within a cell is to downregulate activated RAS proteins, which results in the deactivation of RAS/MEK and PI3K/AKT signaling pathways (27). In NBL cells, NF1 is able to control a response to treatment with retinoids through RAS/MEK signaling because this cascade suppresses the expression of ZNF423 protein functioning as a RAR/RXR coactivator. Moreover, the combined expression status of NF1 and ZNF423 proteins was identified as a powerful prognostic marker in NBL: low levels of both of these proteins were associated with the worst prognosis for NBL patients, while high levels of expression of both proteins were related to the best progression-free interval (11). Despite these findings, other studies on the possible role of NF1 in tumorigenesis have indicated that expression of NF1 can be considered a negative prognostic factor in several cancer types (28). Thus, although our data showed no differences in NF1 expression between responders and non-responders, in both initial and post-induction tumor samples, it should be noted that high proportions of NF1-positive cells were detected in the majority of examined samples regardless of the response category or biopsy status (**Figures 1J**, **2J**). Moreover, we found that high expression of NF1 in terms of immunoscore (**Figures 5G,H**) was significantly related to reduced OS ($p = 0.027$). As all the patients in our cohort were diagnosed with high-risk NBL, all of our results on NF1 correspond to the hypothesis on the relationship between NF1 overexpression associated with aggressive tumor behavior. Similar findings were recently published for colorectal carcinoma (29).

The HMGA subfamily of high-mobility-group (HMG) proteins consists of several members that serve as transcription factors directly binding to DNA or that regulate the expression of target genes via protein–protein interactions (30). Treatment with retinoids can change the expression of HMGA1, and these changes are closely related to MYCN status (30, 31). Although there are no data on the possible relationship between HMGA1 expression and clinical outcome in patients suffering from NBL, published studies on other cancer types suggest that HMGA1 overexpression is associated with aggressive tumor behavior and poor prognosis: such findings were reported for breast carcinoma (32–34), pancreatic adenocarcinoma (35), esophageal squamous cell carcinoma (36), non-small cell lung cancer (37), and uveal melanomas (38). In contrast, such results were not confirmed by other research groups for gastric cancer (39) and non-small cell lung cancer (40). Our findings showed slightly higher HMGA1 expression in initial biopsies taken from non-responders, as well as an inverse expression pattern in post-induction biopsies (**Figure 4B**), but these results and, similarly, the results of the survival analysis (**Figures 5C,D**) were not statistically significant. Nevertheless, such trends in expression—although non-significant—are in accordance with recent knowledge on the importance of HMGA1 as a "master regulator" in tumorigenesis and its association with tumor aggressiveness (32, 34, 38).

The most interesting of our results concerns pre-B-cell leukemia homeobox-1 (PBX1) protein. This molecule is a member of the three-amino-acid loop extension TALE family of atypical homeodomain proteins with characteristic three-residue insertion in the first helix of the homeodomain. PBX1 protein forms heterodimeric transcription complexes by interacting with other homeodomain-containing nuclear proteins, such as HOX and MEIS-1. PBX1 is involved in a variety of biological processes, including cell differentiation and tumorigenesis (41, 42). Very recently, PBX1 has been considered a group of pioneering factors that are able to initiate cell fate changes (43). PBX1 was identified as a critical component in NBL differentiation, and this is unique among the three-amino-acid loop extension family proteins. In NBL cell lines treated with 13-cis retinoic acid, PBX1 expression was induced only in sensitive cell lines, and reduced PBX1 levels led to an aggressive growth phenotype and resistance to 13-cis retinoic acid. In the same study, it was also demonstrated that PBX1 expression correlates with histological NBL subtypes, with the highest expression in benign ganglioneuromas and the lowest expression in high-risk NBL (13). In contrast, our study revealed that the highest levels of PBX1 in tumor tissue are associated with poor response to induction chemotherapy, whereas PBX1 levels were decreased in non-responders (**Figures 1M–O**, **2M–O**). More interestingly, the PBX1 expression pattern was inverted after induction chemotherapy, and this change was statistically significant (**Figure 4E**). Furthermore, the survival analysis clearly demonstrated that high levels of PBX1 in tumor tissue are significantly associated with a worse clinical prognosis (**Figures 5I,J**). The explanation of such different results can be found in the heterogeneity of samples and methods used in the previous study mentioned above (13): (i) the evaluation of PBX1 prognostic value was performed by reverse transcription quantitative PCR, not by the IHC method used in our study, and (ii) their samples were taken from tumors of various risk categories, which is in contrast to our samples acquired solely from high-risk NBL.

To summarize, our study provides new insight into the usefulness of the biomarkers described above for the prediction of responses to multiagent chemotherapy in patients suffering from high-risk NBL. Although these molecules were still considered prognostic biomarkers, our results showed that the expression patterns of only two of those biomarkers HMGA1 and especially PBX1 differ before and after induction chemotherapy. Moreover, high levels of PBX1 are significantly associated with a poor response to induction chemotherapy and with worse clinical outcome in our cohort of patients. Similarly, we found a significant relationship between high levels of NF1 and worse survival probability in terms of OS. We argue that, although the reported statistical significances were not corrected, we consider the findings robust and significant. First, we observed a good agreement of the results (namely, for PBX1) across different analyzes such as the immunoscores and the survival. Second,

there is an issue of the risk of overcorrection, which was already shortly described in *Material and Methods*. Owing to relatively small number of patients involved in our study, this interesting finding should be verified in the independent larger case series. As all of these molecules were also reported to be involved in the treatment of NBL cells with retinoids, it would be helpful to elucidate this issue. Because it is very difficult to collect a large set of paired NBL samples before and after treatment with retinoids, this study cannot answer the question about the usefulness of these markers for predicting the response of patients to retinoids. Nevertheless, our already published study on this topic using a set of primary NBL cell lines confirmed the association of low levels of PBX1 with the sensitivity to retinoids (15).

DATA AVAILABILITY STATEMENT

All datasets generated for this study are included in the article/**Supplementary Material**.

ETHICS STATEMENT

The studies involving human participants were reviewed and approved by The Research Ethics Committee of the School of Science, Masaryk University (Brno, Czech Republic). Written informed consent was obtained from the minor(s)' legal guardian/next of kin for the publication of any potentially identifiable images or data included in this article.

AUTHOR CONTRIBUTIONS

RV, PC, and JS designed the study. PM and JS provided tumor samples and relevant clinical data. MJ performed immunohistochemical analyses. MK performed statistical analyses. RV composed the manuscript. PC and VD participated in data analyses and manuscript preparation. All authors reviewed and approved the final version of the manuscript.

FUNDING

This study was supported by project no. 15-34621A from the Ministry of Healthcare of Czech Republic, project no. LQ1605 from the National Program of Sustainability II (MEYS CR), project no. MUNI/A/1586/2018 from Masaryk University, Brno, Czech Republic, and by project no. FNBr 65269705 from the Ministry of Healthcare of Czech Republic—DRO Program.

ACKNOWLEDGMENTS

The authors thank Lenka Zlamalikova and Kvetoslava Liskova for their technical assistance.

SUPPLEMENTARY MATERIAL

The Supplementary Material for this article can be found online at: https://www.frontiersin.org/articles/10.3389/fonc.2019.01221/full#supplementary-material

REFERENCES

1. Park JR, Bagatell R, London WB, Maris JM, Cohn SL, Mattay KK, et al. Children's Oncology Group's 2013 blueprint for research: neuroblastoma. *Pediatr Blood Cancer*. (2013) 60:9859–93. doi: 10.1002/pbc.24433
2. Irwin MS, Park JR. Neuroblastoma: paradigm for precision medicine. *Pediatr Clin North Am*. (2015) 62:225–56. doi: 10.1016/j.pcl.2014.09.015
3. Kholodenko IV, Kalinovsky DV, Doronin II, Deyev SM, Kholodenko RV. Neuroblastoma origin and therapeutic targets for immunotherapy. *J Immunol Res*. (2018) 2018:7394268. doi: 10.1155/2018/7394268
4. Nakagawara A, Li Y, Izumi H, Muramori K, Inada H, Nishi M. Neuroblastoma. *Jpn J Clin Oncol*. (2018) 48:214–41. doi: 10.1093/jjco/hyx176
5. Kushner BH, Modak S, Kramer K, Basu EM, Roberts SS, Cheung NK. Ifosfamide, carboplatin, and etoposide for neuroblastoma: a high-dose salvage regimen and review of the literature. *Cancer*. (2013) 119:665–71. doi: 10.1002/cncr.27783
6. Reynolds CP, Matthay KK, Villablanca JG, Maurer BJ. Retinoid therapy of high-risk neuroblastoma. *Cancer Lett*. (2003) 197:185–92. doi: 10.1016/S0304-3835(03)00108-3
7. Matthay KK, Reynolds CP, Seeger RC, Shimada H, Adkins ES, Haas-Kogan D, et al. Long-term results for children with high-risk neuroblastoma treated on a randomized trial of myeloablative therapy followed by 13-cis-retinoic acid: a children's oncology group study. *J Clin Oncol*. (2009) 27:1007–13. doi: 10.1200/JCO.2007.13.8925
8. Masetti R, Biagi C, Zama D, Vendemini F, Martoni A, Morello W, et al. Retinoids in pediatric onco-hematology: the model of acute promyelocytic leukemia and neuroblastoma. *Adv Ther*. (2012) 29:747–62. doi: 10.1007/s12325-012-0047-3
9. Chlapek P, Slavikova V, Mazanek P, Sterba J, Veselska R. Why differentiation therapy sometimes fails: molecular mechanisms of resistance to retinoids. *Int J Mol Sci*. (2018) 19:E132. doi: 10.3390/ijms19010132
10. Dobrotkova V, Chlapek P, Mazanek P, Sterba J, Veselska R. Traffic lights for retinoids in oncology: molecular markers of retinoid resistance and sensitivity and their use in the management of cancer differentiation therapy. *BMC Cancer*. (2018) 18:1059. doi: 10.1186/s12885-018-4966-5
11. Hölzel M, Huang S, Koster J, Ora I, Lakeman A, Caron H, et al. NF1 is a tumor suppressor in neuroblastoma that determines retinoic acid response and disease outcome. *Cell*. (2010) 142:218–29. doi: 10.1016/j.cell.2010.06.004
12. Shahhoseini M, Taghizadeh Z, Hatami M, Baharvand H. Retinoic acid dependent histone 3 demethylation of the clustered HOX genes during neural differentiation of human embryonic stem cells. *Biochem Cell Biol*. (2013) 91:116–22. doi: 10.1139/bcb-2012-0049
13. Shah N, Wang J, Selich-Anderson J, Graham G, Siddiqui H, Li X, et al. PBX1 is a favorable prognostic biomarker as it modulates 13-cis retinoic acid-mediated differentiation in neuroblastoma. *Clin Cancer Res*. (2014) 20:4400–12. doi: 10.1158/1078-0432.CCR-13-1486
14. Mao L, Ding J, Zha Y, Yang L, McCarthy BA, King W, et al. HOXC9 links cell-cycle exit and neuronal differentiation and is a prognostic marker in neuroblastoma. *Cancer Res*. (2011) 71:4314–24. doi: 10.1158/0008-5472.CAN-11-0051
15. Dobrotkova V, Chlapek P, Jezova M, Adamkova K, Mazanek P, Sterba J, et al. Prediction of neuroblastoma cell response to treatment with natural or synthetic retinoids using selected protein biomarkers. *PLoS ONE*. (2019) 14:e0218269. doi: 10.1371/journal.pone.0218269
16. Mikulenkova E, Neradil J, Zitterbart K, Sterba J, Veselska R. Overexpression of the ΔNp73 isoform is associated with centrosome amplification in brain tumor cell lines. *Tumour Biol*. (2015) 36:7483–91. doi: 10.1007/s13277-015-3474-3

17. R Core Team. *R: A Language and Environment for Statistical Computing*. R Foundation for Statistical Computing. Vienna (2018). Available online at: https://www.R-project.org/
18. Nakata D, Nakao S, Nakayama K, Araki S, Nakayama Y, Aparicio S, et al. The RNA helicase DDX39B and its paralog DDX39A regulate androgen receptor splice variant AR-V7 generation. *Biochem Biophys Res Commun*. (2017) 483:271–6. doi: 10.1016/j.bbrc.2016.12.153
19. Otake K, Uchida K, Ide S, Kobayashi Y, Kobayashi I, Kusunoki M. Identification of DDX39A as a potential biomarker for unfavorable neuroblastoma using a proteomic approach. *Pediatr Blood Cancer*. (2016) 63:221–7. doi: 10.1002/pbc.25778
20. Kikuta K, Kubota D, Saito T, Orita H, Yoshida A, Tsuda H, et al. Clinical proteomics identified ATP-dependent RNA helicase DDX39 as a novel biomarker to predict poor prognosis of patients with gastrointestinal stromal tumor. *J Proteomics*. (2012) 75:1089–98. doi: 10.1016/j.jprot.2011.10.005
21. Kato M, Wei M, Yamano S, Kakehashi A, Tamada S, Nakatani T, et al. DDX39 acts as a suppressor of invasion for bladder cancer. *Cancer Sci*. (2012) 103:1363–9. doi: 10.1111/j.1349-7006.2012.02298.x
22. Ma J, Chang W, Zhang W. Relationship between the expression of DDX39 protein and prognosis of colorectal cancer. *Zhonghua Wei Chang Wai Ke Za Zhi*. (2018) 21:336–41.
23. Wang X, Choi JH, Ding J, Yang L, Ngoka LC, Lee EJ, et al. HOXC9 directly regulates distinct sets of genes to coordinate diverse cellular processes during neuronal differentiation. *BMC Genomics*. (2013) 14:830. doi: 10.1186/1471-2164-14-830
24. Wang X, Yang L, Choi JH, Kitamura E, Chang CS, Ding J, et al. Genome-wide analysis of HOXC9-induced neuronal differentiation of neuroblastoma cells. *Genom Data*. (2014) 2:50–2. doi: 10.1016/j.gdata.2014.04.002
25. Xuan F, Huang M, Liu W, Ding H, Yang L, Cui H. Homeobox C9 suppresses Beclin1-mediated autophagy in glioblastoma by directly inhibiting the transcription of death-associated protein kinase 1. *Neuro Oncol*. (2016) 18:819–29. doi: 10.1093/neuonc/nov281
26. Hur H, Lee JY, Yang S, Kim JM, Park AE, Kim MH. HOXC9 induces phenotypic switching between proliferation and invasion in breast cancer cells. *J Cancer*. (2016) 7:768–73. doi: 10.7150/jca.13894
27. Philpott C, Tovell H, Frayling IM, Cooper DN, Upadhyaya M. The NF1 somatic mutational landscape in sporadic human cancers. *Hum Genomics*. (2017) 11:13. doi: 10.1186/s40246-017-0109-3
28. Sabova L, Kretova M, Luciakova K. New insights into the role of NF1 in cancer. *Neoplasma*. (2013) 60:233–9. doi: 10.4149/neo_2013_031
29. Elzagheid A, Emaetig F, Elsaghayer W, Torjman F, Latto M, Syrjänen K, et al. Neurofibromin expression is associated with aggressive disease and poor outcome in colorectal carcinoma. *Anticancer Res*. (2016) 36:5301–6. doi: 10.21873/anticanres.11102
30. Cerignoli F, Ambrosi C, Mellone M, Assimi I, di Marcotullio L, Gulino A, et al. HMGA molecules in neuroblastic tumors. *Ann N Y Acad Sci*. (2004)1028:122–32. doi: 10.1196/annals.1322.013
31. Giannini G, Cerignoli F, Mellone M, Massimi I, Ambrosi C, Rinaldi C, et al. High mobility group A1 is a molecular target for MYCN in human neuroblastoma. *Cancer Res*. (2005) 65:8308–16. doi: 10.1158/0008-5472.CAN-05-0607
32. Huang R, Huang D, Dai W, Yang F. Overexpression of HMGA1 correlates with the malignant status and prognosis of breast cancer. *Mol Cell Biochem*. (2015) 404:251–7. doi: 10.1007/s11010-015-2384-4
33. Zhang S, Lei R, Wu J, Shan J, Hu Z, Chen L, et al. Role of high mobility group A1 and body mass index in the prognosis of patients with breast cancer. *Oncol Lett*. (2017) 14:5719–26. doi: 10.3892/ol.2017.6963
34. Qi C, Cao J, Li M, Liang C, He Y, Li Y, et al. HMGA1 overexpression is associated with the malignant status and progression of breast cancer. *Anat Rec*. (2018) 301:1061–7. doi: 10.1002/ar.23777
35. Liau SS, Rocha F, Matros E, Redston M, Whang E. High mobility group AT-hook 1 (HMGA1) is an independent prognostic factor and novel therapeutic target in pancreatic adenocarcinoma. *Cancer*. (2008) 113:302–14. doi: 10.1002/cncr.23560
36. Toyozumi T, Hoshino I, Takahashi M, Usui A, Akutsu Y, Hanari N, et al. Fra-1 regulates the expression of HMGA1, which is associated with a poor prognosis in human esophageal squamous cell carcinoma. *Ann Surg Oncol*. (2017) 24:3446–55. doi: 10.1245/s10434-016-5666-5
37. Zhang Z, Wang Q, Chen F, Liu J. Elevated expression of HMGA1 correlates with the malignant status and prognosis of non-small cell lung cancer. *Tumour Biol*. (2015) 36:1213–9. doi: 10.1007/s13277-014-2749-4
38. Qu Y, Wang Y, Ma J, Zhang Y, Meng N, Li H, et al. Overexpression of high mobility group A1 protein in human uveal melanomas: implication for prognosis. *PLoS ONE*. (2013) 8:e68724. doi: 10.1371/journal.pone.0068724
39. Jun KH, Jung JH, Choi HJ, Shin EY, Chin HM. HMGA1/HMGA2 protein expression and prognostic implications in gastric cancer. *Int J Surg*. (2015) 24:39–44. doi: 10.1016/j.ijsu.2015.10.031
40. Lin SY, Peng F. Association of SIRT1 and HMGA1 expression in non-small cell lung cancer. *Oncol Lett*. (2016) 11:782–8. doi: 10.3892/ol.2015.3914
41. Schnabel CA, Selleri L, Cleary ML. Pbx1 is essential for adrenal development and urogenital differentiation. *Genesis*. (2003) 37:123–30. doi: 10.1002/gene.10235
42. Thiaville MM, Stoeck A, Chen L, Wu RC, Magnani L, Oidtman J, et al. Identification of PBX1 target genes in cancer cells by global mapping of PBX1 binding sites. *PLoS ONE*. (2012) 7:e36054. doi: 10.1371/journal.pone.0036054
43. Grebbin BM, Schulte D. PBX1 as pioneer factor: a case still open. *Front Cell Dev Biol*. (2017) 5:9. doi: 10.3389/fcell.2017.00009

Conflict of Interest: The authors declare that the research was conducted in the absence of any commercial or financial relationships that could be construed as a potential conflict of interest.

frontiers in Oncology

ORIGINAL RESEARCH
published: 10 January 2020
doi: 10.3389/fonc.2019.01436

Personalized Treatment of H3K27M-Mutant Pediatric Diffuse Gliomas Provides Improved Therapeutic Opportunities

Johannes Gojo[1,2], Zdenek Pavelka[3], Danica Zapletalova[3,4], Maria T. Schmook[5], Lisa Mayr[1,2], Sibylle Madlener[1,2], Michal Kyr[3,4], Klara Vejmelkova[3,4], Martin Smrcka[6], Thomas Czech[2,7], Christian Dorfer[2,7], Jarmila Skotakova[8], Amedeo A. Azizi[1,2], Monika Chocholous[1,2], Dominik Reisinger[1,2], David Lastovicka[6], Dalibor Valik[9], Christine Haberler[10], Andreas Peyrl[1,2], Hana Noskova[11], Karol Pál[12], Marta Jezova[13], Renata Veselska[11], Sarka Kozakova[9], Ondrej Slaby[12,13], Irene Slavc[1,2†] and Jaroslav Sterba[3,4,9†]*

[1] Department of Pediatrics and Adolescent Medicine and Comprehensive Center for Pediatrics, Medical University of Vienna, Vienna, Austria, [2] Comprehensive Cancer Center Vienna, Medical University of Vienna, Vienna, Austria, [3] Department of Pediatric Oncology, University Hospital Brno and Faculty of Medicine, Masaryk University, Brno, Czechia, [4] International Clinical Research Center, St. Anne's University Hospital, Brno, Czechia, [5] Department of Biomedical Imaging and Image-Guided Therapy, Medical University of Vienna, Vienna, Austria, [6] Department of Neurosurgery, University Hospital Brno and Faculty of Medicine, Masaryk University, Brno, Czechia, [7] Department of Neurosurgery, Medical University of Vienna, Vienna, Austria, [8] Department of Pediatric Radiology, University Hospital Brno and Faculty of Medicine, Masaryk University, Vienna, Czechia, [9] Regional Centre for Applied Molecular Oncology, Masaryk Memorial Cancer Institute, Brno, Czechia, [10] Institute of Neurology, Medical University of Vienna, Vienna, Austria, [11] Laboratory of Tumor Biology, Department of Experimental Biology, School of Science, Masaryk University, Brno, Czechia, [12] Central European Institute of Technology, Masaryk University, Brno, Czechia, [13] Department of Pathology, Faculty Hospital Brno, Brno, Czechia

OPEN ACCESS

Edited by:
Hatem E. Sabaawy, Rutgers, The State University of New Jersey, United States

Reviewed by:
Theodore Nicolaides, Langone Medical Center, New York University, United States
Shiv K. Gupta, Mayo Clinic, United States

***Correspondence:**
Jaroslav Sterba
sterba.jaroslav@fnbrno.cz

[†] These authors share senior authorship

Specialty section:
This article was submitted to Cancer Molecular Targets and Therapeutics, a section of the journal Frontiers in Oncology

Received: 16 July 2019
Accepted: 03 December 2019
Published: 10 January 2020

Citation:
Gojo J, Pavelka Z, Zapletalova D, Schmook MT, Mayr L, Madlener S, Kyr M, Vejmelkova K, Smrcka M, Czech T, Dorfer C, Skotakova J, Azizi AA, Chocholous M, Reisinger D, Lastovicka D, Valik D, Haberler C, Peyrl A, Noskova H, Pál K, Jezova M, Veselska R, Kozakova S, Slaby O, Slavc I and Sterba J (2020) Personalized Treatment of H3K27M-Mutant Pediatric Diffuse Gliomas Provides Improved Therapeutic Opportunities. Front. Oncol. 9:1436. doi: 10.3389/fonc.2019.01436

Diffuse gliomas with K27M histone mutations (H3K27M glioma) are generally characterized by a fatal prognosis, particularly affecting the pediatric population. Based on the molecular heterogeneity observed in this tumor type, personalized treatment is considered to substantially improve therapeutic options. Therefore, clinical evidence for therapy, guided by comprehensive molecular profiling, is urgently required. In this study, we analyzed feasibility and clinical outcomes in a cohort of 12 H3K27M glioma cases treated at two centers. Patients were subjected to personalized treatment either at primary diagnosis or disease progression and received backbone therapy including focal irradiation. Molecular analyses included whole-exome sequencing of tumor and germline DNA, RNA-sequencing, and transcriptomic profiling. Patients were monitored with regular clinical as well as radiological follow-up. In one case, liquid biopsy of cerebrospinal fluid (CSF) was used. Analyses could be completed in 83% (10/12) and subsequent personalized treatment for one or more additional pharmacological therapies could be recommended in 90% (9/10). Personalized treatment included inhibition of the PI3K/AKT/mTOR pathway (3/9), MAPK signaling (2/9), immunotherapy (2/9), receptor tyrosine kinase inhibition (2/9), and retinoic receptor agonist (1/9). The overall response rate within the cohort was 78% (7/9) including one complete remission, three partial responses, and three stable diseases. Sustained responses lasting for 28 to 150 weeks were observed for cases with *PIK3CA* mutations treated with either

miltefosine or everolimus and additional treatment with trametinib/dabrafenib in a case with *BRAFV600E* mutation. Immune checkpoint inhibitor treatment of a case with increased tumor mutational burden (TMB) resulted in complete remission lasting 40 weeks. Median time to progression was 29 weeks. Median overall survival (OS) in the personalized treatment cohort was 16.5 months. Last, we compared OS to a control cohort ($n = 9$) showing a median OS of 17.5 months. No significant difference between the cohorts could be detected, but long-term survivors (>2 years) were only present in the personalized treatment cohort. Taken together, we present the first evidence of clinical efficacy and an improved patient outcome through a personalized approach at least in selected cases of H3K27M glioma.

Keywords: diffuse midline glioma, H3K27M, pediatric oncology, precision medicine, comprehensive molecular profiling

INTRODUCTION

Central nervous system (CNS) tumors represent the most common solid malignancies in childhood and are the leading cause of cancer-related death in this age group (1). Diffuse midline gliomas (DMG) with histone H3 lysine27-to-methionine mutations (H3K27M glioma) represent a highly aggressive subtype of glioma, which predominantly arise in children and young adults (2–4). The overall prognosis of H3K27M glioma is poor, displaying median survival rates of approximately 9 to 11 months irrespective of the tumor localization (5–9). Based on its uniform fatal prognosis, the presence of *H3K27M* mutation has already been implemented into the new WHO classification as being diagnostic for high-grade gliomas (10). To date, focal irradiation therapy remains the mainstay of therapy for H3K27M glioma, resulting in improved overall survival rates (11). Although additional systemic therapy is generally considered as beneficial (7, 12), no therapy regimen has yet been shown to exert superior effects (11, 13–15). Consequently, novel, improved therapeutic strategies for H3K27M glioma are needed.

Since the discovery of the molecular basis of H3K27M glioma, we and others have intensively studied the underlying molecular biology (8, 16–19). Large international efforts have enabled molecular analysis of a substantial number of these rare tumors showing that H3K27M glioma also comprises biologically and genetically heterogeneous tumors (8, 19). These studies have resulted in the identification of additional oncogenic driver alterations in H3K27M glioma. Interestingly, these events include mutation of well-described oncogenic pathways including cell-/DNA-damage repair mechanisms (*TP53, PPM1D, ATM, ATRX*) and receptor tyrosine kinase signaling pathways (*ACVR1, FGFR1, PIK3CA, PIK3R1, BRAF)* (4, 8, 18). Many of these genomic alterations represent therapeutically actionable targets (8). Similarly, DNA copy number aberrations leading to amplifications of known oncogenes such as *PDGFRA*, *EGFR*, *CDK6*, *KIT*, *KDR*, and *MET* as well as deletion of tumor suppressors such as *CDKN2A* (8) denote equally appealing therapeutic targets. Additionally, we and others have shown that major driver alterations are present throughout the tumor tissue, suggesting that these trunc mutations are feasible therapeutic targets for the entire tumor bulk (19, 20). Moreover, the H3K27M protein has been proposed as promising neo-antigen making H3K27M gliomas potential candidates for immunotherapy (21).

Considering the fatal prognosis and the discovery of novel therapeutic targets in DMG, a variety of small clinical trials with novel targeted agents has already been conducted. Treatment with vinorelbine in combination with nimotuzumab, an antibody directed against *EGFR*, for example, has been shown to prolong survival, resulting in a median overall survival of 15 months (13). However, other studies with either EGFR-directed small molecules (gefitinib, erlotinib) or antibodies could not confirm this effect for all DMGs but showed individual cases of longer survival (7, 15, 22–24). Similarly, also therapy with dasatinib and crizotinib, two small-molecule PDGFRA inhibitors, has not shown overall survival benefit (25). Therefore, considering the aforementioned heterogeneity within H3K27M glioma, a "one-size-fits-all" approach does not appear to substantially improve patient outcome.

Comprehensive dissection of the molecular signatures and specific targeting of these molecular driver signals is hoped to significantly improve mortality and morbidity of cancer patients (26). Personalization of therapy is of particular interest in poor prognosis tumors such as H3K27M glioma and in tumors where inconsistent gene alterations exist (27). As pediatric tumors harbor much less mutations than do adult cancers, precision targeted therapy is likely to be more effective against these tumors than standard population-based approaches (27, 28). This has been corroborated by a recent prospective analysis confirming the presence of potentially targetable alterations in 76% of H3K27M-positive pontine gliomas (29). Additionally, a recently reported pilot study for DIPG has also reported feasibility of personalized treatment recommendations (30). Although multiple interventional molecular matching studies are ongoing (NCT01182350, NCT02233049), evidence for the clinical benefit of this approach in H3K27M glioma is still lacking.

Here, we investigated the feasibility and clinical benefit of comprehensive molecular profiling for H3K27M glioma in an international collaboration of two centers.

MATERIALS AND METHODS

Case Selection

All prospectively evaluated patients aged 0–21 years with DMG diagnosed between 2015 and 2018 were retrospectively collected and included into the case series. Tumor biopsies yielding fresh tissue were performed at diagnosis as part of standard of care treatment. Confirmed histopathological diagnosis of high-grade glioma with H3K27M mutation was necessary for inclusion and further comprehensive molecular profiling. Informed consent was obtained from every participating patient and/or legal representative.

Patient Treatment

All patients received backbone therapy consisting of focal irradiation and a systemic therapy backbone as by institutional guidelines (**Table 1**). Following comprehensive molecular profiling performed at CEITEC, Massaryk University Brno, patients were assigned to additional concomitant personalized treatment plans according to the consensus report of an interdisciplinary molecular tumor board. Respective treatment approaches were suggested according to previously described target actionability described in the INFORM trial (42), FDA datasheets, and Drugbank Canada (35), at mycancergenome.org, or described in other tumors, preclinical studies, or case reports as outlined in **Table 1**. If information on blood–brain barrier penetrance or effect in brain tumors was available from the literature, CNS-penetrant drugs were favored. Patient treatment with innovative therapeutics was based on named-patient use and informed consent was obtained from patients and/or legal representatives. Medication doses were chosen according to the literature and previous experience in the pediatric population if available.

Patient Data

Clinical data were obtained from patient charts available at the respective treating centers.

Criteria for Response and Progression

Radiological response was assessed by experienced pediatric neuroradiologists using regular magnetic resonance imaging (at least every 3 months) according to modified RANO criteria (43).

Survival Analysis

Patients with confirmed *H3K27M* mutation where comprehensive molecular profiling was not possible ($n = 2$) or without targetable alterations ($n = 1$) were included into the control group. Moreover, 6 patients with confirmed *H3K27M* mutation treated at the respective centers before comprehensive molecular profiling became available were included in the control group. All patients of the control group were treated according to institutional guidelines with focal radiotherapy and systemic chemotherapy (**Table 2**). Overall survival was defined as time between first diagnosis by imaging until death.

Whole Exome Sequencing

DNA was extracted from FFPE tumor tissue samples using the QIAmp DNA FFPE Tissue Kit (Qiagen, Netherlands). The whole exome libraries were prepared using TruSeqExome Kit (Illumina, CA, USA) according to the manufacturer's recommendations. Quantity and quality of exome libraries were checked using Qubit 2.0 Fluorometer and NanoDrop2000c spectrophotometer (Thermo Fisher Scientific). Prepared libraries were loaded onto NextSeq 500/550 Mid Output Kit (150 cycles) and sequenced on the NextSeq 500 instrument (both Illumina). Sequencing coverage for both exomes was $>20\times$ at $>90\%$ of capture regions.

Bioinformatic Analysis

Sequencing reads in fastq format were mapped to the human reference genome GRCh37 with the bwamem algorithm for both the tumor and the healthy control sample. The resulting alignments in "bam" format were postprocessed with the samblaster program for marking PCR duplicates. The final alignment file of the control sample was used to assess single nucleotide variants (SNVs) and short insertions/deletions (indels). Two variant callers were used for germline variant calling; the GATK HaplotypeCaller and VarDict (AstraZeneca, Waltham, MA, USA). Reported variants were annotated with Annovar and Oncotator annotation programs. Tumor-specific variants were assessed by somatic (paired; tumor vs. control) variant calling. For this purpose, we used Mutect (SNVs), Scalpel (Indels), and VarDict (SNVs and Indels) variant callers. The annotation of somatic variants was performed with the addition of the COSMIC database.

Variants were filtered manually based on the virtual panel filtering (genes analyzed by FoundationOne CDx panel, genes that are cataloged in the Cancer Gene Census, and variants that have previously been reported in COSMIC, MD Anderson). Mutations in genes that have been causally implicated in cancer are then manually checked in other available databases or scientific literature sources (e.g., cBioPortal, The Clinical Knowledgebase—JAX CKB, MyCancerGenome) where their potential oncogenic biological effect and references to relevant clinical trials or studies can be found. Selected gene variants with known or potential clinical significance are outlined in the final report; other variants found are listed separately (**Table S1**) and are considered as variants of uncertain clinical significance (VUS).

Tumor Mutational Burden Estimation

An annotated list of somatic variants from the previous step is used to assess the tumor mutation burden (TMB). For TMB calculation from WES data only somatic point mutations were considered, since indels (short insertions and deletions) tend to be called with high false-positive rates and could potentially skew the outcome. Additionally, two bases before and after each exon are considered for splicing mutations. Synonymous variants are filtered out, as they do not fit the definition of TMB. Finally, variants with variant allele frequency of $<5\%$ are filtered out. The coding region locations on the hg19 genome were downloaded from the UCSC genome browser.

TABLE 1 | Clinical parameters, molecular alterations, line of treatment, treatment modalities, and backbone treatment of patients treated with personalized approaches.

#	Center	Age	Gender	Localization	Molecular alteration	Line of treatment	Personalized treatment	Mode of action /rationale	Literature	Backbone treatment	OS (months)
1	Brno	4.9	m	Pons	PIK3CA(E545K)	First	Miltefosin (2 mg/kg/day once daily)	AKT inhibitor	(31, 32)	RTX, nimotuzumab 150 mg/m^2 + vinorelbine 20 mg/m^2 every 7 days for 12 weeks, followed by nimotuzumab 150 mg/m^2 + vinorelbine 25 mg/m^2 every 14 days, valproate (plasma level 80–100 μg/ml)	44.5
2	Brno	4.9	f	Pons	ACVR1(R206H)	First	Palovarotene (0.4 mg/kg/day once daily)	Active in germline ACVR1 mutation	(33)	RTX, nimotuzumab 150 mg/m^2 + vinorelbine 20 mg/m^2 every 7 days for 12 weeks, followed by nimotuzumab 150 mg/m^2 + vinorelbine 25 mg/m^2 every 14 days, valproate (plasma level 80–100 μg/ml)	16.5
3	Brno	18.2	m	Pons	TMB 20 mut/MB	First	Nivolumab (1 mg/kg every 2 weeks first 4 months followed by 3 mg/kg every 2 weeks)	Immune checkpoint inhibitor	(34)	RTX, nimotuzumab 150 mg/m^2 + vinorelbine 20 mg/m^2 every 7 days for 12 weeks, followed by nimotuzumab 150 mg/m^2 + vinorelbine 25 mg/m^2 every 14 days, valproate (plasma level 80–100 μg/ml)	17.5*
4	Brno	6.4	f	Pons	PIK3CA(E545K)	First	Miltefosin (2.5 mg/kg/day once daily)	AKT inhibitor	(31, 32)	RTX, nimotuzumab/vinorelbine, valproate	15.0
7	Brno	6.6	f	Pons	FGFR3/CSF1R mRNA overexpression	Second	Pazopanib (5 mg/kg once daily, dose reduction due to side effects to 200 mg every other day)	Receptor tyrosine kinase inhibitor	Drugbank Canada (35)	RTX, nimotuzumab/vinorelbine, valproate	8.0
8	Brno	19.0	m	Spinal (lower thoracic region)	KRAS(G12A)	First	Trametinib (2 mg once daily)	MEK inhibitor	NCT03704688 (36)	RTX, nimotuzumab 150 mg/m^2 + vinorelbine 20 mg/m^2 every 7 days for 12 weeks, followed by nimotuzumab 150 mg/m^2 + vinorelbine 25 mg/m^2 every 14 days, valproate (plasma level 80–100 μg/ml), metoclopramide (0.4 mg/kg/day three times daily)	12.9
9	Vienna	8.2	m	Thalamic	BRAF(V600E)	Second	Dabrafenib (5 mg/kg/day divided twice daily), trametinib (0.04 mg/kg/day once daily), bevacizumab (10 mg/kg every 2 weeks)	BRAF/MEK inhibitors	(37–39)	Re-RTX, temozolomide (concomitant to RTX 75 mg/m²/day once daily)	28.8
10	Vienna	12.9	m	Pons	PIK3CA(G118D)	Second	Everolimus (4.5 mg/m²/day once daily, increased until trough level 5–15 ng/ml)	mTOR inhibitor	(40)	Temozolomide (200 mg/m²/day for 5 days at 28-day cycles), mebendazole 1500 mg/day three times daily	21.4
12	Vienna	4.9	m	Pons	PDGFRA (R841_I843delinsL) XPC(P334H)	First	Pazopanib (260 mg/m²/day once daily) pembrolizumab (2 mg/kg every 3 weeks)	PDGFRA inhibitor Immune checkpoint inhibitor	(34, 35, 41)	RTX, temozolomide (40 mg/m²/day once daily)	6.1

** Alive with disease; OS, overall survival; TMB, tumor mutational burden.*

TABLE 2 | Clinical parameters, histone mutation status, and treatment of cases in the control cohort.

#	Center	Age (years)	Gender	Localization	H3 mutation	First-line treatment	Second-line treatment	OS (months)
5	Brno	4.9	f	Pons	IHC	Nimotuzumab/vinorelbine		19.0
6	Brno	8.2	m	Pons	IHC	Nimotuzumab/vinorelbine	Re-RTX	15.0
11	Vienna	5.9	f	Pons	H3F3A	Temozolomide	Re-RTX, everolimus	19.7
13	Vienna	8.8	m	Pons, mesencephalon	H3F3A	Tumor vaccination	Immune checkpoint inhibitors	10.7
14	Vienna	2.4	m	Pons	HIST1H3B	Temozolomide, tumor vaccination	Re-RTX	20.4
15	Vienna	8.4	m	Pons	H3F3A	Temozolomide		16.8
16	Vienna	9.8	f	Thalamus	H3F3A	Temozolomide	Intrathecal VP-16, PEI	7.9
17	Vienna	11.1	m	Pons, cerebellum	IHC	Nimotuzumab/vinorelbine	Re-RTX, PEI	19.4
18	Vienna	4.4	m	Pons, mesencephalon	IHC	Nimotuzumab/vinorelbine	PEI	17.8

OS, overall survival; IHC, immunohistochemistry.

Detection of Fusion Genes by Next-Generation Sequencing

Total RNA from tumor tissue was extracted using mirVana miRNA Isolation Kit (Thermo Fisher Scientific, MA, USA). Quantity and quality of extracted RNA were checked by Qubit® 2.0 Fluorometer system (Thermo Fisher Scientific, MA, USA) and NanoDrop 2000c Spectrophotometer (Thermo Fisher Scientific, MA, USA). For sequencing libraries preparation, TruSight RNA Pan-Cancer Panel (Illumina, CA, USA), which targets fusions in 1385 genes, was used. Sequencing libraries were subsequently loaded on NextSeq 500/550 Mid Output Kit v2 (150 cycles) and NextSeq 500 sequencing device (both Illumina, CA, USA). All processes were performed according to the manufacturer's instructions. Quantity and quality of sequencing libraries were checked by Qubit® 2.0 Fluorometer system (Thermo Fisher Scientific, MA, USA) and TapeStation 2200 (Agilent Technologies, CA, USA). For data analysis, BreakingPoint tool was used.

Liquid Biopsy Analysis of Cerebrospinal Fluid (CSF)

CSF was obtained via lumbar puncture at the given time points. The cfDNA isolation from 1 ml CSF was performed using the quick cfDNA/cfRNA serum and plasma kit (Zymo Research, CA, USA) following the manufacturer's instructions. The QX200^{TM} digital droplet system from BioRad (CA, USA) was used and the assay was performed according to manufacturer's manuals. In brief, the unique assay ID dHsaMDV2510510 for the *H3F3A* p.K28M mutation from BioRad was used to analyze the mutations in the cfDNA of patient CSF samples. To each run, a sample with known positive H3F3A p.K28M mutation and a negative control (nuclease free water) were included to determine the fluorescence thresholds. The results of ddPCR were analyzed with Quantasoft^{TM} software. Detected counts of *H3F3A* mutant and wild-type cfDNA were normalized to 1 ml CSF volume. Thereby, samples of different time points could be compared for semiquantitative longitudinal analysis.

Statistical Analysis

Analyses were performed using SPSS version 25.0 and Graph Pad Prism version 5.0.

RESULTS

Study Cohort and Comprehensive Molecular Profiling

Twelve patients were included in this study whereby two cases had to be excluded due to insufficient amount of biological material available (**Figure 1**). Comprehensive molecular profiling was performed for 10 tumors (**Figure 1**). Next-generation sequencing could be performed for all 10 cases and transcriptomic profiling in 7 out of 10. *H3K27M* mutations were confirmed in all cases (*HIST1H3B* 2/10, *H3F3A* 8/10). Mutations in *TP53* were detected in 5 of the tumors analyzed (5/10). Potentially targetable mutations included *KRAS* (1/10), *PIK3CA* (3/10), *BRAF* (1/10), *ACVR1* (1/10), *ATM* (1/10), and *ATRX* (1/10) (**Figure 2**). With respect to possible immune checkpoint inhibitor therapy, high TMB (2/10) and overexpression of *IL13RA2* (2/13) were detected. One case was assigned to treatment solely based on transcriptomic profiling due to the lack of targetable mutations (case #7). Only one case (case #11) could not be assigned to a personalized treatment approach. **Table 1** lists clinical details, detected molecular alterations, and personalized as well as backbone treatment for the respective cases. Alteration of the PI3K/AKT/mTOR pathway via mutation of *PIK3CA* was detected in three cases. The two cases harboring a *PIK3CA(E545K)* mutation were subsequently treated with miltefosine, an AKT inhibitor (31, 32), the one case with *PIK3CA(G118D)* mutation with everolimus, a, mTOR inhibitor approved for treatment of tuberosis sclerosis associated tumors (40). Based on effective treatment of germline *ACVR1* mutations with palovarotene, a retinoic receptor agonist, in the literature (33), the case with *ACVR1(R206H)* was treated accordingly. With respect to alterations of the MAPK pathway, one case with *BRAF(V600E)* mutation was subjected to treatment with a combination of dabrafenib, trametinib, together with bevacizumab, and the patient harboring a tumor with *KRAS(G12A)* was subjected to treatment with trametinib (36–39). Two patients (cases #3 and #12) were assigned to receive immunotherapeutic approaches due to high tumor mutational burden (TMB) (34). In one case (case #12), we additionally detected a germline mutation of *XPC,* which has been described as being susceptible toward immune checkpoint inhibition

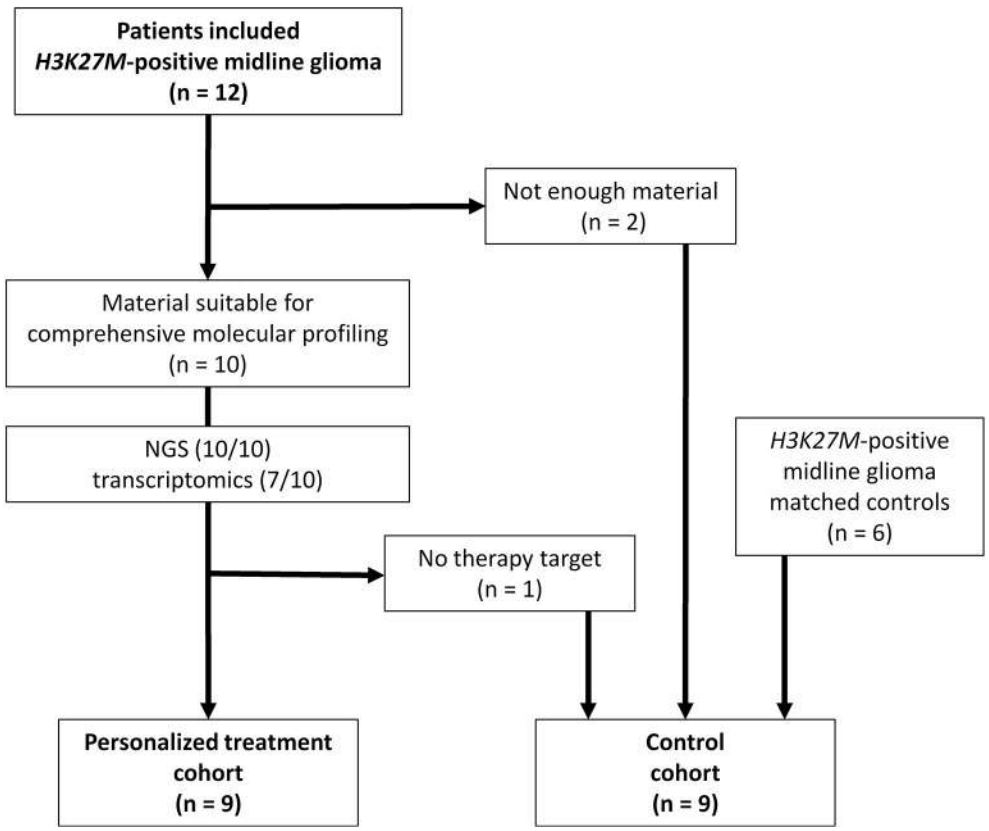

FIGURE 1 | Flow chart of patients included in personalized treatment and control cohort. NGS, next-generation sequencing.

(41). The latter patient was additionally treated with pazopanib, targeting detected mutation and overexpression of *PDGFRA* (35). Last, another patient (case #7) was assigned to treatment with pazopanib based on detected mRNA overexpression of *FGFR3* and *CSF1R* (35).

Response to Personalized Treatment

The overall response rate was 78% (7/9), consisting of two stable diseases, three partial responses, and one complete response (**Figure 3**). Median time to progression was 25 weeks. It is worth noting that the analysis also included three patients who were treated with personalized approaches at first progression as second-line treatment and not upfront. The two responders of this group showed a progression-free survival of 25 and 33 weeks, respectively. The six cases treated upfront with molecularly guided treatment plans exhibited a median time to progression of 29 weeks. Two patients showed disease progression under personalized treatment approaches. Interestingly, both patients not responding to treatment were treated with pazopanib (cases # 7 and #12).

With respect to molecular alterations, miltefosine treatment of tumors harboring *PIK3CA(E545K)* resulted in one stable disease (case #4) and one partial response (case #1, **Table 1**, **Figure 3**). In the latter case, the patient was treated with miltefosine, an AKT inhibitor, in addition to nimotuzumab and vinorelbine following irradiation (case #1, **Figure 4**), resulting in a prolonged partial response of 150 weeks. Everolimus treatment in the case with *PIK3CA(G118D)* led to partial response in second-line treatment (case #10, **Table 1**, **Figure 3**). In the case of a thalamic tumor harboring an additional *BRAF(V600E)* mutation, comprehensive molecular profiling was performed at the time of progression where multiple metastatic lesions were detected (case #9, **Figure 5**). Personalized treatment following re-irradiation in addition to a temozolomide backbone resulted in shrinkage of the lesions and partial response even in second-line treatment. Also in the case of a *KRAS(G12A)* mutation, treatment with trametinib in addition to irradiation, nimotuzumab, vinorelbine, and metoclopramide resulted in stable disease (case #8, **Table 1**, **Figure 3**). Moreover, also personalized treatment of *ACVR1* mutation with palovarotene (case #2, **Table 1**, **Figure 3**) resulted in disease stabilization, providing first evidence of this approach for *H3K27M-ACRV1* commutated tumors. Finally, adding immune checkpoint inhibition to the backbone treatment based on high TMB resulted in a sustained complete remission in one case (case #3, **Figure 6A**). However, after 8 months of treatment, the patient developed severe autoimmune encephalitis necessitating treatment interruption. During steroid treatment, the patient improved markedly. Additionally performed liquid biopsy analysis for *H3K27M* in CSF documented an increase of the *H3K27M* copies during treatment gap, followed by

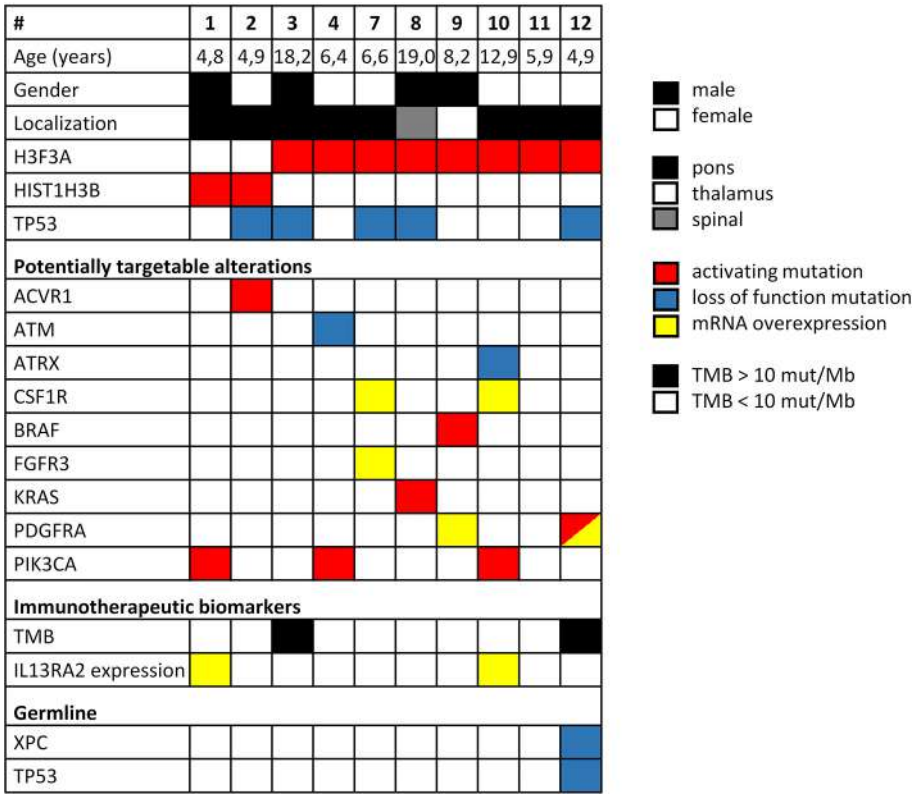

FIGURE 2 | Overview of clinical parameters and detected molecular alterations for H3K27M glioma analyzed by comprehensive molecular profiling. TMB, tumor mutational burden.

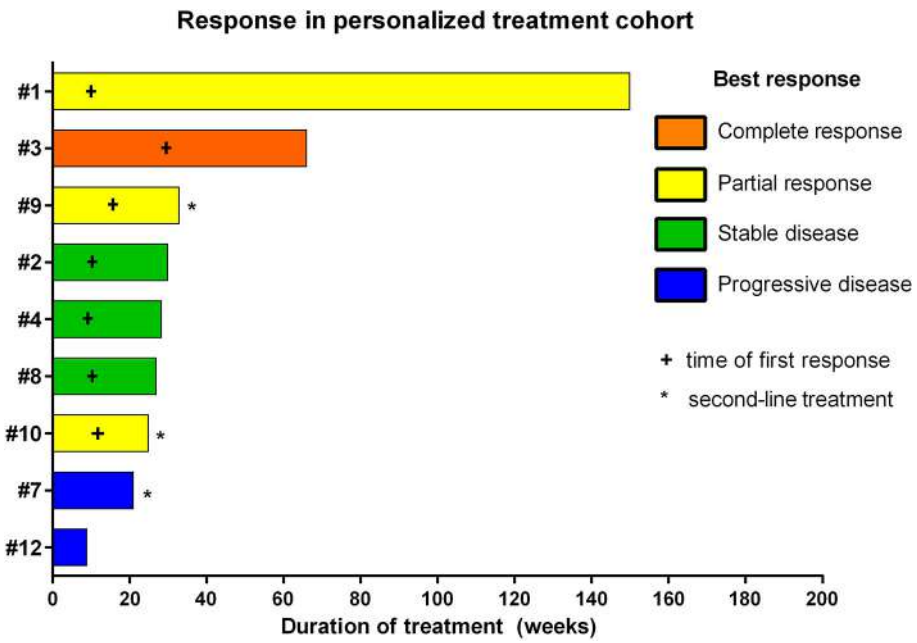

FIGURE 3 | Individual responses of patients treated with personalized treatment approaches based on comprehensive molecular profiling.

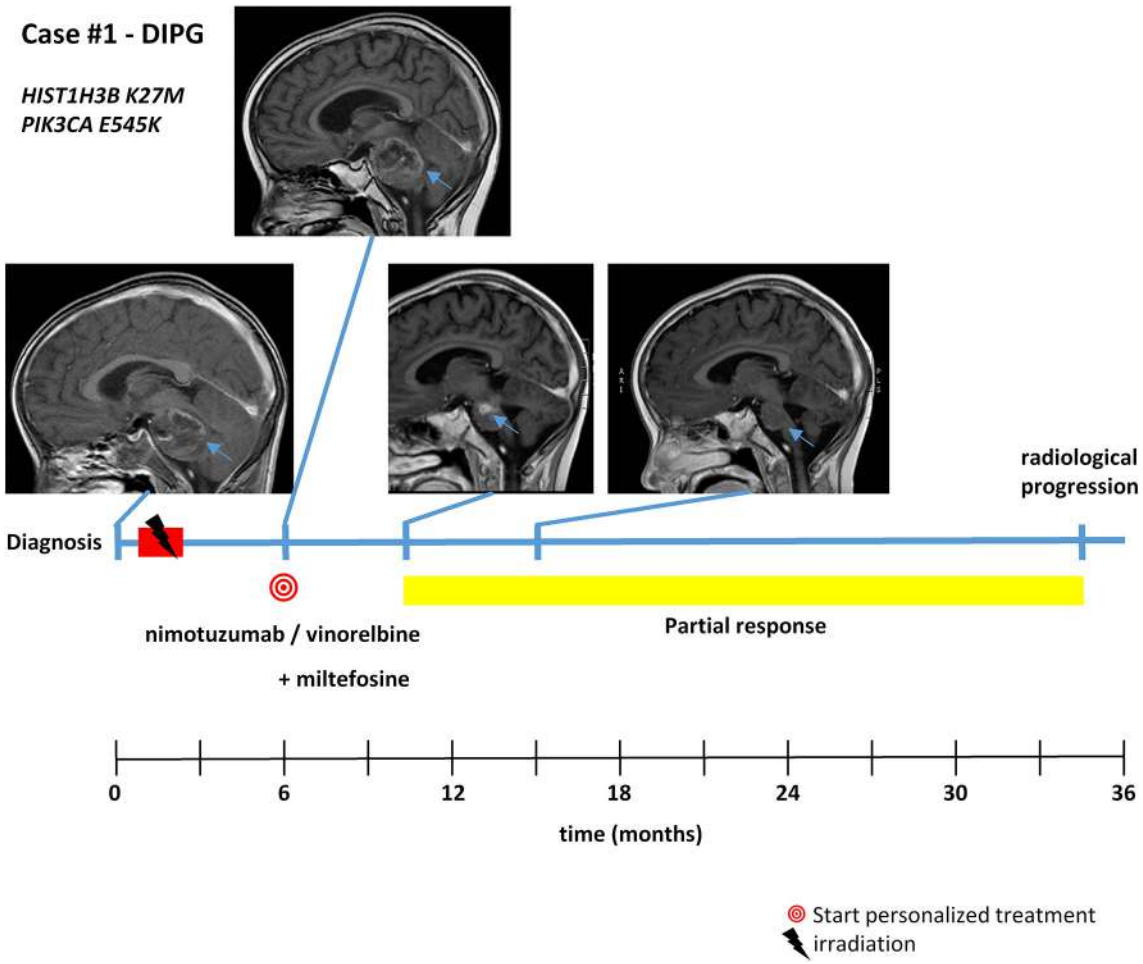

FIGURE 4 | Detailed case description—case #1. Timeline of patient treatment including magnetic resonance images at indicated time points. Blue arrows indicate tumor. DIPG, diffuse intrinsic pontine glioma.

radiological and clinical progression later on (**Figures 6A,B**). The second case treated with immune checkpoint inhibition (case #12, **Table 1**, **Figure 3**) showed no response despite high TMB (27/MB) resulting from a germline *XPC* mutation. It has to be noted, however, that this case displayed an extraordinary aggressive phenotype with massive clinical and radiological progression in only 10 days prior to biopsy and treatment start. Moreover, immune checkpoint inhibitors could only be introduced after the disease had already progressed despite radiotherapy and the patient only received four cycles.

Survival Analysis

To evaluate the potential impact of personalized treatment approaches on the overall survival of H3K27M glioma patients, we set up a control cohort of patients treated at the same centers for comparison. The clinical details of the control cohort are outlined in **Table 2**. Comparison of clinical parameters in the personalized and the control cohort is given in **Table 3**. At the time of data analysis (July 2019), no patient in both the control and the personalized treatment cohort remained alive. Median overall survival was 16.5 months (12.2–20.8 months 95% CI) in the personalized and 17.8 months (14.8–20.7 months 95% CI) in the control cohort, respectively (**Figure 7**). The hazard ratio for personalized treatment was 0.69 (0.25–1.95 95% CI). Accordingly, no significant difference between the two groups was observed. 1-year OS in both cohorts was 77% (±14%). In contrast, 2-year OS was 11% (±10%) in the personalized treatment cohort, whereas no patient in the control cohort survived longer than 2 years. The longest observed survival was 44.5 months. As *TP53* mutation was the second most common recurrent aberration in our case series, we compared survival rates of *TP53* wild-type and mutant cases (**Figure 8**). *TP53* mutant cases showed a markedly shorter overall survival (median survival 12.9 months) as compared to *TP53* wild-type cases (median OS 28.7 months).

DISCUSSION

Due to the uniformly fatal prognosis of H3K27M glioma, improved therapeutic strategies are urgently needed. Recent

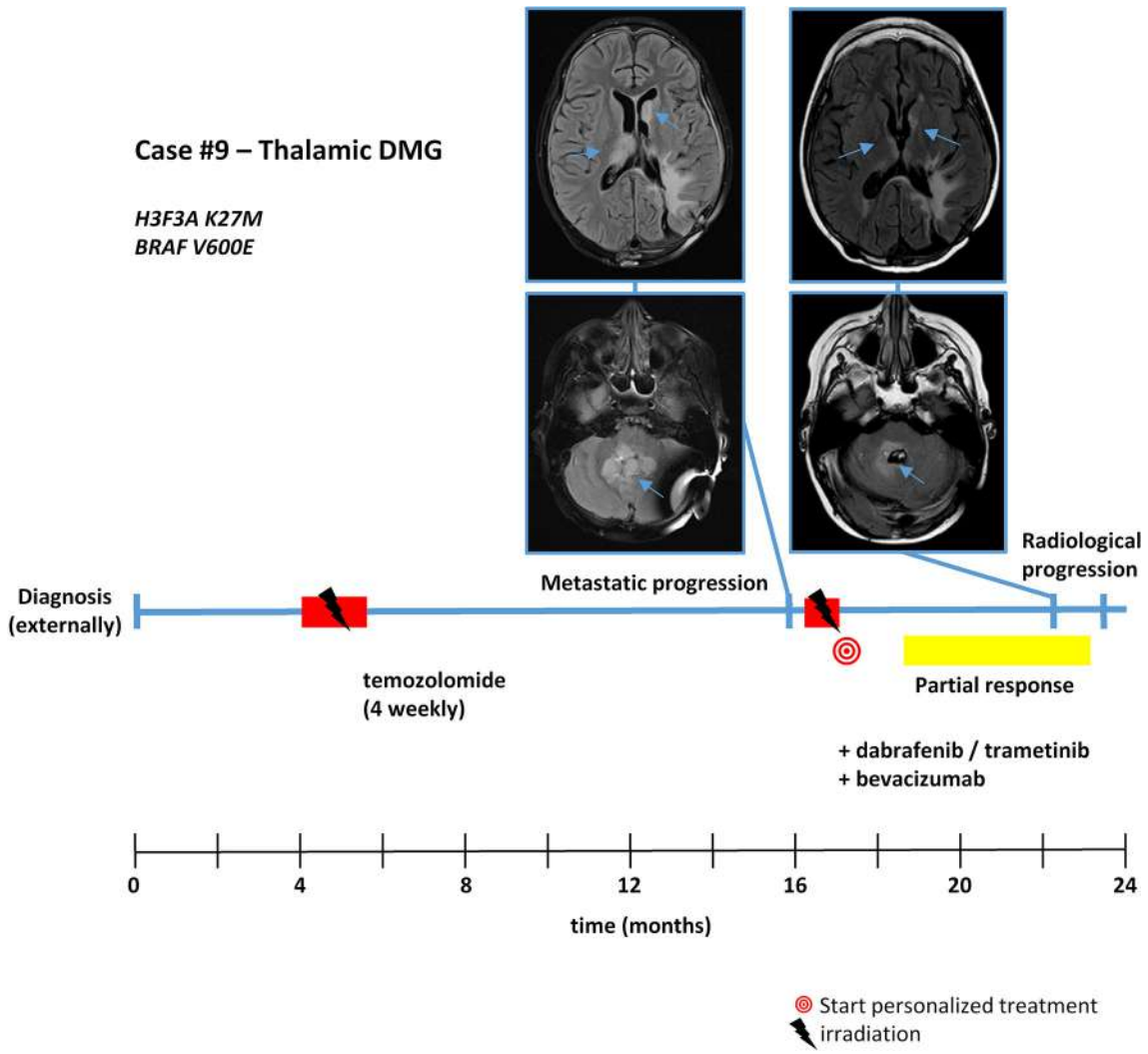

FIGURE 5 | Detailed case description—case #9. Timeline of patient treatment including magnetic resonance images at indicated time points. Blue arrows indicate tumor. DMG, diffuse midline glioma.

high-throughput studies led to the conclusion that despite shared H3K27M mutation, these entity comprises multiple different molecular subgroups (8, 19). Being controversially discussed some years ago, biopsy of DMGs has been shown to be safe, which we could also confirm in our case series (29, 30). Hence, personalized treatment approaches based on comprehensive molecular profiling are considered a particularly promising treatment approach (27). In the underlying study, we investigated not only the presence of potential treatment targets but also clinical benefit via individualized treatment plans. To our knowledge, this is the first personalized medicine-based study describing response rates in H3K27M glioma. Thus, despite low patient number and non-prospective design of the study, we consider these results of high interest to the medical community.

Several previous studies assessed the potential of molecular approaches in H3K27M glioma (4, 8, 18, 29); however, data on the clinical impact is limited (30). In contrast to a recently published study in DIPG (30) our study cohort was restricted to H3K27M glioma (8/10 H3F3A, 2/10 HIST1H3B), also including a thalamic and a spinal case. Comparable to previous studies, 50% of tumors harbored a mutation in *TP53* (29, 30). By comprehensive molecular profiling, we detected targetable alterations in 90% (9/10) of the tumors, which is comparable to previous results from the INFORM study. In contrast to the aforementioned study in DIPG, targeting H3K27M glioma with HDAC inhibitors such as panobinostat was not considered "targeted treatment recommendation" in our study cohort (30). Valproate was used in 6/9 cases as therapy backbone. There were no two molecularly identical patients in our cohort, suggesting the importance of a personalized approach even within a relatively narrow and already molecularly predefined group like H3K27M glioma. While most tumor cells harbor more than one tumor-propagating change within the different cell-signaling pathways,

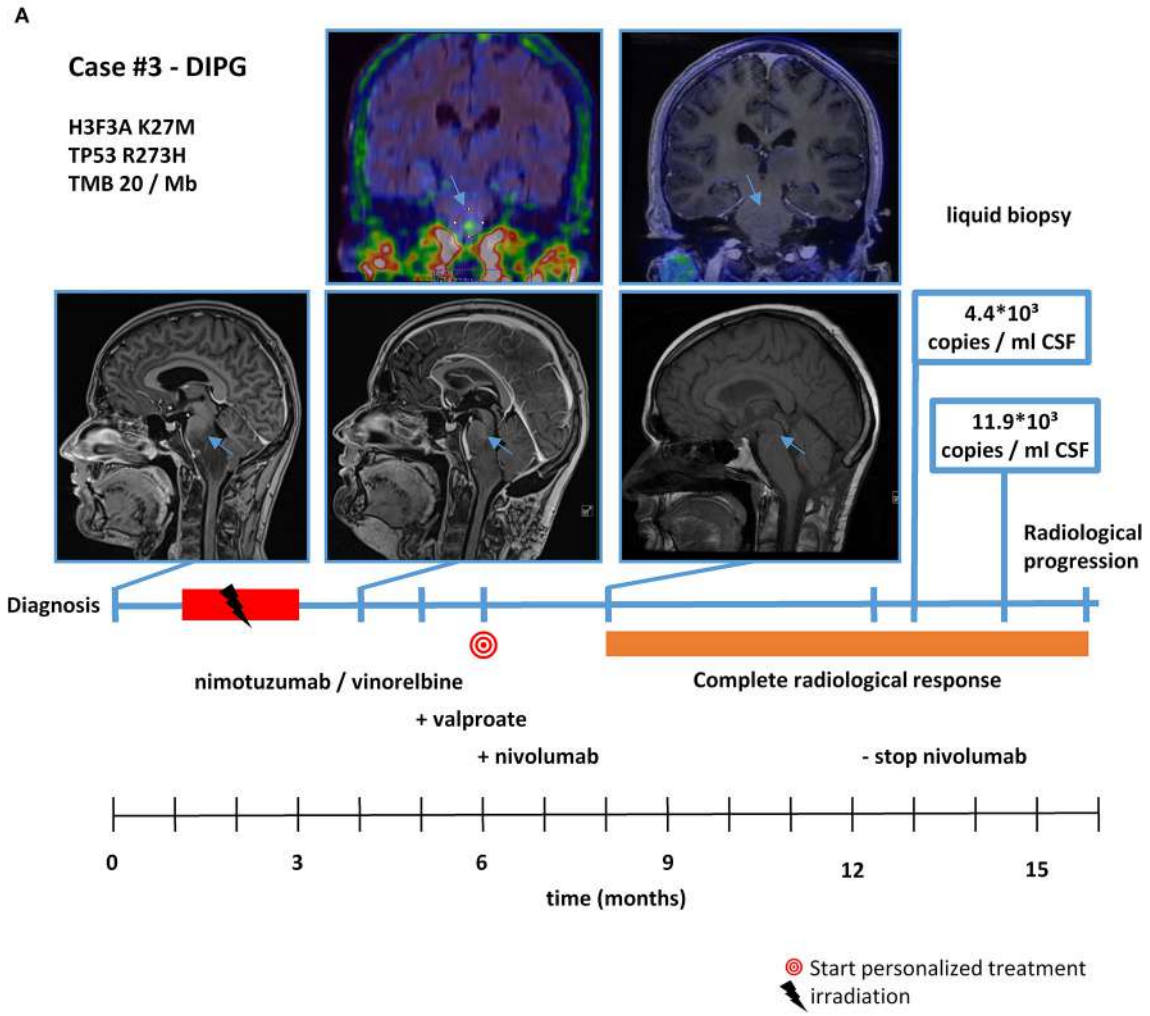

FIGURE 6 | Detailed case description—case #3. **(A)** Timeline of patient treatment including magnetic resonance images, ^{18}F-FET-PET images, and liquid biopsy results at indicated time points. Blue arrows indicate tumor. **(B)** Digital droplet PCR (ddPCR) plot in cerebrospinal fluid (CSF) 1 month after discontinuation of nivolumab. **(C)** ddPCR plate in CSF 3 months after discontinuation of nivolumab. DIPG, diffuse intrinsic pontine glioma.

progressive or relapsed tumors display additional molecular changes mediating resistance to previous treatments as we could document in our serial samples as well (data not shown). It remains a great challenge to address more than one or two such aberrations, and such combination treatments should be based on strong scientific rationale.

In our personalized treatment cohort, the overall response rate was 78% (7/9). Interestingly, the two non-responders were both treated with pazopanib, suggesting poor benefit from pazopanib treatment for H3K27M glioma. However, both tumors also harbored a *TP53* mutation, which we show to be associated with an inferior outcome.

One third of the cases (3/9) exhibited activation of the PI3K/AKT/mTOR pathway that was targeted by either miltefosine or everolimus. All patients responded to a combination with backbone treatment, which also included the case with the longest observed OS (44.5 months) in this cohort. Consequently, our data indicate that targeting molecular alterations of the PI3K/AKT/mTOR pathway in H3K27M glioma might represent a promising therapeutic approach worth validating in clinical trials that have already been initiated (27).

One thalamic case harbored an additional *BRAF(V600E)* mutation. This co-occurrence has already been described and diffusely infiltrating tumors in the midline appear to carry the same dismal prognosis as other H3K27M gliomas (18, 30, 44). However, patients with double-mutant tumors may also show a more benign course of disease, in particular if they show low infiltration, low-grade glioma histology features and can be safely resected (45). In contrast, the case in our cohort showed high proliferation and was treated at metastatic disease progression with a combination of trametinib, dabrafenib, and bevacizumab in addition to backbone treatment. We observed a partial remission lasting 33 weeks. OS in this case was 28.8 months, suggesting a benefit of targeted treatment in *BRAF* commutated H3K27M glioma. The second case treated with the MEK inhibitor trametinib harbored a *KRAS(G12A)* mutation and also showed stable disease lasting 28 weeks.

Activating mutations in *ACVR1* have been reported in approximately 20% of DIPG (8, 46). Interestingly, previous reports in patients with germline *ACVR1* mutations suggested benefit from treatment with palovarotene, a retinoic receptor agonist (33). The single case with *ACVR1* mutation in our cohort was treated accordingly, resulting in disease stabilization lasting 30 weeks.

TABLE 3 | Comparison of clinical and H3K27M-status in personalized and control cohort.

	Personalized	Control
Age in years, median (range)	6.6 (4.8–19)	8.2 (2.4–11.1)
Gender (m:f)	4:5	6:3
Localization		
Pons	7	8
Thalamus	1	1
Spinal	1	–
H3K27M detection		
H3F3A	7	4
HISTH3B	2	1
IHC	0	4
Backbone treatment (first line)		
Nimotuzumab/vinorelbine	6	4
Temozolomide	3	4
Other	0	1

IHC, immunohistochemistry.

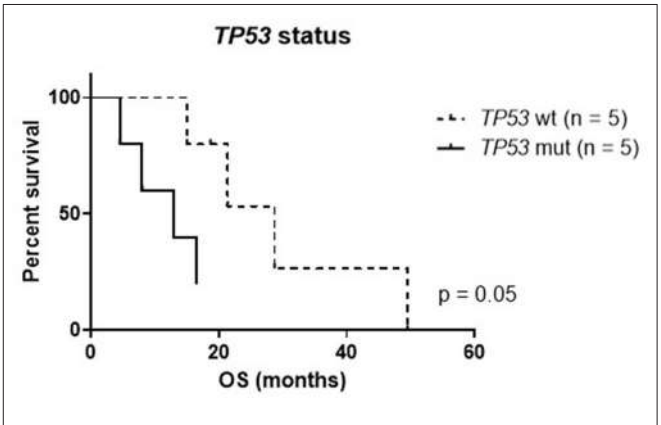

FIGURE 8 | Kaplan–Meier plot of *TP53* mutant (mut) and wild-type (wt) cases within the personalized treatment cohort. OS, overall survival.

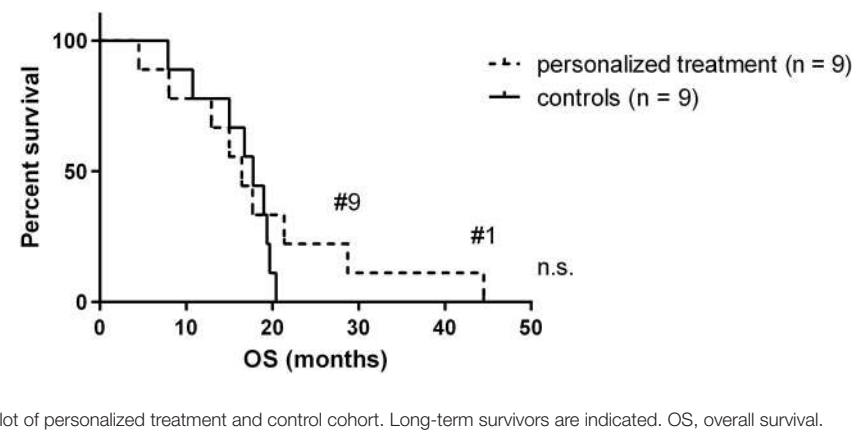

FIGURE 7 | Kaplan-Meier plot of personalized treatment and control cohort. Long-term survivors are indicated. OS, overall survival.

Immunotherapy has revolutionized oncology in the past years and resulted in substantial improvement of treatment outcomes in certain tumor types (47). In pediatric high-grade glioma, best outcomes were described for patients harboring germline mutations in DNA repair mechanisms (34). Within our cohort two patients with increased TMB were treated with immune checkpoint inhibitors. One of these patients showed the sole complete remission in the whole cohort. However, treatment had to be discontinued due to severe side effects, and during steroid treatment, rapid disease progression was observed. In the second case with high TMB due to a germline *XPC* mutation, immune checkpoint inhibitor treatment in addition to pazopanib was recommended. In this case, we observed a highly aggressive course of disease, already prior to personalized treatment approaches and no response under immune checkpoint inhibition. Consequently, immune checkpoint inhibition appears to be a highly effective treatment in selected cases but testing for tumor mutational load appears to be crucial to predict benefit of treatment. However, for future trials, investigation of tumor microenvironment and immune response appear to be crucial in order to further clarify which patient collective may benefit from immune checkpoint inhibitors. Moreover, in our series, immunotherapies were applied following radiotherapy. Interestingly, recent analyses in adult high-grade glioma suggest that immunotherapies may be more effective if applied before irradiation (48). In our longest surviving patient (case #1), immunotherapy was added only after the disease progression as second personalized treatment approach, 35 months from original diagnosis. Therapy consisted of four doses of autologous dendritic cell vaccine according to our institutional protocol (EudraCT number 2014-003388-39). Accelerated disease progression was documented after corticosteroid treatment being a component of terminal antiedematous approach. These observations may stimulate further studies addressing immunotherapeutic approaches for this particularly fatal malignancy.

As the number of oncogenic mutations is generally low in H3K27M glioma, we also included transcriptomic profiling in addition to mutation detection in 70% of the cases. Treatment recommendation was solely based on transcriptomic profiling in one case with elevated *FGFR3* and *CSF1R* expression. Treatment with the receptor tyrosine kinase inhibitor pazopanib did not show an effect. Despite this discouraging observation, we suggest to include transcriptomic profiling also in future personalized medicine approaches as some important aspects like immune evasion or angiogenesis are not reflected just by mutational analyses. The poor effect may have been based on the lack of clinical efficiency with pazopanib treatment, which has also been described for adult high-grade glioma (49). With respect to the emerging treatment with ONC201 (50), being currently assessed within trials, we retrospectively analyzed *DRD2* expression. In all our investigated cases, the *DRD2* expression was decreased (data not shown); however, recent data are suggesting different mechanisms of action for ONC201 (51).

Overall analysis of the clinical benefit demonstrated a median PFS of 29 weeks, also including second-line treatment cases. This might also be the reason for a shorter PFS as compared to other first-line studies (13, 22, 23) but longer median PFS as compared to a previous study for recurrent tumors (24). To assess potential benefit for overall survival of a personalized treatment approach in H3K27M glioma, we compared the cohort to a retrospective control cohort treated at the same centers. No significant difference between the two cohorts was observed (16.5 vs. 17.8 months). It must be noted that in both cohorts, the median OS was markedly higher than in recent meta-analyses reporting an OS of <1 year (7, 9). For example, a recent large retrospective analysis reported a median OS of 10.4 months for *H3F3A*-mutated and 15.0 months for *HIST1H3B* (7). A median OS of 15 months was reported in a study investigating the combination of nimotuzumab and vinorelbine. This backbone was used in 6/9 cases in personalized and in 4/9 cases in the control cohort of our study. Interestingly, median OS for both of the cohorts was longer. Consequently, no significant benefit of personalized treatment approaches was observed, also owing to the good survival rates within the control group. However, longer survival beyond 2 years was only seen in the personalized treatment cohort. We are aware that the study design and results do not allow a clear conclusion whether personalized treatment is of benefit in H3K27M glioma. However, the molecular profiles of the analyzed cases reveal that we did not find any identical case. Consequently, a randomized study approach is less attractive given the strong molecular heterogeneity within this tumor type. Nevertheless, a prospective trial with a larger sample size would be urgently needed to further assess the potential of personalized treatment approaches in this devastating disease.

Liquid biopsy has emerged as a promising diagnostic tool for improved patient monitoring, also in H3K27M glioma (30, 52). The utility in real-world application, however, has not yet been widely investigated. Herein, we report an increase of H3K27M copy numbers in CSF of a patient in complete radiological remission 3 months prior to detection of radiological progression. This underlines the opportunities for tumor DNA detection in CSF for future therapy guidance in H3K27M glioma patients. However, these methods need further validation in larger patient cohorts before they can be routinely applied for assessment of treatment response or recurrence.

Taken together, we show that personalized treatment approaches that address molecular heterogeneity of H3K27M glioma based on tumor biopsies are safe and feasible. Moreover, we demonstrate that clinical efficacy in selected cases is worth validating in future clinical trials with larger patient numbers.

DATA AVAILABILITY STATEMENT

The datasets generated for this study are available on request to the corresponding author.

ETHICS STATEMENT

This study was approved by the local ethics committee of the Medical University of Vienna and the Masaryk University Brno. Informed consent was obtained from every participating patient and/or legal representative.

AUTHOR CONTRIBUTIONS

JG, JSt, and IS designed the study, interpreted data, and wrote the manuscript. JG, ZP, DZ, LM, MK, KV, MS, TC, CD, AA, MC, DR, DL, AP, JSt, and IS acquired clinical data, were involved in molecular tumor board decisions, and managed patients. MTS and JSk performed radiological assessments. CH, DV, HN, KP, OS, MJ, RV, and SK performed histopathological evaluation and molecular analyses for comprehensive molecular profiling. SM performed liquid biopsy analyses.

FUNDING

This study was supported by projects No. 16-34083A and No. 16-33209A from the Ministry of Healthcare of the Czech Republic, by project No. LQ1605 from the National Program of Sustainability II (MEYS CR), by project No. LM15089 (MEYS BBMRI-CZ) and project No. MUNI/A/1586/2018 from Masaryk University, Brno, Czech Republic, and by project MH CZ—DRO (FNBr, 65269705). This study was further supported by the Fellinger Krebsforschung (to JG), the Jubiläumsfonds der Österreichischen Nationalbank (project # 15173 to IS), the "Verein unser_kind," and the Comprehensive Cancer Center Vienna (to SM).

ACKNOWLEDGMENTS

The authors thank all patients, their families, and clinical staff for their contributions.

SUPPLEMENTARY MATERIAL

The Supplementary Material for this article can be found online at: https://www.frontiersin.org/articles/10.3389/fonc.2019.01436/full#supplementary-material

Table S1 | Whole exome sequencing results.

REFERENCES

1. Ostrom QT, Gittleman H, Liao P, Rouse C, Chen Y, Dowling J, Wolinsky Y, Kruchko C, Barnholtz-Sloan J. CBTRUS Statistical Report: Primary Brain and Central Nervous System Tumors Diagnosed in the United States in 2005–2009. *Neuro Oncol*. (2015) 17 (Suppl. 4):iv1–62. doi: 10.1093/neuonc/nov189
2. Sturm D, Bender S, Jones DTW, Lichter P, Grill J, Becher O, et al. Paediatric and adult glioblastoma: Multiform (epi)genomic culprits emerge. *Nat Rev Cancer*. (2014) 14:92–107. doi: 10.1038/nrc3655
3. Schwartzentruber J, Korshunov A, Liu XY, Jones DTW, Pfaff E, Jacob K, et al. Driver mutations in histone H3.3 and chromatin remodelling genes in paediatric glioblastoma. *Nature*. (2012) 482:226–31. doi: 10.1038/nature10833
4. Wu G, Diaz AK, Paugh BS, Rankin SL, Ju B, Li Y, et al. The genomic landscape of diffuse intrinsic pontine glioma and pediatric non-brainstem high-grade glioma. *Nat Genet*. (2014) 46:444–50. doi: 10.1038/ng.2938
5. Khuong-Quang DA, Buczkowicz P, Rakopoulos P, Liu XY, Fontebasso AM, Bouffet E, et al. K27M mutation in histone H3.3 defines clinically and biologically distinct subgroups of pediatric diffuse intrinsic pontine gliomas. *Acta Neuropathol*. (2012) 124:439–47. doi: 10.1007/s00401-012-0998-0
6. Jansen MH, Van Zanten SEV, Aliaga ES, Heymans MW, Warmuth-Metz M, Hargrave D, et al. Survival prediction model of children with diffuse intrinsic pontine glioma based on clinical and radiological criteria. *Neuro Oncol*. (2015) 17:160–6. doi: 10.1093/neuonc/nou104
7. Hoffman LM, Van Zanten SEMV, Colditz N, Baugh J, Chaney B, Hoffmann M, et al. Clinical, radiologic, pathologic, and molecular characteristics of long-term survivors of Diffuse Intrinsic Pontine Glioma (DIPG): a collaborative report from the international and european society for pediatric oncology DIPG registries. *J Clin Oncol*. (2018) 36:1963–72. doi: 10.1200/JCO.2017.75.9308
8. Mackay A, Burford A, Carvalho D, Izquierdo E, Fazal-Salom J, Taylor KR, et al. Integrated molecular meta-analysis of 1,000 pediatric high-grade and diffuse intrinsic pontine glioma. *Cancer Cell*. (2017) 32:520–37.e5. doi: 10.1016/j.ccell.2017.08.017
9. Lu VM, Alvi MA, Mcdonald KL, Daniels DJ. Impact of the H3K27M mutation on survival in pediatric high-grade glioma: a systematic review and meta-analysis. (2019) 23:308–16. doi: 10.3171/2018.9.PEDS18419
10. Louis DN, Perry A, Reifenberger G, von Deimling A, Figarella-Branger D, Cavenee WK, et al. The 2016 world health organization classification of tumors of the central nervous system: a summary. *Acta Neuropathol*. (2016)803–20. doi: 10.1007/s00401-016-1545-1
11. Wagner S, Warmuth-Metz M, Emser A, Gnekow AK, Sträter R, Rutkowski S, et al. Treatment options in childhood pontine gliomas. *J Neurooncol*. (2006) 79:281–7. doi: 10.1007/s11060-006-9133-1
12. El-Khouly FE, Veldhuijzen van Zanten SEM, Santa-Maria Lopez V, Hendrikse NH, Kaspers GJL, Loizos G, et al. Diagnostics and treatment of diffuse intrinsic pontine glioma: where do we stand? *J Neurooncol*. (2019) 145:177–84. doi: 10.1007/s11060-019-03287-9
13. Massimino M, Biassoni V, Miceli R, Schiavello E, Warmuth-Metz M, Modena P, et al. Results of nimotuzumab and vinorelbine, radiation and re-irradiation for diffuse pontine glioma in childhood. *J Neurooncol*. (2014) 118:305–12. doi: 10.1007/s11060-014-1428-z
14. Cohen KJ, Heideman RL, Zhou T, Holmes EJ, Lavey RS, Bouffet E, Pollack IF. Temozolomide in the treatment of children with newly diagnosed diffuse intrinsic pontine gliomas: a report from the Children's Oncology Group. *Neuro Oncol*. (2011) 13:410–6. doi: 10.1093/neuonc/noq205
15. Gokce-Samar Z, Beuriat PA, Faure-Conter C, Carrie C, Chabaud S, Claude L, et al. Pre-radiation chemotherapy improves survival in pediatric diffuse intrinsic pontine gliomas. *Child Nerv Syst*. (2016) 32:1415–23. doi: 10.1007/s00381-016-3153-8
16. Buczkowicz P, Hoeman C, Rakopoulos P, Pajovic S, Letourneau L, Dzamba M, et al. Genomic analysis of diffuse intrinsic pontine gliomas identifies three molecular subgroups and recurrent activating ACVR1 mutations. *Nat Genet*. (2014) 46:451–6. doi: 10.1038/ng.2936
17. Jones C, Baker SJ. Unique genetic and epigenetic mechanisms driving paediatric diffuse high-grade glioma. *Nat Rev Cancer*. (2014) 14:651–61. doi: 10.1038/nrc3811
18. Ryall S, Krishnatry R, Arnoldo A, Buczkowicz P, Mistry M, Siddaway R, et al. Targeted detection of genetic alterations reveal the prognostic impact of H3K27M and MAPK pathway aberrations in paediatric thalamic glioma. *Acta Neuropathol Commun*. (2016) 4:93. doi: 10.1186/s40478-016-0353-0
19. Filbin MG, Tirosh I, Hovestadt V, Shaw ML, Escalante LE, Mathewson ND, et al. Developmental and oncogenic programs in H3K27M gliomas dissected by single-cell RNA-seq. *Science*. (2018) 360:331–5. doi: 10.1126/science.aao4750
20. Hoffman LM, DeWire M, Ryall S, Buczkowicz P, Leach J, Miles L, et al. Spatial genomic heterogeneity in diffuse intrinsic pontine and midline high-grade glioma: implications for diagnostic biopsy and targeted therapeutics. *Acta Neuropathol Commun*. (2016) 4:1. doi: 10.1186/s40478-015-0269-0
21. Ochs K, Ott M, Bunse T, Sahm F, Bunse L, Deumelandt K, et al. K27M-mutant histone-3 as a novel target for glioma immunotherapy. *Oncoimmunology*. (2017) 6:1–7. doi: 10.1080/2162402X.2017.1328340
22. Geoerger B, Hargrave D, Thomas F, Ndiaye A, Frappaz D, Andreiuolo F, et al. Innovative Therapies for Children with Cancer pediatric phase I study of erlotinib in brainstem glioma and relapsing/refractory brain tumors. *Neuro Oncol*. (2011) 13:109–18. doi: 10.1093/neuonc/noq141

23. Pollack IF, Stewart CF, Kocak M, Poussaint TY, Broniscer A, Banerjee A, et al. A phase II study of gefitinib and irradiation in children with newly diagnosed brainstem gliomas: a report from the pediatric brain tumor consortium. *Neuro Oncol*. (2011) 13:290–7. doi: 10.1093/neuonc/noq199
24. Bartels U, Wolff J, Gore L, Dunkel I, Gilheeney S, Allen J, et al. Phase 2 study of safety and efficacy of nimotuzumab in pediatric Patients with progressive diffuse intrinsic pontine glioma. *Neuro Oncol*. (2014) 16:1554–9. doi: 10.1093/neuonc/nou091
25. Broniscer A, Jia S, Mandrell B, Hamideh D, Huang J, Onar-Thomas A, et al. Phase 1 trial, pharmacokinetics, and pharmacodynamics of dasatinib combined with crizotinib in children with recurrent or progressive high-grade and diffuse intrinsic pontine glioma. *Pediatr Blood Cancer*. (2018) 65:1–8. doi: 10.1002/pbc.27035
26. Gajjar A, Pfister SM, Taylor MD, Gilbertson RJ. Molecular insights into pediatric brain tumors have the potential to transform therapy. *Clin Cancer Res*. (2014) 20:5630–40. doi: 10.1158/1078-0432.CCR-14-0833
27. Miklja Z, Pasternak A, Stallard S, Nicolaides T, Kline-Nunnally C, Cole B, et al. Molecular profiling and targeted therapy in pediatric gliomas: review and consensus recommendations. *Neuro Oncol*. (2019) 21:noz022. doi: 10.1093/neuonc/noz022
28. Gröbner SN, Worst BC, Weischenfeldt J, Buchhalter I, Kleinheinz K, Rudneva VA, et al. The landscape of genomic alterations across childhood cancers. *Nature*. (2018) 555:321–7. doi: 10.1038/nature25480
29. Pfaff E, El Damaty A, Balasubramanian GP, Blattner-Johnson M, Worst BC, Stark S, et al. Brainstem biopsy in pediatric diffuse intrinsic pontine glioma in the era of precision medicine: the INFORM study experience. *Eur J Cancer*. (2019) 114:27–35. doi: 10.1016/j.ejca.2019.03.019
30. Mueller S, Jain P, Liang WS, Kilburn L, Kline C, Gupta N, et al. A pilot precision medicine trial for children with diffuse intrinsic pontine glioma—PNOC003: a report from the pacific pediatric neuro-oncology consortium. *Int J Cancer*. (2019) 145:1889–901. doi: 10.1002/ijc.32258
31. Bhutani J, Sheikh A, Niazi AK. Akt inhibitors: mechanism of action and implications for anticancer therapeutics. *Infect Agent Cancer*. (2013) 8:12–5. doi: 10.1186/1750-9378-8-49
32. Romano G, Chen PL, Song P, McQuade JL, Liang RJ, Liu M, et al. A preexisting rare PIK3CA e545k subpopulation confers clinical resistance to MEK plus CDK4/6 inhibition in NRAS melanoma and is dependent on S6K1 signaling. *Cancer Discov*. (2018) 8:556–67. doi: 10.1158/2159-8290.CD-17-0745
33. Han HJ, Jain P, Resnick AC. Shared ACVR1 mutations in FOP and DIPG: opportunities and challenges in extending biological and clinical implications across rare diseases. *Bone*. (2017) 109:91–100. doi: 10.1016/j.bone.2017.08.001
34. Bouffet E, Larouche V, Campbell BB, Merico D, De Borja R, Aronson M, et al. Immune checkpoint inhibition for hypermutant glioblastoma multiforme resulting from germline biallelic mismatch repair deficiency. *J Clin Oncol*. (2016) 34:2206–11. doi: 10.1200/JCO.2016.66.6552
35. Wishart DS, Feunang YD, Guo AC, Lo EJ, Marcu A, Grant JR, et al. DrugBank 5.0: a major update to the DrugBank database for 2018. *Nucleic Acids Res*. (2018) 46:D1074–82. doi: 10.1093/nar/gkx1037
36. Bangi E, Ang C, Smibert P, Uzilov AV, Teague AG, Antipin Y, et al. A personalized platform identifies trametinib plus zoledronate for a patient with KRAS-mutant metastatic colorectal cancer. *Sci Adv*. (2019) 5:1–12. doi: 10.1126/sciadv.aav6528
37. Burger MC, Ronellenfitsch MW, Lorenz NI, Wagner M, Voss M, Capper D, et al. Dabrafenib in patients with recurrent, BRAF V600E mutated malignant glioma and leptomeningeal disease. *Oncol Rep*. (2017) 38:3291–6. doi: 10.1093/neuonc/nox168.877
38. Grossauer S, Koeck K, Murphy NE, Meyers ID, Daynac M, Truffaux N, et al. Concurrent MEK targeted therapy prevents MAPK pathway reactivation during BRAFV600E targeted inhibition in a novel syngeneic murine glioma model. *Oncotarget*. (2016) 7:75839–53. doi: 10.18632/oncotarget.12419
39. Chamberlain MC. Salvage therapy with BRAF inhibitors for recurrent pleomorphic xanthoastrocytoma: a retrospective case series. *J Neurooncol*. (2013) 114:237–40. doi: 10.1007/s11060-013-1176-5
40. Cappellano AM, Senerchia AA, Adolfo F, Paiva PM, Pinho R, Covic A, et al. Successful everolimus therapy for SEGA in pediatric patients with tuberous sclerosis complex. *Child Nerv Syst*. (2013) 29:2301–5. doi: 10.1007/s00381-013-2170-0
41. Salomon G, Maza A, Boulinguez S, Paul C, Lamant L, Tournier E, et al. Efficacy of anti-programmed cell death-1 immunotherapy for skin carcinomas and melanoma metastases in a patient with xeroderma pigmentosum. *Br J Dermatol*. (2018) 178:1199–203. doi: 10.1111/bjd.16270
42. Worst BC, van Tilburg CM, Balasubramanian GP, Fiesel P, Witt R, Freitag A, et al. Next-generation personalised medicine for high-risk paediatric cancer patients – The INFORM pilot study. *Eur J Cancer*. (2016) 65:91–101. doi: 10.1016/j.ejca.2016.06.009
43. Jaspan XT, Morgan XPS, Warmuth-Metz XM, Sanchez Aliaga XE, Warren XD, Calmon XR, et al. Response assessment in pediatric neuro-oncology: implementation and expansion of the RANO criteria in a randomized phase II trial of pediatric patients with newly diagnosed high-grade gliomas ABBREVIATIONS: HERBY a study of avastin (bevacizumab) in combin. (2016) 37:1581–7. doi: 10.3174/ajnr.A4782
44. Mistry M, Zhukova N, Merico D, Rakopoulos P, Krishnatry R, Shago M, et al. BRAF mutation and CDKN2A deletion define a clinically distinct subgroup of childhood secondary high-grade glioma. *J Clin Oncol*. (2015) 33:1015–22. doi: 10.1200/JCO.2014.58.3922
45. Nakano Y, Yamasaki K, Sakamoto H, Matsusaka Y, Kunihiro N, Fukushima H, et al. A long-term survivor of pediatric midline glioma with H3F3A K27M and BRAF V600E double mutations. *Brain Tumor Pathol*. (2019) 36:162–8. doi: 10.1007/s10014-019-00347-w
46. Taylor KR, Mackay A, Truffaux N, Butterfield YS, Morozova O, Philippe C, et al. Recurrent activating ACVR1 mutations in diffuse intrinsic pontine glioma. *Nat Genet*. (2014) 46:457–61. doi: 10.1038/ng.2925
47. Englinger B, Pirker C, Heffeter P, Terenzi A, Kowol CR, Keppler BK, et al. Metal drugs and the anticancer immune response. *Chem Rev*. (2019) 119, 1519–624. doi: 10.1021/acs.chemrev.8b00396
48. Cloughesy TF, Mochizuki AY, Orpilla JR, Hugo W, Lee AH, et al. Neoadjuvant anti-PD-1 immunotherapy promotes a survival benefit with intratumoral and systemic immune responses in recurrent glioblastoma. *Nat Med*. (2019) 25:477–86. doi: 10.1038/s41591-018-0337-7
49. Iwamoto FM, Lamborn KR, Robins HI, Mehta MP, Chang SM, Butowski NA, et al. Phase II trial of pazopanib (GW786034), an oral multi-targeted angiogenesis inhibitor, for adults with recurrent glioblastoma (North American Brain Tumor Consortium Study 06-02). *Neuro Oncol*. (2010) 12:855–61. doi: 10.1093/neuonc/noq025
50. Hall MD, Odia Y, Allen JE, Tarapore R, Khatib Z, Niazi TN, et al. First clinical experience with DRD2/3 antagonist ONC201 in H3 K27M–mutant pediatric diffuse intrinsic pontine glioma: a case report. *J Neurosurg Pediatr*. (2019) 23:1–7. doi: 10.3171/2019.2.PEDS18480
51. Ishizawa J, Zarabi SF, Davis RE, Halgas O, Nii T, Jitkova Y, et al. Mitochondrial ClpP-mediated proteolysis induces selective cancer cell lethality. *Cancer Cell*. (2019) 35:721–37.e9. doi: 10.1016/j.ccell.2019.03.014
52. Stallard S, Savelieff MG, Wierzbicki K, Mullan B, Miklja Z, Bruzek A, et al. CSF H3F3A K27M circulating tumor DNA copy number quantifies tumor growth and *in vitro* treatment response. *Acta Neuropathol Commun*. (2018) 6:7–10. doi: 10.1186/s40478-018-0580-7

Conflict of Interest: The authors declare that the research was conducted in the absence of any commercial or financial relationships that could be construed as a potential conflict of interest.

frontiers in Oncology

ORIGINAL RESEARCH
published: 07 February 2020
doi: 10.3389/fonc.2019.01531

Comprehensive Molecular Profiling for Relapsed/Refractory Pediatric Burkitt Lymphomas—Retrospective Analysis of Three Real-Life Clinical Cases—Addressing Issues on Randomization and Customization at the Bedside

Kristyna Polaskova[1,2], Tomas Merta[1,2], Alexandra Martincekova[1,2], Danica Zapletalova[1,2], Michal Kyr[1,2], Pavel Mazanek[1], Zdenka Krenova[1], Peter Mudry[1], Marta Jezova[3], Jiri Tuma[4], Jarmila Skotakova[5], Ivana Cervinkova[5], Dalibor Valik[6,7], Lenka Zdrazilova-Dubska[6,7], Hana Noskova[8], Karol Pal[8], Ondrej Slaby[8], Pavel Fabian[9], Sarka Kozakova[2,7], Jakub Neradil[2,10], Renata Veselska[2,10], Veronika Kanderova[11], Ondrej Hrusak[11], Tomas Freiberger[8,12,13], Giannoula Lakka Klement[1,14] and Jaroslav Sterba[1,2,7]*

[1] Department of Pediatric Oncology, University Hospital Brno and Faculty of Medicine, Masaryk University, Brno, Czechia, [2] International Clinical Research Center, St. Anne's University Hospital, Brno, Czechia, [3] Department of Pathology, University Hospital Brno and Faculty of Medicine, Masaryk University, Brno, Czechia, [4] Department of Pediatric Surgery, Orthopedics and Traumatology, University Hospital Brno and Faculty of Medicine, Masaryk University, Brno, Czechia, [5] Department of Pediatric Radiology, University Hospital Brno and Faculty of Medicine, Masaryk University, Brno, Czechia, [6] Department of Pharmacology, Faculty of Medicine, Masaryk University, Brno, Czechia, [7] Regional Centre for Applied Molecular Oncology, Masaryk Memorial Cancer Institute, Brno, Czechia, [8] Central European Institute of Technology, Masaryk University, Brno, Czechia, [9] Department of Oncological Pathology, Masaryk Memorial Cancer Institute, Brno, Czechia, [10] Laboratory of Tumor Biology, Department of Experimental Biology, Faculty of Science, Masaryk University, Brno, Czechia, [11] Childhood Leukaemia Investigation Prague, Department of Paediatric Haematology and Oncology, 2nd Faculty of Medicine, Charles University, Prague, Czechia, [12] Faculty of Medicine, Masaryk University, Brno, Czechia, [13] Centre for Cardiovascular Surgery and Transplantation, Brno, Czechia, [14] CSTS Health Care, Toronto, ON, Canada

In order to identify reasons for treatment failures when using targeted therapies, we have analyzed the comprehensive molecular profiles of three relapsed, poor-prognosis Burkitt lymphoma cases. All three cases had resembling clinical presentation and histology and all three patients relapsed, but their outcomes differed significantly. The samples of their tumor tissue were analyzed using whole-exome sequencing, gene expression profiling, phosphoproteomic assays, and single-cell phosphoflow cytometry. These results explain different treatment responses of the three histologically identical but molecularly different tumors. Our findings support a personalized approach for patient with high risk, refractory, and rare diseases and may contribute to personalized and customized treatment efforts for patients with limited treatment options like relapsed/refractory Burkitt lymphoma.

SUMMARY

The main aim of this study is to analyze three relapsed Burkitt lymphoma patients using a comprehensive molecular profiling, in order to explain their different outcomes

OPEN ACCESS

Edited by:
George Calin,
University of Texas MD Anderson Cancer Center, United States

Reviewed by:
Ioana Berindan Neagoe,
Iuliu Haţieganu University of Medicine and Pharmacy, Romania
Barbara Pasculli,
Casa Sollievo della Sofferenza (IRCCS), Italy

***Correspondence:**
Kristyna Polaskova
polaskova.kristyna@fnbrno.cz

Specialty section:
This article was submitted to Cancer Molecular Targets and Therapeutics, a section of the journal Frontiers in Oncology

Received: 18 July 2019
Accepted: 19 December 2019
Published: 07 February 2020

Citation:
Polaskova K, Merta T, Martincekova A, Zapletalova D, Kyr M, Mazanek P, Krenova Z, Mudry P, Jezova M, Tuma J, Skotakova J, Cervinkova I, Valik D, Zdrazilova-Dubska L, Noskova H, Pal K, Slaby O, Fabian P, Kozakova S, Neradil J, Veselska R, Kanderova V, Hrusak O, Freiberger T, Klement GL and Sterba J (2020) Comprehensive Molecular Profiling for Relapsed/Refractory Pediatric Burkitt Lymphomas—Retrospective Analysis of Three Real-Life Clinical Cases—Addressing Issues on Randomization and Customization at the Bedside. Front. Oncol. 9:1531. doi: 10.3389/fonc.2019.01531

and to propose a biomarker-based targeted treatment. In cases 1 and 3, the tumor tissue and the host were analyzed prospectively and appropriate target for the treatment was successfully implemented; however, in case 2, analyses become available only retrospectively and his empirically based rescue treatment did not hit the right target of his disease.

Keywords: Burkitt lymphoma, targeted therapy, precision medicine, theranostics, pediatric oncology

INTRODUCTION

Burkitt lymphoma is a highly aggressive mature B-cell lymphoma commonly associated with translocation of *MYC* gene. The disease is classified as sporadic, endemic, or immunodeficiency related. In pediatric oncology, current standard intensive chemotherapy with anti-CD20 antibody regimens achieve long-term, disease-free survival in almost 95% of patients (1). However, a subset of patients who do not respond to the first-line chemotherapy and who experience relapse have very poor prognosis despite high-dose chemotherapy followed by stem cell transplantation (2). This subset of patients, for whom further chemotherapy-based therapies are futile, is recently often considered for therapies based on molecular analysis of their tumor tissue. We present three cases of relapsed Burkitt lymphoma. Cases 1 and 3 were treated with a therapy that reflected the molecular signature of the child's tumor, but in case 2, the therapy "missed" the target because his molecular signature was not known at the time retrieval therapy was initiated. The findings suggest that molecular signatures are unique, and a tissue biomarker-based customized therapy may be the better approach to address these poor prognosis patients than just another biomarker agnostic randomized trial.

METHODS

A comprehensive molecular profiling consisted of whole-exome, gene expression profiling and a profile of phosphorylated proteins and single-cell phosphoflow cytometry of three cases of relapsed pediatric Burkitt lymphoma searching for biological rationale for different responses to the therapy and different clinical outcomes.

Whole-Exome Sequencing

Whole-exome sequencing (WES) using the TruSeq DNA Exome Kit, the NextSeq 500/550 Mid Output Kit v2.5, and a NextSeq 500 sequencing device (all Illumina, CA, USA) was done in all three cases. Input material was 400 ng of DNA obtained from the peripheral blood (for germline exome) and formalin-fixed, paraffin-embedded (FFPE) tumor sample with $\geq$20% cancer cell count measured in the surface area of tissue slides for somatic exome. WES was done with high coverage where at least 90% of targeted regions were covered 20 times.

Gene Expression Profiling (Transcriptome Examination)

Gene expression profiling using the Affymetrix GeneChip Human Gene 1.0. ST Array (Applied Biosystems, CA, USA) was done in all three cases. Input material was 250 ng of RNA obtained from frozen tumor tissue. Samples were prepared using the GeneChip WT PLUS Reagent Kit (Affymetrix, CA, USA) according to the manufacturer's protocol. Subsequently, chips were hybridized using the GeneChip Hybridization Oven, washed using the GeneChip Fluidics Station, and scanned on the GeneChip Scanner (all Affymetrix, CA, USA), and CEL files were generated. Data were processed using R software version 3.3.3 (3). Gene expressions of 220 selected genes were subsequently compared to accumulated normal tissue samples as described previously (4), utilizing two comparator sets: one consisting of 408 normal tissue samples of different diagnoses (main general comparator) and one consisting of 5 samples of normal germinal center B cells (complementary-specific comparator). Samples were downloaded from Gene Expression Omnibus and ArrayExpress databases, and names of the database samples are listed in **Supplementary Material 1**. Expression data were calculated as Robust Multichip Average (RMA) with background correction and quantile normalization implemented in rma function in oligo package (5). Difference of expression of each gene was calculated as fold change (FC) from the mean of the comparator set and tested using a two-sided one-sample *t*-test, with false discovery rate (FDR) adjustment applied. An FC value of 0.5 and more was considered important. No specific *p*-value was considered limiting the discrimination of differently expressed genes with FC $>$ 0.5. Utilizing the general comparator consisting of 408 samples offers highly significant results corresponding to the power of 10 to -25 for the FDR-adjusted *p*-values for most of the evaluated genes with FC of 0.5 or more, and rising to the power of 10 to -100 for the FDR-adjusted *p*-values for genes with FC $>$ 2.

RNA transcription data from the tumor tissues were analyzed as well using Biogrid (http://thebiogrid.org), and http://www.genome.jp/kegg/pathway.html and mathematical simulations of protein–protein interactions as described before (6).

Profile of Phosphorylated Proteins

Human Phospho-RTK Array Kit (R&D Systems) was used to determine the relative levels of tyrosine phosphorylation of 49 different RTKs. Human Phospho-MAPK Array Kit (R&D Systems) was employed for the detection of phosphorylation status of 26 MAPKs, serine/threonine kinases, and other signaling proteins. Both arrays were performed as previously described (7).

Single-Cell Phosphoflow Cytometry

Peripheral blood mononuclear cells (PBMCs) were separated on Ficoll-Paque (GE Healthcare) according to the manufacturer's

instructions. PBMCs were reconstituted in a culture medium consisting of RPMI 1640 with 25 mM HEPES, L-glutamine, 100 U/ml penicillin, and 100 mg/ml streptomycin (Lonza, Basel, Switzerland) to a final concentration of 2 million cells per milliliter. After a 1-h rest at 37°C in a 5% CO_2 atmosphere, the cells were stimulated on 96-well plate containing coated anti-CD3 (10 μg/ml, Exbio Praha) and free costimulatory anti-CD28/CD49d antibodies (1 μg/ml, BD Biosciences) for 5, 15, and 30 min. The cells were fixed with 4% formaldehyde for 10 min and permeabilized with ice-cold methanol for 30 min. The following fluorochrome conjugates were used for cytometric detection: phospho-Akt (Ser473)-Alexa Fluor 488, phospho-S6 (Ser235/236)-Pacific Blue (Cell Signaling Technologies), phospho-mTOR (Ser2448)-PE (eBioscience, Thermo Fisher), CD45-Pacific Orange, CD45RA-APC (Exbio), CD8-PE-Cy7 (Beckman Coulter), CD4-PerCP-Cy5.5, and CD3-APC-H7 (BD Biosciences). The samples were acquired on Canto II flow cytometer and analyzed using FlowJo software (BD Biosciences).

RESULTS

Case 1

A 7-year-old previously healthy boy presented with $t_{(8;14)}$ positive abdominal stage III Burkitt lymphoma (St. Jude staging system). The boy was initially treated as per the standard BFM B-NHL Registry 2012 protocol with the addition of rituximab according to the most recent published literature (1). He responded well to the therapy and achieved a very good partial response after two cycles. His clinical course was complicated by an episode of duodenal obstruction/intussusception requiring surgical intervention. The histology from this resection revealed sclerosing mesenteritis with no evidence of lymphoma, congruent with the conclusion of a study using ^{18}F-fluorodeoxyglucose positron emission tomography/computed tomography (FDG PET/CT) that revealed a very small residual tumor with only borderline FDG PET avidity. Unfortunately, the patient had disease progression 6 weeks following the completion of protocol therapy (and 3 months from the second surgery) with a new lesion within the tumor resection margin and a new mediastinal mass. A biopsy of the abdominal lesion confirmed the recurrence of Burkitt lymphoma with persistent areas of sclerosing mesenteritis.

As sclerosing mesenteritis has been associated in the literature not only with B-cell lymphomas but also with activation of the PI3K-delta pathway and immunodeficiency (8, 9), a candidate testing for this specific mutation was performed.

In the tumor, there was proven disruption of MYCC and IgH in 97% of cells according to fluorescence *in situ* hybridization (FISH). Karyotype of the tumor showed 46 chromosomes with complex changes. A germline variant of c.935C>G (p.S312C) in the PI3K-delta subunit was found both in the child and in the father. The patient's older sister and mother were negative for this variant. We tested the intracellular signaling downstream of PI3K using flow cytometry assessment of phosphorylation of Akt, mTOR, and S6 proteins in the patient's peripheral blood T-lymphocytes and detected increased basal and T-cell receptor (TCR)-induced activation (**Figure 1A**). Similarly, increased levels of PI3K were confirmed by RNA transcriptome analysis of the tumor tissue with Affymetrix GeneChipST 1.0. This analysis also revealed an increased expression of HR23B, a predictor of response to histone deacetylase (HDAC) inhibitors. Immunohistochemistry revealed a strong expression of PD-1L. The variant p.S312C has been described previously as mutation in brain cancer cell line and prostate cancer cell line (10) but has been classified as benign for development of immunodeficiency according to the ClinVar database. The allele frequency ranges between 0.008 and 0.030 in population databases (gnomAD 0.02, ExAc 0.0217, 1000G/ALL 0.008, 1000G/EUR 0.029) and was found to be 0.018 in our cohort of 508 cord blood samples (not published). Thus, this variant cannot be considered pathogenic. However, it may predispose the PI3K pathway to be activated, if other genetic and/or non-genetic factors are present.

Interestingly, even though the biopsy at the time of initial diagnosis had been tested for *TP53* and no alteration of the gene was found, in the biopsy obtained from the relapse, a new *TP53* R273C somatic mutation was identified in the tumor.

Retrieval therapy was administered with obinutuzumab 550 mg/m^2, ibrutinib 140 mg/m^2, and two cycles of ifosfamide, carboplatin, and etoposide (ICE) chemotherapy. The patient had further progression on this therapy, and a more molecular biomarker-driven theranostic approach was discussed. The therapy was changed to a single-agent window using a specific inhibitor of PI3K idelalisib 200 mg/m^2/d. In 2 weeks, we were able to document a markedly decreased PI3K pathway activation in the patient's peripheral blood T-lymphocytes (**Figure 1B**), but the disease was still showing further radiological progression. Therapy with idelalisib was not discontinued, and ibrutinib 140 mg/m^2 daily was reintroduced. Based on the transcriptome analysis, valproic acid for HDAC inhibition aiming for serum levels of 80–100 μg/ml was added, and nivolumab at 3 mg/kg every second week and metronomic cyclophosphamide at 25 mg/m^2/7 days on/7 days off were introduced for immune modulation. To support local disease management and support the tumor antigen presentation, the patient received 21-Gy radiation to the site of the abdominal relapse. There was evidence of partial remission on FDG PET/CT 3 months later and stable disease 6 months later. Due to persistence of a viable tumor on FDG PET/CT and high toxicity of allogenic stem cell transplant reported in nivolumab-treated patients (11), this approach was not considered as treatment of choice. Consequently, personalized immunotherapy with dendritic cell-based vaccine was preferred to support the antitumor immunity, and treatment with dendritic cells loaded with whole tumor lysate according to phase I/II protocol (EudraCT No. 2014-003388-39) (12) was initiated. The residual tumor resected after 11 months of such therapy consisted of mainly necrotic tissue with lymphocytic infiltration with no evidence of viable tumor. Considering that the child had achieved complete remission, valproic acid, ibrutinib, and idelalisib were gradually discontinued and the patient is continuing to take biweekly intradermal applications of autologous dendritic cell vaccine and nivolumab until May 2018 when all his 37 manufactured doses of dendritic cell-based vaccine were used up.

The progression-free survival (PFS) of 46 months following a customized, tumor tissue molecular analysis-guided regimen was

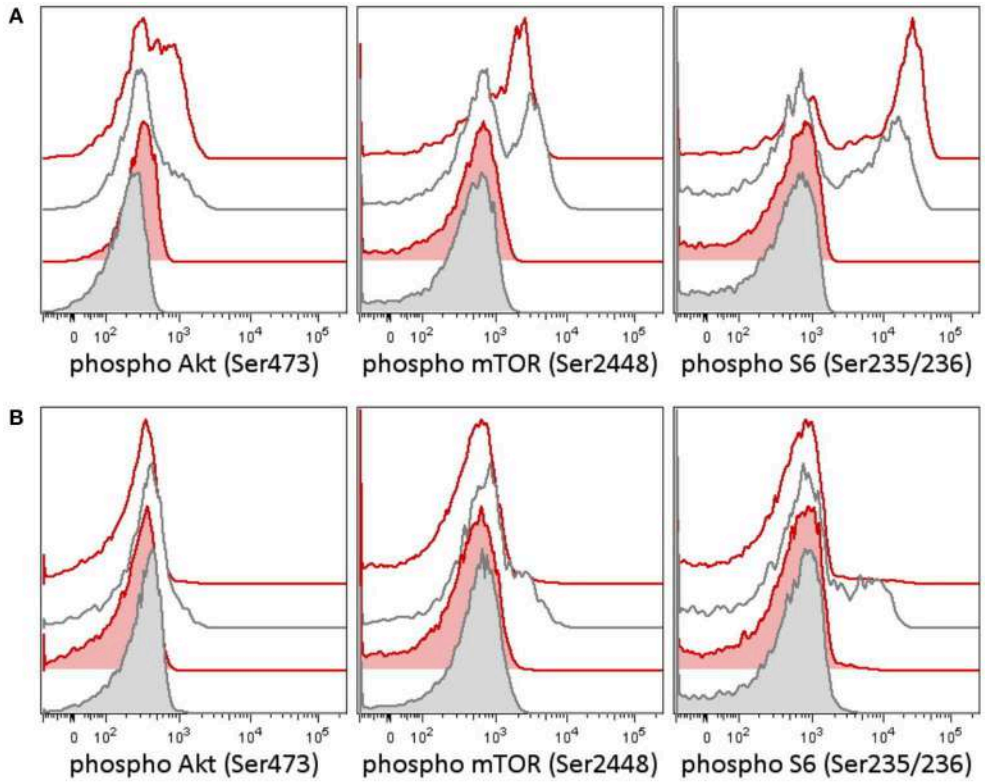

FIGURE 1 | Phosphorylation patterns in the PI3K pathway in peripheral blood T-lymphocytes before **(A)** and after **(B)** therapy in case 1. Case 2 patient had a germline variant of PIK3CD, which was present in the tumor as well. Peripheral blood T-lymphocytes (patient 1's lymphocytes contained only T cells at the time of testing) were tested for activation of the PI3K signaling pathway [reflected as a phosphorylation of Akt (Ser473), mTOR (Ser2448), and S6 ribosomal protein (Ser235/236)] before and following therapy. **(A)** Patient T-lymphocytes showed increased basal phosphorylation of Akt as well as increased phosphorylation of Akt and S6 upon T-cell receptor (TCR) stimulation before treatment compared to an independent healthy control (the result is representative of three independent tests). **(B)** A week following the addition of idelalisib (a PI3K inhibitor), to the patient's therapy, the phosphorylation of Akt, mTOR, and S6 dropped down. CD3+ T-lymphocytes are shown in basal state (tinted histograms) and 15 min upon anti-CD3/CD28/CD49d stimulation (blank histograms). Red, patient 1; black, healthy control.

the longest PFS this child had achieved. The comparison of his earlier therapies reveals that he had achieved PFS1 6 months on the initial standard BFM protocol, and PFS2 only 1 month on the intensive retrieval therapy using anti-CD20 (obinutuzumab), ICE, and ibrutinib. His individualized therapy was outpatient based, associated with minimal treatment-related toxicities and allowed the child to return to school and perform all activities of daily living.

Case 2

A 3-year-old boy diagnosed abroad with widely disseminated Burkitt lymphoma (abdomen, bone marrow, and both kidneys) was initially treated with the same standard BFM-based chemotherapy, but without rituximab. Before the completion of the fifth cycle, the patient had disease progression with a biopsy-positive new lesion in the right cheek. He continued with a relapse ALL protocol/ALL-REZ BFM 2002 in his home country outside the Czech Republic. As no therapeutic response was achieved, he was referred to our institution for a second opinion and management. He received two cycles of R-ICE (rituximab, ifosfamide, carboplatin, etoposide) given as per the ANHL0121 protocol achieving partial response, but the treatment was accompanied with severe life-threatening toxicities. He underwent surgery to obtain specimen for theranostic testing; however, the amount of the tumor tissue was not sufficient for all molecular studies. Based on our previous success in case 1 and as bridging to high-dose chemotherapy, he therefore continued with ibrutinib 140 mg/m^2 daily, idelalisib 100 mg/m^2 daily, and cyclophosphamide 1.5 mg/kg daily week on/week off for 6 weeks. Due to toxicities of intensive therapies and a clinical need for further therapy as bridging to stem cell transplant, the targeted agents were in this case based on our previous experience and a literature review. Despite a high-dose carmustine, etoposide, cytarabine, melphalan (BEAM) chemotherapy as per the AHOD0121 protocol (13) and autologous stem cell transplant being performed, he continued to do poorly. The patient had disease progression 3 weeks after BEAM conditioning and autologous stem cell transplant with a new lesion in the abdomen and continued to progress with massive L3 blast presence in the cerebrospinal fluid. He died due to disease progression 11 months from the initial diagnosis and 6 months after his first progression.

Case 3

A 12-year-old boy was diagnosed with bulky abdominal Burkitt lymphoma. The patient was initially treated as per the standard BFM B-NHL Registry 2012 protocol with the addition of rituximab, but he achieved only partial response after two cycles, and assessment after four cycles revealed residual tumor with still increased FDG PET avidity. Three months later, the FDG PET/CT showed radiological progression of the primary tumor and dissemination in the right retromandibular area and anterior mediastinum. The relapse of Burkitt lymphoma was confirmed by biopsy. However, WES from the relapsed tumor sample revealed high tumor mutation burden−31 mutations/Mb; moreover, gene expression profiling detected strong expression of PD1, and the overall expression patterns of the case 3 were very similar to case 2 patient with very high fibronectin expression. First, participation in the randomized ibrutinib retrieval trial was planned here; however, based on molecular profiling and our previous experience from case 2, we have prioritized immune therapy here. He achieved radiological partial remission after third R-ICE cycle and then continued with nivolumab single agent only. After 12 weeks of nivolumab, he achieved first complete remission. His first PFS on standard intensive protocol was 7 months, but the second PFS with using immunotherapy is 14 months.

Analyses

Somatic exome analysis of relapse samples revealed variants in the *TP53* gene in cases 1 and 2 (p.R273C in case 1 and p.R248L in case 2, NM_000546). p.R273C and p.R248L in *TP53* have been previously described as loss of function mutations based on *in vitro* functional analyses (14–19). Somatic exome analysis in case 1 detected a number of variants; the selected ones are shown in **Supplementary Material 2**. Germline exome analysis in case 1 also confirmed p.S312C (NM_005026) variant in the *PIK3CD* gene in the heterozygous form. Somatic exomes of cases 2 and 3 revealed a number of variants; the selected ones are also available in **Supplementary Material 2**.

Gene expression profiles of all three cases proved to be very similar; the highest expressions showed genes involved in immune system (*BTK*, *CD79A*, *CD79B*, and *KLHL6*). In cases 1 and 2, increased expression also showed genes involved in DNA damage response (*BRCA1*, *BRCA2*, *FANCA*, and *FANCD2*). In case 1, *CSF1R* and *PDGFRA* genes were also found to be increasingly expressed, while no genes coding tyrosine kinases showed to be overexpressed in case 2. In case 3, increased expressions showed genes involved in fibroblast growth factor signaling. In comparison to other pediatric oncology patients analyzed at our institute, transcriptome analysis in cases 1 and 2 revealed significantly increased expression of the *MYC* proto-oncogene.

In case 1, two samples of the tumor tissue were also analyzed for activity of cell signaling pathways using phosphoprotein arrays for detection of RTKs, MAPKs, serine/threonine kinases, and other signaling protein as specified above: tumor tissue sample after the first line of treatment (**Figure 2**: case 1a) and second sample taken during the treatment of relapsed disease (**Figure 2**: case 1b). Phosphorylation profiles showed high relative activities of EGFR, PDGFRβ, ROR2, CREB, ERK1/2, and HSP27 in both samples. Furthermore, a very high level of phosphorylation was detected for p53 protein on Ser46 in the second sample in comparison to the first sample from this patient. This finding is in full accordance with the previous proapoptotic treatment including etoposide administration (20). In case 2, nevertheless, phospho-RTK analysis (**Figure 2**: case 2) revealed high phosphorylation of EGFR and PDGFRβ, and the phosphorylation profile of MAPKs, serine/threonine kinases, and other signaling proteins showed high activities of CREB, ERK1/2, and HSP27 in ascending order of density value.

Serology of Epstein–Barr virus (EBV) revealed the IgG positivity of EBV nuclear antigen (EBNA)-1 and the IgG positivity of viral capsid antigen (VCA) as well case 1 and case 2.

DISCUSSION

The introduction of highly intensive multiagent chemotherapy has dramatically improved the survival rates of primary childhood Burkitt lymphoma. While the initial treatment can have an over 90% success rate using standard intensive chemotherapy with rituximab, the outcome of children with relapsed Burkitt lymphoma is still very poor. The difficulties with treating chemotherapy-resistant relapsed tumors suggest an evolution of a more complex and more resistant disease (21), as could be documented by a new TP53 mutation in our case 1 at relapse, which was suggested by phosphoproteomic assay as well. The overview of our three cases reveals children with some very similar characteristics of their diseases, with alike pattern of cell signaling in tumor tissue, treated with identical agents in the first part of their relapse treatment, who experienced very dissimilar outcomes after the first relapse. It suggests that the tumors with similar histological features may harbor chemotherapy-resistant, genetically and biologically distinct subclones that become more dominant after intensive chemotherapy (21). At presentation, a fraction of these chemotherapy-resistant subpopulations may be small but, following intensive maximum tolerated dose-based chemotherapy, probably increases, and the tumor residuum is subsequently populated by resistant subclones. This evolution was furthermore evident on the evolution of molecular findings in the first patient and supports the need for a careful theranostic analysis and repeated biopsies whenever clinically indicated. Treatment of relapsed disease should be based on a detailed molecular analysis of the most recent available sample, i.e., at the time of relapse or progression rather than on original tumor biopsy only. The choice of drug combinations reflecting a broader molecular profile was based on reports that customized combinatorial therapies may produce more sustained responses (22, 23). Furthermore, as many biological agents are in fact chemotherapy sensitizers, their proper dosage should carefully be titrated to avoid severe systemic toxicity. In case 1, we have started with a single-agent idelalisib to target what was thought to be the driver mutation and gradually added additional targeted agents but at doses about 50% of those recommended in the Summary of Product Characteristics to avoid severe toxicity.

FIGURE 2 | The relative phosphorylation analysis of tumor tissue samples. Human Phospho-MAPK Array Kit (R&D Systems) was employed for the detection of phosphorylation status of 49 RTKs, 26 MAPKs, serin/threonin kinases, and other signaling proteins, which performed using phosphoprotein arrays.

To successfully apply precision oncology principles into clinical practice, a requisite testing for molecular targets for each patient needs to be completed. As pointed above, while all three patients had histologically identical disease and were given the same combination of agents in the first- and two of them as second-line treatments, in case 2, we did not have a representative tumor sample timely available and his therapy was based only on detailed literature review and not the theranostic concept (24–26). The biology of the relapsed disease of case 3 reflected by transcriptome was similar to that of case 2, so a different approach could be undertaken, and while reflecting high mutational burden and increased expression of the PD-1L detected by immunohistochemistry and transcriptome, anti-PD-1 antibody was successfully used here.

While analyzing the transcriptomic results including considerations of gene and network interactions using https://string-db.org/ and http://www.genome.jp/kegg/pathway.html databases (6, 21), we were able to distinguish different patterns of tumor biology among our patients. Case 1 suggested neurotrophic receptor tyrosine kinase 1 (NTRK1) as a signaling protein and one of the best targets. In case 2 and case 3, in contrast, despite being clinically and histologically similar, transcriptomic results suggest an entirely different network, where fibronectin 1 (FN1) has a very complex downstream impact. Because FN1 is not a signaling protein and a druggable target, it is likely that we missed the putatively most important pathway in case 2. One may speculate that integrin inhibitors like cilengitide could be a better therapeutic option here. For case 3, FN1 seemed to be the key molecular hub as well, and it was one of the reasons for clinical decision to rely on tumor mutational burden and PD-1 ligand expression and treat the patient with immune therapies, rather than small molecules.

The localization of *MYC* proto-oncogene on q24 of the human chromosome 8 and its translocation to chromosome 14 is considered pathogenic in most cases of Burkitt lymphoma. In our cases, the RNA transcription analyses as described above indicate the activations of different sets of genes. These patients were almost identical in their clinical presentation, histology, *MYC* status, and initial clinical response to standard chemotherapy. Early clinical testing initiatives are beginning to employ individual profiles/fingerprint analyses to compile patients into histologically or biologically similar series (27), and as these efforts continue, new clinical trial designs will emerge (28, 29).

The research that has emerged over the last 40 years disproves the concept that cancer is a consequence of a single oncogenic change. It is widely accepted that an initiating oncogenic change such as translocation involving MYC is interpreted within the patient's genome, and further genomic alterations lead to the oncogenic inducers hijacking host-specific physiological responses such as angiogenesis, inflammation, and immune evasion. These normal physiological responses are not detected by DNA mutational analysis because they represent reactivation of developmentally silent pathways. We advocate the use of combinations of biological agents addressing not only the DNA mutations but also the normal physiological responses of the host as they are reflected in the individual's molecular signature reflected on transcriptomic and proteomic levels. In case 3, we successfully used immunotherapy reflecting the molecular profile of the tumor. In cases 1 and 2, we used a combination of ibrutinib (inhibitor of BCR signaling), idelalisib (direct PI3Kdelta inhibitor), valproate (HDAC inhibitor with potential to enhance responsiveness to immune therapies), and nivolumab (a host immune response modulator). Both patients were intended to receive an immune-supportive therapy using autologous dendritic cell vaccination with non-immune-suppressive maintenance agents such as checkpoint inhibitors, but only case 1 patient had achieved sufficient duration of the clinical response to live long enough to enable the preparation of his vaccine. Unfortunately, because we did not have the benefit of molecular information on genome or transcriptome in case 2, the therapy could not be customized enough to provide a more effective therapeutic combination. Our results revealing highly phosphorylated EGFR, PDGFRβ, ROR2, ERK1/2, or Hsp27 in all samples are also in accordance with previously published findings on Burkitt lymphoma (30, 31). Interestingly, activation of EGFR and ERK signaling via EBV oncoprotein LMP1 was also reported (32, 33) and our results thus concur with the latent EBV infection as suggested by serological analysis.

One of the most interesting observations was the discordance between laboratory and clinical responses to biomarker-based targeted therapy in case 1. Even though there was evidence of normalization of PI3K pathway activity, the evidence of radiological response was significantly delayed and gave an impression that the patient continued to progress. As has been frequently observed with biological therapies, the biomarker response may be more informative and preceded in this case the radiological response. While using biological therapies, we must allow sufficient time to pass before the patient is evaluated using present radiomorphological methods.

As we show, in cases where individualization of treatment protocols can be based on the recent molecular information, the likelihood of successful therapy may be increased, but the use of a targeted agent without laboratory evidence of contemporary target activation may not only lack benefit—it may even be harmful. Similarly, while treating sepsis, we are not using several-month-old microbiology results to guide antimicrobial treatment. Considering that there are presently numerous initiatives intending to study the addition of idelalisib and/or ibrutinib to existing retrieval therapies for relapsed and refractory mature B-cell lymphomas, it may be of value to collect enough samples for tumor tissue analysis and enable similar retrospective comparisons of patients who either failed or responded to therapy. An attractive concept inspired by our cases may be the successful sequence of different treatment modalities, such as intensive chemotherapy to debulk the initial tumor volume, followed by targeted biomarker-based treatment and stimulation of autologous immune response later on to consolidate the response.

CONCLUSION

Precision medicine has significantly altered the practice of clinical oncology, but no standardized approach to the choice of these therapies exists. The three cases presented here emphasize that despite similarities in the presentation, histology, age, tumor site, and initial treatment response, the biology of tumors may differ significantly between cases and may change over time. Case 2 patient had an entirely different molecular signature and thus biology, without underlying relevant germline mutation, but such differences in molecular profile could be appreciated in retrospect only. We conclude that considering the dire outcomes of relapsed Burkitt lymphoma, theranostic testing may identify the most frequent molecular profiles that lead to therapeutic resistance and may help to improve frontline therapies sufficiently to prevent relapses and 1 day to replace our decade-old and toxic drugs like anthracyclines and alkylating agents.

DATA AVAILABILITY STATEMENT

The datasets for this article are not publicly available because it is not in accordance with our institutional policy. We handle data of rare entities that may be at risk of identification. Requests to access the datasets should be directed to Kristyna Polaskova, polaskova.kristyna@fnbrno.cz.

ETHICS STATEMENT

The studies involving human participants were reviewed and approved by Ethics Committee for Multicenter Clinical Trials of the University Hospital Brno. Written informed consent to participate in this study was provided by the participants' legal guardian/next of kin.

AUTHOR CONTRIBUTIONS

KP wrote the draft of the manuscript and evaluated patient record. TM wrote the manuscript. DZ and AM evaluated patient records. MK did the statistical analyses. PMa, ZK, and PMu participated on the treatment decision and evaluated patient records. MJ performed pathological investigation. JT performed surgical procedures. JS and IC performed the radiological evaluations. DV, LZ-D, and SK participated on the manuscript. HN, KP, OS, PF, JN, RV, VK, OH, and TF performed biological samples analyses. GK supervised and wrote the manuscript. JS conceived and supervised the project and wrote the manuscript.

FUNDING

The study was supported by projects 16-33209A, 16-34083A from the Ministry of Healthcare of the Czech Republic, project No. MUNI/A/1586/2018 from Masaryk University, Brno, Czechia, project MH CZ - DRO (FNBr, 65269705), by projects LQ1605, LO1604, LO1413, and LQ1601 from the National Program of Sustainability II (MEYS), and by Charles University, UNCE 204012.

SUPPLEMENTARY MATERIAL

The Supplementary Material for this article can be found online at: https://www.frontiersin.org/articles/10.3389/fonc.2019.01531/full#supplementary-material

REFERENCES

1. Meinhardt A, Burkhardt B, Zimmermann M, Borkhardt A, Kontny U, Klingebiel T, et al. Phase II window study on rituximab in newly diagnosed pediatric mature B-cell non-hodgkin's lymphoma and Burkitt leukemia. *J Clin Oncol.* (2010) 28:3115–21. doi: 10.1200/JCO.2009.26.6791
2. Attarbaschi A, Dworzak M, Steiner M, Urban C, Fink FM, Reiter A, et al. Outcome of children with primary resistant or relapsed non-Hodgkin lymphoma and mature B-cell leukemia after intensive first-line treatment: a population-based analysis of the Austrian cooperative study group. *Pediatr Blood Cancer.* (2005) 44:70–6. doi: 10.1002/pbc.20121
3. R Core Team. *A Language and Environment for Statistical Computing.* R Foundation for Statistical Computing (2018).
4. Ahn T, Lee E, Huh N, Park T. Personalized identification of altered pathways in cancer using accumulated normal tissue data. *Bioinformatics.* (2014) 30:i422–9. doi: 10.1093/bioinformatics/btu449
5. Carvalho BS, Irizarry RA. A framework for oligonucleotide microarray preprocessing. *Bioinformatics.* (2010) 26:2363–7. doi: 10.1093/bioinformatics/btq431
6. Rietman EA, Scott JG, Tuszynski JA, Klement GL. Personalized anticancer therapy selection using molecular landscape topology and thermodynamics. *Oncotarget.* (2017) 8:18735–45. doi: 10.18632/oncotarget.12932
7. Skoda J, Neradil J, Zitterbart K, Sterba J, Veselska R. EGFR signaling in the HGG-02 glioblastoma cell line with an unusual loss of EGFR gene copy. *Oncol Rep.* (2014) 31:480–7. doi: 10.3892/or.2013.2864
8. Kracker S, Curtis J, Ibrahim MA, Sediva A, Salisbury J, Campr V, et al. Occurrence of B-cell lymphomas in patients with activated phosphoinositide 3-kinase δ syndrome. *J Allergy Clin Immunol.* (2014) 134:233–6.e3. doi: 10.1016/j.jaci.2014.02.020
9. Lucas CL, Kuehn HS, Zhao F, Niemela JE, Deenick EK, Palendira U, et al. Dominant-activating germline mutations in the gene encoding the PI(3)K catalytic subunit p110δ result in T cell senescence and human immunodeficiency. *Nat Immunol.* (2014) 15:88–97. doi: 10.1038/ni.2771
10. Dan S, Okamura M, Seki M, Yamazaki K, Sugita H, Okui M, et al. Correlating phosphatidylinositol 3-kinase inhibitor efficacy with signaling pathway status: *in silico* and biological evaluations. *Cancer Res.* (2010) 70:4982–94. doi: 10.1158/0008-5472.CAN-09-4172
11. Jiménez-Ubieto A, Rodriguez A, Martinez Sánchez P, Gómez A, Rodriguez Y, Carreno-Tarragona G, et al. Fatal graftversus-host disease after allogeneic stem cell transplantation in a patient recently exposed to nivolumab. *J Oncol Pharm Pract.* (2019) 25:502–6. doi: 10.1177/1078155217743069
12. Hlavackova E, Pilatova K, Cerna D, Selingerova I, Mudry P, Mazanek P, et al. Dendritic cell-based immunotherapy in advanced sarcoma and neuroblastoma pediatric patients: anti-cancer treatment preceding monocyte harvest impairs the immunostimulatory and antigen-presenting behavior of dcs and manufacturing process outcome. *Front Oncol.* (2019) 9:1034. doi: 10.3389/fonc.2019.01034
13. Forrest DL, Hogge DE, Nevill TJ, Nantel SH, Barnett MJ, Shepherd JD, et al. High-dose therapy and autologous hematopoietic stem-cell transplantation does not increase the risk of second neoplasms for patients with Hodgkin's lymphoma: a comparison of conventional therapy alone versus conventional therapy followed by autologous hematopoietic stem-cell transplantation. *J Clin Oncol.* (2005) 23:7994–8002. doi: 10.1200/JCO.2005.01.9083
14. Freed-Pastor WA, Prives C. Mutant p53: one name, many proteins. *Genes Dev.* (2012) 26:1268–6. doi: 10.1101/gad.190678.112

15. Chen JY, Funk WD, Wright WE, Shay JW, Minna JD. Heterogeneity of transcriptional activity of mutant p53 proteins and p53 DNA target sequences. *Oncogene.* (1993) 8:2159–66.
16. Vaughan CA, Singh S, Windle B, Yeudall WA, Frum R, Grossman SR, et al. Gain-of-function activity of mutant p53 in lung cancer through up-regulation of receptor protein tyrosine kinase Axl. *Genes Cancer.* (2012) 3:491–502. doi: 10.1177/1947601912462719
17. Odell AF, Odell LR, Askham JM, Alogheli H, Ponnambalam S, Hollstein M. A novel p53 mutant found in iatrogenic urothelial cancers is dysfunctional and can be rescued by a second-site global suppressor mutation. *J Biol Chem.* (2013) 288:16704–14. doi: 10.1074/jbc.M112.443168
18. Lin RK, Wu CY, Chang JW, Juan LJ, Hsu HS, Chen CY, et al. Dysregulation of p53/Sp1 control leads to DNA methyltransferase-1 overexpression in lung cancer. *Cancer Res.* (2010) 70:5807–17. doi: 10.1158/0008-5472.CAN-09-4161
19. Kondo E, Tanaka T, Miyake T, Ichikawa T, Hirai M, Adachi M, et al. Potent synergy of dual antitumor peptides for growth suppression of human glioblastoma cell lines. *Mol Cancer Ther.* (2008) 7:1461–71. doi: 10.1158/1535-7163.MCT-07-2010
20. Smeenk L, van Heeringen SJ, Koeppel M, Gilbert B, Janssen-Megens E, Stunnenberg HG, et al. Role of p53 serine 46 in p53 target gene regulation. *PLoS ONE.* (2011) 6:e17574. doi: 10.1371/journal.pone.0017574
21. Klement GL. Eco-evolution of cancer resistance. *Sci Transl Med.* (2016) 8:327fs5. doi: 10.1126/scitranslmed.aaf3802
22. Simeone E, Grimaldi AM, Festino L, Vanella V, Palla M, Ascierto PA. Combination treatment of patients with BRAF-mutant melanoma: a new standard of care. *BioDrugs.* (2017) 31:51–61. doi: 10.1007/s40259-016-0208-z
23. Hu-Lieskovan S, Robert L, Homet Moreno B, Ribas A. Combining targeted therapy with immunotherapy in *BRAF* -mutant melanoma: promise and challenges. *J Clin Oncol.* (2014) 32:2248–54. doi: 10.1200/JCO.2013.52.1377
24. Sorge CE, McDaniel JK, Xavier AC. Targeted therapies for the treatment of pediatric non-hodgkin lymphomas: present and future. *Pharmaceuticals.* (2016) 9:28. doi: 10.3390/ph9020028
25. Eyre TA, Osborne WL, Gallop-Evans E, Ardeshna KM, Kassam S, Sadullah S, et al. Results of a multicentre UK-wide compassionate use programme evaluating the efficacy of idelalisib monotherapy in relapsed, refractory follicular lymphoma. *Br J Haematol.* (2018) 181:555–9. doi: 10.1111/bjh.14665
26. Davies A. Idelalisib for relapsed/refractory indolent B-cell non-Hodgkin's lymphoma: an overview of pharmacokinetics and clinical trial outcomes. *Expert Rev Hematol.* (2015) 8:581–93. doi: 10.1586/17474086.2015.1071663
27. Egas-Bejar D, Anderson PM, Agarwal R, Corrales-Medina F, Devarajan E, Huh WW, et al. Theranostic profiling for actionable aberrations in advanced high risk osteosarcoma with aggressive biology reveals high molecular diversity: the human fingerprint hypothesis. *Oncoscience.* (2014) 1:167–79. doi: 10.18632/oncoscience.21
28. Woodcock J, LaVange LM. Master protocols to study multiple therapies, multiple diseases, or both. *N Engl J Med.* (2017) 377:62–70. doi: 10.1056/NEJMra1510062
29. Schork NJ. Personalized medicine: time for one-person trials. *Nature.* (2015) 520:609–11. doi: 10.1038/520609a
30. Ogasawara T, Yasuyama M, Kawauchi K. Constitutive activation of extracellular signal-regulated kinase and p38 mitogen-activated protein kinase in B-cell lymphoproliferative disorders. *Int J Hematol.* (2003) 77:364–70. doi: 10.1007/BF02982645
31. Fuchs D, Berges C, Opelz G, Daniel V, Naujokat C. Increased expression and altered subunit composition of proteasomes induced by continuous proteasome inhibition establish apoptosis resistance and hyperproliferation of Burkitt lymphoma cells. *J Cell Biochem.* (2008) 103:270–83. doi: 10.1002/jcb.21405
32. Kung C-P, Meckes DG, Raab-Traub N. Epstein-Barr Virus LMP1 activates EGFR, STAT3, and ERK through effects on PKC. *J Virol.* (2011) 85:4399–408. doi: 10.1128/JVI.01703-10
33. Huang YC, Lin SJ, Lin KM, Chou YC, Lin CW, Yu SC, et al. Regulation of EBV LMP1-triggered EphA4 downregulation in EBV-associated B lymphoma and its impact on patients' survival. *Blood.* (2016) 128:1578–89. doi: 10.1182/blood-2016-02-702530

Conflict of Interest: The authors declare that the research was conducted in the absence of any commercial or financial relationships that could be construed as a potential conflict of interest.

Advantages of publishing in Frontiers

OPEN ACCESS
Articles are free to read for greatest visibility and readership

FAST PUBLICATION
Around 90 days from submission to decision

HIGH QUALITY PEER-REVIEW
Rigorous, collaborative, and constructive peer-review

TRANSPARENT PEER-REVIEW
Editors and reviewers acknowledged by name on published articles

Frontiers
Avenue du Tribunal-Fédéral 34
1005 Lausanne | Switzerland

Visit us: www.frontiersin.org
Contact us: info@frontiersin.org | +41 21 510 17 00

REPRODUCIBILITY OF RESEARCH
Support open data and methods to enhance research reproducibility

DIGITAL PUBLISHING
Articles designed for optimal readership across devices

FOLLOW US
@frontiersin

IMPACT METRICS
Advanced article metrics track visibility across digital media

EXTENSIVE PROMOTION
Marketing and promotion of impactful research

LOOP RESEARCH NETWORK
Our network increases your article's readership